

Silvia Catarina Peixeira Carvalho

RAINFALL: MEASUREMENTS, VARIABILITY AND LABORATORY SIMULATIONS

Thesis submitted to the Civil Engineering Department, Faculty of Sciences and Technology of the University of Coimbra, in fulfilment of the requirements for the degree of Doctor of Philosophy in Environmental Engineering, under the supervision of Prof. Dr. Maria Isabel M. L. P. Pedroso de Lima and Prof. Dr. João Luís Mendes Pedroso de Lima

2014



UNIVERSIDADE DE COIMBRA



FCTUC DEPARTAMENTO DE ENGENHARIA CIVIL
FACULDADE DE CIÊNCIAS E TECNOLOGIA
UNIVERSIDADE DE COIMBRA

Rainfall: measurements, variability and laboratory simulations

Thesis submitted to the Civil Engineering Department, Faculty of Sciences and Technology of the University of Coimbra, in fulfilment of the requirements for the degree of Doctor of Philosophy in Environmental Engineering

Author

Sílvia Catarina Peixeira Carvalho

Supervisors

Prof. Dr. Maria Isabel M. L. P. Pedroso de Lima

Prof. Dr. João Luís Mendes Pedroso de Lima

Coimbra, 2014

*“I can foretell the way of celestial bodies,
but can say nothing of the movement of a small drop of water”*
- Galileo Galilei

ABSTRACT

The characterization of rainfall is of fundamental importance to many fields in hydrology, and engineering applications, such as modelling of runoff, soil erosion, and climate, calibrating remote sensing data, designing rainwater harvesting systems, among others. The work presented in this thesis focuses on some aspects related to rainfall. Special attention is dedicated to measuring and charactering the rainfall variability, both within individual rain events and historical time series. Characterizing the raindrop properties (sizes and fall speeds) is also an emphasis in this research study, which is particularly important for water erosion studies, whether under natural or laboratory conditions.

The first part of the thesis focuses on natural rainfall. The data sets used comprise: (i) annual and monthly time series dating from the 19th century, obtained from meteorological stations scattered over Portugal; (ii) three-year rainfall measurements obtained on an outdoor experimental site set up at Coimbra, using different types of rain gauges, including a laser disdrometer which provided records with one-minute temporal resolution. The longest time series allowed the study of full monotonic trends and partial trends in the annual and monthly rainfall; whereas, the high temporal resolution series were used to characterize the rainfall events according to e.g. the raindrop properties.

The increased variability has been reported for inter- and intra-annual rainfall, which leads to increased concern about water resources management and water scarcity issues. In this thesis when full monotonic trends were investigated in annual rainfall, there was no evidence for rejecting the null hypothesis of no trend. In order to deal with the non-monotonic character of the trends obtained, shorter periods were then analysed; the partial trends showed a sequence of alternately decreasing and increasing trends in annual and monthly rainfall.

The high variability of rainfall is also observed in shorter time scales. Variations can occur, for instance, within individual rainfall events. In this thesis, this fact is considered, for example, in relation to the rainwater chemical composition, which can vary over relatively

short time periods. A rain sampler that has low manufacturing costs was developed for collecting sequential small volume rain samples, and this way, allowing the assessment of variations of rainwater composition during individual rain events.

Instead of centring on the rainfall average properties over large volumes and long time intervals, rainfall can be modelled as a discrete process consisting of numerous individual raindrops that differ in size and fall speed. Relationships were estimated between these raindrops' characteristics and the rain rates and kinetic energy based on the disdrometric data from 35 rain events. Results confirmed that, for example, power laws fitted well the relationship between the kinetic energy and the mass-weighted mean drop diameter, and the kinetic energy-rain rate relationship.

The second part of this thesis focuses on rainfall simulation, which is a widely used tool that allows the repetition of experiments under controlled conditions and in a less time consuming manner. There has been a tendency to use constant intensity at the expense of considering the temporal variability and rainfall patterns. In this thesis, laboratory experiments were carried out in order to study the effects of heavy rainfall bursts within storm events on runoff and soil loss. Results showed that the instant at which rainfall bursts occur during long duration rain events has a strong influence on the discharge hydrographs and associated transport processes; if ignored it might cause both under and over estimation of runoff discharge and soil loss.

Rainfall simulators were also studied in relation to the drop properties. A laboratory set-up that combines spray nozzle simulators and meshes was tested, suggesting that meshes can be used to increase the mean rainfall intensity and kinetic energy on the control plot (mainly through the formation of bigger drops). The exploratory experiments were then important to characterize simulated rainfall and promote the versatility of the nozzles by using meshes.

RESUMO

A caracterização da precipitação assume uma importância fundamental em diversos domínios da hidrologia e em aplicações de engenharia, como por exemplo na modelação do escoamento, da erosão dos solos, e do clima, na calibração de dados de deteção remota, na conceção de sistemas de captação de água da chuva, entre outros. O trabalho apresentado nesta tese foca alguns aspetos relacionados com a precipitação, dando especial atenção à medição e caracterização da variabilidade da precipitação, tanto à escala do evento como em séries temporais históricas. A caracterização das propriedades das gotas de chuva (tamanho e velocidades de queda) é também destacada neste trabalho tanto sob condições naturais como laboratoriais, sendo particularmente importante para estudos de erosão hídrica.

A primeira parte da tese foca-se na precipitação natural. O conjunto de dados usados inclui: (i) séries temporais anuais e mensais que datam do século XIX, obtidas por estações meteorológicas dispersas por Portugal; (ii) mais de 3 anos de medições obtidas numa instalação experimental localizada em Coimbra, usando diferentes tipos de pluviómetros, incluindo um distrómetro que regista dados com resolução de 1 minuto. As séries temporais longas permitiram o estudo de tendências monotónicas e parciais na precipitação mensal e anual; enquanto que os dados com elevada resolução temporal foram usadas para caracterizar os eventos pluviosos de acordo, por exemplo com as propriedades das gotas de chuva.

O aumento da variabilidade tem sido assinalado para a precipitação inter e intra-anual, o que suscita uma crescente preocupação no âmbito da gestão de recursos hídricos e escassez da água. Nesta tese quando foram investigadas as tendências monotónicas da precipitação anual, não houve evidências para rejeitar a hipótese nula de ausência de tendência. Com o intuito de lidar com o carácter não-monotónico das tendências obtidas foram realizados testes de tendência para diferentes sub-períodos que indicaram alternância entre períodos de aumento e diminuição da precipitação anual e mensal.

A elevada variabilidade manifestada pela precipitação estende-se também a escalas temporais menores. As variações podem ocorrer, por exemplo, ao nível dos eventos pluviosos. Nesta tese, este facto é considerado, por exemplo, em relação à composição química da água, que pode variar para períodos de tempo curtos. Um amostrador com baixo custo de fabrico foi desenvolvido para recolher sequencialmente pequenas amostras de água da chuva e, deste modo, permitir estimar a variabilidade da composição da água durante os eventos pluviosos.

Em alternativa a uma abordagem sobre as propriedades médias da precipitação para elevados volumes e longos intervalos de tempo, a precipitação pode ser modelada como um processo discreto, uma vez que consiste em numerosas gotas individuais que diferem no tamanho e na velocidade de queda. A relação entre as características das gotas, intensidade e energia cinética da chuva foi analisada com base em 35 eventos pluviosos registados com um distrómetro. Os resultados confirmaram, por exemplo, que a lei de potência ajusta-se bem à relação entre a energia cinética e o diâmetro médio das gotas (ponderado pela massa), e à relação entre energia cinética e intensidade da chuva.

A segunda parte da tese foca-se na simulação de chuva em laboratório, ferramenta amplamente utilizada que permite a repetição das experiências sob condições controladas e num curto espaço de tempo. Em laboratório é frequente utilizarem-se intensidades de chuva constantes em detrimento da reprodução de variabilidade temporal e diferentes padrões de chuva. Neste trabalho realizaram-se experiências laboratoriais com a intenção de estudar os efeitos de picos de intensidade de eventos pluviosos no escoamento superficial e transporte sólido. Os resultados mostram que os instantes em que os picos de chuva ocorrem durante longos eventos podem ter uma grande influência nos hidrogramas e nos processos de transporte sólido; no caso de serem ignorados podem causar estimativas por defeito ou por excesso das descargas líquidas e perdas de solo.

Os simuladores de chuva foram também estudados no que concerne às propriedades das gotas. Foi testada uma instalação experimental que combina simuladores de chuva por aspersão e redes; sugerindo que estas podem ser utilizadas para aumentar a intensidade e

energia cinética da chuva na zona de controlo (principalmente pela formação de gotas maiores). As experiências laboratoriais foram, portanto, importantes para caracterizar as chuvas simuladas e promover a versatilidade dos aspersores através do uso de redes.

ACKNOWLEDGEMENTS

First of all, I would like to thank my supervisors for their advice and insightful discussions. The achievement of this thesis would not have been possible without their accurate criticism.

I am grateful for the institutional support received from University of Coimbra during this Ph.D. program. In particular, I am heavily indebted to Mr. Joaquim Cordeiro, technical assistant at the Laboratory of Hydraulics, Water Resources and Environment; his involvement and creativity has made the fieldwork possible, but mostly I should thank him for being on hand when reassurance was needed.

A debt of gratitude is also owed to my colleagues, Giovana, Ina, Ricardo, João, Pedro, Patricia, Romeu and so many that passed at some point through the laboratory. They provided me with countless amusing times and made this place so pleasant to work in. Special thanks also go to Professors Jorge Isidoro and Mário Franca for sharing with me their knowledge and life experience, which inspires me to be successful.

My sincere thanks are extended to Susana, Pedro, Ana, Luís, and the entire wonderful group from University Campus I for “adopting me”. I bumped into them this last year and they turned out to be the breath of fresh air that I needed in the final sprint.

To my friends, I would like to thank them for teaching me 'Life isn't about waiting for the storm to pass...It's about learning to dance in the rain' (Vivian Greene). To Patricia, Cristiana and Fátima, who have provided unconditional support and constant encouragement throughout, and to Ashenafi, Merkebe, Miguel, Maria and Carlos, who have definitely make this trip unforgettable.

Finally, I would like to express my deepest gratitude to my family as all my accomplishments are the extension of their valuable efforts and pure belief in me.

The author is grateful to the IMAR - Marine and Environmental Research Centre, as a host institution, and the Foundation for Science and Technology (FCT) of the Portuguese Ministry of Education and Science for the financial support of the Doctoral Grant SFRH/BD/60213/2009, through the National Strategic Reference Framework (QREN) and the Human Potential Operational Program (POPH), co-financed by the European Social Fund (ESF).

The research presented in this thesis was also partially funded by the following projects:

- PTDC/GEO/73114/2006, funded by the FCT;
- PTDC/ECM/105446/2008, funded by the FCT and by the Operational Programme 'Thematic Factors of Competitiveness' (COMPETE), shared by the European Regional Development Fund (ERDF);
- Project RISK of the MIT-Portugal Program, funded by the FCT.

The author acknowledges the Portuguese Sea and Atmosphere Institute (IPMA) for the precipitation data provided. In particular, the author thanks the collaboration of M. F. E. S. Coelho, in the study presented in the Chapter 6.

The author also acknowledges the participation of Romeu Gerardo (IMAR/DEC-FCTUC) and Raquel Silva (trainee ESAC/IPC) in some of the laboratory runs carried out for the study presented in the Chapter 7.



CONTENTS

ABSTRACT	I
RESUMO	III
ACKNOWLEDGEMENTS.....	VII
CONTENTS	XI
LIST OF FIGURES.....	XV
LIST OF TABLES.....	XXIII
1. INTRODUCTION.....	1
1.1. RATIONALE AND OBJECTIVES	1
1.2. OUTLINE.....	3
1.3. PUBLICATIONS	5
2. RESEARCH REVIEW.....	11
2.1. INTRODUCTION	11
2.2. RAINFALL MEASUREMENTS	12
2.3. RAINFALL SPACE AND TIME VARIABILITY.....	15
2.4. VARIABILITY OF RAINDROP CHARACTERISTICS.....	18
2.5. REPRODUCING RAIN EVENTS IN LABORATORY	20
PART I – NATURAL RAINFALL: MEASUREMENTS AND VARIABILITY	23
3. COMPARISON OF MEASUREMENTS FROM AN OUTDOOR EXPERIMENTAL SITE WITH SEVERAL TYPES OF RAIN GAUGES	25
3.1. INTRODUCTION	26
3.2. MATERIAL AND METHODS	27
3.2.1. <i>Measuring site and rain gauges</i>	27
3.2.2. <i>Rainfall data</i>	29
3.3. METHODOLOGY	31
3.3.1. <i>Analysis of rainfall accumulation for 60 rainy periods.....</i>	31
3.3.2. <i>Analysis of 1-min rain rate measurements.....</i>	32
3.4. RESULTS AND DISCUSSION	32

3.4.1.	<i>Analysis of rainfall accumulation for 60 rainy periods</i>	32
3.4.2.	<i>Analysis of 1-min rain rate measurements</i>	35
3.5.	CONCLUDING REMARKS	38
4.	RAINWATER SEQUENTIAL SAMPLER: ASSESSING INTRA-EVENT WATER COMPOSITION VARIABILITY	41
4.1.	INTRODUCTION	42
4.2.	RAINWATER SEQUENTIAL SAMPLER	43
4.2.1.	<i>Design of the equipment</i>	43
4.2.2.	<i>Advantages and disadvantages of the equipment</i>	45
4.3.	TESTING THE SAMPLER	46
4.3.1.	<i>Measuring site</i>	46
4.3.2.	<i>Data acquisition</i>	47
4.3.3.	<i>Data analysis</i>	50
4.4.	CONCLUDING REMARKS	56
5.	ANALYSIS OF RAINFALL EVENTS IN COIMBRA, PORTUGAL: VARIABILITY OF RAINDROP CHARACTERISTICS	57
5.1.	INTRODUCTION	58
5.2.	MATERIAL AND METHODS	60
5.2.1.	<i>Study area and experimental equipment</i>	60
5.2.2.	<i>Rainfall events</i>	61
5.2.3.	<i>Rainfall rates, raindrop properties, and rainfall kinetic energy</i>	63
5.3.	RESULTS AND DISCUSSION	66
5.3.1.	<i>Characterization of drop size</i>	67
5.3.2.	<i>Characterization of drop fall speed</i>	72
5.3.3.	<i>Characterization of rainfall kinetic energy</i>	75
5.4.	CONCLUDING REMARKS	77
6.	INVESTIGATING ANNUAL AND MONTHLY TRENDS IN PRECIPITATION STRUCTURE: AN OVERVIEW ACROSS PORTUGAL	79
6.1.	INTRODUCTION	80
6.2.	STUDY AREA AND PRECIPITATION DATA	81
6.3.	METHODOLOGY	84
6.4.	RESULTS AND DISCUSSION	86
6.4.1.	<i>Analysis of annual precipitation</i>	86
6.4.2.	<i>Analysis of monthly precipitation</i>	94

6.5.	CONCLUDING REMARKS	98
PART II – SIMULATED RAINFALL: LABORATORY EXPERIMENTS.....		101
7. RAINFALL SIMULATOR EXPERIMENTS ON THE IMPORTANCE OF WHEN RAINFALL BURST OCCURS DURING STORM EVENTS ON RUNOFF AND SOIL LOSS		
103		
7.1.	INTRODUCTION	104
7.2.	MATERIALS AND METHODS.....	106
7.2.1.	<i>Simulated rainfall patterns</i>	106
7.2.2.	<i>Laboratory set-up</i>	108
7.2.3.	<i>Laboratory procedure</i>	110
7.3.	RESULTS	114
7.4.	CONCLUDING REMARKS	123
8. USING MESHES TO CHANGE THE CHARACTERISTICS OF SIMULATED RAINFALL PRODUCED BY SPRAY NOZZLES		
125		
8.1.	INTRODUCTION	126
8.2.	MATERIALS AND METHODS.....	128
8.2.1.	<i>Laboratory set-up</i>	128
8.2.2.	<i>Methodology</i>	131
8.3.	RESULTS AND DISCUSSION	135
8.3.1.	<i>Rainfall intensities</i>	135
8.3.2.	<i>Diameter and fall speed of drops</i>	139
8.4.	CONCLUDING REMARKS	142
9. INCREASING THE RAINFALL KINETIC ENERGY OF SPRAY NOZZLES BY USING MESHES		
145		
9.1.	INTRODUCTION	146
9.2.	MATERIALS AND METHODS.....	148
9.2.1.	<i>Laboratory installation</i>	148
9.2.2.	<i>Methodology</i>	150
9.3.	RESULTS AND DISCUSSION	153
9.4.	CONCLUDING REMARKS	161
10. CONCLUSIONS AND FUTURE RESEARCH		
163		
10.1.	CONCLUSIONS.....	163
10.2.	FUTURE RESEARCH	167
11. REFERENCES.....		
169		

APPENDIX A: CHARACTERISTICS OF THE USED GAUGES	199
APPENDIX A.1. NON-CONVENTIONAL RAIN GAUGE (SRG.1)	201
APPENDIX A.2. STANDARD RAIN GAUGES (SRG.2 AND SRG.3).....	203
APPENDIX A.3. TIPPING BUCKET RAIN GAUGE (TBG.4)	205
APPENDIX A.4. WEIGHING PRECIPITATION GAUGE (WPG.5).....	207
APPENDIX A.5. MULTI-PARAMETER WEATHER SENSOR (MWS.6)	209
APPENDIX A.6. DISDROMETER (DIS.7)	211
APPENDIX B: CHRONOGRAM AND LIST OF MEASURED DATA SERIES	213

LIST OF FIGURES

Figure 1. Precipitation measurement by satellite, radar and rain gauges (UCAR, 2009).	12
Figure 2. (a) View of the laser disdrometer manufactured by Thies Clima installed in the Department of Civil Engineering of the University of Coimbra; (b) Detail of the disdrometer measuring precipitation particles that pass through the laser beam (Thies, 2007).	14
Figure 3. Representation of mean annual rainfall (1971-2003) in mainland Portugal. The map was created using the Inverse-Distance-Weighted interpolation method.....	16
Figure 4. Monthly rainfall for three measuring stations in mainland Portugal (the characteristics of the data series can be seen in the Table 11, Chapter 6).	17
Figure 5. Scheme of space distribution of raindrops in a volume of air (Jaffrain, 2012).	18
Figure 6. Views of laboratory experiments making use of a nozzle rainfall simulator at the Civil Engineering Department of the Faculty of Science and Technology of the University of Coimbra.	21
Figure 7. (a) Position of the rain gauges at the top of the building; (b) View of the instruments. Measurements are in meters. See Table 4.	29
Figure 8. Hyetograph of 60 rainy periods selected from the period between March, 2011 and March, 2013: (a) Rainfall depths (mean of 7 gauges) and maximum rain intensity detected with the disdrometer (DIS.7); (b) Accumulated rainfall from the 60 rainy periods, for each gauge.	30
Figure 9. Box-and-whisker plots representing the relative error of rainfall measurements provided by the 7 studied instruments; 60 rainy periods were investigated.	33
Figure 10. (a) Scatter plot of rainfall depths measured by each gauge against the reference values (b) and corresponding fitted trend lines.	35
Figure 11. Representation of time series of wind speed, rain rates (mean of four gauges), and accumulated rainfall (for each gauge). The rainy periods were observed in: (a) 26-27 March 2011; (b) 7-8 May 2012; (c) 7-8 March 2013. Broken scales for the x-axis of (a) and (c) were created to better visualize the rainy period.	36

Figure 12. Box-and-whisker plots of the coefficient of variation of rain rate measurements in relation to rain rate classes. The resolution of data is 1-min and is related to the measurements of four gauges (TBG.4, WPG.5, MWS.6 and DIS.7) in the three rainy periods observed in 26-27 March 2011, 7-8 May 2012 and 7-8 March 2013.....	38
Figure 13. (a) Setup of the rainwater sequential sampler. Distances are in meters; (b) Hydraulic scheme of the rainwater sampling.....	44
Figure 14. (a) Location of Coimbra in mainland Portugal; (b) Location of the study site in the city of Coimbra (black triangle); (c) Photograph of the equipment.....	47
Figure 15. Hyetographs of the four rainy periods (see Table 6). Time needed to fill each sampling bottle is represented on the hyetographs (time between two vertical dotted lines).	51
Figure 16. (a) Turbidity measured for each sample collected during the four rainy periods. Power laws are fitted to the data; (b) pH measured in the rainwater samples collected during the four rainy periods.....	53
Figure 17. Electrical conductivity (EC) measured in each sample during the four rainy periods. Rainfall intensity was averaged over each sampling interval.	54
Figure 18. (a) Concentrations of chloride, sulphates and nitrates during the rainy period 4 (23-09-2012); (b) Concentrations of chloride, sulphates and nitrates plotted against the mass-weighted mean drop diameter (D_m).....	55
Figure 19. (a) D_m (mass-weighted mean diameter) for the 35 rainfall events; the dots are scaled according to the maximum drop diameter recorded in each event. (b) D_m plotted against the coefficient of variation of drop diameter. The fit line is indicative of the tendency in the data.....	67
Figure 20. Time series of drop size and rain rate for three rainfall events. Since disdrometers can not measure the very small drops, the minimum diameter measured is truncated at 0.125 mm.....	68
Figure 21. D_m -R relationships fitted with power law equations based on data from: (a) the individual rainfall events 8, 12 and 19; (b) all the 35 rainfall events. The Spearman's rho is reported.....	69

Figure 22. Empirical raindrop size distributions fitted with gamma distributions for: (a) event 8; (b) event 12; (c) event 19; (d) 8 rain rate classes obtained from the entire data set (35 rainfall events), defined in Table 9.	70
Figure 23. Total number of drops as a function of drop diameter and drop fall speed for 8 rain rate classes and the 35 rain events. The Gunn and Kinzer (1949) measurements are represented (with crosses) as a reference.	72
Figure 24. (a) v_m (mean raindrop fall speed) for the 35 rainfall events; (b) v_m plotted against the coefficient of variation of drop fall speed.	73
Figure 25. Time series of drop fall speed and rain rate of the rainfall events 8, 12 and 19.	74
Figure 26. Mean raindrop fall speed (v_m) plotted against R based on data from all the 35 rainfall events. The Spearman's rho is indicated.	75
Figure 27. Absolute frequency of raindrop fall speeds for 8 rain rate classes obtained from the 35 rainfall events.	75
Figure 28. Hyetograph and time-specific kinetic energy of the rainfall event 8.	76
Figure 29. KE_{time} -R relationship based on data from: (a) the rainfall events 8, 12 and 19 (b) all the 35 rainfall events. Power laws are fitted to the data.	76
Figure 30. KE_{time} - D_m relationship based on data from: (a) the rainfall events 8, 12 and 19 (b) all the 35 rainfall events. Power laws are fitted to the data.	77
Figure 31. Study area: (a) location of mainland Portugal and the Madeira and Azores archipelagos; (b) location of ten precipitation measuring stations in mainland Portugal; (c) location of four precipitation measuring stations in the Madeira and Azores archipelagos.	82
Figure 32. Annual precipitation series for six stations in mainland Portugal and four stations in the islands. Sen's estimator of the slope of monotonic trends over the full record periods (blue line) is indicated in the legend. The red line is the fit for partial trends. For better visualization, note that the Y axes scales are not the same for all the plots.	90
Figure 33. The 50-year moving average series of the annual precipitation from Portugal; the data from the islands are plotted with dashed lines. The data are centred on the 50-year window. See also Table 13.	91

Figure 34. Partial trend fits to the annual precipitations for: (a) ten locations in mainland Portugal (adapted from de Lima et al., 2010b); (b) four locations in the Madeira and Azores archipelagos. The time series are not plotted.	93
Figure 35. Monthly precipitation trends in selected periods for: (a) five locations in mainland Portugal; (b) four locations in Azores and Madeira. The periods analysed are identified in the legend and were selected based on the partial trend analyses and results, and correspond to decreasing trend sub-periods in annual precipitation.	96
Figure 36. Partial trends in monthly precipitation in mainland Portugal: (a) January; (b) March; (c) October; (d) December. The time series are not plotted.	97
Figure 37. Sketch (not to scale) of the different basic hyetographs referred in the text.	107
Figure 38. Sketch of the laboratory set-up used in the experimental runs.	108
Figure 39. Simulating different temporal rainfall intensities: Left, representation (top view) of the two soil flume positions with respect to the wetted area under the nozzle; Right, corresponding rainfall intensities observed along the soil flume for the average intensities of 8 and 100 mm h ⁻¹	112
Figure 40. Raindrop mean diameter and fall velocities. Soil flume positions 1 and 2 are indicated in Figure 39 – left. The measurements were taken at the flume installation level, 2.25 m below the nozzle (vertical distance). The nozzle was operated at 73 kPa.	113
Figure 41. Histograms of simulated raindrops observed for the soil flume at positions 1 (left) and 2 (right); the data are for 15 minutes of simulated rainfall. The rain simulator was operated at 73 kPa. For better visualization, the vertical axes are scaled differently in the two plots.	114
Figure 42. Measured runoff hydrographs: (top) first set of experiments, (bottom) second set of experiments. The origin of the horizontal axes coincides with the beginning of each burst of intense rainfall: 1 – advanced, 2 – advanced-centred, 3 – centred, 4 – centred-delayed and 5 – delayed.	115
Figure 43. Measured transported sediment graphs: (top) first set of experiments, (bottom) second set of experiments. The origin of the horizontal axis coincides with the beginning of each burst of intense rainfall. See also Figure 42 which shows the measured runoff hydrographs.	116
Figure 44. Infiltration in time for rainfall patterns 1, 3 and 5 (first set of experiments).	119

-
- Figure 45. For the five rainfall bursts: (a) total runoff volume, (b) peak runoff, (c) total amount of sediment transported, and (d) peak sediment flux. Squares and triangles represent empirical data from the first and second set of experiments, respectively, whereas the adjusted lines are only indicative of the tendency in the data..... 120
- Figure 46. For the five rainfall bursts: (a) relation between the total amount of sediment transported and total runoff volume, and (b) relation between peak sediment flux and peak runoff rate. Squares and triangles represent empirical data from the first and second set of experiments, respectively, whereas the adjusted lines are only indicative of the tendency in the data..... 121
- Figure 47. For the five rainfall bursts in the 8 hour event: (a) time to runoff, in relation to the beginning of corresponding high intensity rainfall periods, and (b) duration of surface runoff. Squares and triangles represent empirical data from the first and second set of experiments, respectively, whereas the adjusted lines are only indicative of the tendency in the data..... 122
- Figure 48. Set-up of the laboratory experiments. 128
- Figure 49. Spray angle and spray limit boundary for the 4 nozzles used in the experiments; the 3 mesh positions beneath the nozzles are represented. The nozzle vertical distance to the target surface is 2.35 m; operating pressure is 1.5 bar; on the target surface, measures are for the wetted area. Distances are in mm. 132
- Figure 50. (a) Position of the 41 rain gauges used to measure the rainfall intensity on a 1 m² square plot (control plot, top view); (b) Spatial distribution of the simulated rainfall intensity [mm h⁻¹] under the 7G-1 nozzle, estimated using Kriging; (c) Position of 15 rain gauges used to measure the rainfall intensity along a given direction (top view); (d) The position of the disdrometer used to measure drop properties (top view). The black ring identifies the position of the nozzle. 133
- Figure 51. Rainfall intensities observed along the 3.5 m diameter of the nozzle spray wetted circle, for simulations conducted without combining the nozzles with meshes and combining the nozzles with a plastic mesh (square aperture of 20 mm) that was positioned beneath the spray nozzles, at vertical distances of 200, 400 and 600 mm: (a) HH-22; (b) HH-14W; (c) HH-4.3W and (d) 7G-1. Data are average values of 3 replicates..... 137
-

Figure 52. (a) Mean rainfall intensities observed combining nozzles with plastic meshes (square aperture of 12 mm and 20 mm) as a function of the vertical distances between the meshes and the nozzle; data are average values for the control plot and lines are only indicative of trends. (b) Comparison between the rainfall intensities observed along the control plot when combining the spray nozzle HH-14W with plastic meshes (square apertures of 12, 20 and 40 mm) and steel meshes (square apertures of 20 mm and 40 mm); the distance between the mesh and the nozzle was 600 mm..... 138

Figure 53. Comparison of simulated raindrops' properties observed combining the spray nozzle with a plastic mesh (square aperture of 20 mm) and without mesh: (a) mass-weighted mean diameter; (b) mean fall speed. The spray nozzles tested are identified in the legend. The results are for meshes positioned at three vertical distances from the nozzles: 200, 400 and 600 mm. The data were collected during 15 s (3 replicates) with a laser disdrometer positioned in three positions that correspond to the 3 data points for each combination nozzle type-distance (see Figure 50d)..... 140

Figure 54. Rain drop size distribution produced by spray nozzles combined with a plastic mesh (square aperture of 20 mm) and without mesh: (a) HH-22; (b) HH-14W; (c) HH-4.3W; (d) 7G-1. The data were collected with the disdrometer positioned in the centered position, on the measuring plane, and the meshes were positioned at three distances from the nozzle..... 141

Figure 55. View of the laboratory installation, showing the nozzle, the suspended mesh underneath and the disdrometer. 149

Figure 56. For 4 nozzles types, total number of drops counted in each size and fall speed interval for: mesh-free nozzle simulations (left); and for simulations combining the nozzle with a mesh positioned at 400 mm from the nozzle (right). The data were collected during 15 s (average of 3 replicates) with the disdrometer positioned just below the nozzles. See also Table 23..... 155

Figure 57. Comparison of the kinetic energy of the rainfall simulated using meshes with the mesh-free simulations: (a) time-specific rainfall kinetic energy; (b) volume-specific rainfall kinetic energy. The results are for the mesh positioned at three vertical distances from the nozzle. The three data points for each combination nozzle type-distance from the nozzle

are for the three positions of the disdrometer; data points are averages of 3 measurement replicates.	157
Figure 58. Time-specific kinetic energy, KE_{time} , for each size and fall speed class for mesh-free simulations (left), and combining a mesh positioned at 400 mm from the nozzle (right). The data were collected during 15 s (3 replicates) with the disdrometer positioned just below the nozzle. The KE_{time} data are average values for the 3 measurement replicates.	158
Figure 59. Time-specific kinetic energy, KE_{time} , as a function of raindrop size classes (left), and drop fall speed classes (right). The data are for the disdrometer positioned just below the nozzle (average for 3 replicates).	160

LIST OF TABLES

Table 1. Publications in international scientific periodicals with referees.....	6
Table 2. Publications (papers) in proceedings of scientific meetings.....	7
Table 3. Communications (abstracts) in scientific meetings.....	8
Table 4. List of the seven rain measuring devices studied.....	28
Table 5. Coefficients of the regression lines illustrated in Figure 10b, and root mean square errors (RMSE).....	35
Table 6. Description of the rainy periods sampled.....	48
Table 7. Description of rainwater parameters for the four rainy periods (see Table 6 and Figure 15): I (Rainfall Intensity), D_m (Mass-Weighted Mean Drop Diameter), EC (Electrical Conductivity), Tr (Turbidity), Cl^- (Chloride), SO_4^{2-} (Sulphates), and NO_3^- (Nitrates), used to test the sampler.....	52
Table 8. Description of the 35 rainfall events selected during the three year records, in the period from July 2009 to June 2012.	62
Table 9. Definition of rain rate class intervals.....	66
Table 10. Parameters of the gamma distribution used for modeling the DSD illustrated in Figure 22 and skewness of the distribution. Pearson's r correlation coefficients are indicated.....	71
Table 11. Identification of the precipitation measuring sites and some descriptive statistics for the annual time series.....	83
Table 12. Statistics of the Shapiro-Wilk and Kolmogorov-Smirnov tests for normality, applied to the annual precipitation time series. The results in bold indicate which series have normal distributions for a 5% significance level. The * mark indicates that the result is a lower bound of the true significance. The classification of the time series as 'useful', 'doubtful' and 'suspect' is based on the results of the homogeneity tests, as proposed by Wijngaard et al. (2003).....	87
Table 13. Sen's estimator of the slope ($mm\ decade^{-1}$) of monotonic and partial trends of the annual precipitation, as well as for the trends in the 50-year moving average series. The confidence levels for the trend tests are marked: ⁺ 90%, *95%, **99% and ***99.9%. The	

periods selected for partial trends were based on breakpoints located using the methodology described by Tomé and Miranda (2005). The 50-year moving average series were taken to be centred on the corresponding period. NH identifies series that were not considered homogeneous. 89

Table 14. Sen’s estimator of the monthly precipitation trends (mm decade-1) and the respective confidence levels: +90%, *95%, **99% and ***99.9%. The data are for the full period and for sub-periods of negative trend in annual precipitation, which were selected for each time series based on the breakpoints located in the partial trend analyses. The results for mainland Portugal were partly reported in de Lima et al. (2010b). 95

Table 15. Particle size distribution of the soil used in the experiments..... 109

Table 16. Rainfall measurements taken along the soil flume at positions 1 and 2 (3 repetitions of 11 samples each), as defined in Figure 39. 112

Table 17. Characteristics of runoff hydrographs and sediment transported (see also Figure 42 and Figure 43), for the two sets of experiments. 117

Table 18. Description of the spray nozzles used in the experiments. All nozzles are manufactured by Spraying Systems Co. 129

Table 19. Properties of the wire meshes used in the experiments. 130

Table 20. Summary of experiments using different combinations of nozzles and meshes. ... 131

Table 21. Descriptive statistics of rainfall intensities measured in the control plot, for nozzles combined with steel and plastic meshes. The spray nozzle type used was HH-14W and the vertical distance between the mesh and the nozzle was 600 mm. Data are for the 5 gauges in the control plot (Figure 50c), 3-minute sampling time, and 3 replicates. 139

Table 22. Description of the spray nozzles used in the experiments. All nozzles are manufactured by Spraying Systems Co. The operating pressure was 1.5 bar for all the experiments. 150

Table 23. Description of rainfall characteristics produced by four spray nozzles, for mesh-free simulations and combining a mesh at three vertical positions from the nozzle. Data are averages for the measurements recorded at three positions of the disdrometer (with 3 replicates for each position). 154

1. INTRODUCTION

1.1. Rationale and objectives

During the last decades, the changes in global climate have been a major concern for the scientific community. Such developments will have significant impact on local, regional and global hydrologic regimes, which can affect the ecological, economic and social systems (e.g. IPCC, 2007; Zereini and Hötzl, 2008). Climate monitoring provides the scientific basis for reducing uncertainty, forecasting areas that are under threats of e.g. flash flooding, and supports decision-making in a complex and changing world. The rainfall is a main driver of variability on water resources, which makes it an essential variable to study.

In Portugal, the spatial, seasonal and inter-annual variability of rainfall follows a complex pattern (e.g. Miranda et al., 2002; de Lima et al., 2007; 2010a). While some areas can have long periods of unusually dry conditions that reduce the availability of water resources, other areas can be affected by an increase in extreme rainfall events (e.g. de Lima et al., 2013a; de Lima et al., 2013b) with a consequent increase in flood risk (e.g. Costa et al., 2008). In this context, reliable estimation of rainfall is of primary importance.

The densification of the national precipitation-monitoring networks has given the opportunity to complement studies already carried out in Portugal, in particular, for studying short-term rainfall variability (e.g. Brandão et al., 2001). In addition, recently techniques such as the use of optical disdrometers have allowed gathering more detailed information on rainfall characteristics that can cover an entire rainfall event, and even study the inter-event variability (e.g. Tokay et al., 2003; Cao et al., 2008; Frasson et al., 2011).

As rain consists of a spectrum of drop sizes, a description of rainfall microstructure is needed to better understand the rainfall variability. In this context, different parameterizations have

been proposed to model discrete drop size distributions, such as the exponential distribution (e.g. Marshall and Palmer, 1948) the lognormal distribution (e.g. Levin, 1954), and the gamma distribution (e.g. Ulbrich, 1983). Nevertheless, our understanding of the raindrop size variation is still far from complete, and more analyses of in situ measurements under a wide variety of climatic regimes would be helpful.

The lack of accurate data on raindrop characteristics is not only observed in relation to natural conditions, but also in the laboratory for simulated rainfall. Rainfall simulators are a useful tool in the study of geomorphological processes, and the knowledge of drop size and fall speed is especially important for the determination of rainfall erosion ability (e.g. Ghadiri and Payne, 1977; Hudson, 1995).

Different types of rainfall simulators are currently in use, the two most common are the non-pressurized and the pressurized rainfall simulators. Despite the advantages and disadvantages of each type, they typically display considerable differences compared with natural rainfall, for example, because of the difficulty in getting a large range of drop sizes, and adequate drop velocity at the time of incidence with the soil surface (e.g. Agassi and Bradford, 1999). Several research studies using nozzle spray simulators have been carried out in the Civil Engineering Department of the Faculty of Science and Technology of the University of Coimbra (e.g. de Lima and Torfs, 1993; de Lima and Singh, 2003; de Lima et al., 2003, 2008) always seeking for producing simulated rain of different characteristics, for different application purposes.

The work presented in this thesis will focus on some aspects related to rainfall, from the measurement to the characterization of rainfall variability, both within individual rain events, and historical time series. It will also comprise the characterization of raindrop properties (sizes and fall speeds) whether under natural or simulated conditions. More specifically, the objectives of the thesis are:

- study and compare different instruments for rainfall measurement;

- analyse the variability of raindrop characteristics measured at an outdoor experimental site;
- investigate the long-term variability of annual and monthly rainfall in Portugal;
- carry out laboratory experiments on the effects of the temporal variation of rain intensities on runoff and soil loss;
- study the performance of rainfall simulators focusing on rainfall characteristics and explore potential improvements, particularly, in rainfall kinetic energy.

1.2. Outline

The thesis is structured in eleven chapters. Except for the introductory and the concluding chapters, each of the other seven (from Chapter 3 to 9) contain a section of literature review, materials and methodology, discussion of results, and a conclusion section. One can hence read each chapter separately.

The thesis is divided into two main parts. The first part focuses on the study of natural rainfall including the analysis of the field measurements and the rainfall variability. The second part concentrates on the study of the simulated rainfall and describes the laboratory experiments carried out in order to analyse the simulated rain characteristics.

The overview that follows briefly summarizes each chapter:

1. Chapter 1 is an introductory chapter that describes the rationale and objectives of the research study. It also gives the structure of the document, and the publications involved in the achievement of the present thesis.
2. Chapter 2 is the research review, introducing the reader to several basic concepts that support the work contained in the later chapters. This chapter covers issues on both natural and simulated rainfall.

Part I – Natural rainfall: measurements and variability

3. Chapter 3 presents a comparison of rainfall data provided by different types of rain gauges, including four catching gauges and three non-catching gauges. The data comprises 60 rainy periods recorded at an outdoor experimental site, in Coimbra (Portugal).
4. Chapter 4 describes a volume-based sequential rain sampler that allows the assessment of variations in the chemical composition of rainwater during individual rain events in one place. The performance of the apparatus is analysed for a few tests conducted under field conditions in Coimbra (Portugal).
5. Chapter 5 presents the characterization of rainfall events recorded in Coimbra, Portugal, for a three-year period. Time series of raindrop diameter and fall speeds, with 1-min time resolution, are used. The parameterization of the drop size distribution is explored by fitting the gamma distribution to the empirical data.
6. Chapter 6 presents the analysis of annual and monthly rainfall records from meteorological stations in mainland Portugal and in the Madeira and Azores archipelagos. The study analyses the presence of linear monotonic trends in the annual and monthly rainfall over the record period and over sub- periods (i.e. partial trends).

Part II – Simulated rainfall: laboratory experiments

7. In Chapter 7, rainfall simulator experiments are performed focusing on the importance of when rainfall burst occurs during storm events of equal duration and depth on runoff and soil loss processes.
8. Chapter 8 presents the laboratory tests conducted by combining spray nozzle simulators with meshes in order to change simulated rainfall characteristics. Rainfall intensity, drop size distribution and drop fall speeds are analysed.

9. Chapter 9 presents the changes on the rainfall kinetic energy of spray nozzle simulators caused by the incorporation of a mesh underneath.
10. Chapter 10 summarizes the conclusions, and presents a discussion of future research.
11. Chapter 11 lists the studies consulted in the course of this research, and which are referred to in the thesis.
12. Appendix A describes the rain gauges used for data collection including their technical specifications.
13. Finally, Appendix B lists the measured data series recorded on the outdoor experimental site performed at Coimbra during this Ph.D. program.

1.3. Publications

Some chapters of this thesis, Chapters 4, 6, 7, 8 and 9, contain material that has been submitted to international journals. Some of them have been published, while others are currently under review. They are presented as provided to the journals, with the exception of some layout changes (e.g. numbering of figures and tables). Table 1 shows the references of the articles and the corresponding chapters of the thesis.

Table 1. Publications in international scientific periodicals with referees.

Chapter	Reference
6	de Lima, M.I.P., Carvalho, S.C.P. , de Lima, J.L.M.P. 2010. Investigating annual and monthly trends in the precipitation structure: an overview across Portugal. <i>Natural Hazards and Earth System Sciences</i> 10, 2429–2440.
7	de Lima, J.L.M.P., Carvalho, S.C.P. , de Lima, M.I.P. 2013. Rainfall simulator experiments on the importance of when rainfall burst occurs during storm events on runoff and soil loss. <i>Zeitschrift für Geomorphologie</i> 57(1), 91–109.
4	Carvalho, S.C.P. , de Lima, J.L.M.P., de Lima, M.I.P. 2014. Rainwater sequential sampler: assessing intra-event water composition variability. <i>Journal of Engineering Research and Technology</i> 1(1), 1-7.
8	Carvalho, S.C.P. , de Lima, J.L.M.P., de Lima, M.I.P. 2014. Using meshes to change the characteristics of simulated rainfall produced by spray nozzles. <i>International Soil and Water Conservation Research</i> 2 (2), pp. - (in press)
9	Carvalho, S.C.P. , de Lima, J.L.M.P., de Lima, M.I.P. 2014. Increasing the rainfall kinetic energy of spray nozzles by using meshes. <i>Land Degradation & Development</i> . (In revision: revised manuscript submitted)

In the scientific article corresponding to the Chapter 6 the author of this thesis helped in the analysis of data and in the preparation of figures and tables. In the scientific article corresponding to the Chapter 7 the author was responsible for the execution of the laboratory experiments and the preparation of figures and tables.

This research study also contributed to publications in proceedings (Table 2) and communications in scientific meetings (Table 3).

Table 2. Publications (papers) in proceedings of scientific meetings.

Related Chapter	References
6	de Lima, M.I.P., Carvalho, S.C.P. , de Lima, J.L.M.P., Coelho, M.F.E.S. 2010. Variabilidade e tendências da precipitação anual e mensal em Portugal. <i>10º Congresso da Água</i> , Associação Portuguesa dos Recursos Hídricos (APRH), Alvor, Portugal, 21-24 March, 8 p.
6	Carvalho, S.C.P. , de Lima, M.I.P., de Lima, J.L.M.P. Coelho, M.F.E.S. 2011. Comportamento da precipitação em Portugal Continental: tendências anuais e mensais. <i>VII Congresso Ibérico sobre Gestão e Planeamento da Água</i> , Fundação Nova Cultura da Água (FNCA), Talavera de la Reina, Toledo, Spain, 16-19 February, 9 p.
6	de Lima, M. I. P., Coelho, M.F.E.S., Carvalho, S.C.P. , de Lima, J.L.M.P. 2011. Recent variability in the temporal structure of precipitation in Portugal: an analysis across scales. <i>World Environmental and Water Resources Congress 2011: Bearing Knowledge for Sustainability</i> , American Society of Civil Engineers (ASCE), Palm Springs, California, 22-26 May, 1429-1438.
6	de Lima, M. I. P., Coelho, M.F.E.S., Carvalho, S.C.P. , de Lima, J.L.M.P. 2011. Tendências recentes no regime pluviométrico em Portugal Continental. <i>10º Simpósio de Hidráulica e de Recursos Hídricos dos Países de Língua Portuguesa (SILUSBA)</i> , Porto de Galinhas/PE, Brazil, 26-29 September, 7 p.
7	de Lima, J.L.M.P., Carvalho, S.C.P. , de Lima, M.I.P. 2012. Influência da intra-variabilidade temporal da intensidade de chuvadas no escoamento superficial e transporte sólido: ensaios laboratoriais. <i>11º Congresso da Água</i> , Associação Portuguesa dos Recursos Hídricos (APRH), Oporto, Portugal, 6-8 February, 9 p.

Table 3. Communications (abstracts) in scientific meetings.

Related Chapter	References
Appendix A.1.	de Lima, J.L.M.P., de Lima, M.I.P., Carvalho, S.C.P. , Gerardo, R., Isidoro, J. 2010. Conceção de udómetro “low cost”. <i>10^o Congresso da Água</i> , Associação Portuguesa dos Recursos Hídricos (APRH), Alvor, Portugal, 21-24 March.
6	Carvalho, S.C.P. , de Lima, M.I.P., Coelho, M.F.E.S. 2010. Long and short term precipitation trends in Portugal. <i>10th International Precipitation Conference</i> , Coimbra, Portugal, 23-25 June, Book of Abstracts, 79-79.
Appendix A.1.	de Lima, J.L.M.P., Carvalho, S. , Gerardo, R., de Lima, M.I.P., Isidoro, J.M.G.P. 2010. Development of a low cost rain-gauge at the University of Coimbra. <i>10th International Precipitation Conference</i> , Coimbra, Portugal, 23-25 June, Book of Abstracts, 76-76.
5	Carvalho, S.C.P. , de Lima, M.I.P., de Lima, J.L.M.P. 2010. Fine-scale characterization of rainfall events in Coimbra. <i>10th International Precipitation Conference</i> , Coimbra, Portugal, 23-25 June, Book of Abstracts, 74-75.
6	de Lima, M.I.P., Carvalho, S.C.P. , de Lima, J.L.M.P. 2010. Trends in small-scale precipitation: cause for concern in small drainage basins in Portugal? <i>13th Biennial Conference Euromediterranean Network of Experimental and Representative Basins</i> , Seggau Castle, Austria, 5-8 September, Book of Abstracts, 167-167.
6	Carvalho, S.C.P. , de Lima, M.I.P., de Lima, J.L.M.P. 2010. Observed precipitation trends and variability in Portugal. <i>II Seminário Ibérico - International Geosphere-Biosphere Programme</i> , Lisbon, Portugal, 4-5 November.
6	Carvalho, S.C.P. , de Lima, M.I.P., de Lima, J.L.M.P., 2010. Tendências da precipitação em Portugal Continental - períodos de secas e cheias. <i>Workshop - Gestão do Risco em Secas</i> , Instituto Superior de Agronomia, Lisbon, Portugal, 11 November.
5	Carvalho, S.C.P. , de Lima, M.I.P., de Lima, J.L.M.P. 2011. Caracterização de eventos pluviosos em Coimbra: medições com um distrómetro. <i>VII Congresso Ibérico sobre Gestão e Planeamento da Água</i> , Fundação Nova Cultura da Água (FNCA), Talavera de la Reina, Toledo, Spain, 16-19 February.
Appendix A.1.	de Lima, J.L.M.P., de Lima, M.I.P., Carvalho, S.C.P. , Gerardo, R., Isidoro, J. 2011. Conceção de udómetro “low cost” RUC (Rain-gauge University of Coimbra). <i>VII Congresso Ibérico sobre Gestão e Planeamento da Água</i> , Fundação Nova Cultura da Água (FNCA), Talavera de la Reina, Toledo, Spain, 16-19 February.
5	Carvalho, S.C.P. , de Lima, M.I.P., de Lima, J.L.M.P. 2011. Drop-size distribution of rainfall events in Coimbra, Portugal. <i>European Geosciences Union General Assembly 2011</i> , Vienna, Austria, 3-8 April, Geophysical Research Abstracts, Vol. 13, EGU2011-11117.

Table 3. Communications (abstracts) in scientific meetings (continuation).

Related Chapter	References
5	Carvalho, S.C.P. , de Lima, M.I.P., de Lima, J.L.M.P. 2011. Estudo da distribuição de gotas em eventos pluviosos em Coimbra, Portugal. <i>10º Simpósio de Hidráulica e de Recursos Hídricos dos Países de Língua Portuguesa (SILUSBA)</i> , Porto de Galinhas/PE, Brazil, 26-29 September.
Appendix A.1.	de Lima, J.L.M.P., de Lima, M.I.P., Carvalho, S.C.P. , Gerardo, R., Isidoro, J. 2011. Concepção de udómetro de baixo custo. <i>10º Simpósio de Hidráulica e de Recursos Hídricos dos Países de Língua Portuguesa (SILUSBA)</i> , Porto de Galinhas/PE, Brazil, 26-29 September.
5	Carvalho, S.C.P. , de Lima, M.I.P., de Lima, J.L.M.P. 2012. Exploratory analysis of rainfall events in Coimbra, Portugal: variability of raindrop characteristics. <i>European Geosciences Union General Assembly 2012</i> , 22-27 April, Vienna, Austria, Geophysical Research Abstracts, Vol. 14, EGU2012-6560.
8	Carvalho, S.C.P. , de Lima, J.L.M.P., de Lima, M.I.P. 2013. Combining spray nozzle simulators with meshes: characterization of rainfall intensity and drop properties. <i>European Geosciences Union General Assembly 2013</i> , 7-12 April, Vienna, Austria, Geophysical Research Abstracts, Vol. 15.
4	Carvalho S.C.P. , de Lima, J.L.M.P., de Lima, M.I.P. 2013. Rainwater sequential sampler for water quality assessment during single rain events. <i>11th International Precipitation Conference</i> , 30 June -3 July, Wageningen, The Netherlands.
9	Carvalho S.C.P. , de Lima, J.L.M.P., de Lima, M.I.P. 2014. Kinetic energy of simulated rain resulting from combining nozzles and meshes. <i>15th Biennial Conference of Euromediterranean Network of Experimental and Representative Basins (ERB)</i> , 9-13 September, Coimbra, Portugal.

2. RESEARCH REVIEW

2.1. Introduction

Precipitation can be defined as the liquid or solid products of the condensation of water vapour that falls from clouds or are deposited from air onto the earth's surface. The precipitation processes are hence coupled to atmospheric dynamics and thermodynamics through the latent heat released and absorbed during the phases of changes of water. Liquid precipitation includes rain, drizzle, and mist. Solid precipitation can be graupel, hail, snow, rime, glaze, and sleet. The form how the precipitation is found depends on a variety of factors, such as the atmospheric moisture content, temperature at the earth's surface, vertical motion, among others. All forms of precipitation are commonly expressed in terms of the vertical depth of water that would be accumulated on a flat level surface, if all the precipitation remained where it fell. A description of the precipitation types and their formation can be seen in e.g. Chow et al. (1994), Bourgoignie (2000), Ahrens (2006), and Li and Gao (2012).

As regards causes, precipitation is subdivided into (e.g. Bjerknes, 1919; Eliassen, 1962; Smith, 1979): convective, orographic, and frontal. Convective precipitation results from the rapid ascension of moist air due to the instability of the atmosphere; this type of precipitation is more common during the warmer months of the year as localized intense heating of surface is required to initiate the convection cycle. Orographic precipitation occurs when air is forced to rise over a particular topographic barrier; the ascending air expands, promoting cooling, condensation and precipitation. Frontal precipitation results from the contact between two air masses at different temperatures; the warmer less dense air mass is pushed up over the colder dense one.

The complex relationship between precipitation processes and dynamics of the atmosphere is hence a source of continuous concern for scientists. Many studies have been focusing on

finding accurate means to measure precipitation, understanding impacts on precipitation patterns by e.g. climate change, aerosols or land use, and improving prediction models, in order to avoid weather hazards that can cause economic losses and affect livelihood around the world (e.g. Georgakakos and Kavvas, 1987; Pielke et al., 2007; Strangeways, 2007; Michaelides, 2008; Trenberth, 2011).

This chapter reviews briefly some research studies on rainfall that are relevant to the later chapters. Four subsections are presented: rainfall measurements (section 2.2); rainfall space and time variability (section 2.3); variability of raindrop characteristics (section 2.4); and reproducing rain events in laboratory (section 2.5).

2.2. Rainfall measurements

The measurement of rainfall is a critical need to many applications in meteorology, hydrology, agriculture, and climate research, providing input data to e.g. flood zone planning and prediction models, hydrologic and climatological models, and management of water resources. Precipitation monitoring networks have been established comprising different types of rain gauges to guarantee the accuracy of data, and also radar and satellite sensors, which offer a very high spatial resolution (Figure 1).

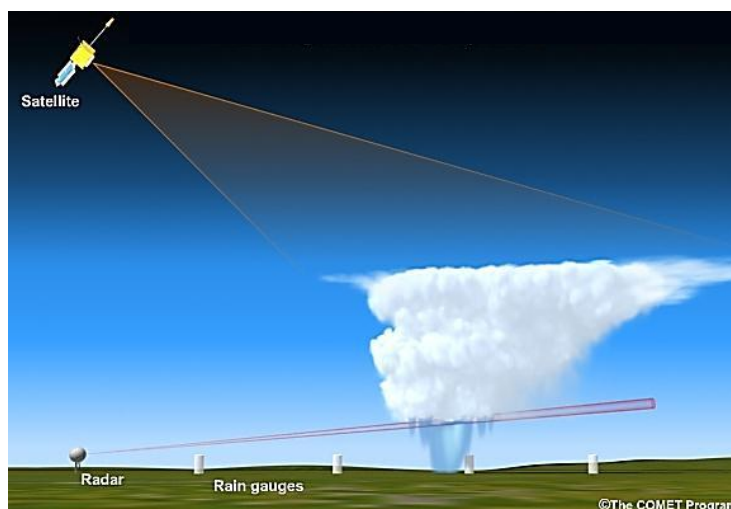


Figure 1. Precipitation measurement by satellite, radar and rain gauges (UCAR, 2009).

The purpose of rain-gauge networks is to provide accurate point measurement of rain rates and rain accumulations at the ground surface. The description of the typical instruments and discussion of aspects of rainfall measurement can be found in e.g. WMO (1994), Michaelides et al. (2009), and Vuerich et al. (2009). These instruments can be classified in: non-recording and recording gauges. The non-recording gauges operate by a collector positioned above a funnel that leads into a container; the most widely used is, probably, the Hellmann gauge (see Appendix A.2.). For recording gauges the most common types are the tipping bucket (see Appendix A.3.) and the weighing gauge (see Appendix A.4.). The tipping bucket consists on capturing a volume of rainwater in one of two small buckets, and once the bucket is full, it overbalances and tips down, registering the time of the tip. The weighing gauge consists on capturing rainwater in a collection system and recording its weight.

Unfortunately, the instruments do not always provide accurate measurements of rainfall. The measurements can be affected by systematic errors caused by the measuring device or human errors that include the observation errors. For example, in Strangeways (2007) and WMO (2008) this issue is discussed with possible preventative measures. The systematic errors vary by e.g. the type of precipitation (rain, drizzle, snow) and gauge design. The choice of the site and the consequent exposure to the effects of e.g. wind, the prevention of loss by evaporation, and splashing effects, are important considerations to be taken into account. Moreover, the number and distribution of the gauges required for a specific area will depend on the rainfall natural variability and the purpose of the data collection.

Radar has been gradually developed as a tool for quantitative rainfall measurement. The advantages of this technology over the traditionally rain-gauge networks include covering large areas and providing high spatial and temporal resolutions (see e.g. Collier, 1989; Krajewski and Smith, 2002). A fundamental problem of radar remote sensing of rainfall is to guarantee accurate conversion of the radar reflectivities measured aloft to rainfall intensities at the ground. In this context, variations in raindrop sizes distributions can have a great impact on the derived algorithms used in rainfall rate estimations associated with radar (e.g. Uijlenhoet, 1999).

In order to measure the raindrop characteristic at the ground level, the disdrometers are the most widely used instruments. Different types of disdrometers are available such as: the impact-type Joss-Waldvogel disdrometer (e.g. Kinnell, 1976), which transform the vertical momentum of an impacting drop into electric pulses whose amplitude is a function of the drop diameter; the 2-dimensional video distrometer (abbreviated to 2DVD) (e.g. Kruger and Krajewski, 2002), which measures the size, shape, orientation and fall velocity of each drop falling through the sensor area by imaging techniques using fast line scan cameras; and the optical disdrometers (e.g. Löffler-Mang and Joss, 2000, see also Appendix A.6), which are able to measure the size and fall speed of raindrops that pass through a laser beam (Figure 2).

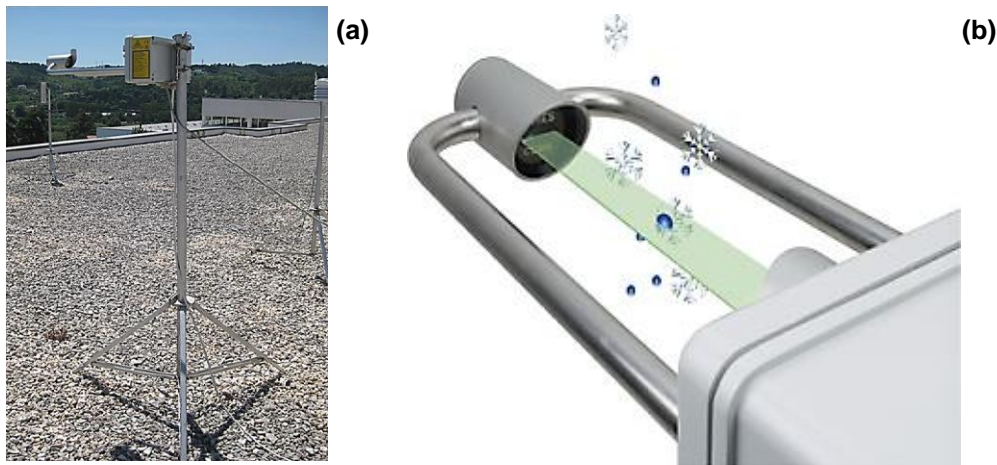


Figure 2. (a) View of the laser disdrometer manufactured by Thies Clima installed in the Department of Civil Engineering of the University of Coimbra; (b) Detail of the disdrometer measuring precipitation particles that pass through the laser beam (Thies, 2007).

The disdrometer measurements can also be affected by different sort of errors, caused for example by undersampling (e.g. Gertzman and Atlas, 1977) and by environmental conditions, such as wind effect (e.g. Nešpor et al., 2000). Some instrument limitations are also related with the resolution and sensitivity as it cannot distinguish drop sizes within a given size interval; there are also some errors related to the light sheet which can make some drops to appear to be smaller than other drops of the same sizes; and the drop splashing on the housing of the instrument, which can lead to the drop fragmentation and produce un-realistically low fall speeds (e.g. Krajewski et al., 2006; Yuter et al., 2006; Niu et al., 2010).

The instruments for measuring rainfall thus differ in the design and measuring principle applied. Instruments, such as tipping bucket gauges, are commonly used in national monitoring networks for already some time, while equipment based on optical techniques have more recently been widely spread; since each one has its own limitations and strengths it is required their comparison to assess the accuracy and suitability to a specific purpose. Several types of equipments have been used in this thesis (see Chapter 3 and Appendix A).

2.3. Rainfall space and time variability

The variety of methods that have been developed for measuring rainfall allows the estimation of its spatial and temporal distribution. The study of changes in space-time rainfall variability is receiving world-wide attention due to global warming and the corresponding urban drainage impacts; floods resulting from extreme rainfall can have significant economic and social implications. There is indeed the need to anticipate and reduce the uncertainty associated with different precipitation (e.g. rainfall) scenarios.

Some relevant researches on the detection of long-term precipitation trends can be seen in e.g. Lettenmaier et al. (1994), Türkeş (1996), Zhang et al. (2000) and Partal and Kahya (2006). Most of these studies that identified hydroclimatologic trends and climatic variations have used the Mann–Kendall test (Mann, 1945; Kendall, 1970). This procedure can be useful as missing values are allowed and the data do not need to follow any particular distribution (e.g. Gilbert, 1987). More detail on this method will be given in Chapter 6. The precipitation trends can be detected in historical records providing that such records are representative and cover a long period of time; in fact, the short length of existing precipitation records are often an limiting factor. In a study on annual and monthly precipitation in mainland Portugal, based on long time series (between 88 and 145 years), de Lima et al. (2010b) highlighted that the majority of the studies focus on the second half of the 20th century or even on smaller periods, and only a few studies report results for longer periods.

For the southern Europe, some studies have predicted drier climate based on climate models and past observed records, as a result of increased evapotranspiration and a relatively slow decrease of rainfall amounts and rain events frequency (e.g. Cubasch et al., 1996; Kostopoulou and Jones, 2005; Vicente-Serrano and Cuadrat-Prats, 2007). As for the southern Europe, in Portugal mainland the annual rainfall amounts are also projected to decrease, within the range of 20 to 40% of its current values, especially in southern regions (Miranda et al., 2006). Moreover, previous studies have reported high variability in the rainfall regime, see e.g. Corte-Real et al. (1998), de Lima et al. (2007), and Durão et al. (2009); the total annual rainfall varies highly with geographical location (Figure 3), and it also exhibits strong seasonal variability (Figure 4).

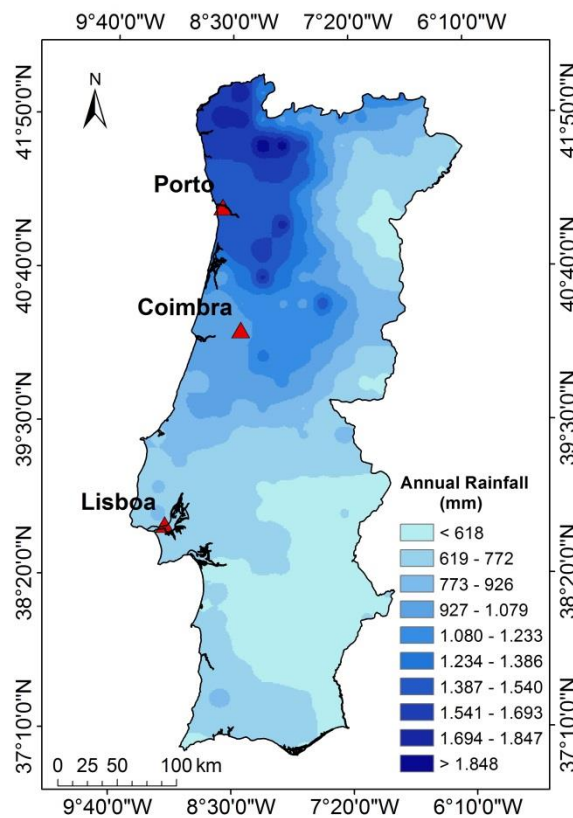


Figure 3. Representation of mean annual rainfall (1971-2000) in mainland Portugal. The map was created using the Inverse-Distance-Weighted interpolation method.

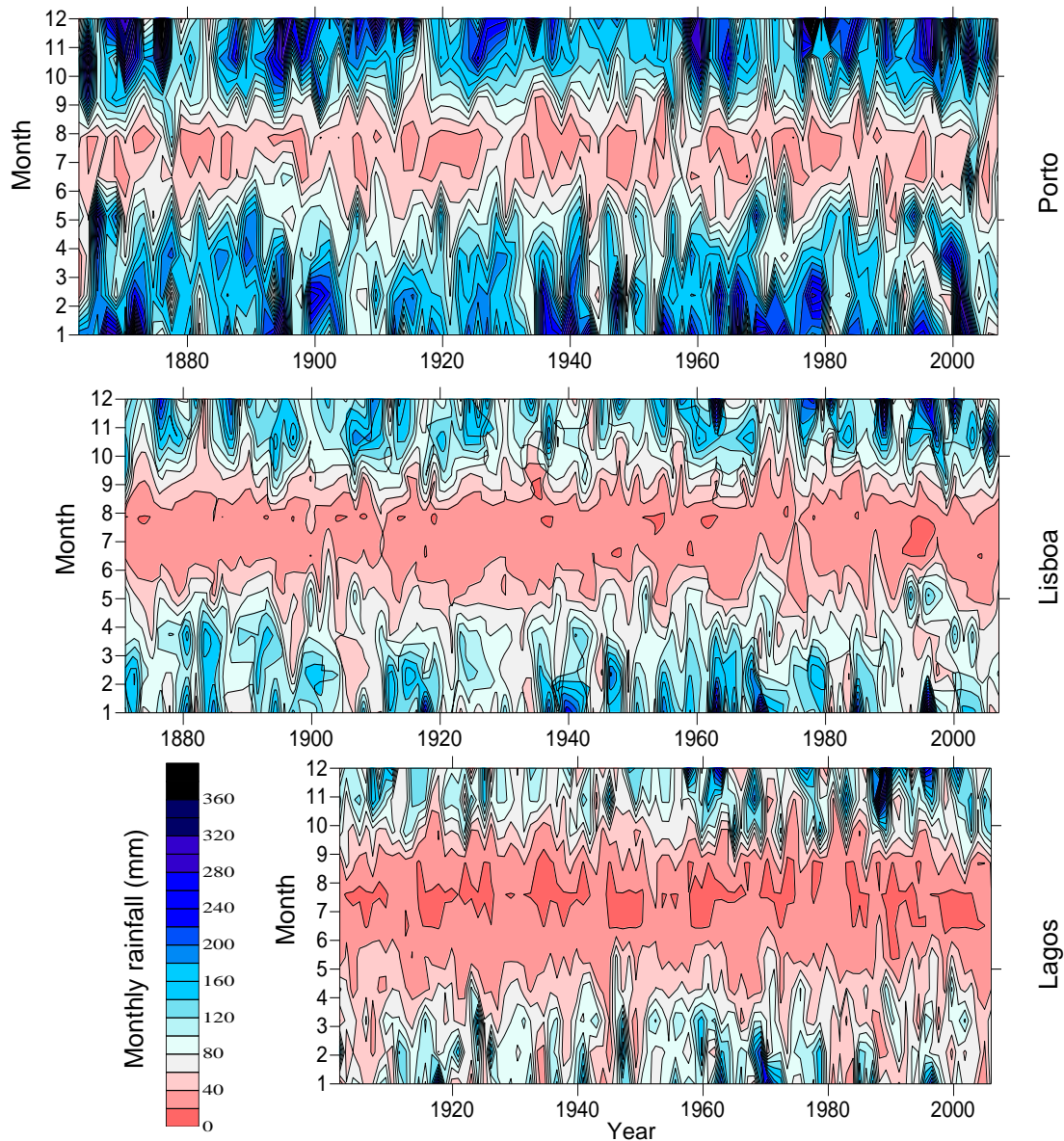


Figure 4. Monthly rainfall for three measuring stations in mainland Portugal (the characteristics of the data series can be seen in the Table 11, Chapter 6).

The characterization of rainfall in the Portuguese North Atlantic Archipelagos of Madeira and Azores has been less studied than that in mainland Portugal. For Madeira the global models show a strong reduction in winter rainfall, in particular in the high grounds, as well as, reductions of spring and autumn rainfall, which are only partially compensated by an increase in the summer; in terms of the annual average, the reduction can be from 20 to 30% by the end of the 21st century (Miranda et al., 2006).

For Azores, it is expected small changes in the annual rainfall; however, some changes may occur in the annual cycle, with the strong winter rainfall being compensated by decreasing rainfall in the other seasons (Miranda et al., 2006).

Besides the long-term trends discussed, short-term variability at different geographical scales should also be considered. Changes can occur for example in the intensity of individual storms or in its length and frequency.

2.4. Variability of raindrop characteristics

Besides concentrating on rainfall average properties over large volumes and time intervals, rainfall should also be considered as a discrete process, consisting of numerous individual raindrops that differ in size and fall speed, landing in different positions (Figure 5). Although, on average, the raindrops are distributed homogeneously in space, for a particular volume their concentration will fluctuate in space and time. In 1 m^3 of air, the number of raindrops is typically of the order of 10^3 (Uijlenhoet, 1999).

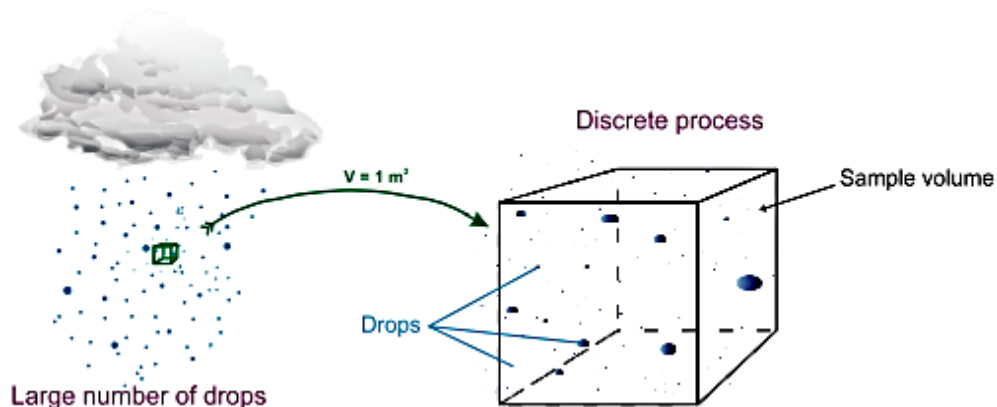


Figure 5. Scheme of space distribution of raindrops in a volume of air (Jaffrain, 2012).

In relation to the drop diameters, they range typically from 0.1 to 6 mm (Uijlenhoet, 1999). The smallest drop size, 0.1 mm, is hence the threshold size which separates the cloud droplets that are kept suspended in the air indefinitely, from the falling raindrops. In relation to the

maximum diameter, in fact, the majority of the raindrops found in nature are smaller than 3 mm (Rogers and Yau, 1989).

As a raindrop is accelerated downward by the effect of gravity, its motion is retarded by the increase of the frictional resistance of the air. The drop velocities range typically from 0.1 m s^{-1} for the smallest raindrops to over 9 m s^{-1} for the largest raindrop (Uijlenhoet, 1999). While for drops smaller than 1 mm, the terminal fall speed increases approximately linearly with increasing drop size, for bigger drops the terminal fall speed increases at a lower rate, and become constant at diameters of around 6 mm (Houze Jr., 1994).

The microstructure of rainfall can then be represented by means of the statistical distribution of the number, size and fall speed of the raindrops within a reference volume or time interval. The number of raindrops that one happens to measure as a function of the diameter, present in a unit volume of air, is the so-called drop size distribution (DSD). In Chapter 5, the calculation of DSD will be described in more detail.

The microphysical processes involved in the development of DSD are known to be complex; the variability of DSD is related with the mechanisms such as condensation/evaporation, coalescence/collision, and breakup (e.g. Pruppacher and Klett, 2010). This variability is not well understood and so as recommended by McFarquhar (2010) efforts should still be done to acquire a large amount of data for investigation of DSD from e.g. heavy rain rates in a variety of locations.

Despite the DSD variability, some theoretical continuous distributions have been fitted to the measured DSD. In order to guarantee sufficient accuracy, DSD parameterization requires large DSD samples (Smith and Kliche, 2005). Different parameterizations of the DSD have been proposed in the literature. One of the pioneering studies was carried on by Marshall and Palmer (1948), who proposed an exponential distribution for DSD. As the exponential parameterizations have been claimed to tend to overestimate the numbers of small drops, distributions using an extra (third) parameter have been suggested, namely the lognormal distribution (e.g. Levin, 1954), and the gamma distribution (e.g. Ulbrich, 1983).

Depending on e.g. geographic location, climatic regime, season, and other factors, the shape and then the parameters deduced from DSD will differ (e.g. Sauvageot and Lacaux, 1995; Rosenfeld and Ulbrich, 2003; Nzeukou et al., 2004; Rao et al., 2009). For example, Kozu et al. (2006) revealed seasonal and diurnal variations of DSD in Asian Monsoon Region; the authors found that e.g. the morning DSDs were narrower than the afternoon ones, implying that the local convection cycle over land, which often causes peak afternoon rainfalls, produces broader DSDs.

The information on the size of drops complemented with their velocities can be used to compute the rainfall kinetic energy. Nevertheless, this approach is not frequently used since direct measurements of these drop characteristics (with e.g. disdrometers) have been uncommon up to the last decade. Instead, the kinetic energy of a given rainfall event has been estimated from kinetic energy-rain rate relationships that have been proposed in the literature (e.g. Wischmeier and Smith, 1958; Carter et al., 1974; Kinnell, 1981; Rosewell, 1986). These relationships are mainly obtained from kinetic energies computed from DSD measurements, which are specific to climate conditions and intensity ranges. Therefore, the use of these relationships in different conditions should be validated before its implementation. Insights on the estimation of kinetic energy based on different DSDs are given in e.g. Smith and De Veaux (1992), Uijlenhoet and Stricker (1999), Salles et al. (2002), Brodie and Rosewell, (2007); power laws relationships between kinetic energy and rain rates were presented in these studies, and it will be also estimated in Chapter 5.

2.5. Reproducing rain events in laboratory

Rainfall simulation has been an important tool in disciplines, such as, hydrology, agronomy, and geomorphology, used for different purposes, e.g. the assessment of overland flow generation, infiltration rates, splash, or process-based experiments on soil surface sealing and crusting dynamics (e.g. Mutchler and Hermsmeier, 1965; de Ploey 1981; de Lima and Singh, 2002; Cerdà and Doerr, 2007; Seeger, 2007; de Lima et al., 2008; 2011).

Because of the unpredictable and infrequent nature of rain, it would be very difficult to study e.g. the effects of soil erosion by water in the field. Rainfall simulators can be used in order to overcome these natural limitations, allowing the repetition of experiments under controlled conditions. With minimum time-consuming, experiments can be performed with the chosen rainfall characteristics (Figure 6a shows the laboratory experiments performed with a rainfall simulator, which are described in Chapter 8).

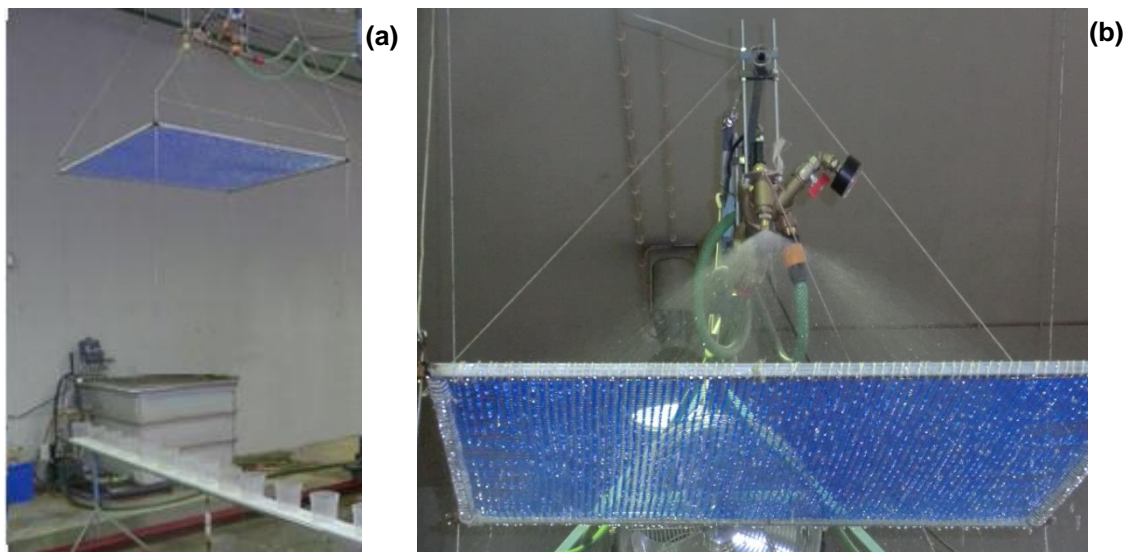


Figure 6. Views of laboratory experiments making use of a nozzle rainfall simulator at the Civil Engineering Department of the Faculty of Science and Technology of the University of Coimbra.

In relation to the drawbacks of using rainfall simulators, Dunkerley (2008a) presents a literature review that claimed a lack of correspondence between natural and simulated rain events in relation to e.g. rain rates, range of drop sizes, kinetic energy, and drop arrival rate. He also highlighted other rain event properties that require attention, such as the intra-event variation in rain rate. Experiments involving the change of the rainfall intensities instantaneously during a simulated storm have been conducted by some authors (e.g. Flanagan et al., 1988; Zhang et al., 1997; Parsons and Stone, 2006), but are not as common as constant intensity experiments, mainly because of difficulties in implementing a sequence of intensities; in Chapter 7, the possibility of using a single nozzle rainfall simulator to simulate rain events of varying intensity will be explored.

Since the 1930's more than 100 rainfall simulators with plot dimensions $<5 \text{ m}^2$ were developed differing in design (from drop-formers to nozzle-type simulators), rainfall intensities and rain characteristics (Iserloh et al., 2013). Rain simulators can be classified according to the way they produce drops. The two major types are: non-pressurized rainfall simulators or drop-former simulators that use hypodermic needles or capillary tubes (e.g. Munn and Huntington, 1976; Kamphorst, 1987); and pressurized rainfall simulators, such as spray nozzles (e.g. Meyer and McCune, 1958; Esteves et al., 2000) (Figure 6b shows a spray nozzle which was used in the laboratory experiments with a mesh suspended underneath, see Chapters 8 and 9).

In the non-pressurized rainfall simulators, the drops fall when their weight overcomes surface tension forces; therefore, the main disadvantage of this type of simulator is that the fall height can be insufficient for drops to reach their terminal velocities. The other widely known disadvantage is that they usually produce a narrow range of drop sizes (e.g. Tossell et al., 1987).

For the pressurized rainfall simulators, theoretically, as the water is released under pressure, drops reach higher fall speeds compared to simulated rainfall from non-pressurized simulators. Due to the high pressure of the supplied water, a broader range of drop sizes is also expected for the pressurized rainfall simulators (e.g. Battany and Grismer, 2000).

Despite the concern and advancements towards rainfall simulation standardization, there is still limited research on the assessment and comparison of simulators' performance in relation to raindrop characteristics, in particular the kinetic energy.

The characterization of simulated drops is crucial to assess, for example, the effect of drop impact on physical properties of the soil surface by evaluating the kinetic energy with which drops impact the soil surface (e.g. Bisal, 1960; Ziegler et al., 1997). Moreover, Thompson and James (1985) showed a decrease in soil infiltration, and increase in hydraulic resistance of the soil surface with increasing drop kinetic energy.

**PART I – NATURAL RAINFALL:
MEASUREMENTS AND VARIABILITY**

3. COMPARISON OF MEASUREMENTS FROM AN OUTDOOR EXPERIMENTAL SITE WITH SEVERAL TYPES OF RAIN GAUGES

Abstract

Instruments for measuring precipitation differ in the design and measuring principle applied; since each one has its own limitations and strengths it is required their comparison to assess the accuracy and suitability to a specific purpose. Rainfall measurements were performed on an outdoor's experimental site, comprising 60 rainy periods corresponding to a total of around 580 mm. The main aim of this study was to compare the measurements from seven different types of rain gauges: catching gauges, namely Hellmann, tipping-bucket and weighing gauges; and non-catching gauges, that included optical and impact sensors. Descriptive analyses were performed to evaluate and compare the rainfall depths provided by each gauge and the reference values. Analyses also included the assessment of rain rate measurements based on 1-min rain rate time series yielded by the continuous-recording gauges. As the rainfall measurements can be affected by different sources of errors, related for example to the wind, time series of wind speed were registered and compared with the variability of rain measurements. The results show high dispersion of the measurements around the reference rain depths, in particular for non-catching rain gauges. Nevertheless, the median of the relative error is within $\pm 5\%$ for the majority of the gauges.

3.1. Introduction

The availability of accurate rainfall data is required for hydrological studies, whether related to water balances, flood forecasting or optimization and verification of climate models. Nevertheless, measuring the rainfall accurately can be challenging, due to its natural variability in both space and time. Several techniques have been used to measure rainfall, namely: in-situ local measurements using e.g. tipping bucket rain gauges or optical disdrometers (e.g. Löffler-Mang and Joss, 2000; WMO, 2008); ground-based remote sensing measurements, by means of e.g. radars (e.g. Krajewski and Smith, 2002); and satellite-based remote sensing techniques (e.g. Barret and Martin, 1981).

The accuracy of the rainfall measurements obtained from the different instruments, as well as their comparative performance, is widely discussed in the literature (e.g. Huffman et al., 1995; Ciach and Krajewski, 1999; Ciach, 2003; Morin et al., 2003; Yilmaz et al., 2005; Keefer et al., 2008; Savina et al., 2012). For example, an important advantage of satellite-based measurements is to cover large areas, but the calibration and validation of satellite sensors raise questions on data reliability (e.g. Rudolf et al., 1996). Regardless of the recent advances in remote sensing of rainfall, the in-situ local measurements are still the basic input for many studies with application to e.g. agriculture, water resources management and calibration of satellite-based rainfall estimation (e.g. Habib et al., 2010).

Rain gauges are widely used for measuring rain rates and accumulations near the surface. Several types of rain gauges have been developed, which have different measuring principles (e.g. quantification of volume, weight or by laser beam attenuation) or design details (e.g. collecting area). These instruments can be classified in (e.g. Lanza et al., 2010): catching gauges (e.g. weighing and tipping buckets rain gauges) or non-catching gauges (e.g. optical and impact disdrometers).

The rainfall data obtained by rain gauges can be affected by various types of measuring errors, including (e.g. Lanza and Vuerich, 2012): catching errors, which means that the instrument does not detect the full amount of water falling through the atmosphere due to, for

example, splashing and evaporation processes, or weather conditions (e.g. wind); and counting errors, which are related to the correct quantification of the amount of water that is collected/detected by the instrument.

In order to assess the temporal variability of rainfall intensity, the instruments should acquire high resolution data. For example, the tipping bucket gauge detects every increment of rainfall (which can be e.g. 0.1 mm for the instrument TE525MM-L manufactured by Campbell Scientific), and it typically records the time of the tip, or the number of tips that have been detected within a selected time period (e.g. one minute); the disdrometer, on the other hand, estimates instantaneous rain rates based on the size and amount of drops over the sensing area per unit time (e.g. 30 seconds) (e.g. Tokay et al., 2003; Michaelides et al., 2009).

The aim of this chapter is the comparison of rainfall data provided by different rain gauges. Instruments, such as tipping bucket gauges, are commonly used in national monitoring networks for already some time while equipment based, for example, on optical techniques have more recently been widely spread. The analysis comprises 60 rainy periods recorded by seven different types of gauges on an outdoor experimental site. The preparation of the network of instruments was undertaken by the author within the ambit of the Ph.D. program.

3.2. Material and methods

3.2.1. Measuring site and rain gauges

Different types of rain gauges were used to monitor rainfall on the same site, in Coimbra (in the centre region of mainland Portugal). Geographic coordinates of the measuring site are 40°11'8" N and 8°24'52" W. The climate of this area is Csb (Mediterranean climate) in the Köppen's classification, which corresponds to humid mesothermal climate with dry or temperate summer.

The analysis reported in this study concerns the comparison of the instruments' measurements recorded for similar field conditions. The instruments consist of catching type gauges, namely two Hellmann gauges, a tipping bucket gauge and a weighing gauge; and non-catching rain gauges that included optical and impact sensors (see Table 4). A non-conventional rain gauge developed in the University of Coimbra was also included in this comparison. The RUC (Rain-gauge University of Coimbra) measures the rainfall accumulated over a given period of time and it is comparable to other standard rain gauges (e.g. Hellmannn rain gauge). The appendix A includes a description of all the instruments used.

Table 4. List of the seven rain measuring devices studied.

Gauge ID	Manufacturer/ model	Gauge type	Reporting method
SRG.1	<i>University of Coimbra / RUC</i>	Non-conventional rain collector	Hand-emptied
SRG.2	<i>VWR / Hellmann rain gauge</i>	Standard rain gauge	Hand-emptied
SRG.3	<i>Wilh.Lambrecht / Hellmann rain gauge</i>	Standard rain gauge	Hand-emptied
TBG.4	<i>Casella Cell / 100000E</i>	Tipping bucket rain gauge	Datalogger
WPG.5	<i>MPS / TRwS 204</i>	Weighing precipitation gauge	Real-time PC monitoring
MWS.6	<i>Vaisala / Weather Transmitter WXT510</i>	Multi-parameter weather sensor	Real-time PC monitoring
DIS.7	<i>Thies Clima / Laser Precipitation Monitor</i>	Disdrometer	Real-time PC monitoring

Because the accuracy of rainfall measurements are significantly influenced by field conditions, the instruments were all collocated at the top of the building of the Department of Civil Engineering of the University of Coimbra (Portugal) to ensure similar exposure conditions (see Figure 7). The rooftop of the University's building was chosen as a way to prevent the instruments from being vandalized. The instruments were positioned at 1.5 m above a flat surface, which is the typical height used in the national udometric networks. It was ensured that the surrounding wall was not closer to the instruments than a distance of 2.5 times the height by which it extends above the instrument (e.g. WMO, 2008).

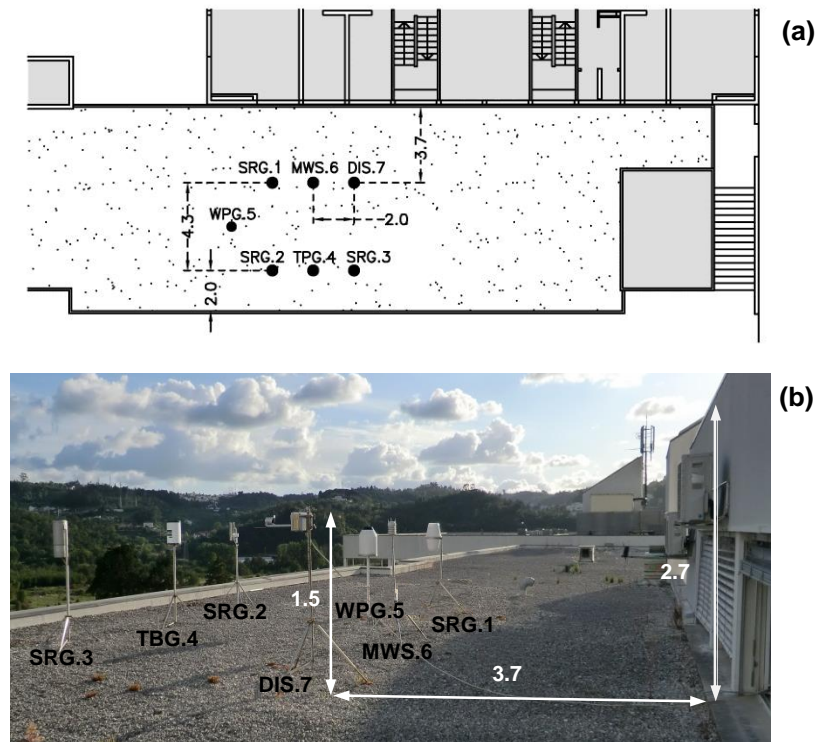


Figure 7. (a) Position of the rain gauges at the top of the building; (b) View of the instruments. Measurements are in meters. See Table 4.

3.2.2. Rainfall data

The rainfall was collected for more than three years (see appendix B, Figure B.1); however, as some of the instruments were set up later, the time period considered in this chapter was only two years, from 26 March, 2011 to 25 March, 2013. Please note that the Chapter 5, which focuses on the disdrometer measurements (with 1-min time resolution), comprises a selection of rainfall events from a three year period starting in July 2009.

An operator (the author) was required to record daily the measurements of the non-recording rain gauges, as well as, checking the data of the continuously recording rain gauges. The term “rainy period” will be used to describe the time intervals for which the accumulated rainfall was recorded (see appendix B, Table B.1).

The dataset selected comprises 60 rainy periods, and corresponds to a total of around 580 mm (mean of 7 gauges); the total rainfall depth of events ranged from 0.4 to 25 mm (mean of 7 gauges), see Figure 8a. Different rainfall conditions were observed during the studied period, which include extreme rain storms reaching rain rates of around 100 mm h^{-1} . Moreover, the selected rainy periods were observed in different seasons, although they are scarce in summer.

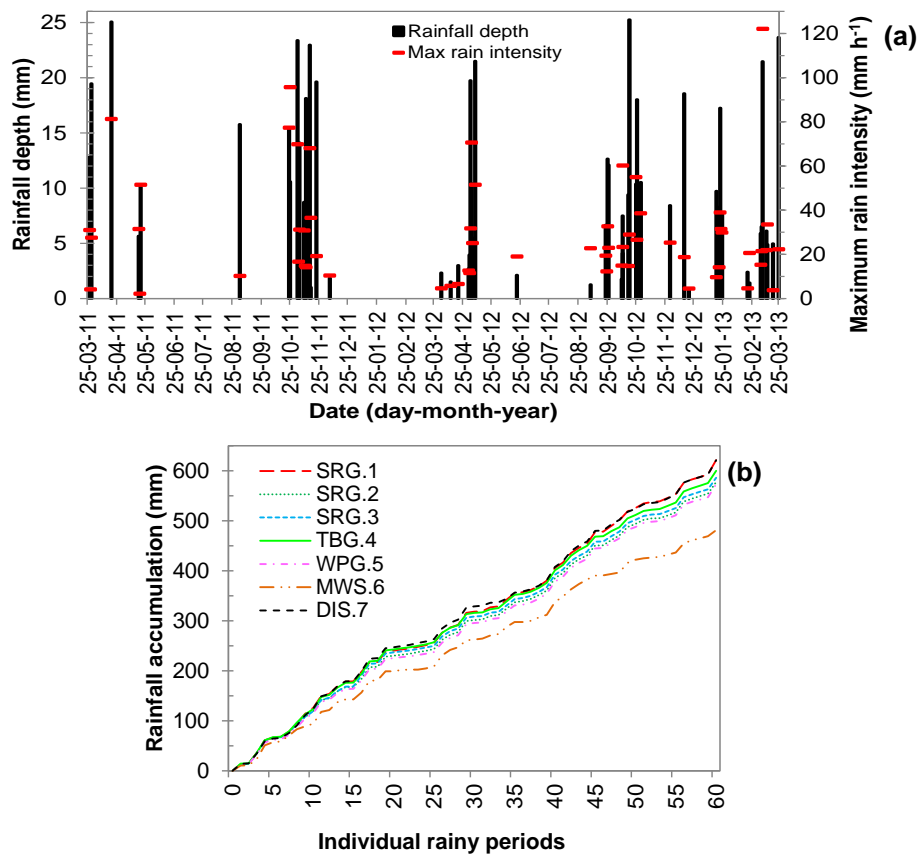


Figure 8. Hyetograph of 60 rainy periods selected from the period between March, 2011 and March, 2013: (a) Rainfall depths (mean of 7 gauges) and maximum rain intensity detected with the disdrometer (DIS.7); (b) Accumulated rainfall from the 60 rainy periods, for each gauge.

3.3. Methodology

3.3.1. Analysis of rainfall accumulation for 60 rainy periods

Preliminary analyses of the rainfall time series included checking the data periods, when all the gauges were collecting data simultaneously, in particular, some of the gaps resulted from repairs and maintenance services on some instruments, and identifying clearly incorrect values. Inaccurate records were excluded.

The rainfall measurements provided by rain gauges can be affected by different sources of errors, related to e.g. the wind, evaporation, and wetting loss on the internal walls of the collector. The “true” rainfall value can be estimated by correcting the systematic errors using empirical relationships based on e.g. gauge design, wind speed and type of precipitation (Sevruk and Hamon, 1984); yet the correction procedures itself can lead to new uncertainties. The comparison of measurements from different type of rain gauges will be performed, and related with the variability of e.g. wind speed.

The assessment of the performance of gauges requires the identification of the “true” rain events’ depth, which is unknown. However, since different gauges were used in this study, it is possible to estimate the uncertainty of one instrument’s measurements by the “deviations” from the mean obtained from all or a set of instruments. In this study, as the rain-accumulation time series provided by the MWS.6 equipment showed several anomalous values, and a much lower total rainfall amount (481 mm), see Figure 8b, its records were excluded from the calculation of the reference rainfall depths.

For a given rainy period T recorded with a rain device A , the relative error of the rain gauge measurements is expressed by:

$$RE_{1,T} = \frac{x_{1,T} - x_{6,T}}{x_{6,T}} \quad (3.1)$$

where $x_{1,T}$ is the rain accumulation measured by a single device for a given rainy period, and $x_{6,T}$ is the mean of the rainfall accumulation from the 6 gauges, taken here as the “true” value.

Regression lines were established for rainfall data from each gauge and the references values. The root mean square error (RMSE) was determined to measure the difference between observed data and the data predicted by the fitted line.

$$\text{RMSE} = \sqrt{\frac{1}{n} \sum_{i=1}^n (x_i - \hat{x}_i)^2} \quad (3.2)$$

where x_i is the observed rainfall depth, \hat{x}_i is the predicted rainfall depth (by the regression line), and n is the number of rainy periods.

3.3.2. Analysis of 1-min rain rate measurements

The comparative study of the different types of rain gauges also includes the analysis of 1-min rain rate measurements yielded by the continuous-recording gauges (WPG.5, MWS.6 and DIS.7), and the data from the tipping bucket gauge (TBG.4), which recorded the exact time of the tip. The measurements from the SRG.1, SRG.2 and SRG.3 were not included as the dataset corresponds to rainfall accumulated during longer time periods (appendix B, Table B.1).

The coefficient of variation for 1-min rain rate measurements (from 4 gauges) were related to the wind speed. The time series of the wind speed were obtained with the MWS.6, i.e. the *Weather Transmitter WXT510* manufactured by Vaisala.

3.4. Results and discussion

3.4.1. Analysis of rainfall accumulation for 60 rainy periods

The performance of the investigated instruments was first determined by the relative error of rain gauge measurements of 60 rainy periods assuming the reference value as the mean of the

rain accumulations from 6 instruments. Figure 9 illustrates the percentage relative errors obtained for each gauge by box-and-whisker plots; the plots indicate the values obtained for the mean (circles), median (thin line), 25–75th percentiles (box limits), 10–90th percentiles (whisker caps) and outliers (rings), which are values that lie more than one and a half times the length of the box from either end of the box.

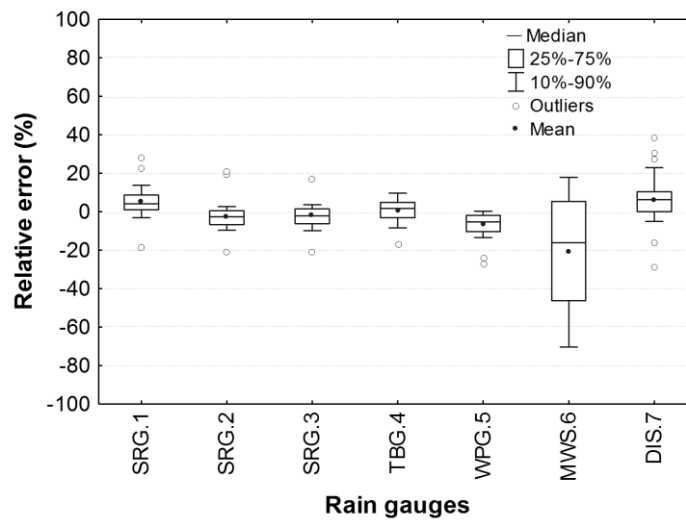


Figure 9. Box-and-whisker plots representing the relative error of rainfall measurements provided by the 7 studied instruments; 60 rainy periods were investigated.

For the majority of the gauges, with the exception of MWS.6 and DIS.7, the median of the relative error was close to $0 \pm 5\%$, and the inter-quartile range was around 8%. In fact, for these rain gauges (SRG.1-3, TBG.4 and WPG.5) approximately half of the observed rain-depth amounts are within the WMO limits of rainfall measurement accuracy, i.e. 5%. The inaccuracy of rain measurements by non-catching rain gauges (MWS.6 and DIS.7) has been already reported in the literature by Lanza and Vuerich (2012) after analysing 1-minute rain intensity measurements.

The assessment of the performance of the non-conventional rain collector and the two standard rain gauges (SRG.1-3) showed that the rainfall measurements are not strictly equivalent as the design of the non-conventional rain collector (SRG.1) differs from the model Hellmann rain gauges (SRG.2 and SRG.3). The non-conventional rain gauge collected

more rainfall amount than the Hellmann gauges; yet the median of the relative error is within the $\pm 5\%$. The collector of SRG.1 does not have a sharp rim (see appendix A.1.), which might increase the error by splashing processes. Although the Hellmann gauges studied (SRG.2 and SRG.3) have different collecting areas (100 cm^2 and 200 cm^2), the results were similar, e.g. the median of the relative error was around -2.3% , and the inter-quartile range was close to 7.4% .

In relation to the recording rain gauges, TBG.4 was the instrument whose mean of the relative error was closer to zero, i.e. 0.7% and a standard deviation of 7.9% ; on the opposite, MWS.6 is the instrument that less agree with the reference time series, with a mean of -20.9% and standard deviation of 35.5% . The MWS.6 tended to underestimate rainfall depths, which might be explained by the difficulty to detect small drops by impact sensors. The optical disdrometer, DIS.7, also showed a high spread of relative errors (standard deviation of 16%), but mainly caused by an overestimation of measurements (mean of 5.8%).

In Figure 10a the rainfall depths provided by each gauge, P_i , were plotted against the reference values (mean of 6 gauges), P_{ref} . The best fit equations were found (Figure 10b):

$$P_i = c_i + m_i P_{ref} \quad (3.3)$$

where m_i and c_i are the coefficients of the regression line, see Table 5.

As observed in Figure 10b, the MWS.6 tended to underestimate the rainfall depths (the majority of the data points are below the 1:1 line). In relation to the other gauges, the measurements were in general close to the 1:1 line. The deviation of the regression lines from the 1:1 line can be related to systematic errors inherent to the devices.

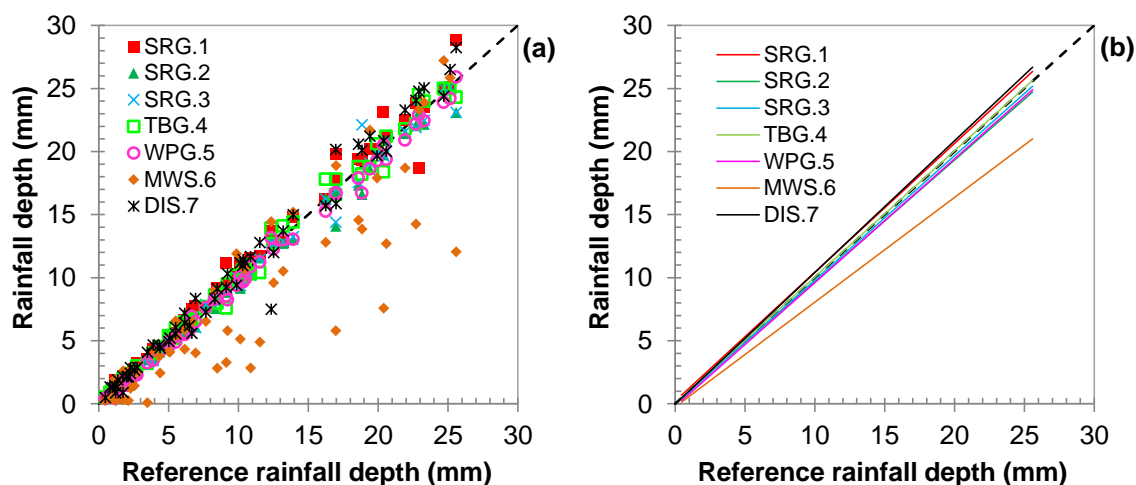


Figure 10. (a) Scatter plot of rainfall depths measured by each gauge against the reference values (b) and corresponding fitted trend lines.

Table 5. Coefficients of the regression lines illustrated in Figure 10b, and root mean square errors (RMSE).

Gauge ID	Coef. regression line		RMSE (mm)
	c_i	m_i	
SRG.1	0.199	1.022	0.903
SRG.2	0.022	0.966	0.588
SRG.3	-0.038	0.986	0.699
TBG.4	0.049	1.001	0.625
WPG.5	-0.203	0.981	0.409
MWS.6	-0.242	0.831	3.299
DIS.7	-0.030	1.044	1.034

The RMSE is a reasonable measure of the difference between the rain-gauge measurements and the estimated rainfall depths by the regression line. The best quality of estimation was obtained with WPG.5 (RMSE was 0.4 mm); whereas the MWS.6 gauge yielded the maximum RMSE (around 3.3 mm).

3.4.2. Analysis of 1-min rain rate measurements

The 1-min rain rate measurements of four gauges (TBG.4, WPG.5, MWS.6 and DIS.7) were compared, taking also into account the time series of wind speeds. In Figure 11 three examples of measured rainy periods are shown (26-27 March 2011, 7-8 May 2012, and 7-8

March 2013); other rainy periods show similar discrepancy of rainfall depths, these three were chosen due to the high wind speeds observed.

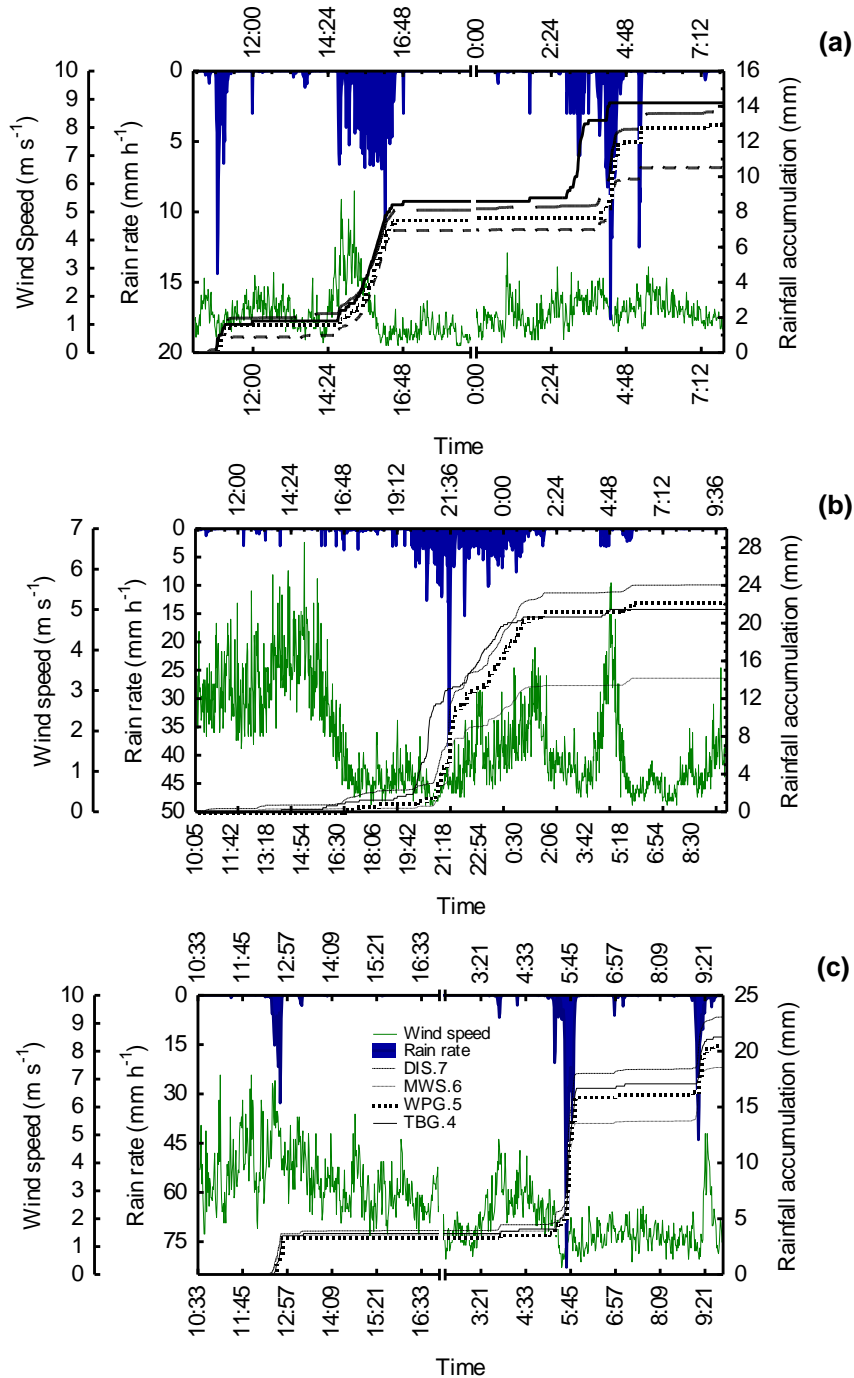


Figure 11. Representation of time series of wind speed, rain rates (mean of four gauges), and accumulated rainfall (for each gauge). The rainy periods were observed in: (a) 26-27 March 2011; (b) 7-8 May 2012; (c) 7-8 March 2013. Broken scales for the x-axis of (a) and (c) were created to better visualize the rainy period.

In Figure 11a the maximum values of rain rate and wind speed observed were 18 mm h^{-1} and 6 m s^{-1} , respectively. Moreover, the highest discrepancy between gauges' measurements was observed in the periods of higher rain rates; for these periods the wind speed was low (around 2 m s^{-1}), and so the wind-induced errors were not expected to be significant. In Figure 11b and Figure 11c the effect of high rain rates (maximum of 51 and 83 mm h^{-1} , respectively) in the discrepancy of measurements is confirmed, in particular for the acoustic gauge (MWS.6).

In relation to the wind, it is known that at higher wind speeds the noise of instrument measurements is likely to increase significantly. The presence of the instruments interferes with the air flow producing turbulence; the wind speed increases at the collecting aperture/detection area which might reduce the amount of raindrops collected/detected. In this context, it could be expected that, for example, in Figure 11c at around 12:57, the high wind speeds (over 5 m s^{-1}) lead to high differences of rainfall accumulations measured by the gauges, but the differences were low (maximum of 0.27 mm in 3.5 mm , i.e. less than 10%). The extent of the differences will then, probably, depend on wind speed, as well as the fall speed of raindrops and the design of the gauge.

In Figure 12 the variation coefficients of rain rate measurements from the four gauges (TBG.4, WPG.5, MWS.6 and DIS.7) were represented in relation to the rain rate classes – results included records from the same three rainy periods shown before (see Figure 11). The higher coefficients of variation were observed for lower rain rates. According to Sevruc et al. (2009), under low rain rates a great amount of small drops are, in fact, blown away even by low wind speeds. Moreover, it is not expected a perfect match between 1-min rain rates provided from instruments such as the disdrometers and the tipping bucket gauges, as their differences in operational factors affect the measurements. In general, the poor performance of the tipping bucket gauges is recognized during light rain periods as the instrument might take too long to record a tip and some evaporation of rain can occur in the bucket; also some rainwater amount can be lost during the tipping movement of the bucket at higher rain rates (e.g. Molini et al., 2005). In relation to the rainfall rates measured by disdrometers, the overestimation of records has already been reported; for example Vuerich et al. (2009)

pointed out that a possible error can occur from coincident drops, which are detected by the laser as one single but large drop.

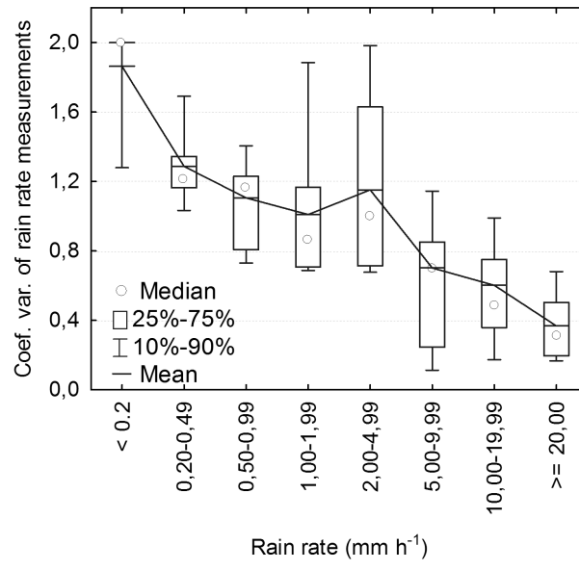


Figure 12. Box-and-whisker plots of the coefficient of variation of rain rate measurements in relation to rain rate classes. The resolution of data is 1-min and is related to the measurements of four gauges (TBG.4, WPG.5, MWS.6 and DIS.7) in the three rainy periods observed in 26-27 March 2011, 7-8 May 2012 and 7-8 March 2013.

3.5. Concluding remarks

This study compared the performance of different types of rain gauges, under field conditions, in recording rainfall depths. The dispersion of the measurements around the reference value was high. Nevertheless, despite the differences found across the seven types of gauges, the median of the relative error is within $\pm 5\%$ for the majority of the gauges. Moreover, the fact that the rainfall time series provided by the different gauges are not strictly equivalent could be expected, as the instruments tested have different designs and measuring principles. For example, the accumulative rainfall depth (from 60 rainy periods) was 8% higher for the disdrometer comparing with the weighing precipitation gauge: a possible error can occur from coincident drops, which are detected by the laser as one single but large drop; or an

underestimation from weighing precipitation gauge as a result of evaporation processes. In order to obtain accurate measurements, attention must be paid to calibration methods, in particular for non-catching rain gauges – optical and impact sensors – which had less agreement with the reference values (mean of 6 gauges).

The discrepancy of 1-min rain rate measurements observed for the continuous-recording gauges is also expected to be a consequence of different sources of errors, e.g. wetting and catching losses due to wind speed and evaporation processes, which can be intensified by their location at the top of the building. It was possible to detect the variation coefficients of rain measurements were high for low rain rates.

4. RAINWATER SEQUENTIAL SAMPLER: ASSESSING INTRA-EVENT WATER COMPOSITION VARIABILITY¹

Abstract

Rainwater sequential sampler instruments can be very useful in characterizing the variability in rainwater composition, which can occur over relatively short time periods. The main aim of this study was to develop a low-cost volume-based sequential rain sampler for the assessment of variations in the chemical composition of rainwater during individual rain events in one place. In order to evaluate the performance of the apparatus a few tests were conducted under field conditions in Coimbra (Portugal). Rainy periods were analysed in relation to the following physicochemical parameters: electrical conductivity, pH, turbidity, nitrates, sulphates and chloride. The results showed that the rainwater composition varied over time; moreover, some parameters were found to be highest at the beginning of the rainy period, followed by a rapid decline of the initial value and then remained approximately constant. The findings suggest that the rainwater sequential sampler is a low-cost solution tool that can be useful for non-continuous assessment of intra-event rainwater composition variability.

¹ Carvalho, S.C.P., de Lima, J.L.M.P., de Lima, M.I.P. 2014. Rainwater sequential sampler: assessing intra-event water composition variability. *Journal of Engineering Research and Technology* 1(1), 1-7.

4.1. Introduction

Rain is a scavenging agent for pollutants present in the atmosphere (e.g. Engelmann, 1968) creating a potential of contamination for terrestrial and aquatic ecosystems. Collecting rainwater sequentially is crucial to understand the variability in rainwater composition during rain events.

The rainwater composition is related to the atmospheric composition. For example, in rural areas that are located far from cities and industrial pollution and are not so much affected by the transport of pollutants, the rainwater is expected to be low polluted, as the air is mostly clean. On the contrary, urban areas are typically marked by intense traffic and industry can produce pollutants that are “washed out” from the atmosphere during rainfall events (e.g. Helmreich and Horn, 2009).

A wide variety of sequential rain samplers have been proposed: manual sampling (e.g. Gatz and Dingle, 1971); linked collection vessels (e.g. Cooper et al., 1976); automatic sequential samplers (e.g. Ronneau et al., 1978); and continuous monitors (e.g. Tomich and Dana, 1990). In addition, a classification of sequential rain samplers can be defined by the way the rain is fractionated, i.e. by volume (e.g. Mangoni et al., 1998) or at fixed time intervals (e.g. Gray et al., 1974). The method used to collect the rainwater might affect the results (e.g. Laquer, 1990a).

The variability in different rainwater components has been explored in relation to, for example, the rainfall event intensity and depth, the season when it occurs, and the antecedent dry periods (e.g. Huff and Stout, 1964; Dawson, 1978; Lim et al., 1991). Some of the studies on rainwater chemical composition use daily or lower time resolutions (e.g. Mantovan et al., 1995; Okuda et al., 2005). However, as pointed out by Raynor and Hayes (1981), and Seymour and Stout (1983) short-period samples (e.g. hourly) can provide crucial information, because the rainwater composition and the meteorological conditions (e.g. wind patterns, temperature, humidity) often change significantly over time during an event, and

important relationships might be masked by inadequate temporal resolution of the observations.

The aim of this research was to present a volume-based sequential rain sampler that can be adapted for low or high volume resolution (by using sampling-bottles with different capacities). The equipment was designed to attain: low manufacturing cost, set-up and maintenance easiness, and no power requirements. It was tested under field conditions in Coimbra (Portugal).

4.2. Rainwater sequential sampler

4.2.1. Design of the equipment

The intra-event variability of rainwater quality can be explored by collecting sequential samples of rainwater (with an appropriate resolution) during the event. In this study a volume-based sequential rain sampler was designed (Figure 13, see also the photograph of the equipment in Figure 14c). The components of this equipment are:

- i) Rainwater collection: a knife-edge collector ring; an aluminium funnel with an aperture diameter of 0.358 m; a flexible hose that connects the funnel to a flume; an adjustable support which keeps the funnel at an height of 1.5 m above the ground; and a support for the flume.
- ii) The sampler: an acrylic flume with 11 openings (regularly spaced at 100 mm) where bottles are attached; and 11 polypropylene bottles to collect/store the rainwater samples.

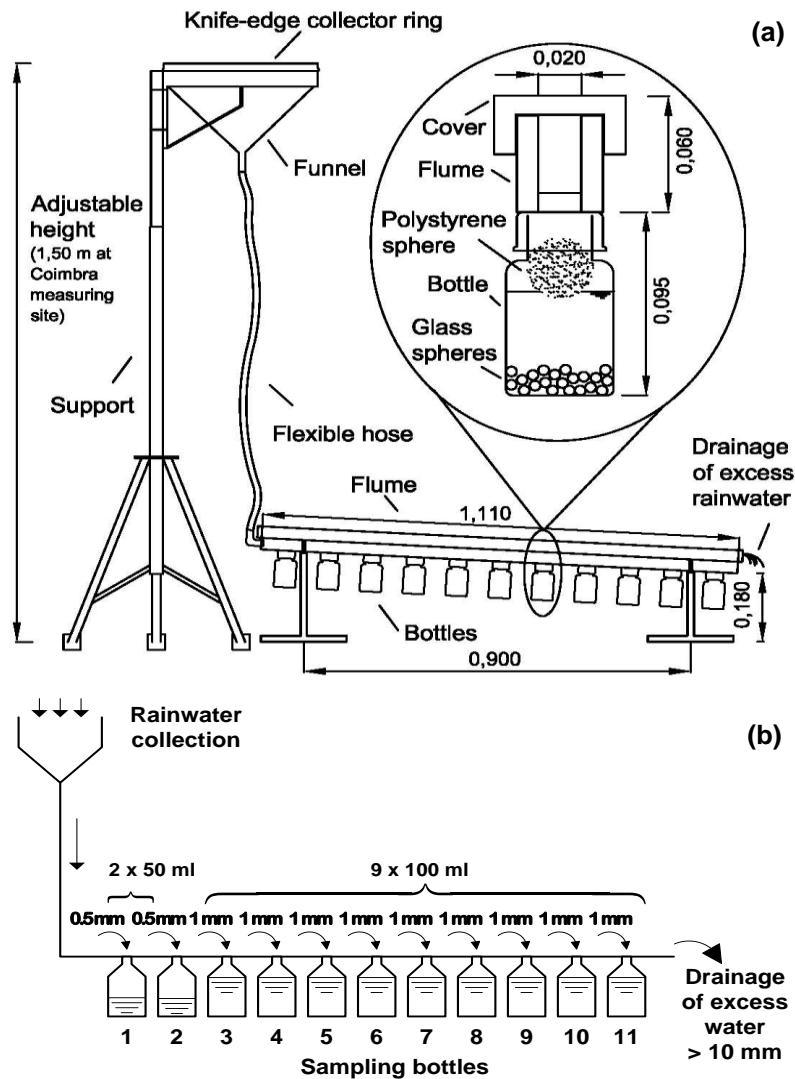


Figure 13. (a) Setup of the rainwater sequential sampler. Distances are in meters; (b) Hydraulic scheme of the rainwater sampling.

This study was performed in a way to provide a continuous storage of rainwater until a maximum of 10 mm of cumulative rainfall depth. For that purpose, and taking into account the funnel aperture/collecting area, i.e. around 0.1 m^2 , a maximum of 1000 ml of rainwater were collected (using a total of 11 individual samples): 50 ml (0.5 mm) for the first two bottles and 100 ml (1 mm) for each of the other bottles (Figure 13b); after all the bottles are filled the additional rain is disregarded. The first two bottles were used to better capture the eventual stronger variation on rainwater composition at the beginning of the events. Because all the sampling bottles attached in the equipment have 100 ml capacity, the volume collected

in each bottle was adjusted by placing small glass spheres in the bottle (Figure 13a); i.e. the first two bottles were filled with small glass spheres until the empty space left were enough for storing a maximum of 50 ml of rainwater. There was also some concern regarding mixing the rainwater from earlier samples and the following ones. Therefore, each bottle also contains a large polystyrene sphere which seals it once it is filled and prevents the inflow of additional rainwater; as entrapped air was present surrounding the float sphere and the water level, the inexistence of rainwater mixing between individual samples was confirmed. This sealing also protects samples from contamination.

4.2.2. Advantages and disadvantages of the equipment

The sequential rainwater samplers found in the literature vary in complexity, but the manual collection of rainwater is the simplest and least expensive method in terms of equipment requirements (e.g. Gatz and Dingle, 1971; Castillo et al., 1985). However, the long term availability of an operator to carry out the experiments makes this procedure difficult to implement. The sampler present in this study has low manufacturing costs and the bottles are filled in sequence by gravitational flow. Indeed, the samplers based on linked collection vessels, such as the present, have a simple construction (e.g. Cooper et al., 1976).

Since these samplers are designed to operate unattended, the number of samples that can be collected is an important specification to consider. The number of sampling bottles typically used in linked collection vessels is five or less (Laquer, 1990b), this equipment is prepared to attach 11 samples.

Depending on the number of samples and the purpose of the analysis, the collection of samples can be based on time or on rainfall volume; automatic sequential samplers are usually able to sample at unit times but in that case some extra care should be taken to avoid incomplete record of the event, for example, if a sample container is not big enough, the excess of water will overflow before the next container is in position to fill.

The total amount of rainfall collected by the present sampler can be easily adapted to different measuring schemes by using bottles with different volume capacities, i.e., decreasing or increasing the sampling volume resolution.

In addition to the assessment of the intra-event water composition variability, if one wants to register the intensity and duration of the rain event, it is necessary to complement the measurements using a recording rain gauge (e.g. tipping bucket rain gauge), which would obviously involve extra costs and power requirements.

This equipment only provides an unrefrigerated collection of samples; some other devices store the samples under refrigeration conditions, see e.g. Kawakubo et al. (2001). For studies aiming at analysing rainwater composition in terms of stable chemical species, the samples can be removed immediately after the end of the event, which guarantee their physicochemical integrity. Nevertheless, this sampler is easily transported to the field and it does not require power. The equipment also has low maintenance requirements (it can be easily cleaned with distilled water).

4.3. Testing the sampler

4.3.1. Measuring site

The sequential rain sampler was tested in the field in the city of Coimbra (Portugal), which is located in the valley of Mondego River, and it is at approximately 50 km from the Atlantic coast (Figure 14). The sampler was installed on the flat roof of the building of the Department of Civil Engineering of the University of Coimbra (with geographic coordinates 40°11'08"N and 08°24'52"W).

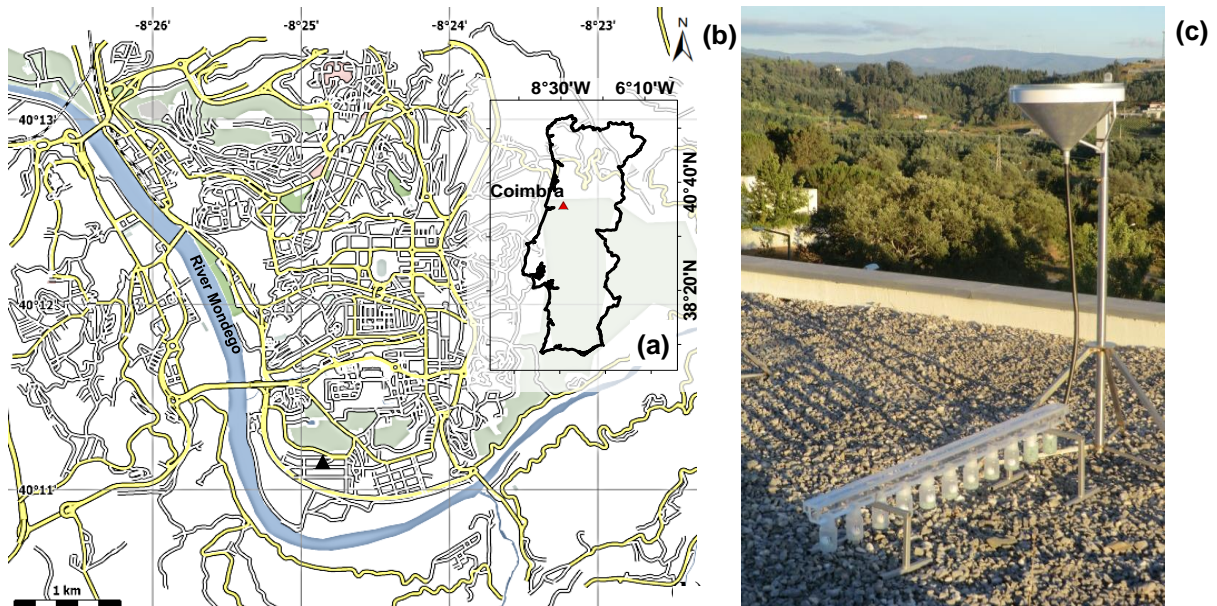


Figure 14. (a) Location of Coimbra in mainland Portugal; (b) Location of the study site in the city of Coimbra (black triangle); (c) Photograph of the equipment.

4.3.2. Data acquisition

The dataset analysed comprises four rainy periods (Table 6), which were selected based on the following criteria: i) a minimum rainfall amount of 6 mm (to provide at least 7 sampling bottles); ii) a minimum of 6 hours of dry period prior to sampling (dry period means here that the rain intensity was lower than 0.05 mm h^{-1}).

Table 6. Description of the rainy periods sampled.

Rainy periods	1	2	3	4
Date (day-month-year)	01-09-2011	02-11-2011	11-11-2011	23-09-2012
(h:min)	17:23 – 20:20	8:08 – 9:36	6:31 – 10:30	3:04 – 6:13
Antecedent dry period (h)	8.0	33.4	43.5	119.6
Total rain amount (mm)	10	10	10	6
Total duration (min)	178	89	240	190
Shortest sampling duration* (min)	7	1	7	2
Longest sampling duration** (min)	51	49	58	134
Mean rain intensity (mm h⁻¹)	3.4	6.8	2.5	1.9
Maximum rain intensity (mm h⁻¹)	10.2	69.8	13.6	63.0
Mass-weighted mean drop diameter, D_m (mm)	1.76	2.11	1.48	1.64

*The “shortest sampling duration” is the minimum interval needed to fill a sampling bottle.

**The “longest sampling duration” is the maximum interval needed to fill a sampling bottle.

In relation to the procedure for collection and analysis of rainwater samples: all the components of the rain sampling equipment were pre-washed with distilled water; the sampling bottles were removed immediately after being filled.

The electrical conductivity (EC), pH and turbidity of rainwater were measured immediately upon completing the removal of samples, using the following portable instruments: HI9033 Multi-range EC meter, HI8314 pH/ORP/Temperature meter, and the HI93125 Turbidity meter, all of them manufactured by Hanna Instruments.

In addition to the electrical conductivity, pH and turbidity measurements, the sampled rainwater from rainy period 4 (23-09-2012) was frozen and transported to an analytical laboratory for analysing nitrates, sulphates, and chloride. The concentrations of sulphates and nitrates were measured by ion chromatography, and the chloride was determined by the Mohr Method.

Although under certain conditions the chemical composition of the rainwater (e.g. pH) can change between the time from filling the first bottle and the time of sampling collection, it is

believed that such time period is not long enough to influence the concentration of the major inorganic ions in the dissolved fraction (e.g. Krupa, 2002).

The rain intensity was measured by a laser disdrometer (“Laser Precipitation Monitor” from Thies Clima) installed next to the sequential rain sampler. This instrument also yields the number of raindrops over 21 size classes and 20 fall speed classes. The rainfall data temporal resolution is one-minute and the depth resolution is 0.001 mm.

The variability in rainwater composition was explored in relation to the distribution of raindrop sizes. The laser disdrometer provided each minute a two dimensional matrix with the count of drops in each size and fall speed classes; the matrices were added over the sampling period to obtain one single matrix, which was used for determining the mass-weighted mean drop diameter (D_m).

The D_m allows the quantification of the overall distribution of raindrop sizes and is obtained by (e.g. Ulbrich, 1983):

$$D_m = \frac{\sum_{i=1}^{21} D_i^4 N(D_i) \Delta D_i}{\sum_{i=1}^{21} D_i^3 N(D_i) \Delta D_i} \quad (4.1)$$

where D_i [mm] is the central diameter of the size class i (21 classes) and $N(D_i)$ [$\text{mm}^{-1} \text{m}^{-3}$] is the expected number of drops, with diameters between D and $D+\Delta D$, present per unit volume of air.

The $N(D_i)$ [$\text{mm}^{-1} \text{m}^{-3}$] defined in the Eq. (4.1) is obtained by (e.g. Krajewski et al., 2006):

$$N(D_i) = \frac{I}{A \Delta t \Delta D_i} \sum_{j=1}^{20} \frac{n_{ij}}{v_j} \quad (4.2)$$

where n_{ij} is the number of detected raindrops in the size class i and fall speed class j (20 classes), which is measured during the time period Δt [s] taken to fill the sampling bottles, v_j

$[m\ s^{-1}]$ is the fall speed at the middle of the fall speed class j , $A\ [m^2]$ is the detection area and $\Delta D_i\ [mm]$ is the width of the size class i .

4.3.3. *Data analysis*

Figure 15 shows the hyetographs of the four rainy periods investigated (see also Table 6). The total amount of rainwater collected in each rainy period was 10 mm, with the exception of rainy period 4 (23-09-2012), which accumulated 6 mm. The time taken to fill all the sampling-bottles for the four rainy periods varied from 89 min (rainy period 2) to 240 min (rainy period 3). The time needed to fill each sampling bottle is also represented in Figure 15; the highest difference in sampling duration was observed for the rainy period 4 (23-09-2012), ranging from 2 to 134 min.

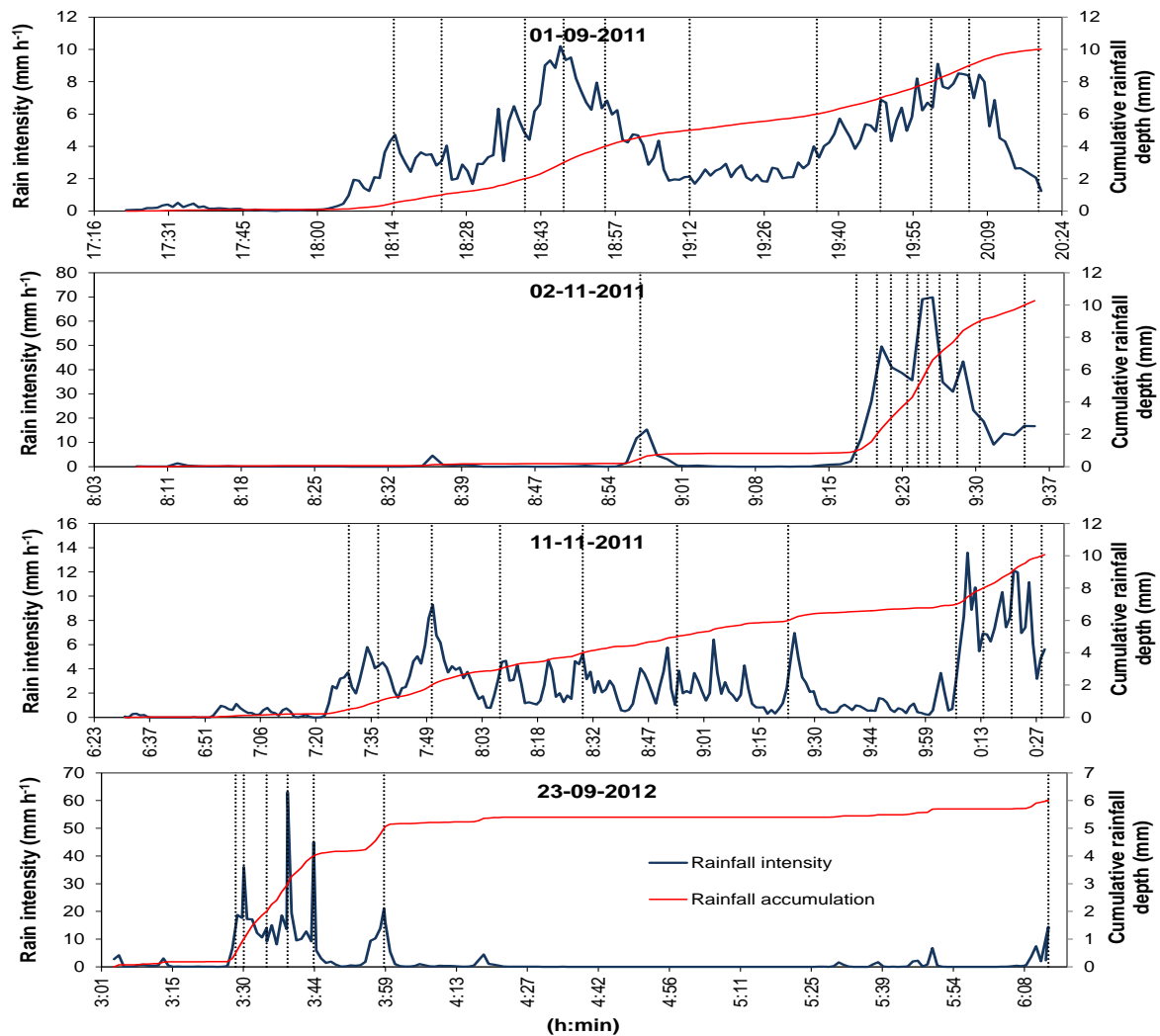


Figure 15. Hyetographs of the four rainy periods (see Table 6). Time needed to fill each sampling bottle is represented on the hyetographs (time between two vertical dotted lines).

The mean intensity for the four rainy periods varied between 1.9 mm h⁻¹ (rainy period 4) and 6.8 mm h⁻¹ (rainy period 2). The mass-weighted mean drop diameter (D_m) ranged from 1.48 to 2.11 mm (Table 6). The highest D_m was observed in rainy period 2 (02-11-2011), which was expected since the highest mean and maximum intensity was found for this sampling period, and bigger drops are typically more abundant in high rain rate episodes.

The physical and chemical parameters that characterize the rainwater of the rainy periods investigated using the rainwater sequential sampler are given in Table 7.

Table 7. Description of rainwater parameters for the four rainy periods (see Table 6 and Figure 15): I (Rainfall Intensity), D_m (Mass-Weighted Mean Drop Diameter), EC (Electrical Conductivity), Tr (Turbidity), Cl^- (Chloride), SO_4^{2-} (Sulphates), and NO_3^- (Nitrates), used to test the sampler.

Samples number	Rainfall amount (mm)	01-09-2011					02-11-2011					11-11-2011					23-09-2012							
		I (mm h ⁻¹)	D_m (mm)	Tr (FNU)	EC (μS cm ⁻¹)	pH	I (mm h ⁻¹)	D_m (mm)	Tr (FNU)	EC (μS cm ⁻¹)	pH	I (mm h ⁻¹)	D_m (mm)	Tr (FNU)	EC (μS cm ⁻¹)	pH	I (mm h ⁻¹)	D_m (mm)	Tr (FNU)	EC (μS cm ⁻¹)	pH	Cl^- (mg L ⁻¹)	SO_4^{2-} (mg L ⁻¹)	NO_3^- (mg L ⁻¹)
1	0.5	0.5	1.38	1.76	48.0	6.73	0.5	2.06	3.79	35.2	7.05	0.5	1.02	2.90	21.2	6.41	0.8	1.42	3.73	75.3	7.34	13.0	0.24	0.04
2	0.5	3.4	1.70	1.14	30.4	6.62	1.4	1.88	3.02	33.0	7.06	3.8	1.62	1.49	11.9	6.79	18.2	2.22	1.40	21.3	7.53	4.1	7.47	0.65
3	1.0	3.7	1.96	0.74	8.4	6.82	19.2	1.92	1.70	9.6	6.98	4.0	2.20	0.74	5.8	6.88	14.3	1.82	1.09	10.8	7.53	2.4	0.17	0.00
4	1.0	7.8	2.21	0.48	5.5	7.20	49.6	2.25	1.07	6.6	6.91	3.6	1.18	0.90	6.0	6.84	12.9	1.73	0.91	7.8	7.40	4.1	2.65	2.71
5	1.0	7.7	1.91	0.47	5.2	7.26	39.8	2.09	0.68	5.4	7.00	2.8	1.22	0.88	6.3	6.75	12.2	1.91	0.95	7.3	7.43	4.1	32.03*	2.00
6	1.0	3.9	1.69	0.57	5.4	7.14	35.6	1.79	0.67	4.2	7.17	2.4	1.18	0.83	4.5	6.84	3.6	1.20	0.65	9.1	7.02	5.9	3.46	0.05
7	1.0	2.4	1.57	0.39	5.2	7.06	69.1	2.53	0.61	3.6	7.10	2.1	1.27	0.76	3.3	7.02	0.5	1.05	0.56	15.8	7.18	2.4	5.14	0.01
8	1.0	4.6	1.69	0.46	5.1	6.96	69.8	2.56	0.65	3.1	6.98	1.4	0.95	0.59	2.8	7.30								
9	1.0	6.2	1.77	0.22	9.9	6.51	32.9	2.14	0.61	2.9	7.10	8.5	1.53	0.47	2.2	6.98								
10	1.0	8.0	1.78	0.39	7.7	6.43	33.3	1.95	0.49	2.7	6.93	7.9	2.10	0.53	2.2	6.86								
11	1.0	4.6	1.63	0.53	11.8	6.50	14.2	1.70	0.42	3.1	7.10	7.6	2.02	0.74	3.3	6.74								
Mean		3.4	-	0.65	12.96	6.84	6.8	-	1.25	9.95	7.03	2.5	-	0.98	6.32	6.86	1.9	-	1.33	21.06	7.35	5.14	3.19	0.78
Coef. of variation		0.80	-	0.67	1.06	0.04	2.16	-	0.91	1.22	0.01	1.03	-	0.70	0.90	0.03	2.27	-	0.83	1.16	0.03	0.71	0.89	1.43

*Apparent anomalous value; it was ignored in the analysis

Empirical turbidity time variation was represented in Figure 16a for the four rainy periods investigated. The turbidity of the rainwater reduced over time; a power law fitted well the data. The results suggest the suitability of high resolution sampling – in particular, the 2 first bottles with 0.5 mm of rain each – to assess the intra-event rainwater composition; in case e.g. 3-mm sampling-bottles were used, the rapid decline of turbidity in the beginning of this particular event would be unnoticed. This variability in rain turbidity is consistent with several studies that report the presence of higher concentration of suspended matter during the beginning of rainfall and decrease throughout the rain event, which is likely to result from “washout” processes (e.g. Jambers et al., 2000).

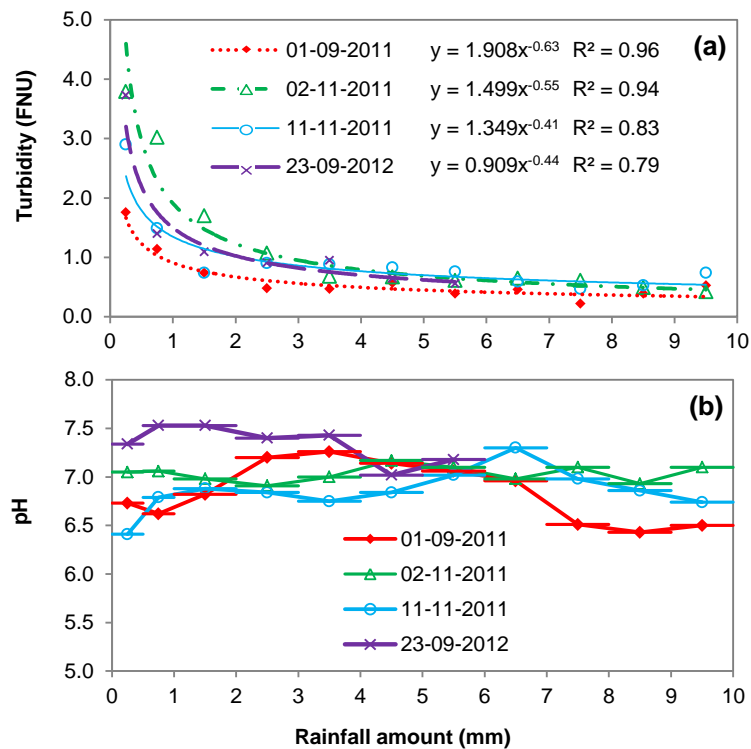


Figure 16. (a) Turbidity measured for each sample collected during the four rainy periods. Power laws are fitted to the data; (b) pH measured in the rainwater samples collected during the four rainy periods.

The rainwater sequential sampling also permitted to identify the pH fluctuations during the rainy periods (Figure 16b). For the four rainy periods investigated, the samples pH values

ranged between 6.4 and 7.5. The mean (\pm standard deviation) for each rainy period was 6.8 (\pm 0.3), 7.0 (\pm 0.1), 6.8 (\pm 0.2), and 7.3 (\pm 0.2) for rainy periods 1 to 4, respectively.

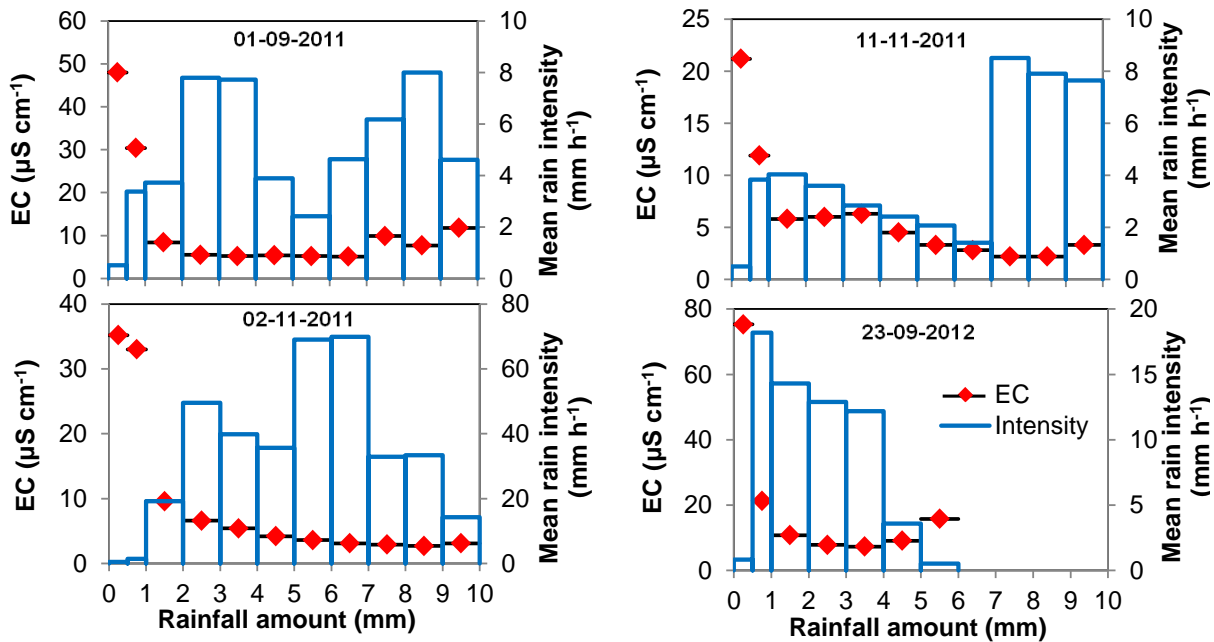


Figure 17. Electrical conductivity (EC) measured in each sample during the four rainy periods. Rainfall intensity was averaged over each sampling interval.

Figure 17 shows the evolution of the electrical conductivity of the rainwater during the four rainy periods. They all show the occurrence of higher electrical conductivity at the beginning of rainfall and a rapid decrease in the first millimetre of rain. Nevertheless, it is possible to observe some differences between the studied rainy periods. For example, the rainy period 4 (23-09-2012) reached the highest electrical conductivity, $75 \mu\text{S cm}^{-1}$, which might be explained by the corresponding longest antecedent dry period, ~ 5 days (see Table 6). This relationship is usually described in the literature, for example Nyika et al. (1996) observed that the rainwater samples had higher electrical conductivity when there was no rainfall on the days before the rainwater collection, in comparison with the samples taken after a rainy day.

The Figure 18a shows the variations of concentrations of chloride, sulphates and nitrates for the rainy period 4 (23-09-2012). The chloride concentration was higher in the first 0.5 mm and, after that, the concentration fluctuated between 2 and 6 mg L^{-1} (see also Table 7). The

rainwater sequential samples have concentrations of sulphates between 0.2 and 7.5 mg L⁻¹, with a mean value of 3.2 mg L⁻¹. In relation to the nitrates, the mean concentration recorded was 0.8 mg L⁻¹; and 2.71 mg L⁻¹ was the maximum value detected, which corresponds to the sample filled at the time of maximum rain intensity (~ 63 mm h⁻¹), see Figure 15.

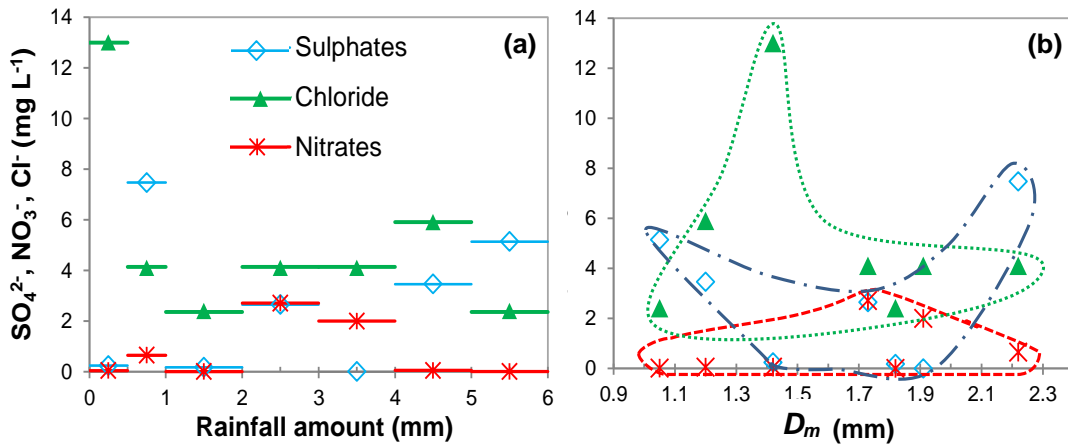


Figure 18. (a) Concentrations of chloride, sulphates and nitrates during the rainy period 4 (23-09-2012); (b) Concentrations of chloride, sulphates and nitrates plotted against the mass-weighted mean drop diameter (D_m).

The relationship between the processes of removal of pollutants from the atmosphere and raindrop sizes has been studied for a long time. For example, Levine and Schwartz (1982) stated that the removal of HNO₃ vapour depend on raindrop size, with the smaller drops (< 1 mm) having the greatest contribution to the washout scavenging. In addition, Ebert et al. (1998) establish different relationships between scavenged particle sizes (0.19 - 1.8 μm) and the most effective raindrop diameter. In Figure 18b the mass-weighted mean drop diameter (D_m) is plotted against the concentrations of chloride, sulphates and nitrates measured in the rainy period 4 (23-09-2012), apparently showing no clear relationship. The variation of D_m , ranging from 1.05 to 2.22 mm, seems to have a different effect on rainwater composition depending on the ionic species. For example, the highest concentrations of sulphates (7.5 and 5.1 mg L⁻¹) were observed for the extreme (highest and lowest) values of D_m (2.22 and 1.05 mm, respectively) (see also Table 7). But the small sample size analysed does not allow any inference of relations between the relevant variables, which in any case was not the main goal of this work.

4.4. Concluding remarks

This study proposed a rainwater sequential sampler that can be useful as a low-cost solution to explore rainwater composition variations during a rainfall event. Because of the simplicity of its design, the apparatus can be easily adapted to include different sample volumes and total amount of sampled rainfall. A drawback is that in order to register the intensity and duration of the rain event it is necessary to use in addition a recording rain gauge.

Sequential samples of rain were collected in Coimbra (Portugal) during four rainy periods to test the performance of the equipment. The higher resolution of the initial rainwater samples (2 bottles with 0.5 mm of rainwater each whereas all other bottles have 1 mm) allowed the detection of higher values of some parameters followed by a rapid decline. Results suggest that the volume resolution of the device is able to assess rainwater composition variability during a rain event, but if necessary this can be easily adapted to specific requirements.

5. ANALYSIS OF RAINFALL EVENTS IN COIMBRA, PORTUGAL: VARIABILITY OF RAINDROP CHARACTERISTICS

Abstract

The characterization of the rainfall structure at small time scales is of particular interest for many hydrological applications. The aim of this study is to characterize rainfall events according to the size and fall speed of drops, including the intra-event variability. Rainfall data comprise a set of 35 independent rainfall events recorded during three years with a laser disdrometer in Coimbra, Portugal. The data temporal resolution is one-minute. Descriptive statistics of time series of raindrop diameter, fall speed, rain rate and kinetic energy were studied. The empirical raindrop size distribution (DSD) was calculated based on data from all the 35 events recorded, and also provided for individual rainfall events: the parameterization of DSD was attained by using the gamma distribution to fit the empirical data. Results confirmed that the gamma DSD parameters varied with rain rates; moreover, the skewness of DSD increased from low to high rain rates. Power laws were shown to fit well the relationships between the mass-weighted mean diameter and kinetic energy, as well as the kinetic energy-rain rate relationship.

5.1. Introduction

The characterization of the rainfall structure at small time scales is of particular interest for many hydrological applications, and the increasing availability of high-resolution records, provided by disdrometers is allowing this study at time scales of e.g. one minute. One study approach is by defining rain events, whose properties are meaningful for specific applications, such as soil erosion, rainfall modelling and rainfall-runoff modelling.

In the early studies, raindrop size was measured using the flour method (Laws and Parsons, 1943), filter paper (Marshall and Palmer, 1948) and photographic cameras (e.g. Jones, 1959), among other approaches. In recent years, instruments such as optical disdrometers have become popular in scientific research (e.g. Do Khac et al., 2004; Brawn and Upton, 2008; King et al., 2010; Frasson et al., 2011). These sensors are able to measure the size of raindrops that pass through a laser beam (e.g. Thies, 2007). Different statistics can then be obtained to characterize the rain in terms of drop sizes: the mass-weighted mean diameter of drops, and drop size distribution (DSD) are commonly analysed (e.g. Haddad et al., 1996; Uijlenhoet, 1999; Fornis et al., 2005; Marzuki et al., 2010).

The relation between the distribution of drop sizes and the rain rate has interested the scientific community for a long time; for early studies see e.g. Laws and Parsons (1943) and Best (1950). For example, Carter et al. (1974) found that the median drop size increases with increasing rain rate up to 63.5 mm h^{-1} and decreases at higher intensities; this could be explained by the instability of large drops which break into smaller ones. The relationship between rain rate and the median drop size or the drop-size distribution is not unique, as there are many factors affecting the drop characteristic. For example, several authors explored the variability of raindrop size distribution according to the rain's type, e.g. stratiform and convective (e.g. Blanchard, 1953; Mason and Andrews, 1960; Tokay and Short, 1996; Caracciolo et al., 2006; Niu et al., 2010).

Despite the variability of raindrop size distributions, the measurements from numerous researchers suggest that averaged distributions tend to be positively skewed, unimodal and

parameterized with a few parameters (e.g. Lu et al., 2008). In order to model discrete drop size distributions (resulting from the size classes established by the disdrometer) different parameterizations have been proposed. The exponential distribution (e.g. Marshall and Palmer, 1948) is the most widely used (Zhang et al., 2008). Because the exponential parameterizations have been claimed to tend to overestimate the number of small drops, distributions using an extra (third) parameter have been suggested, namely the lognormal distribution (e.g. Levin, 1954), and the gamma distribution (e.g. Ulbrich, 1983).

Raindrop falling speed is also an important variable in the characterization of rainfall. The terminal velocity of water drops was measured under laboratory conditions by e.g. Gunn and Kinzer (1949), Beard and Pruppacher (1969), and Beard (1976). Following these findings and because data on drop sizes are usually more easily available in comparison to drop fall speed records, it is often assumed that the terminal velocity of a drop is mainly determined by its size and is the same as that for drops falling in stagnant air; power laws that describe the terminal velocity as a function of the equivalent spherical diameter were derived, and are commonly used (e.g. Atlas et al., 1973; Brandes et al., 2002).

Over the last decades, instruments such as the optical disdrometers have also been used to monitor the drop fall speeds. Some authors (e.g. Krajewski et al., 2006) showed that, in general, their fall speed measurements agreed closely with those of Gunn and Kinzer (1949), which are usually a reference for drop size-terminal velocity relationship. However, Montero-Martínez et al. (2009) claimed that raindrops, in their studied size range of 0.1 - 3 mm, did not all fall at the theoretical terminal velocity during the periods of high rainfall rates as a result of the break-up of larger drops that fall at greater velocities. Recently, Leijnse and Uijlenhoet (2010) concluded that the effect of high-velocity small drops would be negligible, in particular, for remote sensing of rainfall using radar, microwave links, or optical links, since the errors induced by the use of slightly different drop size-terminal velocity relations would be obscured by other error sources. Nevertheless, it has been suggested the importance of further investigation of the drop fall speed at natural outdoor conditions in different places, because for example, adverse environment conditions such as the air pollution, might change the surface tension of water and cause more frequent breakup of drops.

The information about the diameter and fall speed of each individual raindrop permits to estimate the rainfall kinetic energy, which is of particular interest for water erosion studies. A wide variation of relationships between kinetic energy and rain rate have been proposed in the literature (e.g. Kinnell, 1981; Rosewell, 1986; Steiner and Smith, 2000; Assouline, 2009; Petan et al., 2010). For example, Salles et al. (2002) states the most suitable mathematical function to link kinetic energy and rain rate is a power law considering the existing drop-size distribution models from literature.

This study analyses the variability of raindrops' characteristics (size and fall speed) using data from Coimbra (Portugal); the estimation of relationships between these variables and the rain rates and kinetic energy focuses on individual events, and also on data from all the 35 selected events.

5.2. Material and methods

5.2.1. Study area and experimental equipment

Rainfall data were recorded with a laser disdrometer installed in the city of Coimbra (Portugal). The disdrometer used is manufactured by Thies Clima (see Appendix A.6.). In the equipment a laser-optical source produces a light-beam (infrared of 785 nm and measuring area of 4777 mm²) then a receiver transforms the optical intensity into an electrical signal. When a raindrop falls through the light-beam, the receiving signal is reduced. The size of the drop is calculated from the amplitude of the reduction and the fall speed of the drop is determined from the duration of the reduced signal. The equipment provides the distribution of the drops' diameter over 21 size classes ($0.125 \leq D < 8.000$ mm, with irregular class widths) and 20 fall speed classes ($0.0 \leq v < 20.0$ m s⁻¹, with irregular class widths) (Thies, 2007). The data temporal resolution is one-minute.

5.2.2. *Rainfall events*

The study explores a set of 35 independent rainfall events recorded during three years, from July 2009 to June 2012, that correspond to a total of 12321 minutes and 589.3 mm. The following criteria were adopted to identify the individual events (e.g. Dunkerley, 2008b; Jaffrain and Berne, 2012): a minimum rain depth of approximately 10 mm; a minimum inter-event period of at least 15 min (i.e. during at least 15 min the rain rate is lower than 0.05 mm h^{-1}).

The description of the selected rainfall events in relation to rain rate and duration are shown in Table 8. These events were recorded throughout the year, spanning the 4 seasons, although 45% of the events were observed in the fall.

The properties of the selected rainfall events varied considerably. For example, the total amount of rainfall ranged from 9.5 mm (events 1 and 14) to 38.3 mm (event 6). Most of the events (94%) lasted more than 2 hours. The analysis of the events' mean rain rates shows that 90% of the data are below 7 mm h^{-1} , with an average value of 4 mm h^{-1} .

Table 8. Description of the 35 rainfall events selected during the three year records, in the period from July 2009 to June 2012.

Event	Date (day-month-year) / Time (h:min)		Duration (h:min)	Depth (mm)	Mean rain rate (mm h ⁻¹)	1-min maximum rain rate (mm h ⁻¹)	Coef. of Var. of 1-min rain rate	Season
	start	end						
1	22-07-2009 20:36	22-07-2009 21:53	01:18	9.5	8.2	39.3	1.05	Summer
2	20-10-2009 04:54	20-10-2009 09:57	05:04	20.4	4.1	31.1	1.16	Fall
3	21-10-2009 19:18	21-10-2009 23:52	04:35	18.9	4.3	39.4	1.42	Fall
4	14-11-2009 00:10	14-11-2009 02:37	02:28	19.1	7.9	80.1	1.81	Fall
5	15-11-2009 15:19	16-11-2009 04:43	13:25	38.2	2.9	28.1	1.14	Fall
6	16-11-2009 06:50	16-11-2009 14:12	07:23	38.3	5.2	45.3	1.31	Fall
7	16-11-2009 18:52	16-11-2009 20:54	02:03	12.3	6.0	26.9	1.16	Fall
8	29-11-2009 02:05	29-11-2009 05:33	03:29	18.3	5.3	59.2	1.52	Fall
9	06-12-2009 10:32	06-12-2009 15:24	04:53	13.9	2.8	20.7	1.05	Fall
10	06-12-2009 16:43	06-12-2009 20:46	04:04	13.8	3.4	63.3	1.98	Fall
11	22-12-2009 21:37	23-12-2009 06:19	08:43	17.5	2.1	20.1	1.68	Winter
12	30-12-2009 09:09	30-12-2009 09:51	00:43	10.2	14.3	98.6	1.61	Winter
13	12-01-2010 03:29	12-01-2010 11:37	08:09	22.7	2.8	52.5	1.51	Winter
14	13-01-2010 10:10	13-01-2010 15:22	05:13	9.5	1.9	16.0	1.13	Winter
15	16-01-2010 09:39	16-01-2010 18:44	09:06	22.0	2.4	19.5	1.13	Winter
16	17-02-2010 00:58	17-02-2010 09:01	08:04	12.3	1.5	7.7	0.70	Winter
17	05-03-2010 05:46	06-03-2010 01:11	19:26	16.0	0.8	3.0	0.72	Winter
18	20-04-2010 20:19	21-04-2010 00:06	03:48	17.4	4.6	49.3	1.63	Spring
19	13-11-2010 23:05	14-11-2010 04:30	05:26	24.0	4.4	173.9	2.95	Fall
20	16-11-2010 21:56	17-11-2010 06:06	08:11	16.4	2.0	20.8	1.02	Fall
21	20-11-2010 00:20	20-11-2010 03:42	03:23	10.3	3.2	56.0	2.21	Fall
22	07-12-2010 13:19	07-12-2010 15:31	02:13	10.2	4.7	44.3	1.70	Fall
23	30-12-2010 13:06	30-12-2010 19:50	06:45	14.6	2.3	25.1	1.54	Winter
24	06-01-2011 16:28	06-01-2011 19:45	03:18	15.3	4.6	29.2	0.88	Winter
25	13-02-2011 08:36	13-02-2011 12:10	03:35	12.2	3.5	51.7	1.72	Winter
26	18-02-2011 20:34	19-02-2011 06:59	10:26	19.8	2.0	15.2	1.15	Winter
27	28-03-2011 17:05	28-03-2011 21:47	04:43	14.5	3.1	22.9	1.23	Spring
28	18-04-2011 23:09	19-04-2011 07:47	08:39	16.2	1.9	26.8	1.49	Spring
29	29-04-2011 16:00	29-04-2011 20:06	04:07	13.0	3.2	42.9	2.02	Spring
30	01-09-2011 17:23	01-09-2011 21:15	03:53	9.8	2.5	9.1	0.97	Summer
31	02-11-2011 08:08	02-11-2011 11:09	03:02	22.9	8.1	80.3	1.51	Fall
32	22-11-2011 01:40	22-11-2011 09:25	07:46	15.5	2.1	11.2	1.04	Fall
33	10-12-2011 06:53	10-12-2011 10:19	03:27	10.1	2.9	15.5	1.14	Fall
34	13-04-2012 23:32	14-04-2012 05:13	05:42	14.0	2.6	20.8	1.40	Spring
35	25-04-2012 09:56	25-04-2012 18:46	08:51	20.3	2.3	18.7	1.23	Spring
Mean			05:52	16.8	3.9	39.0		
Minimum			00:43	9.5	0.8	3.0		
Maximum			19:26	38.3	14.3	173.9		

5.2.3. Rainfall rates, raindrop properties, and rainfall kinetic energy

As explained before in the description of the disdrometer, the instrument provides a two dimensional matrix with the count of drops in each size and fall speed classes. These data were used to calculate the rainfall intensity, R [mm h^{-1}], by (e.g. Krajewski et al., 2006):

$$R = \sum_{i=1}^{21} R(D_i) \quad (5.1)$$

with $R(D_i)$ being the intensity for a given drop size class i :

$$R(D_i) = \frac{\pi}{6A\Delta t} n_i D_i^3 \quad (5.2)$$

where n_i is the number of drops detected in the size class i during the interval $\Delta t = 1/60$ h, D_i [mm] is the drop diameter at the middle of the size class i , and A [mm^2] is the disdrometer detection area.

Aside from rainfall rate, information on the size and fall speed of drops was explored; basic descriptive statistics of time series of raindrop diameter (D) and fall speed (v) were determined (i.e. the average, maximum, minimum and coefficient of variation).

In order to characterize the rainfall microstructure, a fundamental property commonly used is the raindrop size distribution (DSD), $N(D)$. The $N(D_i)$ [$\text{mm}^{-1}\text{m}^{-3}$] represents the expected number of raindrops in the drop-size class i (21 classes), present per unit volume of air, and is calculated by (e.g. Krajewski et al., 2006):

$$N(D_i) = \frac{1}{A\Delta t\Delta D_i} \sum_{j=1}^{20} \frac{n_{ij}}{v_j} \quad (5.3)$$

where D_i [mm] is the drop diameter at the middle of the size class i , n_{ij} is the number of detected raindrops in the size class i and belonging to the fall speed class j (20 classes), which is measured during the interval Δt (1 min), v_j [m s^{-1}] is the fall speed of the raindrops at the middle of the fall speed class j , A [m^2] is the disdrometer detection area and ΔD_i [mm] is the width of the size class i .

The mass-weighted mean diameter, D_m [mm], is another useful parameter to describe the DSD, and is estimated by (e.g. Ulbrich, 1983; Testud et al., 2001):

$$D_m = \frac{\sum_{i=1}^{21} D_i^4 N(D_i) \Delta D_i}{\sum_{i=1}^{21} D_i^3 N(D_i) \Delta D_i} \quad (5.4)$$

All the variables in Eq. (5.4) were defined before for Eq. (5.3).

The relationship between D_m and rain rates was investigated based on data from all the 35 selected events; Spearman's rho was calculated to assess the correlation between the variables. Compared to the widely used Pearson's r , Spearman's rho is more robust to outliers and to nonlinearity (e.g. Helsel and Hirsch, 2002).

The parameterization of raindrop size distribution was attempted by using the gamma distribution, which is believed to fit the shape of the DSD as more small than large raindrops are found in a particular volume (e.g. Wong and Chidambaram, 1985). The gamma distribution function has the form (e.g. Ulbrich, 1983):

$$N(D) = N_0 D^\mu e^{-\Lambda D} \quad (5.5)$$

where $N(D)$ [$\text{mm}^{-1} \text{m}^{-3}$] is the raindrop size distribution as a function of the raindrop diameter D [mm], N_0 [$\text{mm}^{-1-\mu} \text{m}^{-3}$] is number concentration parameter or scaling parameter, μ [unitless] is the shape parameter, and Λ [mm^{-1}] is the slope parameter.

The parameters N_0 , μ , and Λ were estimated based on the method of moments, where the k th moment, M_k , is calculated by (e.g. Tokay and Short, 1996):

$$M_k = N_0 \frac{\Gamma(\mu+k+1)}{\Lambda^{\mu+k+1}} \quad (5.6)$$

and Γ is the standard gamma function.

Cao and Zhang (2009) have shown that the middle-moment estimators (M_2 , M_4 and M_6) produce smaller errors than lower and higher-moment estimators, provided the DSD follows

the gamma distribution. The gamma DSD parameters were hence obtained (Cao and Zhang, 2009):

$$\mu = \frac{11\eta - 7 + \sqrt{\eta^2 + 14\eta + 1}}{2(1-\eta)} \quad \text{with } \eta = \frac{M_4^2}{M_2 M_6} \quad (5.7) \quad (5.8)$$

$$\Lambda = \sqrt{\frac{M_2}{M_4}} (\mu+3)(\mu+4) \quad (5.9)$$

$$N_0 = \frac{\Lambda^{\mu+3} M_2}{\Gamma(\mu+3)} \quad (5.10)$$

After analysing the drop size data, the drop fall speed (v) analysis was performed. The mean drop fall speed (v_m) was calculated as,

$$v_m = \frac{\sum_{j=1}^{20} n_j v_j}{N} \quad (5.11)$$

where n_j is the number of detected raindrops in the fall speed class j , v_j (m s^{-1}) is the fall speed at the middle of the fall speed class j , and N is the total number of detected raindrops.

The diameter and fall speed of raindrops was also used to estimate the time-specific kinetic energy KE_{time} [$\text{J m}^{-2} \text{h}^{-1}$] (e.g. Usón and Ramos, 2001):

$$\text{KE}_{\text{time}} = \sum_{i=1}^{21} \text{KE}_{\text{time}}(D_i) \quad (5.12)$$

with

$$\text{KE}_{\text{time}}(D_i) = \frac{\rho \pi}{12A\Delta t} \sum_{j=1}^{20} n_{ij} v_j^2 D_i^3 \quad (5.13)$$

where ρ is the water density ($10^{-6} \text{ kg mm}^{-3}$), n_{ij} is the number of detected raindrops in the size class i and fall speed class j , which is measured during the interval $\Delta t = 1/60 \text{ h}$, v_j [m s^{-1}] is the fall speed of the raindrops at the middle of the fall speed class j , A [m^2] is the detection area, and D_i [mm] is the drop diameter at the middle of the size class i .

Power law $KE_{\text{time}}-R$ relationships were obtained based on data from all the 35 events recorded, and also provided for individual rainfall events.

The rainfall kinetic energy can also be estimated in terms of volume-specific rain kinetic energy KE_{mm} [$J\ m^{-2}\ mm^{-1}$], which is obtained by the ratio of KE_{time}/R , see Chapter 9 (section 9.2.2.). Nevertheless, as stated by Salles et al. (2002) estimating $KE_{\text{mm}}-R$ relationships produces erroneous results from a statistical point of view, as relating KE_{mm} to R would be equivalent to relating the ratio KE_{time}/R to R ; the KE_{mm} were hence not studied in this chapter.

The sub division of data into different rain rate classes allows to study drop characteristics (diameter and fall speed) at different rain rates, see e.g. Coutinho and Tomás (1995), Nzeukou et al. (2004), and Islam et al. (2012). Eight rain rate classes were defined such that the width of the range, increases in a roughly exponential manner (Table 9) (Harikumar et al., 2009)

Table 9. Definition of rain rate class intervals.

Class	Class interval (mm h⁻¹)	Total number of 1-min records
R1	$0.2 < R$	2003
R2	$0.2 \leq R < 0.5$	1544
R3	$0.5 \leq R < 1$	1723
R4	$1.0 \leq R < 2$	2283
R5	$2.0 \leq R < 5$	2929
R6	$5 \leq R < 10$	1204
R7	$10 \leq R < 20$	437
R8	$R \geq 20$	198

5.3. Results and discussion

The results on the variability of raindrop characteristics are given in three sections: drop size (section 5.3.1), drop fall speed (section 5.3.2), and rainfall kinetic energy (section 5.3.3).

5.3.1. Characterization of drop size

Figure 19a shows the mass-weighted mean drop diameter (D_m) and the maximum drop diameter for the 35 rainfall events. The D_m varied from roughly 0.6 to 1.7 mm, whereas the maximum drop diameter varied from 4 to 8 mm. Despite the wide spread of the data points, the coefficient of variation of drop diameter seems to be directly related to D_m , i.e. events with higher D_m have a higher coefficient of variation of diameters (Figure 19b).

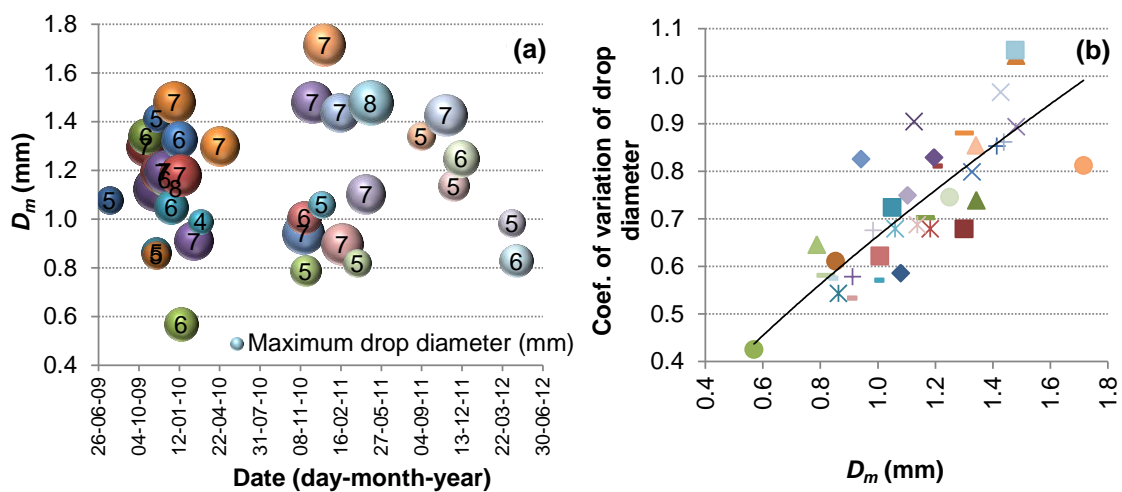


Figure 19. (a) D_m (mass-weighted mean diameter) for the 35 rainfall events; the dots are scaled according to the maximum drop diameter recorded in each event. (b) D_m plotted against the coefficient of variation of drop diameter. The fit line is indicative of the tendency in the data.

The intra-event variability of drop sizes was also assessed. Figure 20 shows examples of time series of drop size (minimum and maximum diameter, and mass-weighted mean diameter), and rain rates; rainfall events were selected from the Table 8 (event 8, 12 and 19) as their 1-min maximum rain rate was particularly higher, from 59 to 174 mm h⁻¹. Please note that in Figure 20 (and Figure 25), event 12, there are not periods of time without rain, although some instants have very low rain rates (around 1 mm h⁻¹). The figure suggests a tendency for the mass-weighted mean diameter to increase with the increasing of the rain rate, so in the next step this relationship will be explored.

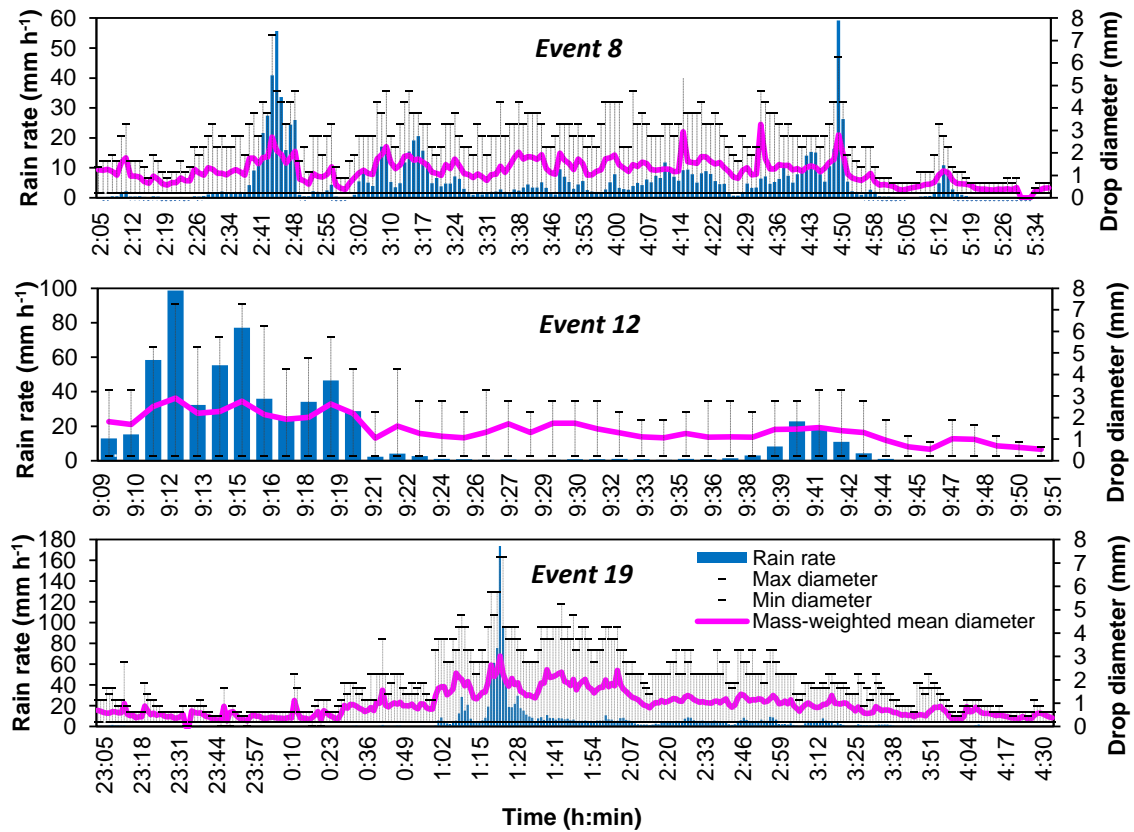


Figure 20. Time series of drop size and rain rate for three rainfall events. Since disdrometers can not measure the very small drops, the minimum diameter measured is truncated at 0.125 mm.

In Figure 21, the R is plotted as a function of D_m in a log scale in order to accommodate their large variation. Figure 21a shows the scatterplot of the rainfall events 8, 12 and 19 (the same as Figure 20) fitted with power laws. For the three rain events the Spearman's rho is higher than 0.80 and there is enough statistical significance to reject the null hypothesis of no correlation.

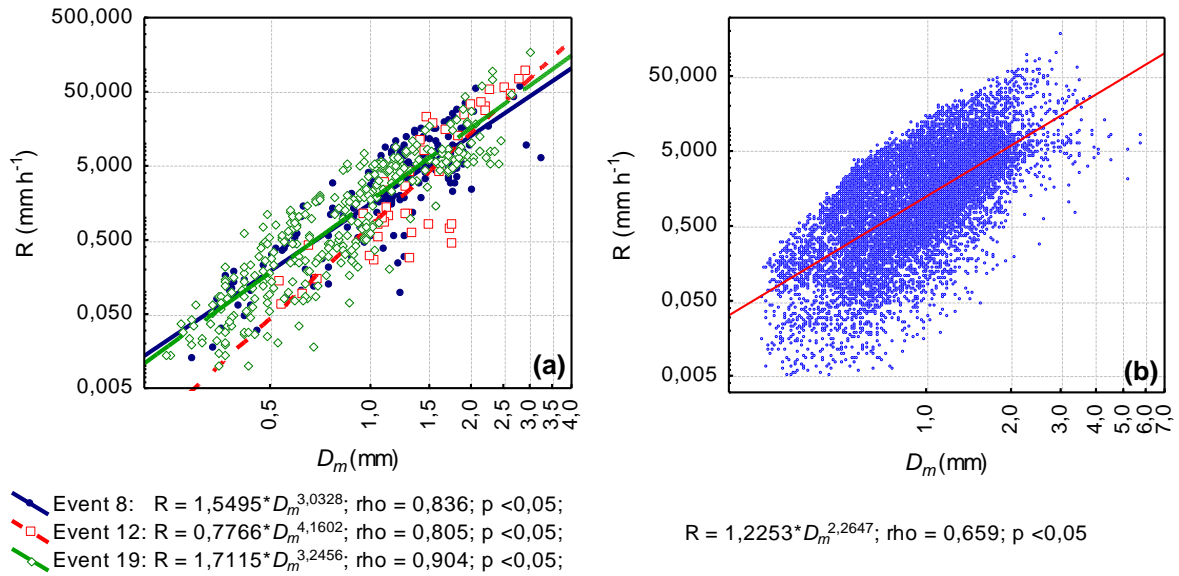


Figure 21. D_m -R relationships fitted with power law equations based on data from: (a) the individual rainfall events 8, 12 and 19; (b) all the 35 rainfall events. The Spearman's rho is reported.

A similar relationship between D_m and R was used to characterize the rainfall based on data from all the 35 rainfall events (Figure 21b). D_m is not able to explain all observed variability of the rain rate, $\rho = 0.66$, which is acceptable as the attempt is to explain the rain rate variability over 12321 minutes using one single parameter estimated from each raindrop size spectra.

As the mass-weighted mean diameter provides limited information on drops properties, other statistics need to be studied, such as the drop size distribution. Figure 22a to Figure 22c illustrates the raindrop size distributions for the rainfall events 8, 12 and 19. The variation of the DSD is observed not only from event to event but also across a specific rain event (Figure 22a to Figure 22c, grey dots). The drop size distribution for a whole event (Figure 22a to Figure 22c, black triangles) was generated by averaging the total number of rain drops in each size class recorded at 1-min resolution. The gamma distribution was adjusted to the data, see parameters in Table 10 estimated based on the method of moments; the Pearson's r correlation coefficients were determined to measure the goodness-of-fit.

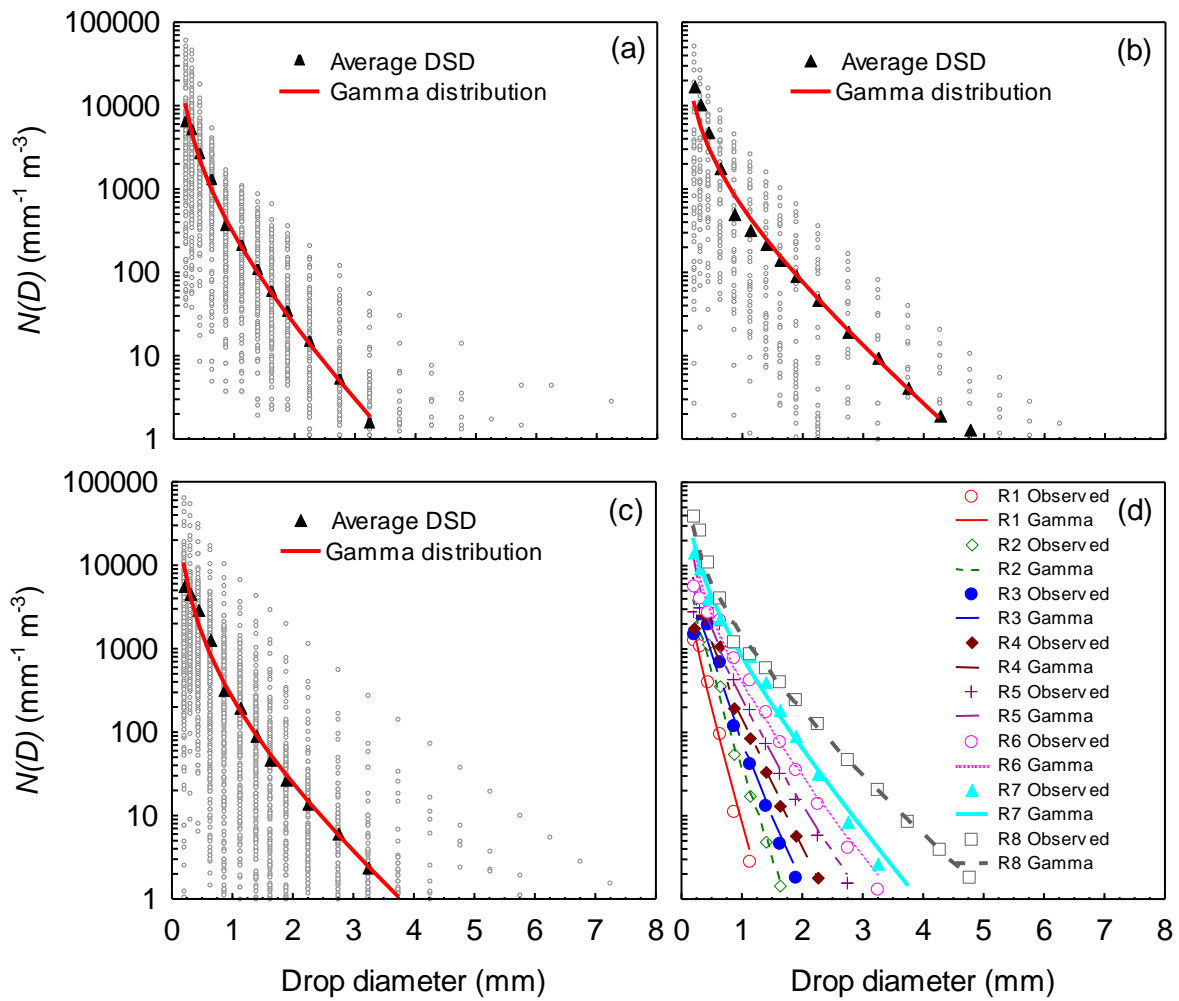


Figure 22. Empirical raindrop size distributions fitted with gamma distributions for: (a) event 8; (b) event 12; (c) event 19; (d) 8 rain rate classes obtained from the entire data set (35 rainfall events), defined in Table 9.

Table 10. Parameters of the gamma distribution used for modeling the DSD illustrated in Figure 22 and skewness of the distribution. Pearson's r correlation coefficients are indicated.

Rain event	Rain rate classe	Average number of drops	Coef. of gamma distribution			Skewness	r
			μ	Λ (mm ⁻¹)	N_0 (mm ^{-1-μ} m ⁻³)		
Event 8	-	1153	-1.45	1.48	1242.8	3.90	0.943
Event 12	-	2390	-1.13	1.29	2189.2	3.62	0.990
Event 19	-	1217	-1.65	1.21	860.2	4.12	0.922
All events (35)	R1	180	-0.62	5.46	1951.0	2.57	0.930
	R2	371	-0.50	4.64	4081.8	2.75	0.836
	R3	540	-0.88	3.49	2714.6	3.06	0.708
	R4	709	-0.83	3.02	3186.4	3.05	0.731
	R5	1068	-1.48	1.90	1667.0	3.80	0.734
	R6	1475	-1.47	1.59	2005.6	3.89	0.921
	R7	2574	-1.10	1.77	4785.1	3.46	0.990
	R8	5355	-1.17	1.30	5502.2	3.69	0.985
All events	-	858	-1.72	1.46	781.1	4.06	0.842

The variation of drop distribution as a function of rain rate is also explored. The next step consists in taking the whole data set (the 35 rainfall events) and trying to fit gamma distributions to the empirical raindrop size distributions obtained according to different ranges of R (see Table 9).

As expected the variation of DSD gamma parameters are clearly dependent on rain rate classes (Figure 22d, Table 10). The narrower DSD (and lower skewness, 2.57) correspond to lower values of R, i.e. class R1, which indicates lesser concentration of large drops. As the value of R increases (from R1 to R8), the concentration of large drops per unit of volume, $N(D)$, also increases. The gamma DSD model showed smaller shape parameters (μ), and higher slope parameters (Λ) for lower rain rates, e.g. R2, and the opposite, i.e. higher μ , and smaller Λ , for higher rain rates, e.g. R5. Note that the gamma distribution reduces to the exponential distribution when $\mu = 0$; in this study for all rain rate classes the μ is negative, which means the DSD is concave upward on a semilogarithmic plot. The highest concentrations of drops were hence found for the minimum drop size classes, <0.50 mm.

5.3.2. Characterization of drop fall speed

Within certain limits, raindrop fall speed increases with an increase in drop size. Figure 23 shows the total number of drops as a function of drop diameter and drop fall speed obtained by averaging rain drops in each size and fall speed classes over the 8 rain rate classes, and the 35 rain events. The laboratory measurements of drop terminal velocities by Gunn and Kinzer (1949) in stagnant air (pressure of 760 mm, temperature of 20°C, and relative humidity of 50%) are also shown as a reference.

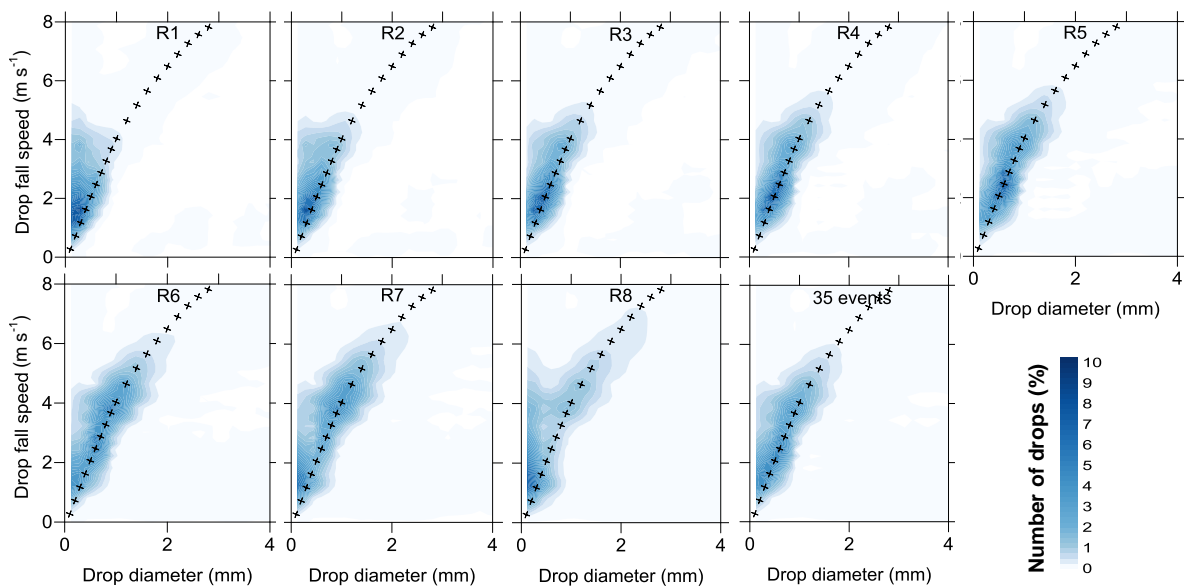


Figure 23. Total number of drops as a function of drop diameter and drop fall speed for 8 rain rate classes and the 35 rain events. The Gunn and Kinzer (1949) measurements are represented (with crosses) as a reference.

In general, the observed diameter-fall speed relationship followed the Gunn-Kinzer measurements, but for some rain rate classes, e.g. R1 and R8, it is clear the spread of fall speeds of smaller drops; in fact, for the drops with diameters lower than 1 mm the observed fall speeds tend to be higher than the corresponding Gunn-Kinzer measurements. For all the eight rain rate classes, the highest concentration of drops had diameters smaller than 2 mm, which is consistent with drop size distributions shown in the section 5.3.1, and fall speeds

lower than 5 m s^{-1} . The following analysis will focus on the characterization of drop fall speeds of the 35 rainfall events.

The mean drop fall speed of all observed rainfall events is shown in Figure 24a and it ranges from 2.0 to 3.0 m s^{-1} ; in particular, the majority of the events (80%) have a v_m between 2.4 and 2.8 m s^{-1} . The variability of the drop fall speed for all rainfall events is illustrated in Figure 24b by the coefficient of variation, ranging from 0.37 to 0.66. It does not seem to have a direct relationship between v_m and the variation coefficient of drop fall speed, i.e. events with higher v_m are not necessarily the ones with higher coefficient of variation.

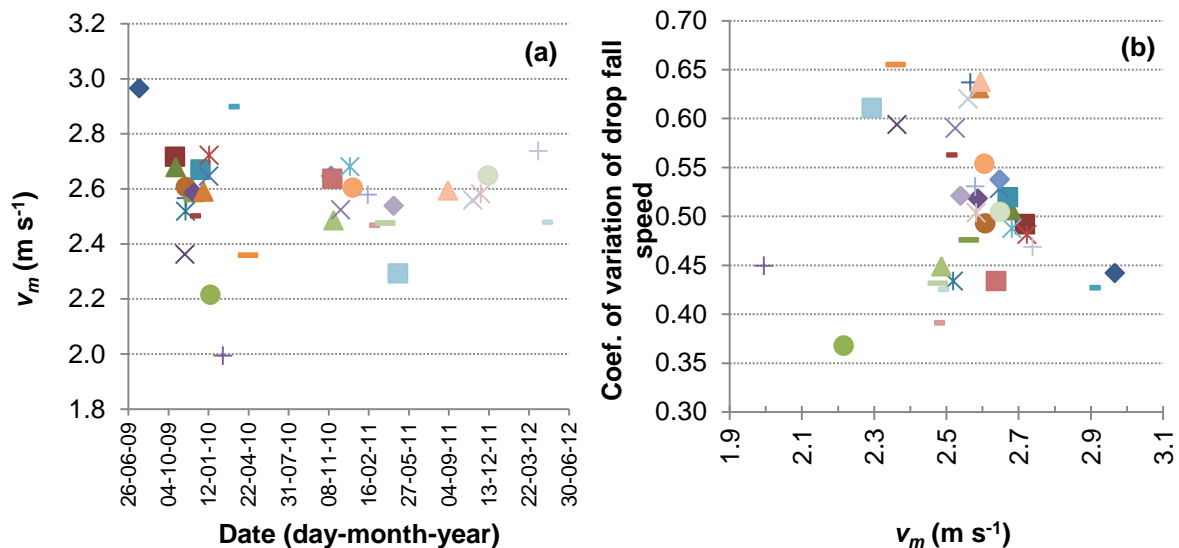


Figure 24. (a) v_m (mean raindrop fall speed) for the 35 rainfall events; (b) v_m plotted against the coefficient of variation of drop fall speed.

Using the same three events studied before in drop size analysis, Figure 25 shows the time series of drop fall speed (mean, minimum and maximum) and rain rate with 1-min resolution. The v_m shows some fluctuations during the whole event that occurs without an evident correlation with the rain rate variation (see also Figure 26). For example, in the event 12 at the time of the highest rain rate (98.6 mm h^{-1} , recorded at 09:12), the v_m (2.3 m s^{-1}) for that 1 minute interval was lower than the mean fall speed for the whole event (2.7 m s^{-1}).

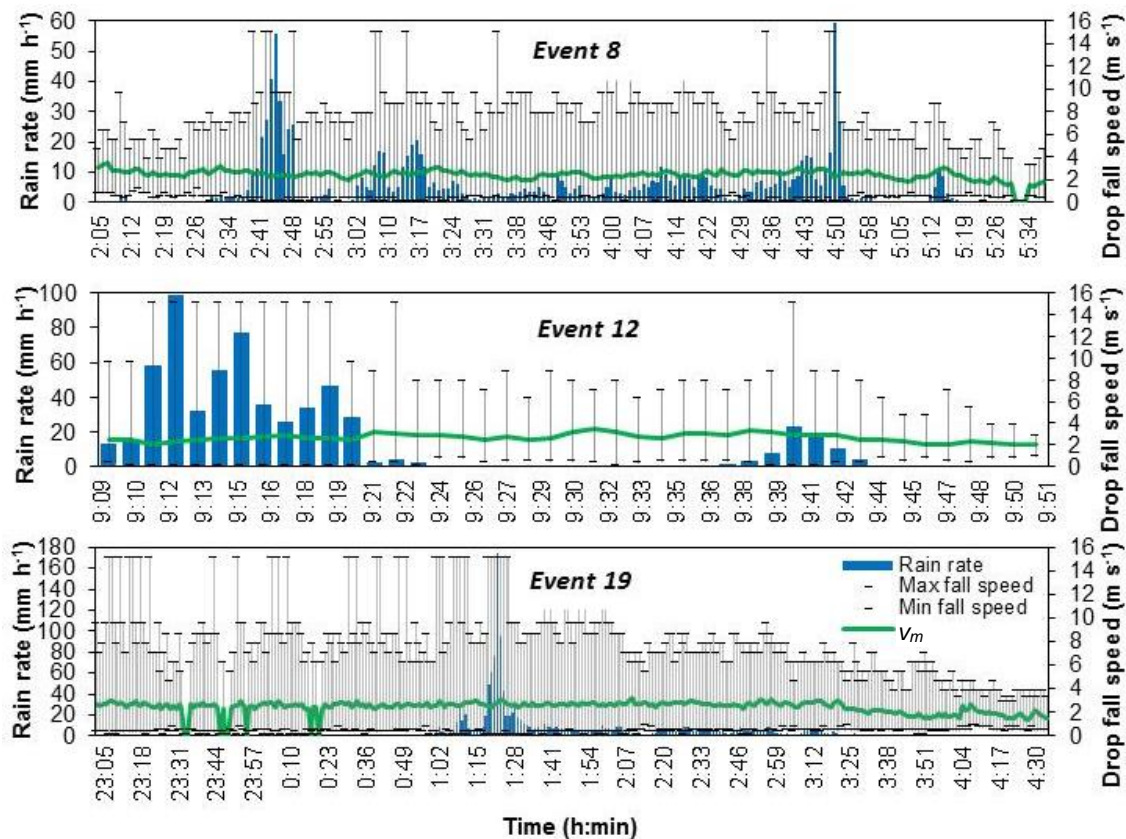


Figure 25. Time series of drop fall speed and rain rate of the rainfall events 8, 12 and 19.

In order to understand the relation between the drop fall speed and the rain rate, this time for all studied rainfall events, in Figure 26 v_m was plotted against R . The v_m seems not to be related with the rain rate ($\rho = 0.292$). It is common knowledge that larger drops fall faster than smaller ones, and as noticed before higher rain rates indicate increased concentration of large drops. However, despite this fact, the existence of a great amount of small drops might explain the low values of mean fall speeds, when the rain rates and the concentration of large drops are the highest. In Figure 27 the absolute frequency of raindrop fall speed is shown for the 8 rain rate classes by averaging rain drops in each fall speed classes over the rain rate class; it is possible to observe that for R8 the highest concentration of drops is for fall speeds of 1.2 m s^{-1} , whereas for lower rain rates, class R6, the highest concentration is for drops that fall quicker, 3.8 m s^{-1} .

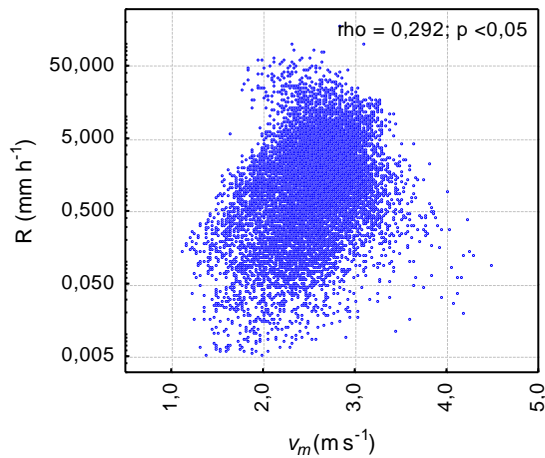


Figure 26. Mean raindrop fall speed (v_m) plotted against R based on data from all the 35 rainfall events. The Spearman's rho is indicated.

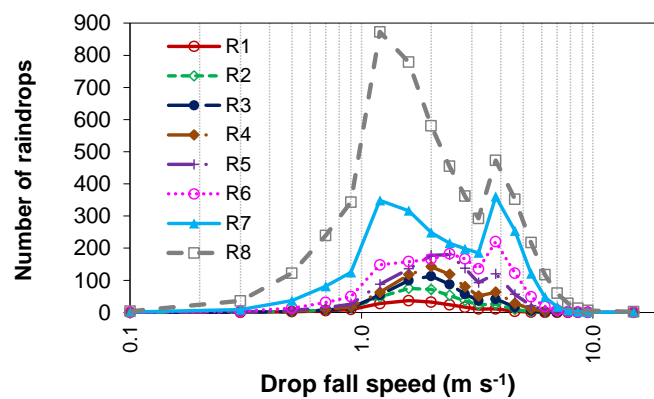


Figure 27. Absolute frequency of raindrop fall speeds for 8 rain rate classes obtained from the 35 rainfall events.

5.3.3. Characterization of rainfall kinetic energy

Here we explore the variability of rainfall kinetic energy within the individual rainfall events and from all the 35 rainfall events. Figure 28 shows the hyetograph and the time-specific kinetic energy of rain event 8. In the figure it is observed that as the rain rate increases so does the kinetic energy.

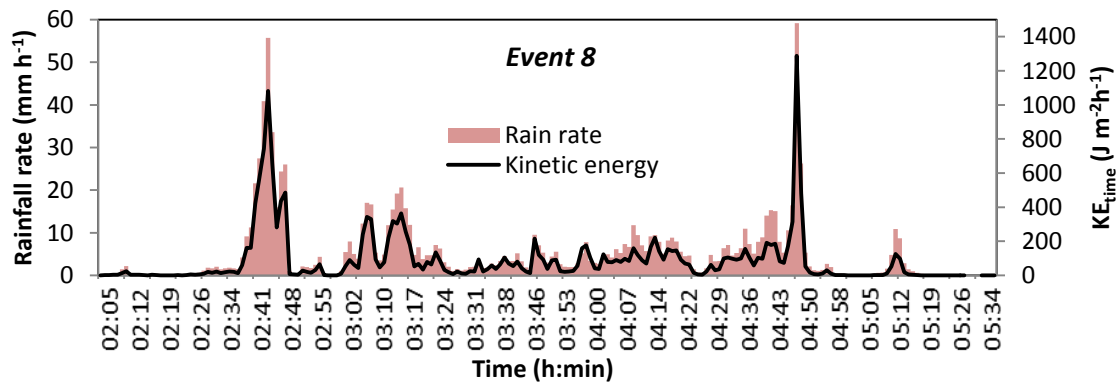


Figure 28. Hyetograph and time-specific kinetic energy of the rainfall event 8.

To investigate the correlation between kinetic energy and rain rate, KE-R relationship was plotted for the three rainfall events (Figure 29a). Power laws fitted well the data. Figure 29b (dash line) confirms that type of relation based on the data from all the 35 rainfall events; indeed, the KE-R relationship follows the power law, $KE=aR^b$, where $a = 7.4246$ and $b = 1.2476$.

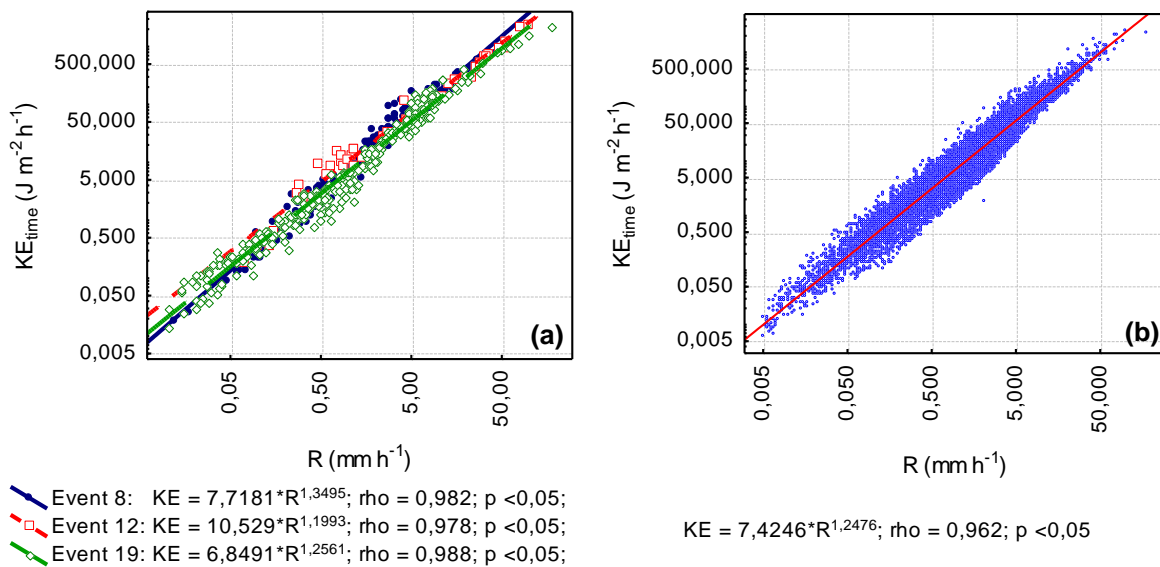


Figure 29. KE_{time} -R relationship based on data from: (a) the rainfall events 8, 12 and 19 (b) all the 35 rainfall events. Power laws are fitted to the data.

The kinetic energy is estimated based on drop size (and drop fall speed) measurements (see Eq. 5.13). When relating the volume-weighted mean diameter to the kinetic energy, the power

law function fitted well $KE-D_m$ relationship (Figure 30). Nevertheless, because of the natural variations of raindrop characteristics, the estimation of the kinetic energy from the $KE_{\text{time}}-D_m$ relationship is limited ($\rho = 0.813$).

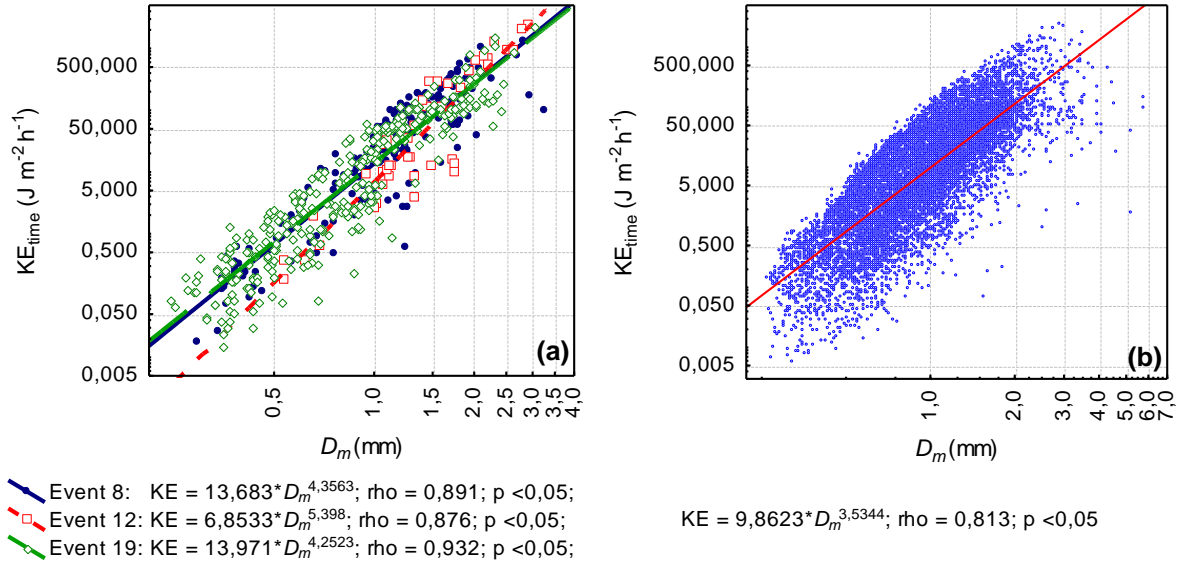


Figure 30. $KE_{\text{time}}-D_m$ relationship based on data from: (a) the rainfall events 8, 12 and 19 (b) all the 35 rainfall events. Power laws are fitted to the data.

5.4. Concluding remarks

The study provided information on the variability of rain rate, kinetic energy and raindrop characteristics (diameter and fall speed) for single event scale and based on data from all the 35 events recorded in Coimbra from July 2009 to June 2012, in order to attempt the estimation of relationships between these rainfall parameters.

In relation to the characterization of drop sizes, it was observed noticeable differences between the events; for example, events with the same mean rain rate differ in the maximum size recorded and the dispersion of drops diameter. Nevertheless, the variability of mass-weighted mean diameter is reflected in the rain rate; power laws fitted well the relationships between D_m and rain rates. Detailed analysis of data comprised the parameterization of raindrop size distributions by using the gamma distribution, whose parameters varied with

rain rate classes; in the case of lower rain rates, e.g. $< 2 \text{ mm h}^{-1}$, the distribution was characterized by a large number of small to medium sized drops $< 2.5 \text{ mm}$, whereas higher rain rates indicated increased concentration of larger drops, from 2.5 to 5 mm.

Unlike the raindrop sizes, analysis of the drop fall speeds revealed that the mean fall speed did not increase progressively with the rain rate. The existence of a great amount of small drops, which fall with less velocity, is likely to explain the low values of mean fall velocities, even when the rain rates and the concentration of large drops are the highest.

The relationship between rain rate and kinetic energy was well described by power laws. This might be explained as both rainfall rate and kinetic energy are estimated based on the number of drops and their size. Moreover, power laws also fitted well $\text{KE}-D_m$, despite the natural variations of raindrop characteristics.

6. INVESTIGATING ANNUAL AND MONTHLY TRENDS IN PRECIPITATION STRUCTURE: AN OVERVIEW ACROSS PORTUGAL²

Abstract

This work investigates recent changes in precipitation patterns manifested in long annual and monthly precipitation time series recorded in Portugal. The dataset comprises records from 14 meteorological stations scattered over mainland Portugal and the Portuguese North Atlantic Islands of Madeira and Azores; some of the time series date back to the 19th century. The data were tested for trends using the Mann-Kendall non-parametric test and Sen's non-parametric method, searching both for full monotonic trends over the record period and for partial trends. Results provide no evidence for rejecting the null hypothesis of no trend in annual precipitation, when a monotonic linear model was used. Nevertheless, the analyses of 50 years' moving averages showed an increase over time, in the recent past, for many of the series in mainland Portugal and the Islands. For the longest time series this behaviour was preceded by a decrease over time. The analyses of partial trends in the time series suggested a sequence of alternately decreasing and increasing trends in annual and monthly precipitation, which are sometimes statistically significant. The trend changing points were identified.

² de Lima, M.I.P., Carvalho, S.C.P., de Lima, J.L.M.P. 2010. Investigating annual and monthly trends in the precipitation structure: an overview across Portugal. *Natural Hazards and Earth System Sciences* 10, 2429–2440.

6.1. Introduction

Variations in precipitation over daily, seasonal, annual, and decadal time-scales have an impact on water balances. Thus it is important to understand the recent changes in precipitation patterns as part of the long term behaviour of this process, e.g. to predict changes in other hydrological processes. For these studies, one limiting factor is the short length of many existing precipitation records and the spatial representativeness of the available data. Thus, the majority of the studies on this topic are based on relatively short time series, covering a few decades, over periods of about 40–50 years. Only a few studies report results for longer periods, essentially covering the 20th century as a whole. The fact that many studies may be reporting different results highlights the need for further insight into both empirical findings, based on point precipitation data analyses, and numerical models of climate change projection. Several studies of precipitation trends over the Mediterranean Basin and the Iberian Peninsula are reported in Lionello et al. (2006).

This study aims at improving our understanding of the dynamics of precipitation and of the recent changes in this process over the Portuguese territory. It complements previous studies for mainland Portugal which have reported high variability in the precipitation regime and discussed recent patterns of change. Among these studies are: Corte-Real et al. (1998), Goodess and Jones (2002), de Lima et al. (2007, 2010b), Rodrigo and Trigo (2007), Durão et al. (2009), Mourato et al. (2010). There are also projections for the future behaviour of this process over the territory including Miranda et al. (2002, 2006) and López-Moreno et al. (2009). For example, Miranda et al. (2006) predict that the annual precipitation in mainland Portugal will decline within the range of 20 to 40% by the end of the 21st century. Climate change scenarios in the Portuguese North Atlantic Archipelagos of Madeira and Azores are discussed by e.g. Santos et al. (2004). Nevertheless, the characterization of precipitation in these archipelagos has been less studied than that in mainland Portugal. In particular, the problem of fluctuations in precipitation variability over time has not been fully explored yet for these islands.

The work reported here investigates annual and monthly precipitation records that include the longest time series available for Portugal that we are aware of. The data are from 14 meteorological stations in mainland Portugal and in the Madeira and Azores island groups. The study focused on the presence of linear monotonic trends in the temporal structure of precipitation over the record period and over sub-periods (i.e. partial trends). Trends were examined using the Mann-Kendall non-parametric test and Sen's non-parametric method. Partial trends were investigated using the method proposed by Tomé and Miranda (2005), with a view to performing a piecewise linear fitting to climate data and to detecting the associated trend change points.

6.2. Study area and precipitation data

This work examines 14 long precipitation data sets from mainland Portugal and the Portuguese North Atlantic Archipelagos of Madeira and Azores. The data were obtained by the Institute of Meteorology (IM) and the Institute for Water (INAG), of Portugal, and have annual and monthly resolutions. Some of the time series date back to the 19th century, spanning periods that range between 88 and 145 years. The first records are from 1863. The location of the precipitation measuring sites is shown in Figure 31 and Table 11: ten sites are in mainland Portugal and four are in the islands. Three sites are located in the Azores, specifically on the islands of Faial, Terceira and S. Miguel, and the fourth site is on Madeira Island. Table 11 also presents some descriptive statistics for the annual time series.

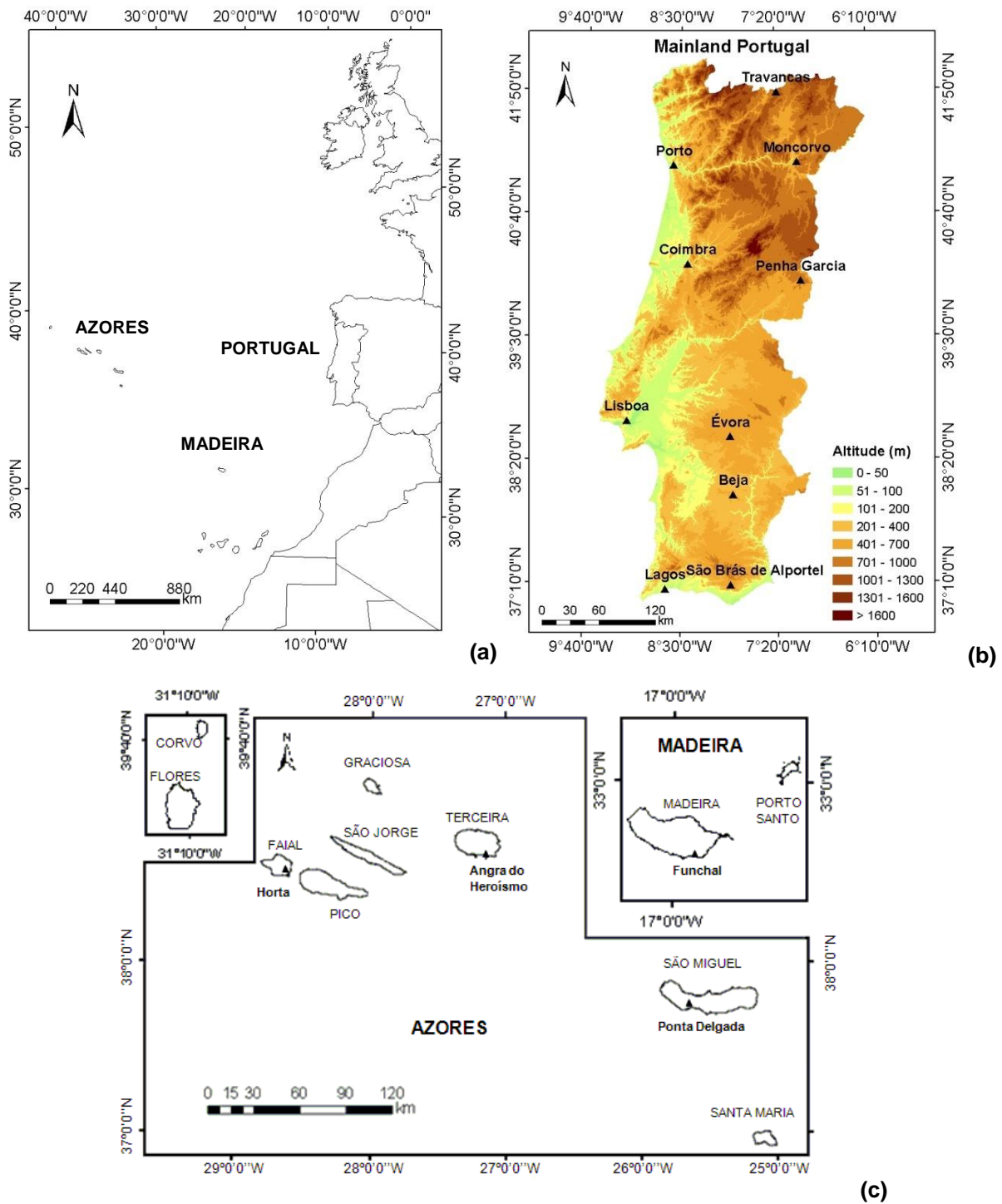


Figure 31. Study area: (a) location of mainland Portugal and the Madeira and Azores archipelagos; (b) location of ten precipitation measuring stations in mainland Portugal; (c) location of four precipitation measuring stations in the Madeira and Azores archipelagos.

Table 11. Identification of the precipitation measuring sites and some descriptive statistics for the annual time series.

	Measuring Station (Code)	Latitude (N)	Longitude (W)	Altitude (m)	Period	Annual precipitation			
						Mean (mm)	Coef. of Variation	Max. (mm)	Min. (mm)
Mainland Portugal	Travancas (03N-01G)	41°50'	07°18'	884	1914-2006	985	0.252	1636	499
	Moncorvo (06O-04UG)	41°10'	07°03'	385	1878-1995	569	0.263	1095	253
	Porto (546)	41°08'	08°36'	93	1863-2007	1237	0.251	2255	604
	Coimbra (549)	40°12'	08°25'	141	1900-1998	982	0.216	1651	524
	Penha Garcia (13O-01UG)	40°03'	07°01'	495	1911-1998	808	0.264	1597	432
	Lisboa (535)	38°43'	09°09'	77	1871-2007	733	0.250	1421	416
	Évora (557)	38°34'	07°54'	309	1871-2007	629	0.253	1186	346
	Beja (562)	38°01'	07°52'	246	1900-2007	563	0.246	1042	301
	São Brás de Alportel (31J-01C)	37°10'	07°45'	325	1909-2002	837	0.306	1693	431
	Lagos (31E-01UC)	37°06'	08°40'	14	1902-2006	527	0.302	1098	187
Azores	Horta/Faial (506)	38°31'	28°38'	60	1901-1994	1020	0.168	1623	692
	Angra do Heroísmo /Terceira (511)	38°40'	27°13'	74	1865-2004	1065	0.204	1650	588
	Ponta Delgada/S. Miguel (513)	37°45'	25°40'	35	1865-1994	884	0.234	1459	432
Madeira	Funchal (522)	32°38'	16°53'	49	1865-2000	623	0.343	1419	200

Mainland Portugal lies in the transitional region between the sub-tropical anticyclone and the sub-polar depression zones, between latitudes 36°56' and 42°09' N and longitudes 6° 10' and 9°34' W. The climatic variables exhibit strong north-south and west-east gradients, and precipitation also exhibits strong seasonal variability. The dominant climate in mainland Portugal is mild Mediterranean with a warm, dry summer period. These characteristics are more pronounced in the south. The climate is greatly influenced by the latitude, the orography and the proximity of the Atlantic Ocean (see e.g. Miranda et al., 2002).

The Madeira archipelago is situated in the North Atlantic Ocean, about 900 km from mainland Europe (Figure 31). It is formed by two main islands of volcanic origin: Madeira (728 km²) and Porto Santo (42 km²). It is in the Atlantic subtropical belt under the direct influence of the Azores high pressure system. The geographical position of the Madeira archipelago is between parallels 30°01' and 33°07' N and between longitudes 15°51' and 17°15'

W. The complex topography of Madeira Island and its small size play a crucial role in the local precipitation regime, which is marked by high spatial variability (e.g. de Lima and de Lima, 2009). The winter months are quite wet, particularly at higher altitudes, and stormy and cloudy conditions may last for several days at a time.

The Azores archipelago is located in the North Atlantic ridge, between latitudes 36°45' and 39°43' N and longitudes 24°45' and 31°17' W. It comprises 9 islands of volcanic origin, in 3 groups: Western, Central and Eastern. The warm Gulf Stream and their latitudinal position affect the islands' climatic conditions. For most of the year the Atlantic depressions track across the Azores islands. The precipitation is heavier and more frequent in winter. In late spring and summer the Azores region is under the influence of the Azores anticyclone (e.g. Santos et al., 2004; Miranda et al., 2006).

6.3. Methodology

This section gives a brief overview of the methods used in the data analyses. All the methods are extensively described in the literature so there is no need to go into their details here.

Preliminary analyses of the precipitation time series included checking the data for gaps and clearly incorrect (i.e. anomalous) precipitation values. Then the data were statistically tested for normality using the Shapiro-Wilk test (e.g. Royston, 1982) and the Kolmogorov-Smirnov (e.g. Deheuvels, 1981) non-parametric tests. In the Kolmogorov-Smirnov test the p-value was computed using the analytical approximation to the test statistics of Lilliefors, proposed by Dallal and Wilkinson (1986).

The preliminary analyses were complemented with the investigation of the homogeneity of the data. Inhomogeneities in time series can result, for example, from changes in observational routines, relocation of the measuring station, and changes in station surroundings or in measurement techniques. The four tests selected to check the time series homogeneity were: Standard Normal Homogeneity Test (SNHT) (Alexandersson and

Moberg, 1997), the Buishand range test (Buishand, 1982), the Pettitt test (Pettitt, 1979), 1979), and the Von Neumann ratio test (von Neumann, 1941). All tests but the Pettitt test are parametric. The Pettitt test is based on the ranks of the elements of a series rather than on the values themselves (Pettitt, 1979). It can be very useful to apply more than one statistical test when it comes to detecting inhomogeneities in time series (e.g. Wijngaard et al., 2003; Costa and Soares, 2009).

All the homogeneity tests assume as null hypothesis that the variable tested is independent and identically distributed. In the SNHT, Buishand range and Pettitt tests the alternative hypothesis is associated with the existence of deviations in the mean, whereas the Von Neumann ratio test assumes that the distribution is not random. This last test is the only one that cannot locate the change-point. But the sensitivity of these tests to detect the break differs: the SNHT is better at identifying breaks near the beginning and the end of a series, whereas the the Buishand range and the Pettitt tests identify the breaks in the middle of a time series more easily (Hawkins, 1977).

With respect to their homogeneity, the precipitation time series were assembled in categories based on the classification used by Wijngaard et al. (2003). Therefore, the precipitation series were classified as “useful”, “doubtful” and “suspect”, depending on the number of tests that rejected the null hypothesis at the 1% significance level. This classification amounts to a qualitative assessment of the adequacy of the time series to conduct trend and variability analyses.

The presence of trends in the precipitation time series was examined using the Mann-Kendall non-parametric test (e.g. Gilbert, 1987) and Sen’s non-parametric method (Sen, 1968; Gilbert, 1987). The Mann-Kendall test is useful if the possible trend in a time series can be considered monotonic; moreover, the time series should not be characterized by seasonality. The null hypothesis, H_0 , of no trend assumes that the observations are randomly ordered in time and is tested against the alternative hypothesis, H_1 , associated with increasing or decreasing monotonic trends. In this work the null hypothesis is tested at the 10, 5, 1 and 0.1% significance levels; the test is taken in its two-sided form (see e.g. Sneyers, 1990). Sen’s

estimator can be used for estimating the change per unit time in time series that exhibit linear trends.

The method described in Tomé and Miranda (2005) was used to deal with the non-monotonic character of trends in the data. This method was built based on a study developed by Karl et al. (2000) about global warming changes and corresponds to an extension of the method proposed in Tomé and Miranda (2004). The methodology aims at fitting an unknown number of continuous straight-line segments to a time series and at detecting the trend change-points. The number and location of the breakpoints are optimized simultaneously. Thus, the method searches for such segments that best fit the data, in a least-squares sense, while satisfying a pair of conditions: a minimum time distance between breakpoints and a minimum trend change at each breakpoint. The conditions imposed in our study are explained below.

6.4. Results and discussion

6.4.1. Analysis of annual precipitation

This section first presents the results of the preliminary analyses of the annual data and afterwards the results of the trend analyses.

The statistics for the Shapiro-Wilk and Kolmogorov-Smirnov tests for normality applied to the annual precipitation time series are given in Table 12. The statistics provided evidence to reject the null hypothesis of normality for the data from Horta and São Brás de Alportel. Even though normality is a pre-condition for some of the subsequent tests of homogeneity, the tests are applied to all the data sets. However, one should keep in mind that the results of the normality and homogeneity testing of the precipitation time series might affect the validity of the conclusion of the subsequent trend tests (below) and should be carefully taken into account.

Table 12. Statistics of the Shapiro-Wilk and Kolmogorov-Smirnov tests for normality, applied to the annual precipitation time series. The results in bold indicate which series have normal distributions for a 5% significance level. The * mark indicates that the result is a lower bound of the true significance. The classification of the time series as ‘useful’, ‘doubtful’ and ‘suspect’ is based on the results of the homogeneity tests, as proposed by Wijngaard et al. (2003).

	Measuring Station	Period	Normality tests		Classification based on homogeneity tests
			Shapiro-Wilk	Kolmogorov--Smirnov	
Mainland Portugal	Travancas	1914-2006	0.159	0.200*	Useful
	Moncorvo	1878-1995	0.029	0.200*	Useful
	Porto	1863-2007	0.013	0.200*	Useful
	Coimbra	1900-1998	0.148	0.200*	Useful
	Penha Garcia	1911-1998	0.010	0.079	Useful
	Lisboa	1871-2007	0.001	0.091	Useful
	Évora	1871-2007	0.011	0.200*	Useful
	Beja	1900-2007	0.037	0.200*	Useful
	São Brás de Alportel	1909-2002	0.001	0.015	Useful
	Lagos	1902-2006	0.008	0.200*	Useful
Azores	Horta (Faial)	1901-1994	0.001	0.017	Useful
	Angra do Heroísmo (Terceira Island)	1865-2004	0.406	0.048	Doubtful
	Ponta Delgada (S. Miguel Island)	1865-1994	0.834	0.200*	Suspect
Madeira	Funchal (Madeira)	1865-2000	0.008	0.200*	Useful

The outcomes of the four homogeneity tests (SNHT, the Buishand range test, the Pettitt test and the Von Neumann ratio test) yielded the classification for each precipitation series that is presented in Table 12. Although almost all data sets are classified as “useful”, results indicate that some time series may not be homogeneous over the full record period. Two time series were not classified as “useful”: the data from Ponta Delgada are classified as “suspect” and the data from Angra do Heroísmo are classified as “doubtful”. It was not possible to explain these behaviours from the existing metadata. Taking into consideration the results of the normality tests for the time series from São Brás de Alportel and Horta, the tests for homogeneity might be considered inconclusive; the data sets were classified as “useful”. Thus, for some time series the results of the trend analysis over the full period should be

interpreted cautiously. But for the sub-periods considered in the partial trends analyses, all the precipitation series are classed as “useful”.

Results of the annual precipitation trend analyses are given in Table 13 and Figure 32. This figure shows the annual time series for selected locations, the monotonic linear trend fitting to the data and the partial trends identified using the method described in Tomé and Miranda (2005). Table 13 gives the results of the trend analysis for the full record period and for two selected contiguous periods having distinct behaviour. The statistical significance of the results was assessed using the Mann-Kendall test. Over the full time span of the records there was no evidence to reject the null hypothesis of no trend in annual precipitation at any of the stations from mainland Portugal. For the Azores, the results indicate a decrease of 19 mm decade⁻¹ in the annual precipitation from Horta (Faial Island). But this result could be biased, taking into consideration the results of the normality and homogeneity tests discussed above. Because the other time-series from the Azores were not found to be homogeneous over the full period of the records they were not tested for trends over that period. For Funchal (Madeira Island), results show a reduction in annual precipitation of about 10.5 mm decade⁻¹ over the record period.

Table 13. Sen's estimator of the slope (mm decade⁻¹) of monotonic and partial trends of the annual precipitation, as well as for the trends in the 50-year moving average series. The confidence levels for the trend tests are marked: ⁺90%, *95%, **99% and ***99.9%. The periods selected for partial trends were based on breakpoints located using the methodology described by Tomé and Miranda (2005). The 50-year moving average series were taken to be centred on the corresponding period. NH identifies series that were not considered homogeneous.

Measuring Station	Monotonic Trends		Partial Trends		50-years moving average		
	Period	(mm dec ⁻¹)	Period	(mm dec ⁻¹)	Period	(mm dec ⁻¹)	
Mainland Portugal	Travancas	1914-2006	-4.32	1940-1960 1960-1981	164.67 -78.80	1937-1980	-4.57**
	Moncorvo	1878-1995	-3.78	1945-1965 1965-1989	164.60** -25.30	1902-1931 1932-1970	-15.85*** 1.75 ⁺
	Porto	1863-2007	-3.35	1947-1967 1967-2002	222.33 52.88	1887-1926 1927-1982	-23.52*** 25.37***
	Coimbra	1900-1998	-1.75	1946-1966 1966-1992	204.85 -68.71	1924-1973	7.45***
	Penha Garcia	1911-1998	-5.64	1945-1965 1965-1993	140.33 ⁺ -56.33	1934-1972	-7.25***
	Lisboa	1871-2007	-2.61	1933-1963 1963-1983	70.54 ⁺ -74.40	1895-1928 1929-1982	-21.02*** 11.46***
	Évora	1871-2007	-3.78	1942-1981 1981-2001	-8.23 44.83	1895-1982	-1.15*
	Beja	1900-2007	-2.92	1933-1961 1961-1981	67.28 -66.31	1924-1982	9.38***
	São Brás de Alportel	1909-2002	12.78	1935-1962 1962-1982	75.60 -139.24	1933-1977	23.10***
	Lagos	1902-2006	7.15	1941-1961 1961-1981	116.67 ⁺ -105.11 ⁺	1926-1981	18.52***
Azores	Horta	1901-1994	-19.00**	1947-1967 1967-1994	-70.40 ⁺ 19.55	1925-1969	-14.69***
	Angra do Heroísmo	1865-2004	NH	1944-1964 1964-1992	-5.89 -35.69	n.a.	n.a.
	Ponta Delgada	1865-1994	NH	1923-1943 1943-1989	200.46** 4.30	n.a.	n.a.
Madeira	Funchal	1865-2000	-10.49*	1950-1970 1970-2000	231.00*** -32.68	1889-1942 1943-1975	-30.65*** 8.74***

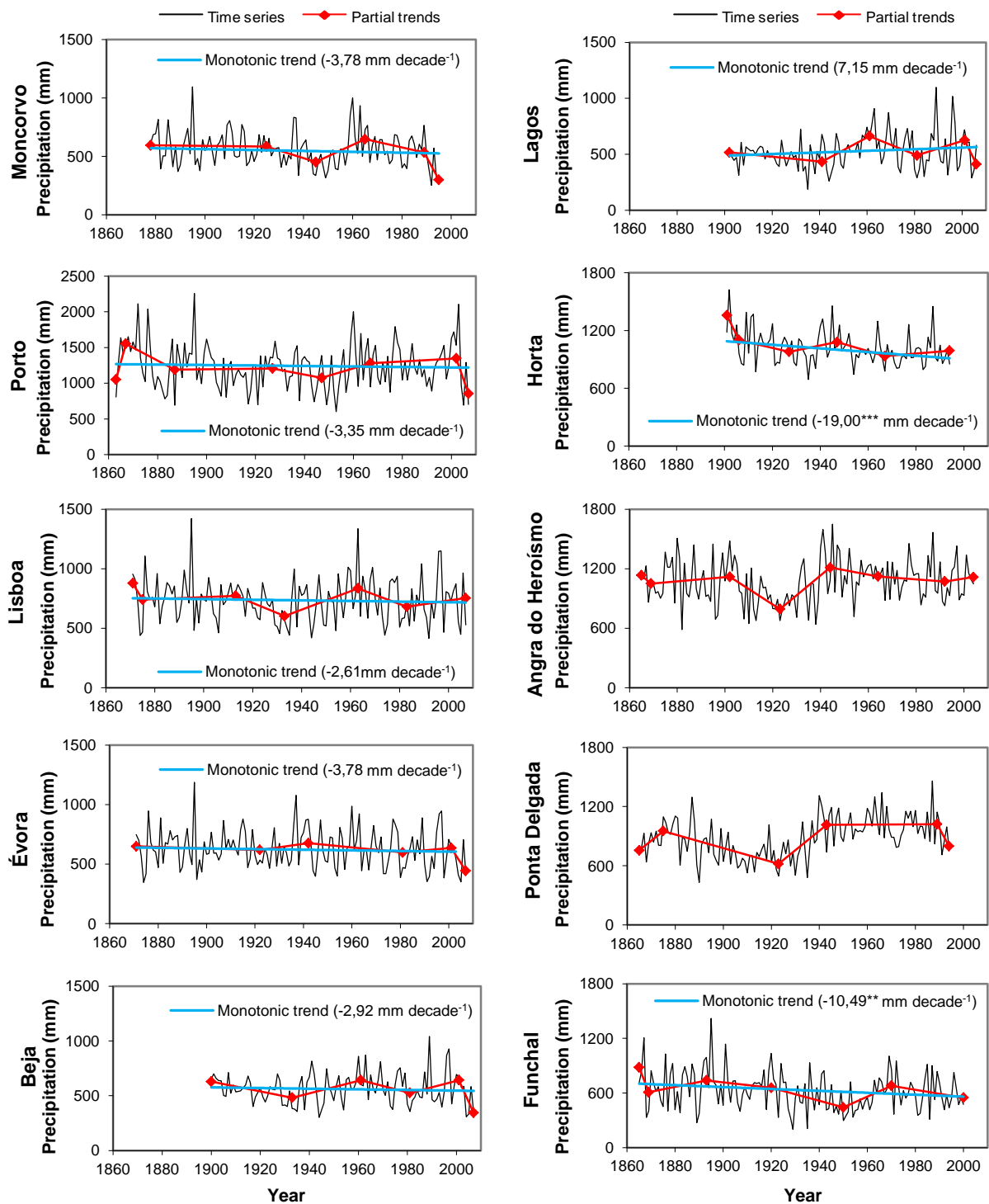


Figure 32. Annual precipitation series for six stations in mainland Portugal and four stations in the islands. Sen's estimator of the slope of monotonic trends over the full record periods (blue line) is indicated in the legend. The red line is the fit for partial trends. For better visualization, note that the Y axes scales are not the same for all the plots.

The 50-year moving average series of annual precipitation were also examined. The reason for adopting 50 years as the time-window instead of a shorter period was to reduce the impact of precipitation cycles of a few decades on the analyses. Figure 33 shows a plot of the 50-year moving average series where each data point is centred on the corresponding 50-year period. Overall, the 50-year moving average analyses suggest an increasing tendency in annual precipitation (i.e. positive trend slope) in the recent past for many of the series in mainland Portugal and the islands. For the longest time series this behaviour was sometimes preceded by a decrease over time. The rate of change observed for different sub-periods is given in Table 13; results are not given for the series that were not considered homogeneous. It is worth noting that the presence of correlation in the data may cause errors in trend analysis and frequently lead to rejecting the null hypothesis, which means that trend is accepted even in cases when it does not exist.

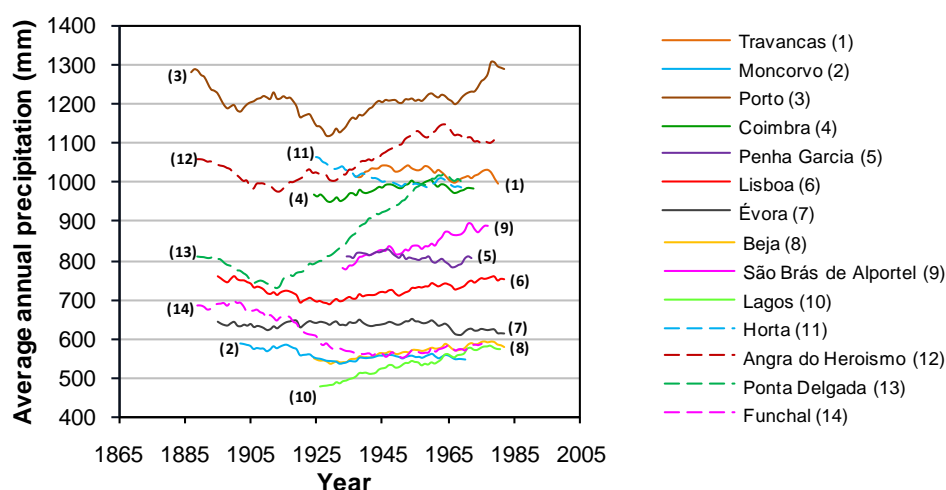


Figure 33. The 50-year moving average series of the annual precipitation from Portugal; the data from the islands are plotted with dashed lines. The data are centred on the 50-year window. See also Table 13.

Examination of the 50-year moving average data and the non-monotonic character of the behaviour observed led us to investigate partial trends in precipitation. For that purpose the method proposed in Tomé and Miranda (2005) was used. This methodology identifies times of significant change in the precipitation series. The results for annual precipitation that are

shown in Figure 32 and Figure 34 were obtained by unconstraining (in practical terms) the minimum rate of change, set at $0.01 \text{ mm year}^{-1}$, at consecutive breakpoints by imposing a minimum allowed interval of 20 years between breakpoints and a minimum allowed length of 5 years for the first and last segments. These conditions were empirically chosen based on the application examples given in Tomé and Miranda (2005) and on the examination of the data. In certain cases, these conditions may introduce some bias in the results, with the location of the breakpoints (i.e. times of significant change) in particular being affected.

Figure 34 reveals that the patterns of precipitation variation over time are not the same for all the data sets investigated. Nevertheless, results suggest that in mainland Portugal sub-periods of increasing and decreasing trends in annual precipitation occur in the records and that they alternate over time. The dominant common annual precipitation pattern is, therefore, alternating periods of increasing and decreasing trends. The characterization of the frequency associated with this behaviour is hampered by the short length of the time series. In addition there are some small shifts in the breakpoints from data set to data set. The minimum interval between breakpoints and the minimum length of the first and last segments that were imposed for the automatic search for times of significant change in the series can bias the results. Also, the very low spatial density information provided by the data used in this study makes it difficult to evaluate the influence of local factors (e.g. topographical factors) on the results. With respect to the Atlantic archipelagos, the scarcity and dispersion of the data do not allow us to conclude whether there is a pattern in annual precipitation there.

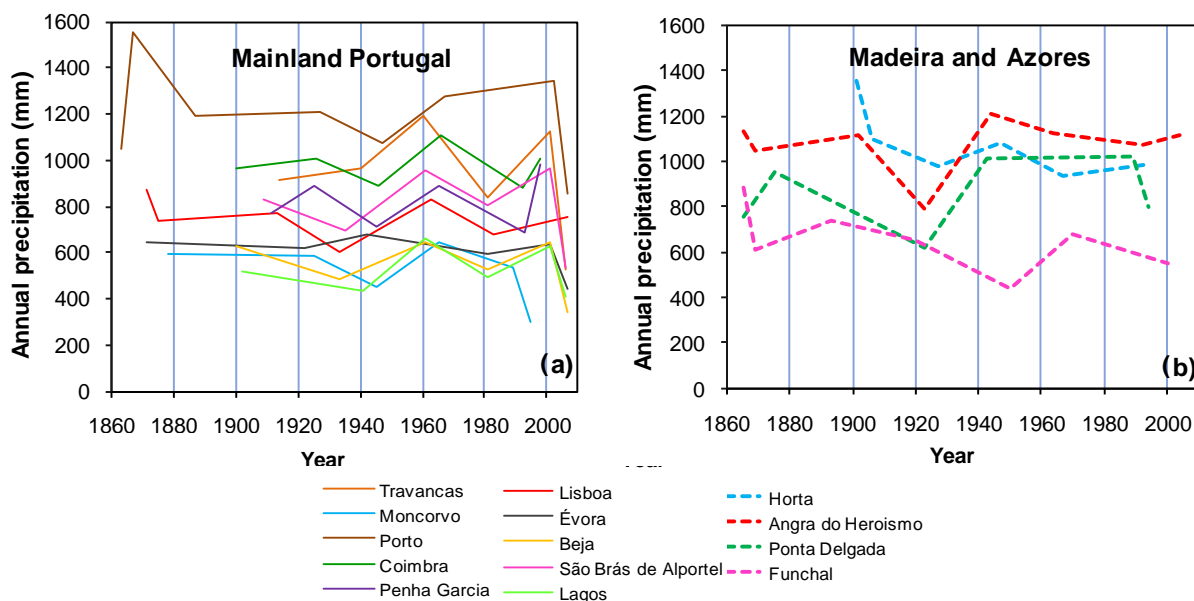


Figure 34. Partial trend fits to the annual precipitations for: (a) ten locations in mainland Portugal (adapted from de Lima et al., 2010b); (b) four locations in the Madeira and Azores archipelagos. The time series are not plotted.

Table 13 shows the rate of change associated with partial trends for two consecutive periods; these were individually selected for the different stations, respecting the breakpoints between periods with significantly different trends that were identified by the methodology used in this analysis. It highlights how the results can be completely different depending on the period analysed, and that extrapolations beyond these periods can be extremely dangerous without a comprehensive understanding of larger scale precipitation dynamics.

For example, in the period between roughly 1940 and 1960 in mainland Portugal there was an increase in annual precipitation, followed by a decreasing trend from about 1960 to 1980 (see Figure 34a). It should be noted that there are shifts in the corresponding breakpoints between the data sets and that these dates are only indicative. Table 13 shows the results of partial precipitation trends for such consecutive periods. From the information in this table, Sen's estimator confirms reductions in annual precipitation over mainland Portugal in the period roughly from the 60s–70s until the 80s–90s for almost all locations; but 75% of these trends are not statistically significant. Moreover, in many locations this behaviour changed into an

increasing trend period which has recently apparently been followed again by another period of decreasing trend. It is worth noting that the first and last segments are too short to allow a reliable estimation of trend since this estimator could easily be biased.

The partial trends in annual precipitation for the four data sets from the Azores and Madeira are shown in Figure 34b. The reduced number of time series does not allow the same type of comparative analysis, nor can we draw conclusions about whether there is a regular pattern in the precipitation structure. But the results do suggest the presence of a sequence of alternating decreasing and increasing trends in annual precipitation in these locations. This behaviour is qualitatively similar to that exhibited by the data from mainland Portugal, although the two patterns are not in phase. The drivers of precipitation are known to be different in the several locations, and so there was no expectation that the results would coincide.

6.4.2. Analysis of monthly precipitation

Table 14 presents the results of the trend analyses of monthly precipitation recorded in mainland Portugal and the Islands for the full record period and for sub-periods. Some monthly trends obtained for sub-periods are also shown in Figure 35.

Table 14. Sen's estimator of the monthly precipitation trends (mm decade⁻¹) and the respective confidence levels: +90%, *95%, **99% and ***99.9%. The data are for the full period and for sub-periods of negative trend in annual precipitation, which were selected for each time series based on the breakpoints located in the partial trend analyses. The results for mainland Portugal were partly reported in de Lima et al. (2010b).

	Station name	Period	Jan	Feb	Mar	Apr	May	Jun	Jul	Aug	Sep	Oct	Nov	Dec
Mainland Portugal	Travancas	1914-2006	-1.56	-2.97	-5.30 ⁺	-1.13	-0.49	-1.20	0.06	0.92 [*]	0.48	7.00 ^{**}	-1.18	-4.36
		1960-1981	-24.17	0.80	-23.20	-1.94	22.52	-0.58	-1.56	-0.40	-10.50	-7.14	-58.00 [*]	-3.81
	Moncorvo	1878-1995	0.32	0.12	-2.03 [*]	-0.99	-0.53	0.13	0.00	0.00	-0.57	-1.56	-1.52	-0.14
		1965-1989	-25.47 ⁺	-15.52	-14.77	12.25	-3.92	3.49	0.00	0.00	0.02	3.72	5.18	18.10
	Porto	1863-2007	0.84	0.68	-2.52	-0.89	-0.04	-0.57	-0.17	0.31	-0.24	-0.97	-0.82	1.85
		1967-2002	-12.25	-19.38	-17.45 ⁺	6.46	-6.43	-6.34	4.75 [*]	1.33	-0.67	24.88 ⁺	9.36	24.06
	Coimbra	1900-1998	4.13	1.25	-6.41 ^{**}	-0.10	2.10	0.02	-0.25	-0.17	-0.58	0.79	-1.10	-1.02
		1966-1992	-42.24 [*]	-28.50	-11.80	10.69	-22.75 ⁺	-1.91	-0.33	2.00	-2.62	18.54	-9.38	13.05
	Penha Garcia	1911-1998	2.72	0.74	-10.90 ^{***}	0.06	1.75	-0.40	0.00	0.00	0.00	0.07	-0.14	0.00
		1965-1993	-35.22 ⁺	-26.29	-7.39	7.25	0.04	-3.84	0.00	0.00	0.05	12.77	-2.53	7.97
	Lisboa	1871-2007	0.89	-0.64	-2.83 ^{**}	-1.13	-0.47	-0.36	0.00	0.02	-0.08	-0.35	-0.29	-0.63
		1963-1983	-73.29 [*]	-35.93	-23.68	7.00	2.64	-3.64	1.59 [*]	0.00	-3.54	-6.58	-22.79	8.58
	Évora	1871-2007	-0.07	-0.63	-2.15 [*]	-0.85	-0.77	-0.45	0.00	0.00 ⁺	0.21	0.32	-1.24	-0.07
		1981-2001	11.27	-5.96	-0.71	-24.45 [*]	34.13 ⁺	-1.16	0.00	0.00	5.55	20.94	-18.42	-8.29
	Beja	1900-2007	0.19	-0.81	-3.25 ^{**}	0.17	-0.54	-0.26	0.00	0.00	0.05	1.44	-1.51	0.33
		1961-1981	-14.89	-6.37	-13.53	3.58	6.13	-11.33	0.17	0.10	-4.58	3.22	-32.44 [*]	17.79
	São Brás de Alportel	1909-2002	4.35	-2.88	-5.16 [*]	1.42	1.00	0.00	0.00 ^{***}	0.00 ^{**}	1.18 ^{***}	0.95	-1.16	8.92 ⁺
		1962-1982	-56.14	-28.07	-20.73	3.10	-2.38	-11.97	0.22 ^{**}	0.00	2.00	-14.15	-33.54	13.81
Lagos	1902-2006	0.18	-0.08	-1.15	0.74	-0.07	-0.11 ⁺	0.00	0.00 ⁺	0.00	1.66	-0.70	1.33	
	1961-1981	-40.62	9.39	-29.12 [*]	5.98	-1.86	-4.55	0.00 [*]	0.00	-1.91	-3.10	-49.08 [*]	-14.19	
Horta	1901-1994	-2.79	-0.50	-1.73	-2.53 ⁺	-2.86 [*]	-2.02 ⁺	-0.68	-1.82 ⁺	-0.46	1.81	1.02	-0.91 ^{**}	
	1967-1994	-25.90 [*]	-1.60	-7.78	-7.20	6.46	-2.62	-2.65	2.50	-4.25	16.53 ⁺	25.99 [*]	0.89	
Azores	Angra do Heroísmo (Terceira Island)	1865-2004	1.17	-0.53	1.08	-0.02	-0.73	0.09	0.15	0.51	0.89	1.32	-0.72	1.18
		1964-1992	-41.28 [*]	-18.27	-10.60	11.06	13.23	-6.05	-5.29	2.82	23.27 [*]	-4.43	16.50	-4.43
Ponta Delgada (S. Miguel Island)	1865-1994	3.42 ⁺	2.00 ⁺	1.88	0.26	-0.05	-0.03	0.45	-0.17	1.99 [*]	2.71 ⁺	3.55 ^{**}	1.41	
	1943-1989	-7.38	0.29	-8.28	5.58	-4.00	1.83	-1.00	1.27	6.14	-6.17	2.52	12.17 ⁺	
Madeira	Funchal	1865-2000	-1.57	-0.15	-1.78	-0.68	0.00	0.00	0.00	0.00 ⁺	-0.08	0.00	-2.95 ⁺	-0.34
		1970-2000	-9.60	-16.75 [*]	-9.50	-9.40 [*]	5.05	-0.17	0.00	0.00	-1.00	13.62	-11.50	11.29

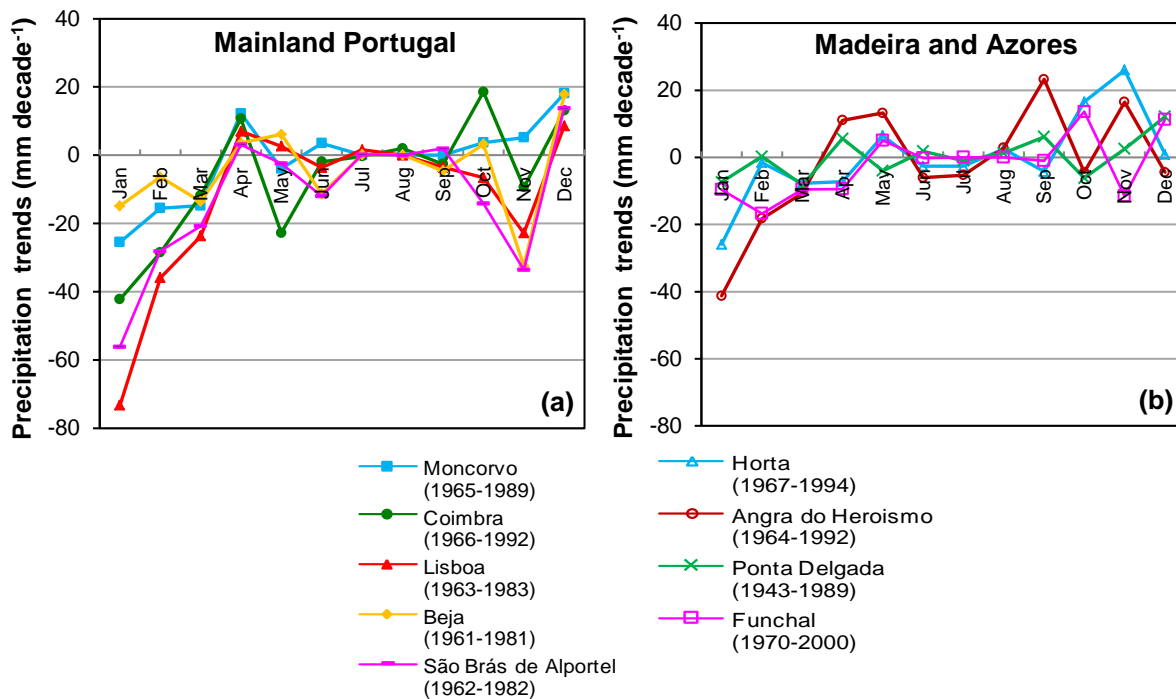


Figure 35. Monthly precipitation trends in selected periods for: (a) five locations in mainland Portugal; (b) four locations in Azores and Madeira. The periods analysed are identified in the legend and were selected based on the partial trend analyses and results, and correspond to decreasing trend sub-periods in annual precipitation.

Results for the full record period do not suggest important overall changes in precipitation distribution over the year. The exception is the precipitation in March: over time spans ranging from 88 to 145 years precipitation exhibits a decreasing trend in all the ten stations in mainland Portugal that were investigated; for seven of the data sets the trends are statistically significant, at least at the 5% significance level. For the Azores, only the data from Horta showed a decreasing pattern for March, which was not statistically significant. Similar behaviour was revealed by the data from Funchal.

The analyses of sub-periods yield different results. An example is given in Table 14 for periods from roughly 1960 to 1980, when a decreasing trend in annual precipitation was observed; but this result is only significant for the data from Lagos. The exception is the data from Porto; it reveals an increasing trend over this period, but not statistically significant. The

selection of the sub-periods was based on the results of partial trend analysis of annual precipitation, and so the sub-periods studied are not exactly the same for all the data sets. This may help explain some of the different results obtained for the rate of change in monthly precipitation for the various data sets (Figure 35), apart from local factors.

Figure 36 shows the analysis of partial trends in monthly precipitation observed in mainland Portugal for January, March, October and December. For each month, the tendencies are given in Table 14 for selected sub-periods and suggest that the distribution of precipitation over the year (i.e. seasonal distribution) changes over time; some of the results are statistically significant. When analysed individually, monthly precipitation exhibits alternately decreasing and increasing trends. This type of pattern was also observed for annual precipitation.

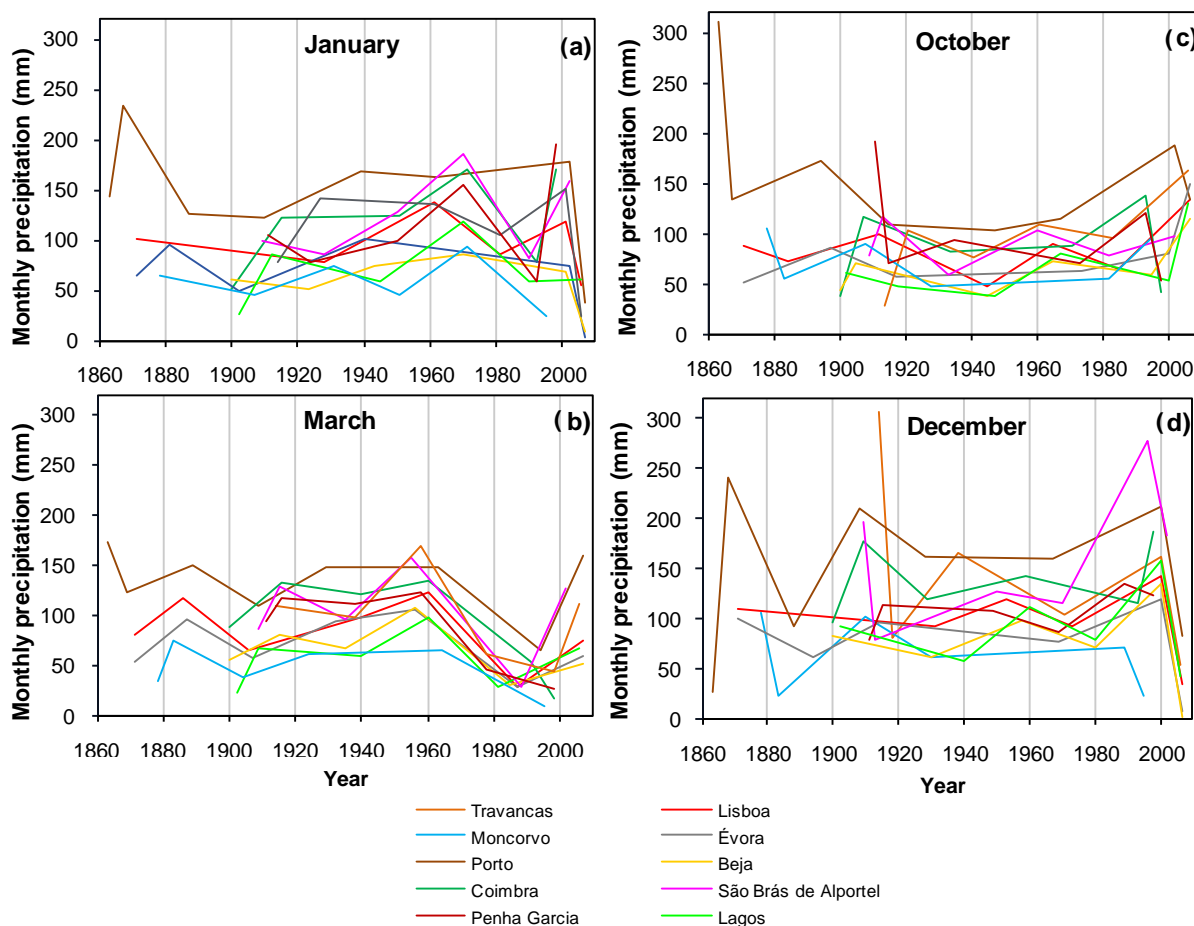


Figure 36. Partial trends in monthly precipitation in mainland Portugal: (a) January; (b) March; (c) October; (d) December. The time series are not plotted.

6.5. Concluding remarks

The investigation of monotonic linear trends in long precipitation time series was used as an exploratory tool to detect long term patterns of variation in this climate element in mainland Portugal and the Azores and Madeira archipelagos. On the whole this analysis did not reveal statistical evidence for rejecting the null hypothesis of no trend in annual precipitation over the full record period, in those geographical locations, based on the data that were explored in this study. However, the analyses of the 50-year moving averages of annual precipitation revealed an increase over time, in the recent past, for many of the series. For the longest time series this behaviour was preceded by a decrease over time.

The analyses of partial trends in the time series revealed a sequence of alternating periods of decreasing and increasing trends in annual and monthly precipitation, and these are sometimes statistically significant. These contiguous periods, exhibiting distinct tendencies, are defined by turning points in the behaviour of precipitation which are times of significant change in the properties of precipitation. The study of monthly precipitation suggested that redistribution of precipitation during the year took place over several decades, which means that some seasons were wetter while others were drier. However, results also show that this behaviour is not persistent and that changes can occur rapidly, in terms of the relevant time scales being discussed here. The limited number and origin of the precipitation time series used in this work means that it is not possible to perceive the presence of regional patterns. This issue is more pertinent for the Azores and Madeira, where the spatial variability of precipitation is very marked; at the same time, the homogeneity tests identified some probable problems in the data that may reduce the usefulness of some of the time series for trend studies and, therefore, affect the reliability of the results. It is noticeable, however, that over the longest period of records, which ranges from 88 to 145 years, March exhibits a decreasing trend in all the ten stations in mainland Portugal, seven of which are statistically significant at the 5% significance level. This type of behaviour was not revealed by the data from the islands, for this study. There is evidence that global and local factors can both affect the spatial distribution of trends in mainland Portugal and in the Portuguese archipelagos, which has been also reported in the literature for other locations in the Iberian Peninsula and nearby

territories (see e.g. Zhang et al., 1997; Lionello et al., 2006; de Lima et al., 2007; Costa et al., 2010; González-Hidalgo et al., 2011; Mourato et al., 2010).

This study also confirms that the results from precipitation trend analyses based on a monotonic (linear) model should be handled carefully, especially if only a small number of data sets are studied. In addition, it demonstrates that the analyses of short precipitation records consisting of only a few decades can be biased by the period studied. Complementary methods should therefore be used to better understand the structure of precipitation.

We have already stressed these issues in a previous publication (de Lima et al., 2010b), based on the analyses of data sets from mainland Portugal which have been reanalysed and further explored in the present work. But this fuller study of precipitation time series from Portugal, which is now more focused on the variability of monthly precipitation (i.e. seasonal variability), and the study of additional data (i.e. the study of long series from the Azores and Madeira islands), lends more weight to our previous conclusions. Thus, this work provides a more comprehensive and in-depth discussion of the long-term behaviour of annual and monthly precipitation in Portugal than is found in de Lima et al. (2010b), thanks to the greater diversity of analytical methods used and the overall analyses of precipitation records for mainland Portugal and the Portuguese islands of Madeira and the Azores. This compilation of results is also important for the overall understanding of the local conditions and regional specificities of precipitation in Portugal.

**PART II – SIMULATED RAINFALL:
LABORATORY EXPERIMENTS**

7. RAINFALL SIMULATOR EXPERIMENTS ON THE IMPORTANCE OF WHEN RAINFALL BURST OCCURS DURING STORM EVENTS ON RUNOFF AND SOIL LOSS³

Abstract

The influence of the temporal structure of rainfall on the discharge hydrographs and associated transport processes has not yet been fully explored. Nevertheless, the expectation is that characteristics of the rain spells have important effects on both runoff and soil loss, in particular the time when heavy rainfall bursts occur during storm events. This experimental study focuses especially on the influence of when such bursts occur during rain storm events of equal duration and depth on runoff and soil loss processes.

Laboratory experiments were conducted using a rainfall simulator and a soil flume to study the different responses caused by rain events characterized by a constant base intensity interrupted by short 5-minute rainfall bursts. These bursts occurred at different times during the event. On average, the greatest runoff and amount of sediment transported were caused by the rainfall bursts that occurred later in the event. Results obtained in the laboratory experiments are expected to represent the response typical of advanced, centred and delayed rainfall patterns.

Thus, rain storm temporal variability and patterns should be considered in the definition of design hyetographs for rainfall-runoff and rainfall-erosion modelling. Ignoring the time of occurrence of the heaviest rain intensity within storm events can cause both under and over estimation of runoff discharge and soil loss.

³ de Lima, J.L.M.P., Carvalho, S.C.P., de Lima, M.I.P. 2013. Rainfall simulator experiments on the importance of when rainfall burst occurs during storm events on runoff and soil loss. *Zeitschrift für Geomorphologie* 57(1), 91–109.

7.1. Introduction

The occurrence of extreme rainfall events severely affects society and can have a significant economic impact. Rainfall characteristics, which include intensity, duration, direction of movement, moving speed and temporal and spatial variability, affect both the integrated response of a catchment area (e.g. runoff hydrograph) and the distributed response (e.g. the temporal and spatial variability of soil moisture), several studies have already focused on these problems (e.g. Black, 1972; Foroud et al., 1984; Singh, 1997; 2005; Assouline et al., 2007; Chang, 2007; Cerdà and Doerr, 2007; de Lima et al., 2009). Knowledge of these characteristics and the probability of their occurrence is very important for designing engineering structures and urban drainage systems, reservoir management, pollution and erosion control, and agricultural practices (e.g. Stedinger et al., 1993; Hosking and Wallis, 1997). In this context, design hyetographs determine the shape and timing of the corresponding runoff hydrograph and are also expected to affect strongly soil loss.

A number of design hyetographs have been proposed by e.g. Bonta and Rao (1988), Grimaldi and Serinaldi (2006) and Ellouze et al. (2009). Some examples of hyetograph patterns are: rectangular, which has been commonly used, but in certain cases it has been found to underestimate both, volume and peak discharge (e.g. Lambourne and Stephenson, 1987), triangular (Yen and Chow, 1980), Chicago hyetograph (Keifer and Chu, 1957), and best linear unbiased estimation (BLUE) hyetograph (Veneziano and Villani, 1999). In these hyetographs, maximum intensities (bursts) can occur at any instant during a storm event. Researchers have tried to assess the influence of when these rainfall bursts occur during the event on runoff hydrographs (e.g. El-Jabi and Sarraf, 1991; Alfieri et al., 2008). Rain storm patterns have been classified depending on the part of the event duration in which the heaviest intensity falls (Dunkerley, 2012). One example of a classification of rain patterns defines advanced, centred or intermediate, delayed and uniform patterns. A storm event pattern is classified as advanced when high rainfall intensities take place early in the event, and the delayed pattern is the opposite. In the centred pattern high rainfall intensities occur in the middle part of the event. Finally, the uniform pattern assumes constant rainfall intensity for the entire duration of the event (no temporal variability). Other pattern classification considers which quartile delivers

the greatest rain depth: first quartile events, second quartile events, etc. Both criteria are found in e.g. Huff (1967), Chukwum and Schwab (1983), Zhang et al. (1997), Ng et al. (2001), de Lima and Singh (2002), Tsai (2008), and de Oliveira et al. (2010). In many cases the application of the two criteria leads to the same classification of a given pattern. It should be noted that no attempt is made in this paper to review in depth the already significant literature on representative rainfall patterns.

Water resources engineering projects require analysis of the relationship between the rainfall structure and the runoff response (e.g. Chow, 1964; Hewlett et al., 1977; Segond et al., 2007). According to Singh (1997) the shape, timing and peak flow of a stream flow hydrograph are influenced by watershed and drainage network characteristics, storm rainfall dynamics (amount, intensity, duration, velocity and direction of storm movement), infiltration and antecedent soil moisture conditions. The hydrologic response is also affected by the temporal and spatial distribution of rainfall induced by wind (e.g. Erpul et al., 2003; 2004; Ries et al., 2009; Vermang et al., 2011).

Experiments using varying simulated rainfall intensities have been attempted by several authors but are not as common as constant intensity experiments, mainly because of difficulties in implementing a sequence of intensities. Rainfall simulations permit the control of parameters such as rain intensity and duration. In fact, producing rain events to order, with pre-defined patterns and durations, is one of the main advantages of using rainfall simulators in hydrological research, both in the field and in the laboratory (e.g. Mermut et al., 1997; Cerdà, 1999; Clarke and Walsh, 2007; Ries et al., 2009; Fister et al., 2011). In a recent paper, Dunkerley (2012) refers a number of authors that used varying simulated rainfall intensities (e.g. Flanagan et al., 1988; Zhang et al., 1997; Parsons and Stone, 2006). When using nozzle-spray rainfall simulators the rainfall intensity can be changed by: (i) adjusting the operating pressure to change the discharge at the nozzles, (ii) using several sets of independent nozzles that can be switched on and off, and (iii) changing the position of the drainage area relative to the location of the nozzles and wetted area, to achieve specific rainfall intensities. When experiments are conducted using low discharges it is difficult to change the operating pressure

in a replicable way. Also, it is complicated to use different sets of nozzles to achieve a variety of rainfall intensities. In this study we implemented the third option, as explained below.

The aim of this study is to quantify the importance of when rainfall bursts occur, during the simulated storm event, on runoff and sediment production. The study involved laboratory experiments using a rainfall simulator and a soil flume. The following features were explored: time to runoff, final runoff time, peak runoff rate, total runoff volume, peak sediment flux and total sediment transported. The experimental set-up used in this work provided data on runoff and sediment transport flows over time.

7.2. Materials and methods

7.2.1. Simulated rainfall patterns

The selected conceptualized storm events used in the experiments are shown schematically in Figure 37. Two sets of experiments were done and the empirical data will be discussed separately for each set. They used a storm characterized by: a duration of 8 hours, a constant base intensity of 8 mm h^{-1} interrupted by five periods of intense rainfall (bursts) of 100 mm h^{-1} and 5-minute duration. These periods of high intensity rainfall are located at the beginning, 25 %, 50 %, 75 % and at the end of the total duration of the rainfall event, and are expected to simulate different rain patterns (advanced, advanced-centred, centred, centred-delayed and delayed, in Figure 37, or simply three categories: 1 and 2 – advanced, 3 – centred, and 4 and 5 – delayed). The rainfall intensities used in these laboratory experiments are comparable to the intensities used by several other authors (e.g. Frauenfeld and Truman, 2004; Parsons and Stone, 2006; Dunkerley, 2008b).

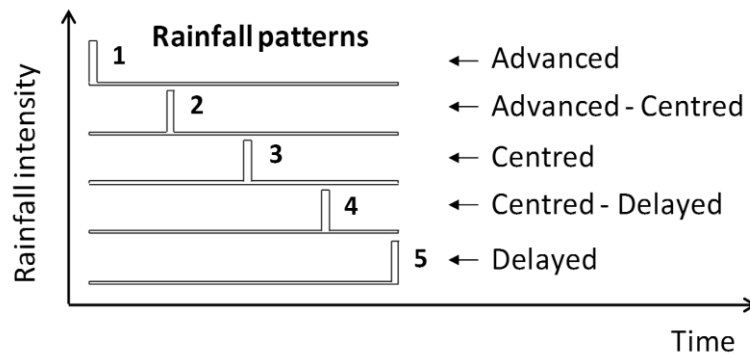


Figure 37. Sketch (not to scale) of the different basic hyetographs referred in the text.

Different times of occurrence of high intensity bursts of rainfall during a rain event can be embraced by usual rainfall patterns classification (see section 1, e.g. advanced, centred or delayed patterns). The proposed laboratory scheme sought to create laboratory conditions that would lead to an understanding of how the time a high intensity rainfall burst occurs during a rain event affects runoff and soil loss. It is extremely difficult to replicate the soil conditions exactly, because: (i) of soil sample variability, (ii) of compaction of the soil when filling the flume, and (iii) the characteristics of the top surface layer of the soil, which has a major influence on the availability of soil particles for the transport by overland flow. Thus a long simulated rain event was conceptualized with low intensity, interrupted from time to time by high intensity bursts. Because the base intensity did not produce runoff at any time, the effect of the rain burst could be comparable to different rainfall patterns such as the patterns defined in Figure 37.

These synthetic patterns are clearly oversimplified rainfall patterns which cannot represent the wide variability observed in natural conditions. But, even though their intrinsic simplicity, they make comparisons of the response more clear and results easier to interpret. The use of a simple hyetograph with two fixed intensities can be justified by: (i) difficulty in changing rainfall intensities, accurately, when using nozzle rainfall simulators, and (ii) keep hyetograph simple and prominent to make results more noticeable.

7.2.2. Laboratory set-up

The experiments were carried out using a rainfall simulator and a soil flume. The schematic representation of the experimental set-up is shown in Figure 38. A similar set-up has been used in other laboratory works (e.g. de Lima et al., 2008; 2009; 2011).

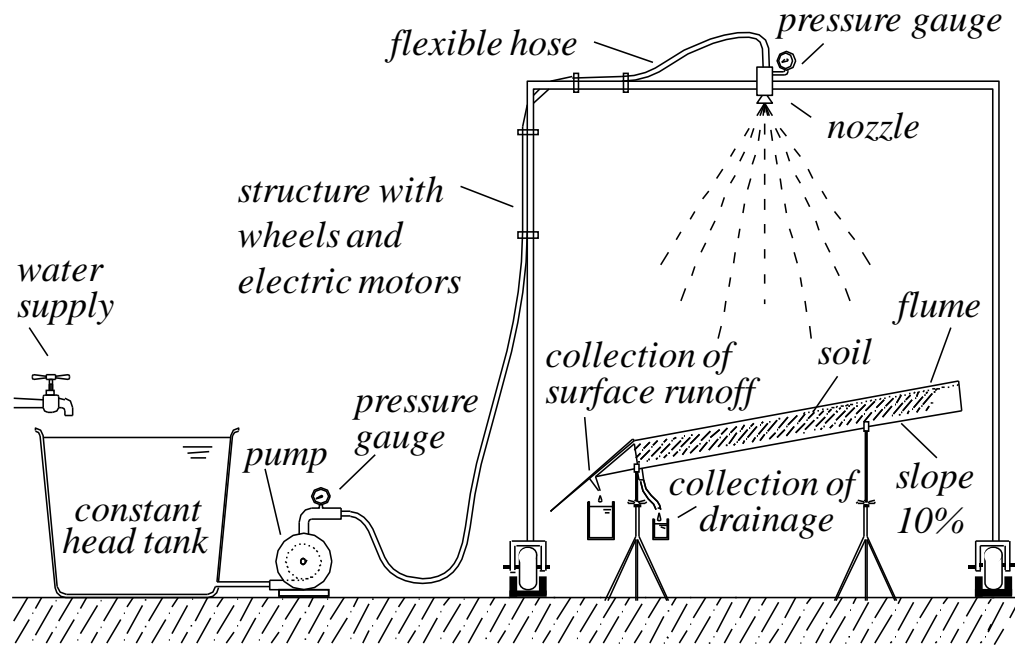


Figure 38. Sketch of the laboratory set-up used in the experimental runs.

Rainfall simulator

The rainfall simulator consists of: a constant level reservoir; a pump; a hose carrying water from the pump to the nozzle; an automatic pressure gauge to monitor the pressure at the nozzle, and a single downward-oriented full-cone nozzle which was fixed 2.25 m above the geometric centre of the soil flume surface. The nozzle was from Spraying Systems Co.; it is made of stainless steel and is a standard type (HH) with the capacity-size code of 22 (an orifice diameter of 4.8 mm). The operating pressure of the simulator was kept constant at 73 kPa. A detailed description of this equipment is given in de Lima et al. (2008, 2009, 2011).

Soil and soil flume

The use of laboratory soil flumes is well established in runoff–erosion research (e.g. Frauenfeld and Truman, 2004; Parsons and Stone, 2006; de Lima et al., 2008; 2009; Dunkerley, 2012). The soil flume used in these experiments was built of metal sheets and was 2.0 m long, 0.1 m wide and 0.12 m deep. A 0.10 m layer of soil was placed over a metal grid bottom covered by a permeable fabric that allows free drainage. The use of a small flume can be justified: (i) easier to use (e.g. smaller volumes of soil, since the flume has to be emptied and refilled, smaller discharges to measure volumetrically and smaller volumes of runoff to oven-dry), (ii) guaranty that the soil was homogeneous, (iii) guaranty that initial soil moisture conditions were the same for the different laboratory sets of experiments, and (iv) guaranty one-dimensional flow (in the downslope direction), namely because no lateral variations of rainfall occurs due to the small width of the flume.

The soil was taken from the right bank of River Mondego, in Coimbra, Portugal. The material consisted of 7 % clay, 9 % silt and 84 % sand and gravel, which classifies it as loamy sand: the classification is based on the criteria proposed by Gerakis and Baer (1999). The soil texture information is listed in Table 15, the grain-size of coarser particles was determined by conventional sieving, while the grain-size of finer particles was determined by laser diffraction

Table 15. Particle size distribution of the soil used in the experiments.

Material	Particle Size (mm)	Distribution (%)
Clay	<0.0062	6.7
Silt	0.0062-0.0233	3.2
	0.0233-0.1500	6.3
Sand and Gravel	0.1500-0.5000	31.6
	0.5000-4.7600	40.7
	4.7600-19.1000	11.5

Water

The characteristics of the water used in rainfall simulation experiments are important because they can affect processes at the soil surface. In these experiments, tap water was used in the various runs and it had the following approximate physical and chemical characteristics: temperature, 23 °C (first set of experiments) and 17 °C (second set of experiments); conductivity, 100 $\mu\text{S cm}^{-1}$; pH, 7; total hardness, 30 mg L^{-1} of CaCO_3 ; turbidity, 3 NTU. Because it is expected that the water properties remained practically unchanged during the various laboratory runs it is assumed that water did not influence the outcome of the experiments, in relative terms.

7.2.3. Laboratory procedure

Soil

The air soil collocated in the flume was previously sieved (high frequency mechanical sieve) using a 4.75 mm aperture square-hole mesh in order to break-down all aggregates, and all vegetative material and unusual coarser particles were removed. Afterwards the soil was mixed up mechanically to guaranty homogeneity for the different repetitions and placed in the soil flume to achieve a 0.10 m thick layer of uniform depth. To obtain a plane surface, a sharp, straight-edged blade that could ride on the top edge of the sidewalls of the flume was used to remove excess soil. Surface slope was set at 10 %. The bulk density of the soil depends greatly on the degree of compaction, therefore the same mass of soil was used each time the flume was filled (1.6 g cm^{-3} for air-dried soil material).

To ensure identical initial conditions (e.g. in terms of soil moisture, soil compaction, soil surface roughness) for the different runs, the soil material in the flume was removed and replaced with new air dried soil material before each set of laboratory experiments. The procedure was repeated for the two sets of experiments.

Runoff, drainage and soil loss

Overland flow and sediment loss were measured by collecting samples in metal containers at the downstream end of the soil flume, non-stop, every 15 seconds, whenever flow occurred. The initiation of overland flow at the flume outlet defined the starting time for the measurements. The sediments were calculated based upon the oven-dry sediment mass.

The total amount of water percolated through the 0.10 m soil depth (free drainage), collected also at the downstream end of the soil flume, was approximately the same for the different experiments and was not taken in consideration in this study.

Rainfall patterns

With the current set-up, specific rainfall intensities were achieved by conveniently setting the position of the drainage area (soil flume) relative to the location of the nozzle (i.e., wetted area). Thus, the position of the nozzle was changed relative to the soil flume during the experimental runs, as appropriate, to capture the intended rainfall intensity over the predefined time intervals. This was achieved with the help of wheels and 2 electric motors (see Figure 38). It took on average 5 seconds to move the nozzle from one position to another.

The rainfall simulator produced a circular wetted area below the nozzle (Figure 39 – left). The main factors affecting water application (water distribution at ground level) are: nozzle type, operating pressure, nozzle diameter, nozzle elevation, wind speed, heat and damp (e.g. Keller and Bliesner, 1990; Tarjuelo et al., 1999; Louie and Selker, 2000). Mean rainfall intensities over the flume were estimated measuring the simulated rain using 11 gauges equally spaced along the flume (at a slope of 10 %), during 5 minutes (Figure 39b, see also Table 16). The spatial distribution of the rainfall simulated in the laboratory over the soil flume, for both positions of the flume relative to the nozzle, resembles natural conditions in that it is not uniform. Moreover, we can consider that it could represent a rain cell, static over the drainage area. For the spatial rain distribution associated with both simulated average intensities, the uniformity coefficient developed by Christiansen (1942) is below 80 % (Table 16), but

considerable lower for position 1 than for position 2 (e.g. Christiansen, 1942; Vories and von Bernuth, 1986; Losada et al., 1990). Another issue is the drop trajectory and impact angle of the drops on the flume surface for the two rainfall intensities. It is observed that the angles of inclination of the trajectories of drops at impact, measured from the vertical, increase as the distance to the nozzle increases, but can be disregarded here because of the set-up geometry (de Lima et al., 2011).

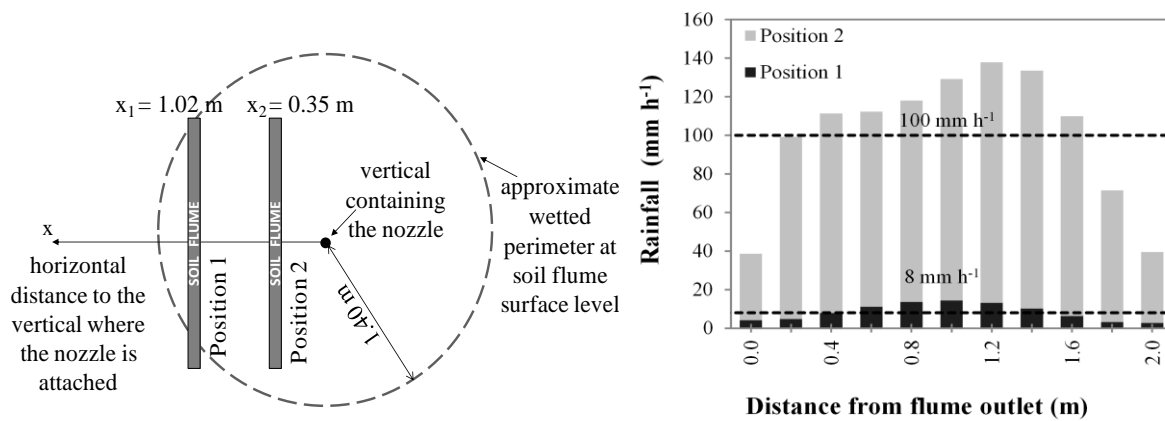


Figure 39. Simulating different temporal rainfall intensities: Left, representation (top view) of the two soil flume positions with respect to the wetted area under the nozzle; Right, corresponding rainfall intensities observed along the soil flume for the average intensities of 8 and 100 mm h⁻¹.

Table 16. Rainfall measurements taken along the soil flume at positions 1 and 2 (3 repetitions of 11 samples each), as defined in Figure 39.

	Position 1	Position 2
	Base rainfall intensity	Rainfall burst
Mean (mm h⁻¹)	8.3	100.1
Minimum (mm h⁻¹)	2.8	38.6
Maximum (mm h⁻¹)	14.4	137.8
Standard deviation (mm h⁻¹)	4.4	35.1
Coefficient of variation	0.31	0.25
Uniformity coefficient (%)	54.5	72.5

For the two average rainfall intensities that were applied in the laboratory experiments, the simulated raindrop size distribution and fall velocities were determined using a Laser Disdrometer, usually used in outdoor conditions. This disdrometer has a time resolution of 1-minute. The mean drop diameter and velocity are presented in Figure 40. The measurements were taken under windless conditions over 15 minutes at several horizontal distances from the vertical that contains the nozzle, at the level of the soil surface of the flume. The mean raindrop diameter ranged from 0.66 to 0.76 mm, while the mean drop velocity ranged from 2.08 to 2.79 m s⁻¹.

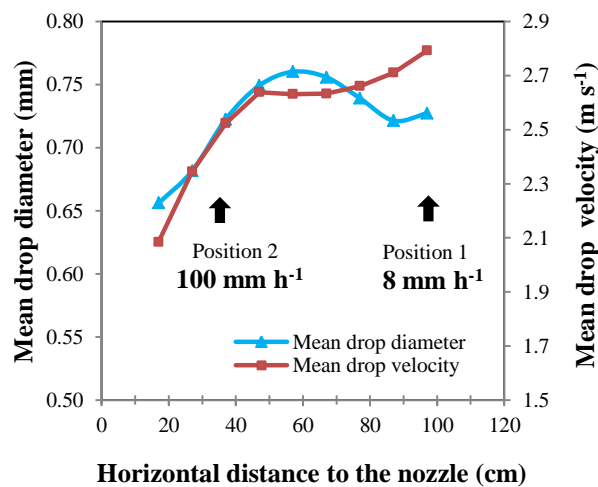


Figure 40. Raindrop mean diameter and fall velocities. Soil flume positions 1 and 2 are indicated in Figure 39 – left. The measurements were taken at the flume installation level, 2.25 m below the nozzle (vertical distance). The nozzle was operated at 73 kPa.

Figure 41 presents the distribution of the number of drops as a function of drop diameter and fall velocity measured at positions 1 and 2 (see Figure 39 and Figure 40). At position 1, where the mean rainfall intensity is low (8 mm h⁻¹) and so the number of drops is small, the maximum number of drops was recorded around the 0.5 –1 mm diameter class and velocities of 3.5 m s⁻¹. But at position 2, where the rainfall intensity is higher (100 mm h⁻¹), there were more drops belonging to lower diameter classes, i.e. less than 0.5 mm diameter, and exhibiting velocities of around 2 m s⁻¹.

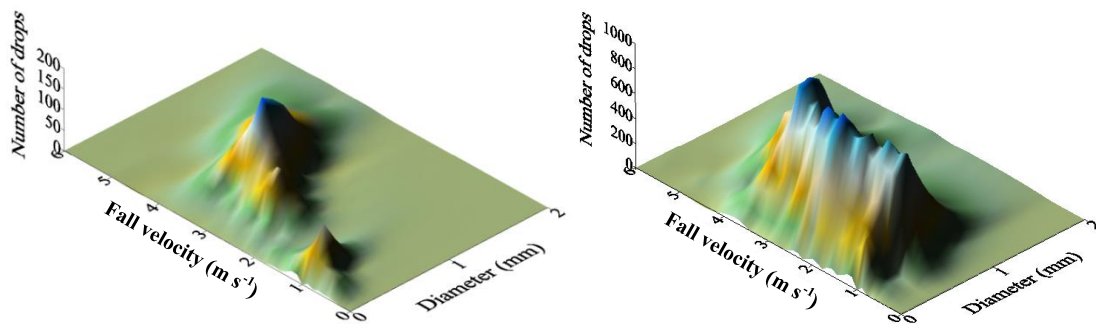


Figure 41. Histograms of simulated raindrops observed for the soil flume at positions 1 (left) and 2 (right); the data are for 15 minutes of simulated rainfall. The rain simulator was operated at 73 kPa. For better visualization, the vertical axes are scaled differently in the two plots.

7.3. Results

Rainfall-runoff experiments were conducted using simulated rainfall events that aimed at recreating responses to advanced, centred and delayed rainfall patterns (see the conceptualized hyetographs shown in Figure 37).

The main characteristics of runoff (Figure 42) and soil loss (Figure 43) triggered by the 5 high intensity rainfall bursts that occurred at different times during the simulated event are summarized in Table 17 for the two sets of experiments. Whereas the soil used to fill the flume had the same origin and expectable characteristics, it is likely that the characteristics of the soil and the final result for the deposition of the soil material in the flume (e.g. soil compaction), for the two sets of experiments, were not exactly the same. Although the experimental procedure was carried out carefully and similar experimental conditions were established each time, in fact, these conditions are not strictly reproducible and this might have affected the results. During the simulated events, Hortonian overland flow took place only during and shortly after the rainfall bursts: no runoff was generated during periods of lower (base) intensity rainfall. The free drainage provided prevented the 0.10 m soil layer

placed in the flume from approaching saturation except, probably, on the top surface layer during the high intensity bursts.

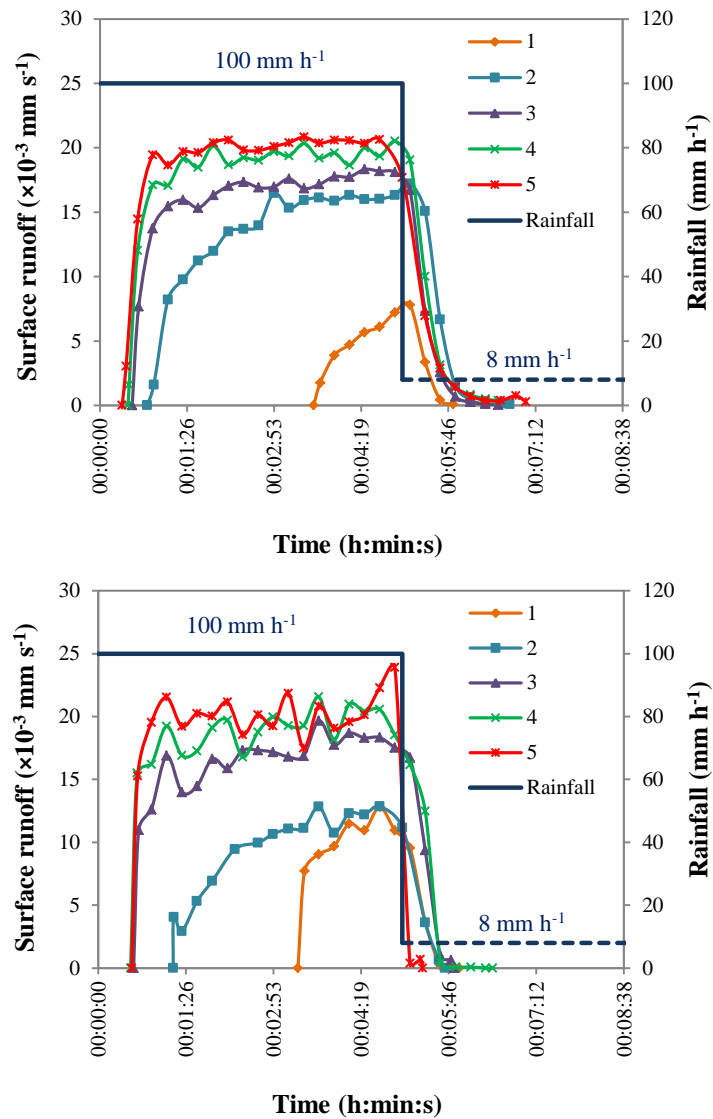


Figure 42. Measured runoff hydrographs: (top) first set of experiments, (bottom) second set of experiments. The origin of the horizontal axes coincides with the beginning of each burst of intense rainfall: 1 – advanced, 2 – advanced-centred, 3 – centred, 4 – centred-delayed and 5 – delayed.

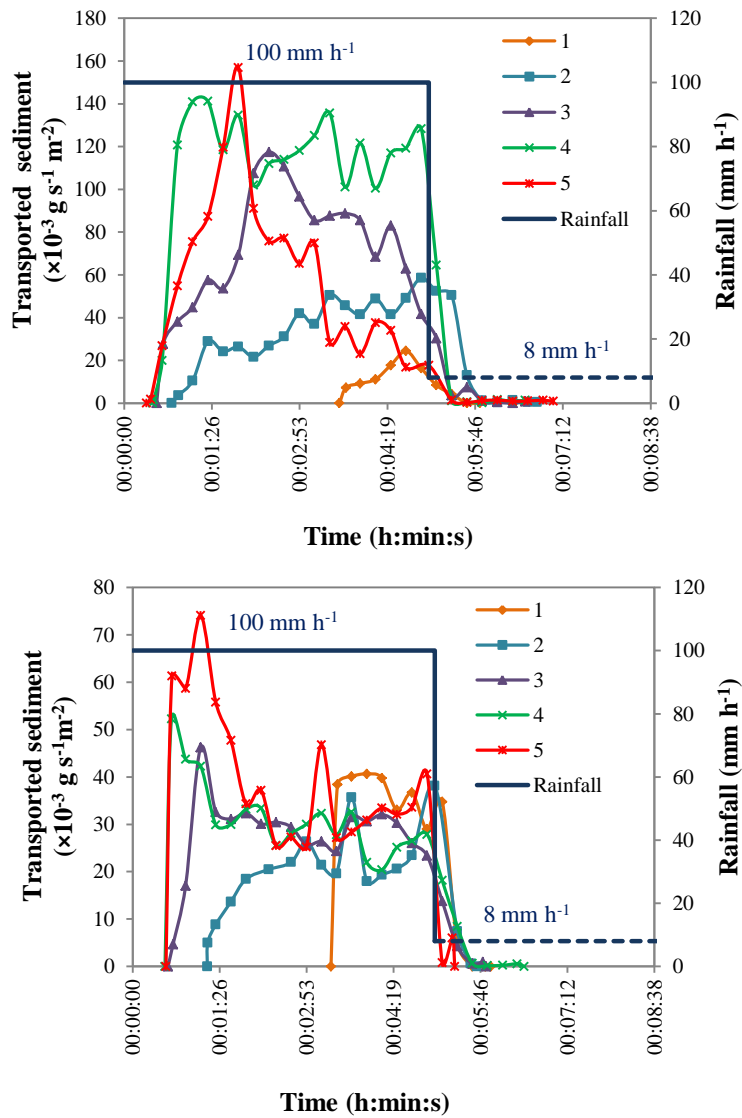


Figure 43. Measured transported sediment graphs: (top) first set of experiments, (bottom) second set of experiments. The origin of the horizontal axis coincides with the beginning of each burst of intense rainfall. See also Figure 42 which shows the measured runoff hydrographs.

Table 17. Characteristics of runoff hydrographs and sediment transported (see also Figure 42 and Figure 43), for the two sets of experiments.

	1 st set					2 nd set				
Rainfall bursts	1	2	3	4	5	1	2	3	4	5
Rainfall patterns	Advanced	Advanced-centred	Centred	Centred-Delayed	Delayed	Advanced	Advanced-centred	Centred	Centred-Delayed	Delayed
Initial runoff time (min:s)*	03:32	00:47	00:32	00:28	00:22	03:17	01:14	00:35	00:32	00:33
Final runoff time (min:s)*	05:56	06:48	06:40	06:40	07:05	05:56	05:42	05:51	06:29	05:20
Peak runoff ($\times 10^{-3}$ mm s ⁻¹)	8	17	18	21	21	13	13	20	22	24
Total runoff volume (mm)	0.6	4.0	4.8	5.6	5.6	1.3	2.2	4.8	5.5	5.4
Peak sediment flux ($\times 10^{-3}$ g s ⁻¹ m ⁻²)	24	59	117	141	157	41	38	46	52	74
Total sediment transported (g m ⁻²)	1.5	10.6	20.6	32.1	16.6	4.4	4.7	7.8	8.8	10.7

* from the start of the period of intense rainfall

Notice that in Figure 42 and Figure 43 the origin of the horizontal axes ($t=0$) coincides with the beginning of each intense rainfall burst, for the different rain patterns. Thus, hydrographs and sediment graphs are superimposed to highlight the differences between the graphs. Also, the 8 mm h⁻¹ rainfall intensity (dashed line) does not exist for the period of high intensity located at the end of the event (i.e., the end of the 5-minute 100 mm h⁻¹ intensity is the end of the simulated rainfall).

Runoff volumes and peak discharges that originated from the high-intensities in the simulated rain increased perceptibly as the bursts were occurring progressively later (Figure 42), thus, this increase in the response might be expected for the advanced to the delayed rainfall patterns (Figure 37). Furthermore, the beginning of runoff was strongly delayed for the early burst (thus, also expected for advanced rainfall patterns), compared with the response observed for the other bursts (Figure 42).

For the different rain and runoff events, the collected soil loss at the downstream end of the flume was the result of raindrop impacted overland flow transport. There were no signs of concentrated flow, there was no rill formation observed during the short period of time that overland flow existed because runoff only occurred during the intense rainfall bursts. Whereas the difference in runoff between the two sets of experiments is not relevant, the difference in the results for the total sediment transport and peak sediment flux was very marked: total sediment transported in the second set of experiments was approximately 50 % less in relation to the first set. Table 17 shows that the total sediment transported, for the first set of experiments, varied between 1.5 and 32.1 g m⁻² whereas for the second set it varied between 4.4. and 10.7 g m⁻².

Infiltration in time for rainfall bursts 1 (advanced), 3 (centred) and 5 (delayed), of the first set of experiments, is shown in Figure 44. The soil was able to infiltrate most of the rainfall during the burst that occurred earlier, causing a strong delay in the ponding time and consequent runoff generation, therefore runoff volume and sediment loss are small. On the other hand, for the more delayed burst, runoff started quickly after it began because infiltration capacity decreased fast as the result of higher moisture content due to nearly 8 hours of rainfall. In this case runoff volume is large with repercussions on the competence for sediment transport.

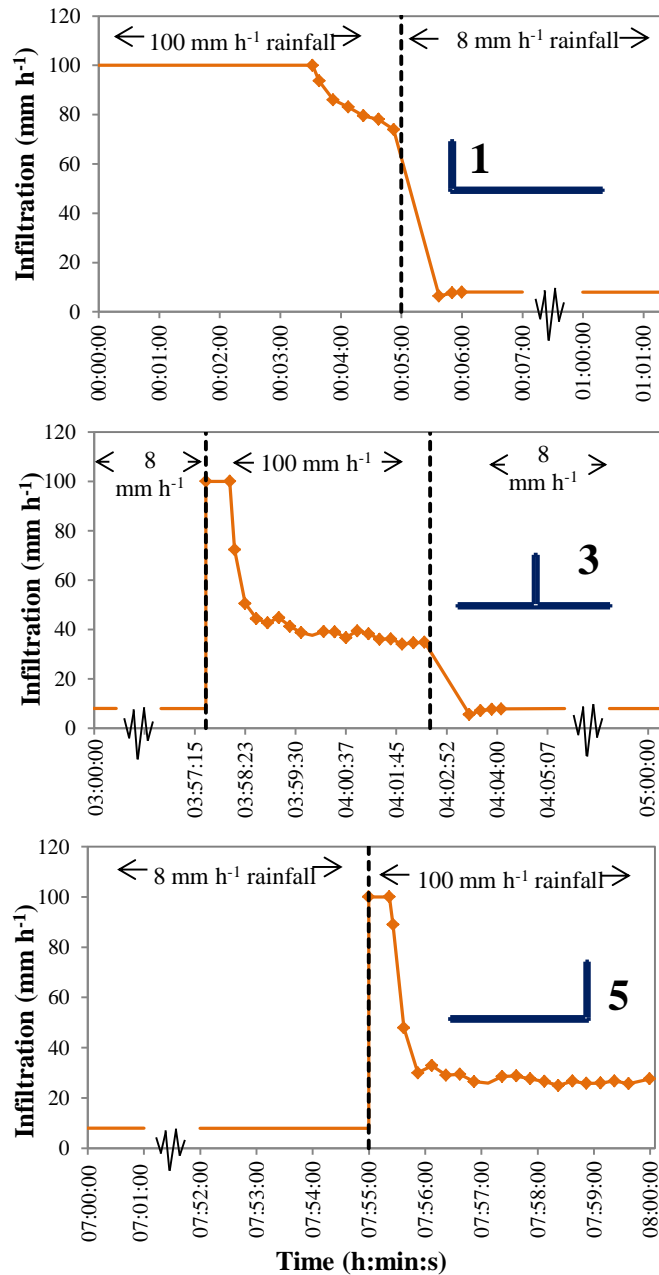


Figure 44. Infiltration in time for rainfall patterns 1, 3 and 5 (first set of experiments).

Higher transport capacity was noticed as water depth and stream power increased from upslope to downslope. The runoff generated by rainfall bursts was responsible for the total sediment transport. Sediment loss followed the behaviour of runoff; the outflow and soil loss increased over time as the bursts of intense rainfall occurred later in the different rainfall patterns (Figure 45). For the more opposite cases (i.e., burst occurring in the beginning and

end of the simulated event), for the first set, an increase of 10 times is observed for the total runoff volume and 11 times for the total sediment loss, whereas, for the second set the increase is 4 and 2.4, respectively (see Table 17). Some of these differences might be due to different initial conditions in the soil flume, which are always expected in this type of laboratory work, regardless of how much care is taken in the preparation of the experiments.

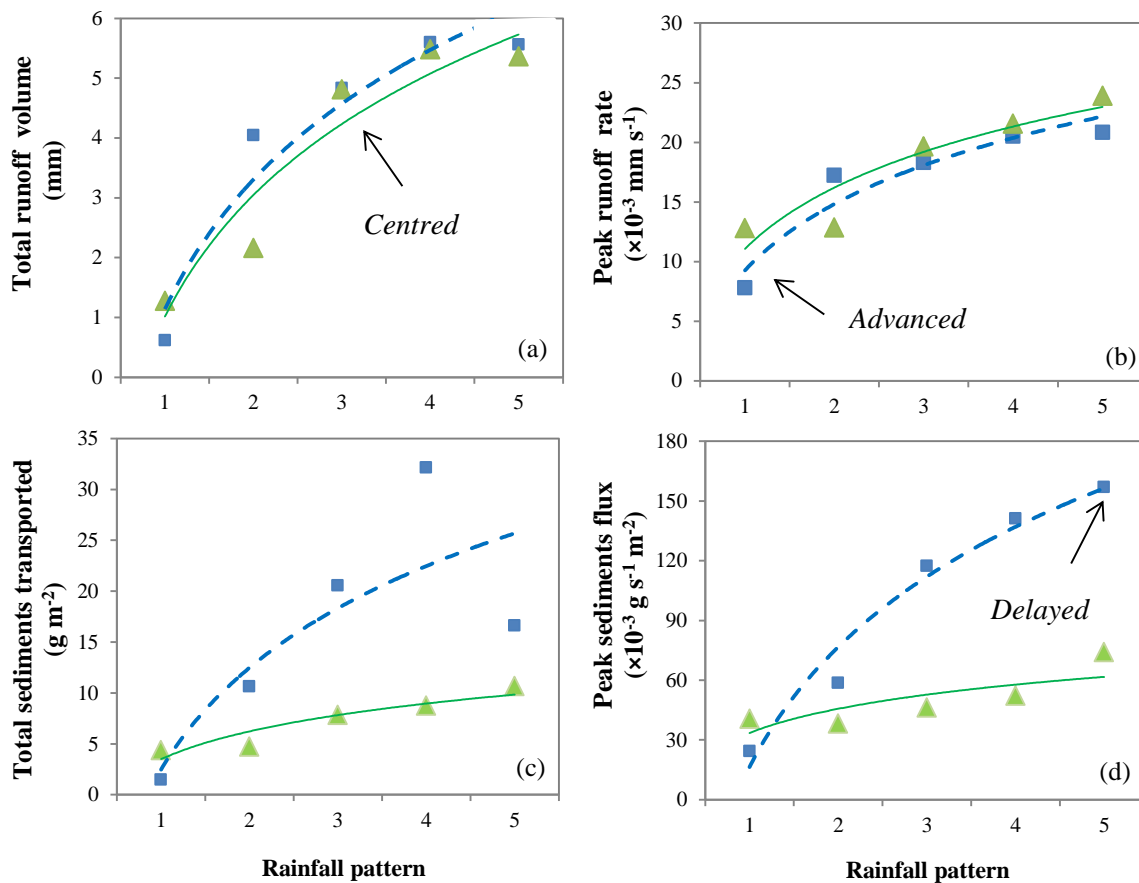


Figure 45. For the five rainfall bursts: (a) total runoff volume, (b) peak runoff, (c) total amount of sediment transported, and (d) peak sediment flux. Squares and triangles represent empirical data from the first and second set of experiments, respectively, whereas the adjusted lines are only indicative of the tendency in the data.

Figure 45 illustrates more clearly the behaviour of runoff and soil loss for the five rainfall bursts and for the two sets of experiments. Total runoff volumes and peak discharges show a tendency to be lower for the advanced rainfall bursts and higher for the delayed bursts. The adjusted lines are only indicative of the trend observed for the two sets of experiments. For

example: (i) the peak runoff rate and total runoff volume are exactly the same for the rainfall patterns 4 and 5, (ii) the two data sets present similar runoff behaviour but rather different soil loss for both total amounts and fluxes. The fluctuations in the results and the marked differences amongst the two sets of experimental runs can be explained, at least partly, by: (i) measurement errors (e.g. manual collection of runoff), (ii) characteristics of the soil placed on the flume, including compaction effects (iii) changing properties of the top soil as a result of crusting, and (iv) eventual incorrect positioning of nozzle relative to the flume. Although a tendency is revealed by the experiments, these results are preliminary; laboratory procedures are being developed seeking for more control over some variables (e.g. soil) that are expected to have strongly affected here the outcome of the experiments, in addition to the different rain patterns.

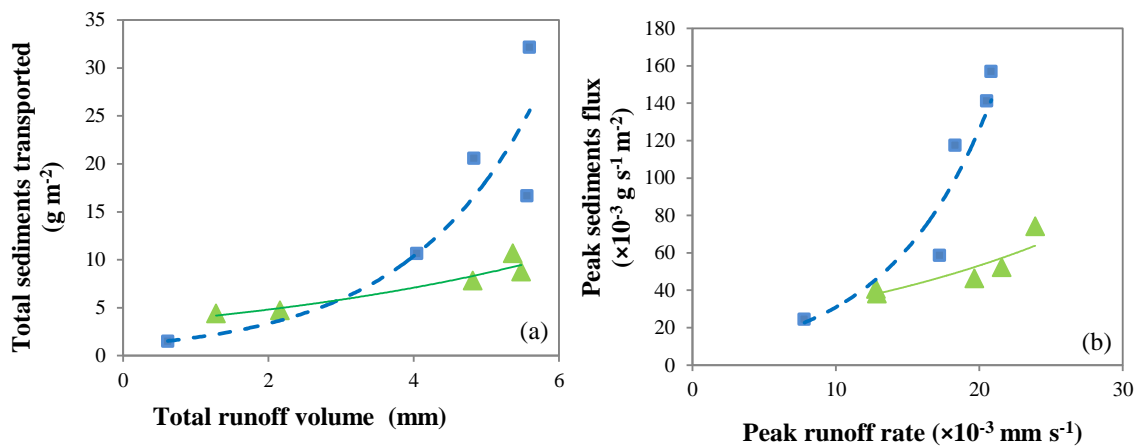


Figure 46. For the five rainfall bursts: (a) relation between the total amount of sediment transported and total runoff volume, and (b) relation between peak sediment flux and peak runoff rate. Squares and triangles represent empirical data from the first and second set of experiments, respectively, whereas the adjusted lines are only indicative of the tendency in the data.

In both series of experiments the five rainfall bursts yielded total soil loss and peak sediment flux that increased with runoff volumes and peak discharges, respectively. This can also be seen in Figure 46 where sediment transport is plotted against runoff: higher runoff volumes are associated with greater amounts of soil loss since more energy is available to displace

sediment. Nevertheless, when handling the soil in the laboratory to fill the flume it is difficult to attain the same compaction of the soil material, particularly at the top layer where water erosion processes take place. Therefore, when the surface layer is more compacted, more runoff but less soil loss are expected, since fewer loose particles are expected to be available. This interpretation might help to explain the different behaviour observed between the first and second experimental runs in terms of runoff production and sediment loss.

With respect to the duration of overland flow (Figure 47), as bursts of intense rainfall are located more and more to the end of the events it is observed that the time to runoff decreased, whereas the corresponding base time increased. These trends could also be observed in the overland flow hydrographs (Figure 42) and the infiltration plots (Figure 44). Note that time to runoff is taken from the beginning of the corresponding rainfall burst since there is no runoff observed during the low intensity periods.

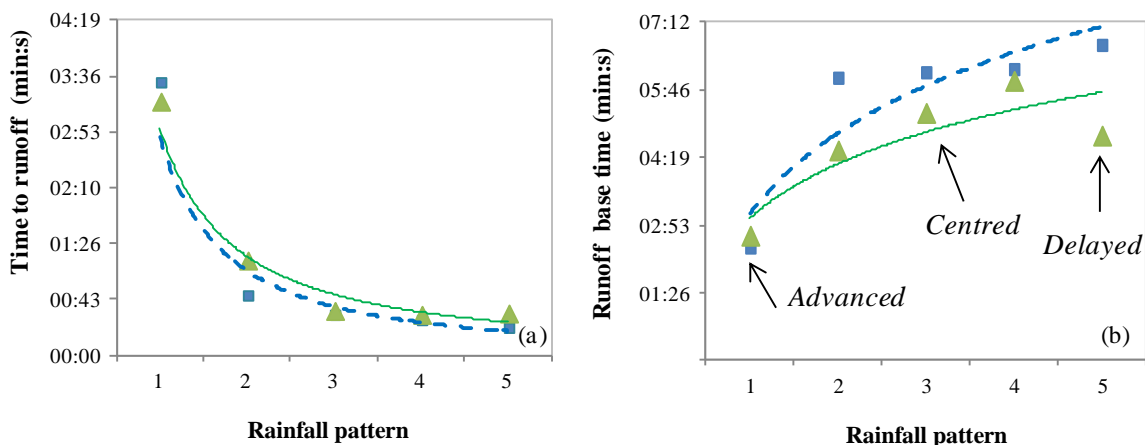


Figure 47. For the five rainfall bursts in the 8 hour event: (a) time to runoff, in relation to the beginning of corresponding high intensity rainfall periods, and (b) duration of surface runoff. Squares and triangles represent empirical data from the first and second set of experiments, respectively, whereas the adjusted lines are only indicative of the tendency in the data.

Although Figure 45, Figure 46 and Figure 47 show a non-linear response, this behaviour cannot be easily extrapolated to other situations without many repetitions, with different soils, slopes and rainfall intensities and patterns, such data will permit to conduct statistical analysis

of the results and thus to get a better insight on the influence of the type of rainfall patterns on runoff and water erosion. Therefore, for the exploratory study reported here the fit lines are merely indicative of a trend in the data and applied only to these specific experiments conducted on the soil flume. But qualitatively, results justify further investigation on the topic of this study.

7.4. Concluding remarks

It is known that heavy rainfall intensities lead to marked detachment of soil particles and facilitate soil loss through increased overland flow. However, the variation of rain intensity within an event is also crucial for the processes of overland flow and soil erosion. But the system is complex and highly nonlinear. All rainfall-runoff processes occurring over permeable surfaces and water erosion processes are tough to model exactly because of the imbricate phenomena involved. This work focused on the effect of the timing of high intensity bursts within events of a given duration and mean intensity. The main findings from this study are:

- It is possible to simulate in the laboratory rain events of varying intensity using a single nozzle rainfall simulator.
- The instant at which rainfall bursts occur during long duration rain events has a strong influence on runoff and associated soil loss.
- In these experiments, the delayed rainfall bursts led to greater runoff depth and total sediment loss, these bursts also generated higher runoff peaks and sediment fluxes than were observed for bursts occurring earlier in the rain event.
- The earlier the intense rainfall period occurs in a given event (advanced pattern), the more delayed is the initiation of runoff, and the runoff base time tends to be smaller.

All these conclusions can largely be explained by the changes in soil moisture content observed as the rainfall event developed, as a consequence of the temporal variability of the infiltration capacity and overland flow (i.e., water depths and velocities). It is likely that alteration of the structure of the soil surface over time (in particular the repeated and cumulative effect of the impact of high intensity rain on the soil surface) might also have contributed to the observed runoff and sediment production. The empirical data used in this exploratory work could also be influenced by the actual soil conditions obtained when filling the flume.

Despite some limitations, this research has practical implications for understanding the runoff and water erosion response to varying rainfall intensities. Ignoring intra-event rainfall variability (e.g. when high intensity burst occurs during a rainfall event) can cause both under- and overestimation of runoff discharge and soil loss. For flood risk management, special attention should be paid to the assessment of the hydrological response to rain events exhibiting a delayed pattern. Although the results obtained in this study, in quantitative terms, cannot be extrapolated to plots or drainage basins, they clearly indicate qualitatively the trend expected in the overland flow and soil erosion processes, triggered by different rainfall patterns. However, it is expected that for very impervious surfaces (i.e., urban drainage basins) the issue of when a high intensity burst occurs during a given rain event is less important than for pervious surfaces because the initial abstractions are smaller.

Further studies should investigate more complex rainfall patterns, other soil types and surface slopes, and be extended to runoff plots and small catchment areas. Special attention should be given to soil moisture monitoring when exploring these processes.

8. USING MESHES TO CHANGE THE CHARACTERISTICS OF SIMULATED RAINFALL PRODUCED BY SPRAY NOZZLES⁴

Abstract

Rainfall simulators have been used for many years contributing to the understanding of soil and water conservation processes. Nevertheless, rainfall simulators' design and operation might be rather demanding for achieving specific rainfall intensity distributions and drop characteristics and are still open for improvement. This study explores the potential of combining spray nozzle simulators with meshes to change rainfall characteristics, namely drop properties (drop diameters and fall speeds). A rainfall simulator laboratory set-up was prepared that enabled the incorporation of different wire meshes beneath the spray nozzles. The tests conducted in this exploratory work included different types of spray nozzles, mesh materials (plastic and steel), square apertures and wire thicknesses, and positions of the meshes in relation to the nozzles. Rainfall intensity and drop size distribution and fall speed were analysed. Results showed that the meshes combined with nozzles increased the mean rainfall intensity on the 1 m² control plot below the nozzle and altered the rain drops' properties, by increasing the mass-weighted mean drop diameter, for example.

⁴ Carvalho, S.C.P., de Lima, J.L.M.P., de Lima, M.I.P. 2014. Using meshes to change the characteristics of simulated rainfall produced by spray nozzles. *International Soil and Water Conservation Research* 2 (2), pp. - (in press)

8.1. Introduction

Rainfall simulation is a common tool that has been widely used in studies related to soil erosion, nutrient and pollutant transport, water conservation and agricultural management practices. One of the main advantages of rainfall simulation is the possibility to generate and replicate rainfall with a specific intensity and duration (e.g. de Lima and Singh, 2003; Potter et al., 2006; de Lima et al., 2013c). In laboratory controlled conditions, it is also possible to reduce the effects of the variability of temperature, humidity and wind, as experienced in the field (e.g. de Lima et al., 2003; Fister et al., 2012). Nevertheless, rainfall simulators' design is demanding, raising questions on rainfall distribution and intensity, drop characteristics, manpower required, energy availability, costs and transportability.

In the literature, one finds many studies that have used rainfall simulators. These include studies by Mutchler and Hermsmeier (1965), de Ploey (1981), Bowyer-Bower and Burt (1989), and de Lima et al. (2003, 2008). However, the rainfall simulators' drop properties and spatial intensity distribution is often not discussed (e.g. Lascelles et al., 2000; Ries et al., 2009) although some studies report on the mean drop size of the simulated rain (e.g. Arnaez et al., 2007; Marques et al., 2007). In natural rain, large mean drop sizes are associated with high rain intensities, but in simulated rain the relationship between drop size and intensity may be different. For example, Parsons and Stone (2006) reported simulated intensities ranging from 59 to 170 mm h⁻¹, but the median drop size remained constant at 1.2 mm.

Rain simulators can be classified according to the way they produce drops. The two most common types of simulators are: (i) non-pressurized rainfall simulators or drop-former simulators which drip water from hypodermic needles and capillary tubes (e.g. Munn and Huntington, 1976; Kamphorst, 1987; Elbasit et al., 2010); (ii) pressurized rainfall simulators, such as spray nozzles (e.g. Meyer and McCune, 1958; Esteves et al., 2000).

Non-pressurized rainfall simulators are less used in the laboratory; but they are a convenient technique for places experiencing difficult access and limitations in water supply (e.g. Humphry et al., 2002). The well-known disadvantage in these simulators is that they produce

a narrow range of drop sizes (e.g. Tossell et al., 1987) and a small drop fall speed. Some non-pressurized rainfall simulators include meshes below the drop formers in order to break up water drops into a distribution of drop sizes closer to that of natural rainfall and to randomize drop landing positions (e.g. Holden and Burt, 2002; Clarke and Walsh, 2007; Fernández-Gálvez et al., 2008).

Pressurized rainfall simulators have an important advantage over the non-pressurized simulators: drops do not rely on gravity to reach terminal velocity, but are sprayed under pressure. For example, the hydraulic spray nozzles, which are commonly used in scientific and technical experiments on soil and water conservation, operate by discharging the water under pressure through an exit orifice with a small diameter. This leads to an increase in water velocity, causing instability in the nozzle exit and subsequent breakup into small drops; typically a spray nozzle provides a broader range of drop sizes compared to non-pressurized simulators (e.g. Battany and Grismer, 2000). Moreover, drops' properties and hence the entire simulated event will depend on the pressure applied, the flow rate, and the nozzle design (e.g. Kincaid, 1996; Cerdà et al., 1997; Erpul et al., 1998).

To our knowledge, meshes have been combined with drop-former simulators but not with nozzle type simulators. However, Schindler Wildhaber et al. (2012) recently described a “field hybrid simulator”, and claimed that the performance of the simulator improved in relation to the mean drop size and kinetic energy when a mesh grid (aperture size of 2 mm × 1.7 mm) was fixed at a distance of 0.5 m under a spray nozzle.

The objective of this study was to further explore the effect of meshes on spray nozzle rain simulations, namely on rain intensity, drop size and drop fall speed. In particular, we are interested in the raindrop properties which are important for calculating rainfall erosivity. These properties depend on the design and operation of rainfall simulators.

8.2. Materials and methods

8.2.1. Laboratory set-up

Figure 48 shows a schematic representation of the laboratory set-up used in this study. The main components are: the rainfall simulator which includes a downward-oriented spray nozzle operating in a static position; a mesh suspended by a system of cables and pulleys at variable vertical distances to the nozzle; and rainfall measuring devices, namely rain gauges and a disdrometer. These measuring devices were set at 2.35 m below the nozzles, on an horizontal plane. The rainfall simulator installation also includes a constant head reservoir, a submersible pump, a pressure tank, a pressure sensor, two pressure gauges, a pressure switch, pipes and a flexible hose.

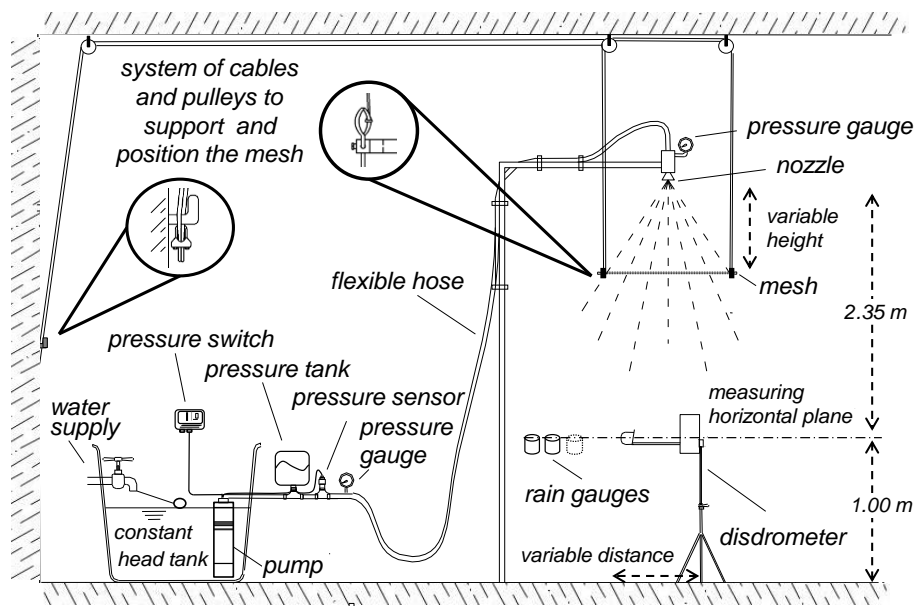


Figure 48. Set-up of the laboratory experiments.

Nozzles

Four types of spray nozzles were used to simulate rainfall with different intensities and drop size distributions. The nozzles selected were single full-cone nozzles (HH-22, HH-14W and

HH-4.3W) and a multiple full-cone nozzle (7G-1). All were manufactured by Spraying Systems Co. Table 18 gives a description of the spray nozzles used in the experiments, including the pressure at the nozzle, spray angle (i.e. angle of the water cone; see Figure 49) and discharge. The pressure at the nozzle was kept constant at 1.5 bar for all the experiments. Spraying Systems Co. (2013) claims that the spray angle of the nozzles is higher at this pressure and that, in general, increasing operating pressure is expected to lead to decreasing drop sizes and increasing drop velocities.

Table 18. Description of the spray nozzles used in the experiments. All nozzles are manufactured by Spraying Systems Co.

Spray nozzle code	HH-22	HH-14W	HH-4.3W	7G-1
Type	Full-cone spray nozzle: standard	Full-cone spray nozzle: wide angle	Full-cone spray nozzle: wide angle	Fine spray nozzle (multiple full cone pattern)
Pressure (bar)	1.5	1.5	1.5	1.5
Discharge (L min ⁻¹)	11.9	7.6	2.3	4.3
Spray angle (°)	90	120	120	170

Meshes

The rain simulator was adapted to allow for the installation of meshes at different distances beneath the nozzles, with the purpose to change the characteristics of the simulated sprays. Thus, the set-up included a system of cables and pulleys that were used to support and position the meshes, which were stretched and attached to a 1 m² metal square frame. The main characteristics of the meshes used in the experiments are described in Table 19. The meshes had different square apertures and wire thicknesses, defining different percentages of open area in relation to the area of the frame. Since the adhesion and surface tension forces depend on the material, two materials were tested: steel and plastic.

Table 19. Properties of the wire meshes used in the experiments.

Meshes	1	2	3	4	5	6
Material	Plastic (polyethylene and polypropylene)			Steel (welded wire)		
Square aperture (mm)	12	20	40	20	40	40
Weight (g m⁻²)	210	470	235	1200	600	5500
Wire thickness (mm)	1.0 - 1.5	2.0 - 3.0	2.0 - 3.0	1.4	1.4	4.0
Open area (%)	82	79	89	87	93	83

Instrumentation

Characteristics of the nozzle sprays such as drop size and fall speed, and raindrop count over time were measured using a Laser Precipitation Monitor, manufactured by Thies Clima (e.g. Thies, 2007). The instrument includes a laser-optical source which produces a light-beam (infrared, 785 nm); in a receiver, the optical intensity is transformed into an electrical signal. When a raindrop falls through the light-beam (measuring area: 4777 mm²) the receiving signal is reduced. The diameter of the drop is calculated from the amplitude of the signal reduction and the drop fall speed is determined from the duration of the reduced signal. The disdrometer used in the laboratory yields the distribution of the raindrops over 21 diameter-size classes (from 0.125 mm to 8.000 mm) and 20 fall speed classes (up to 20.0 m s⁻¹). The class intervals do not all have the same width.

The rain intensity on the target surface was assessed using rain gauges with an opening diameter of 0.116 m, corresponding to a collection area of 10568 mm² (see section 8.2.2 – rainfall intensities).

8.2.2. Methodology

The laboratory experiments were comprised of rain simulations from spray nozzles combined with meshes and spray nozzles only (i.e. the meshes were absent from the rain simulations). For these two cases, the simulated rainfall intensity and drop size and fall speed were examined. The laboratory procedures included: (1) selection of the nozzle and operating pressure of 1.5 bar; (2) selection of a mesh, which was positioned at a certain vertical distance from the nozzle; (3) start of the rainfall simulation; (4) rain measurements (rain gauges and disdrometer). We have undertaken the measurements defined in Table 20 and explained below.

Table 20. Summary of experiments using different combinations of nozzles and meshes.

	Material	Aperture (mm)	Thickness (mm)	Vertical distance to the nozzle (mm)	Spray Nozzles							
					HH-22		HH-14W		HH.4.3W		7G-1	
					Rain gauges	Disdrometer	Rain gauges	Disdrometer	Rain gauges	Disdrometer	Rain gauges	Disdrometer
Meshes	Plastic	12	~1.25	200	✓	•	✓	•	✓	•	✓	•
				400	✓	•	✓	•	✓	•	✓	•
				600	✓	•	✓	•	✓	•	✓	•
		20	~2.5	200	✓	•	✓	•	✓	•	✓	•
				400	✓	•	✓	•	✓	•	✓	•
				600	✓	•	✓	•	✓	•	✓	•
	40	~2.5	600			✓	•					
	Steel	20	1.4	600			✓	•				
		40	4.0	600			✓	•				
		40	1.4	600			✓	•				
without meshes					✓	•	✓	•	✓	•	✓	•
✓	3 replicates; 15 rain gauges (5 rain gauges located on the control plot), see Figure 50c.											
•	disdrometer in 3 positions, 3 replicates (sampling time was 15 seconds), see Figure 50d.											
	Not measured											

Position of the meshes

The meshes were suspended at three positions: 200, 400 and 600 mm vertical distances below the nozzles. These three positions of the meshes are represented schematically in Figure 49,

which also shows the spray angle and the spray boundary for each nozzle, obtained for an operation pressure of 1.5 bar. This figure illustrates the expected interception of the sprays by the square meshes ($1 \times 1 \text{ m}^2$), which varies with the vertical distance between the meshes and the nozzles. At some positions the meshes are able to intercept the whole spray. The information on the nozzles' sprays was based on photographs captured during the experiments.

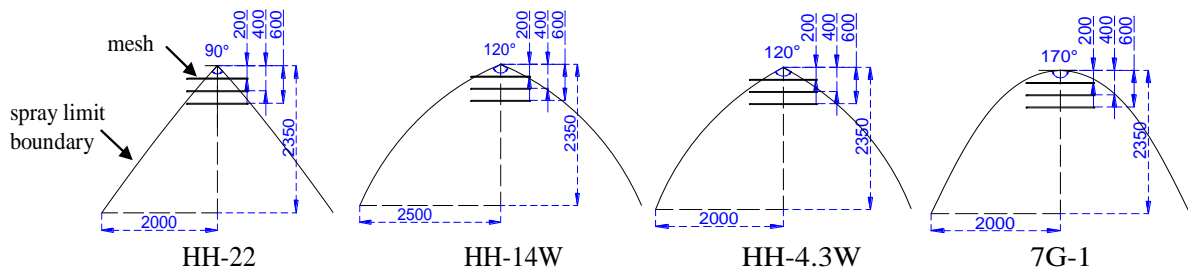


Figure 49. Spray angle and spray limit boundary for the 4 nozzles used in the experiments; the 3 mesh positions beneath the nozzles are represented. The nozzle vertical distance to the target surface is 2.35 m; operating pressure is 1.5 bar; on the target surface, measures are for the wetted area. Distances are in mm.

Rainfall intensities

A control square plot of 1 m^2 was used for assessing the simulated rainfall intensities on the target surface. This plot (horizontal measuring plane, in Figure 48) was defined at a height of 1 m above the floor and at a vertical distance of 2.35 m below the nozzle, and was centred in relation to the nozzle position. We will refer to this area as “control plot”. We noticed that this control plot size has been adopted in many soil and water conservation studies on small scale field plots that have used rainfall simulators.

The distribution of the simulated rainfall intensity on the control plot was evaluated with 41 rain gauges scattered over the plot (Figure 50a); the sampling interval for the rain measurements was three minutes and 3 replicates were undertaken. The uniformity of the distribution was assessed using the coefficient of uniformity (CU) defined by Christiansen (1942).

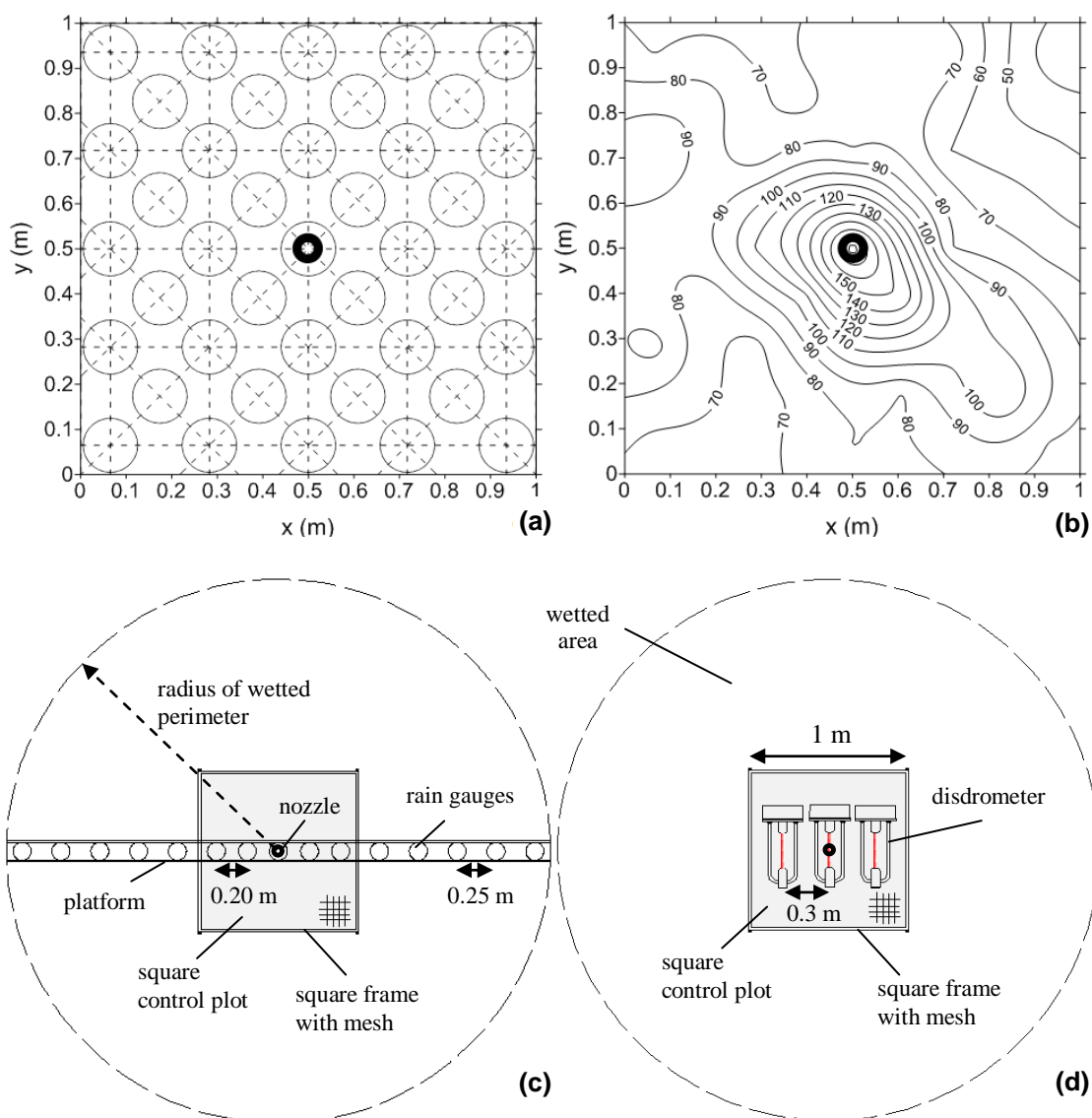


Figure 50. (a) Position of the 41 rain gauges used to measure the rainfall intensity on a 1 m² square plot (control plot, top view); (b) Spatial distribution of the simulated rainfall intensity [mm h⁻¹] under the 7G-1 nozzle, estimated using Kriging; (c) Position of 15 rain gauges used to measure the rainfall intensity along a given direction (top view); (d) The position of the disdrometer used to measure drop properties (top view). The black ring identifies the position of the nozzle.

The laboratory work involved 32 experiments that included combinations of 4 nozzles with 6 meshes, positioned at 3 vertical distances from the nozzle (not all possible combinations were considered in this exploratory work; see Table 20). In addition, 3 replicates were carried out

for each case. Because using a 41 rain-gauge grid for assessing the rainfall spatial distribution for all these cases would imply a great number of measurements, and because the rainfall intensity distribution was observed to be approximately symmetric (see Figure 50b, for nozzle 7G-1), then the rainfall distribution on the target surface was estimated by studying the rain distribution along a single transect; this is illustrated in Figure 50c that shows equally distributed rain gauges set along a given direction defined on the wetted area, at the target surface level. Thus, estimates of rainfall intensity on the control plot used data from 5 rain gauges, distributed along 1 m; and across the whole wetted area rain intensity was estimated using data from 15 rain gauges that covered a 3.5 m distance (Figure 50c).

Drop properties

Raindrop diameter and fall speed were recorded with a laser disdrometer, which was positioned with the light-beam coinciding with the target surface (i.e. measuring plane of the rain gauges). Three measuring positions were adopted on this plane (Figure 50d). Measurements' sampling time was 15 seconds; this small sampling time is explained by limitations of the disdrometer and its software in handling a large number of raindrops during the usual 1-minute resolution of the device, because counting limits of the number of particles were surpassed during the laboratory runs and the 1-minute data were then not reliable. So, to avoid exceeding the number of drops' counting limit we have restricted the observation time; we expect that the time variability in the simulations is small and that this procedure did not introduce important bias in the results; we nevertheless took 3 replicates of the measurements and calculated the mean. For each measurement the instrument provides a two dimensional matrix with the count of drops in each of the size and fall speed classes, which is used for determining the drop size distribution of the simulated rain.

The number and size of raindrops within a unit volume of air can be described by the number concentration, $N(D)$ [$\text{mm}^{-1}\text{m}^{-3}$], also called the raindrop size distribution (DSD), where D [mm] is the spherical equivalent diameter of each raindrop. The expected number of drops $N(D_i)$ [$\text{mm}^{-1}\text{m}^{-3}$] in the raindrop size class i (21 classes, with D_i [mm] being the central diameter of the size class i) is obtained by :

$$N(D_i) = \frac{1}{A\Delta t\Delta D_i} \sum_{j=1}^{20} \frac{n_{ij}}{v_j} \quad (8.1)$$

where n_{ij} is the number of detected raindrops in the size class i and belonging to the fall speed class j (20 classes) that is measured during the interval Δt (here is $\Delta t=15$ s, as explained above), v_j [m s^{-1}] is the fall speed of the raindrops at the middle of the fall speed class j , A [m^2] is the disdrometer detection area and ΔD_i [mm] is the width of the drop size class i .

The DSD can also be described in general by the mass-weighted mean drop diameter, D_m [mm], which is estimated using (e.g. Ulbrich, 1983):

$$D_m = \frac{\sum_{i=1}^{21} D_i^4 N(D_i) \Delta D_i}{\sum_{i=1}^{21} D_i^3 N(D_i) \Delta D_i} = \frac{\sum_{i=1}^{21} D_i^4 \left(\frac{1}{A\Delta t} \sum_{j=1}^{20} \frac{n_{ij}}{v_j} \right)}{\sum_{i=1}^{21} D_i^3 \left(\frac{1}{A\Delta t} \sum_{j=1}^{20} \frac{n_{ij}}{v_j} \right)} \quad (8.2)$$

The mean fall speed of the raindrops, v_m [m s^{-1}], is calculated by:

$$v_m = \frac{\sum_{j=1}^{20} n_j v_j}{N} \quad (8.3)$$

where n_j is the number of detected raindrops in the fall speed class j , v_j [m s^{-1}] is the central fall speed of the fall speed class j , and N is the total number of detected raindrops.

8.3. Results and discussion

This section is dedicated to exploring simulated rainfall intensities and drop properties. The control runs were for mesh free simulations (i.e. without combining nozzles and meshes).

8.3.1. Rainfall intensities

The distribution of the simulated rainfall intensity on the target surface (at 2.35 m below the nozzle) were examined for different experimental runs (Table 20). We aimed at investigating the impact of the following variables on the simulated rain intensities:

-
- i) *Nozzle type*: rainfall intensities simulated by different nozzles were compared, with each nozzle being combined with one plastic mesh (20 mm square aperture), and for 3 mesh positions;
 - ii) *Mesh position*: rainfall intensities obtained for 3 mesh positions were compared for combinations of 4 nozzles and 2 plastic meshes (12 mm and 20 mm square aperture);
 - iii) *Mesh characteristics*: rainfall intensities obtained using different mesh characteristics (material, aperture and wire thickness) were compared for rain simulated by one nozzle type (HH-14W) and the meshes positioned at one fixed position (i.e. at 600 mm vertical distance below the nozzle).
 - a) *Material*: the influence of the meshes' material on the simulated rain was studied by comparing the effects of 3 plastic meshes with those of 3 steel meshes.
 - b) *Aperture*: the effect of different meshes' apertures was studied by comparing the rainfall intensities obtained using plastic meshes with square aperture of 20 mm and 40 mm (both with ~2.5 mm wire thicknesses). The same effect was studied for the steel meshes with squares apertures of 20 mm and 40 mm (both with 1.4 mm wire thicknesses).
 - c) *Wire thickness*: the influence of the wire thicknesses was explored by comparing the impact of 40 mm square aperture steel meshes with wires of 1.4 mm and 4 mm thicknesses.

With and without combining the nozzles with meshes

The mesh-free rainfall simulations were compared with the rainfall altered by combining the four nozzles with plastic meshes of 20 mm square aperture, positioned at three different distances from the nozzles (200, 400 and 600 mm). Figure 51a to Figure 51d show the rain intensities observed along the 3.5 m diameter of the wetted area on the target surface.

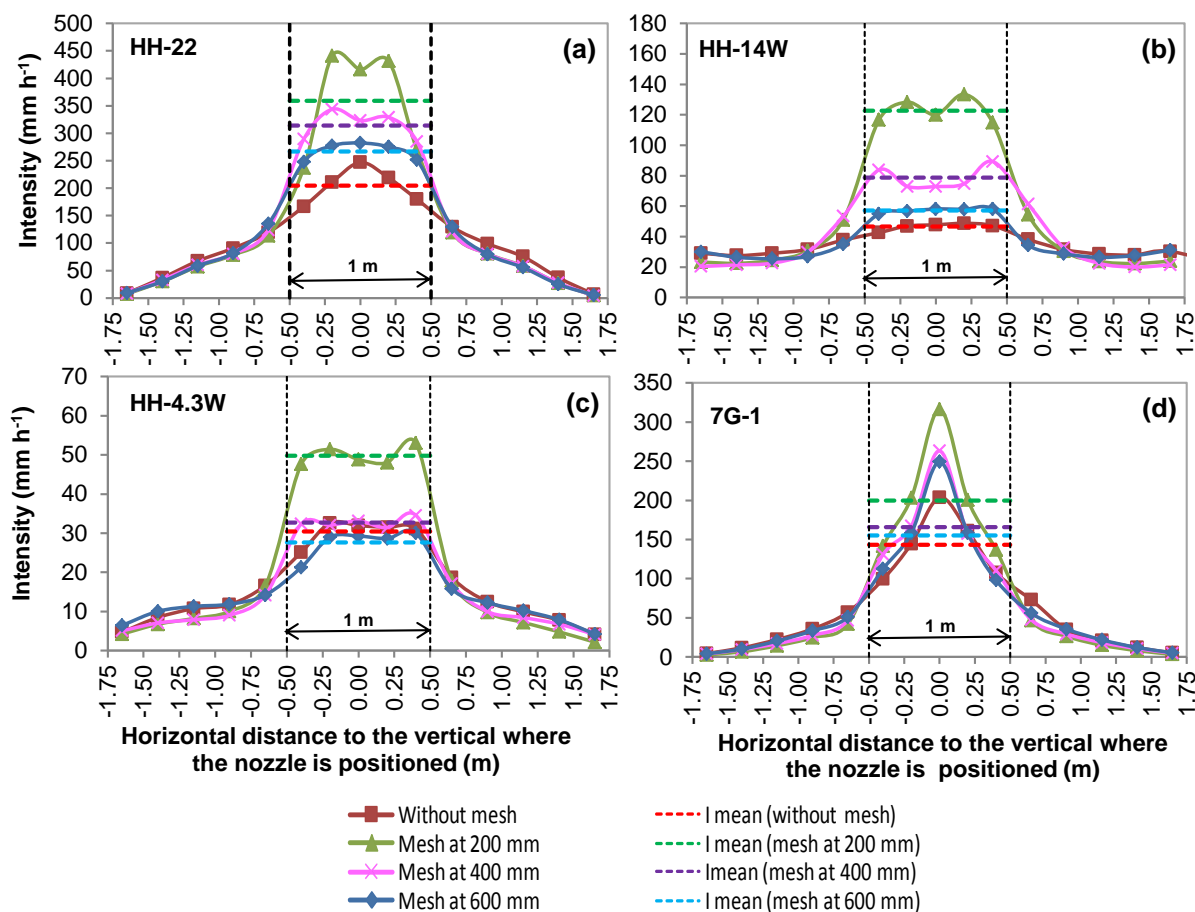


Figure 51. Rainfall intensities observed along the 3.5 m diameter of the nozzle spray wetted circle, for simulations conducted without combining the nozzles with meshes and combining the nozzles with a plastic mesh (square aperture of 20 mm) that was positioned beneath the spray nozzles, at vertical distances of 200, 400 and 600 mm: (a) HH-22; (b) HH-14W; (c) HH-4.3W and (d) 7G-1. Data are average values of 3 replicates.

Nozzles HH-22 and 7G-1 are the ones producing the highest intensities beneath the nozzle, which decreases strongly a short distance away (Figure 51a and Figure 51d); they also yield less uniform water distribution on the control plot. Figure 51 shows that the mean rainfall intensities were higher for meshes combined with the nozzles than for mesh-free simulations. The mesh used affects the distribution of the rainfall intensity generated by nozzles: it is responsible for concentrating the rainfall intensity on the area below the nozzle because most drops that hit the meshes will fall vertically underneath, although some drops can also be ejected away from the meshes by splash.

Meshes at different distances from the nozzle

The importance of the vertical distance adopted between the nozzle and the mesh underneath was assessed for the control plot; we tested distances of 200, 400 and 600 mm. Results show that, in general, this distance affects the mean rainfall intensity simulated, which tends to increase as this distance decreases (Figure 52a). The corresponding wire thickness of the meshes are different (see Table 19) but this variable seems not to affect the results.

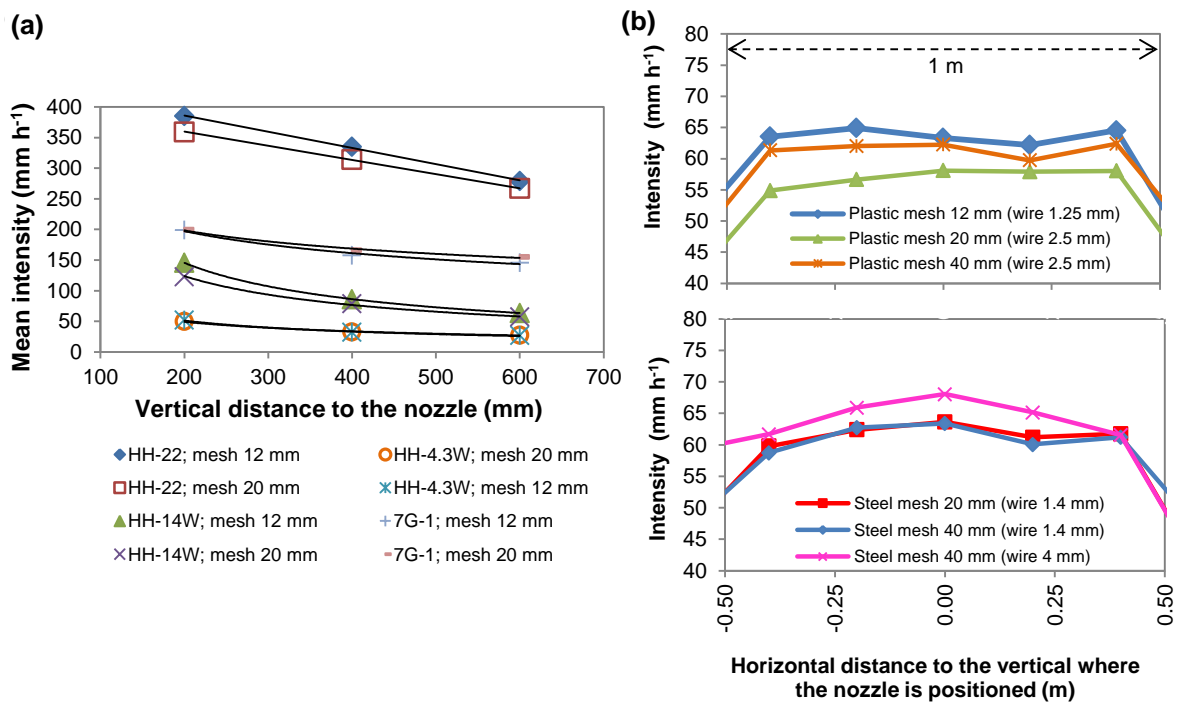


Figure 52. (a) Mean rainfall intensities observed combining nozzles with plastic meshes (square aperture of 12 mm and 20 mm) as a function of the vertical distances between the meshes and the nozzle; data are average values for the control plot and lines are only indicative of trends. (b) Comparison between the rainfall intensities observed along the control plot when combining the spray nozzle HH-14W with plastic meshes (square apertures of 12, 20 and 40 mm) and steel meshes (square apertures of 20 mm and 40 mm); the distance between the mesh and the nozzle was 600 mm.

Meshes made of two materials, different square apertures and thicknesses

The effect of the meshes' material (plastic and steel) was attempted by using only one nozzle type (HH-14W), one distance to the nozzle (600 mm), and two square apertures for both the plastic and steel meshes (20 mm or 40 mm).

Descriptive statistics of the measured rainfall intensities are given in Table 21. The mesh material (plastic and steel) seems not to influence much the measured rain intensities (Figure 52b). The results obtained using plastic and steel meshes with different square apertures also show that the aperture of the meshes used seems not to affect significantly the intensity of the simulated rainfall (Figure 52b). Also, there is no clear evidence of the impact of the wire thickness on the measured rain intensities.

Table 21. Descriptive statistics of rainfall intensities measured in the control plot, for nozzles combined with steel and plastic meshes. The spray nozzle type used was HH-14W and the vertical distance between the mesh and the nozzle was 600 mm. Data are for the 5 gauges in the control plot (Figure 50c), 3-minute sampling time, and 3 replicates.

Material	Meshes						Without mesh
	Plastic wire			Steel wire			
Square aperture (mm)	12	20	40	20	40	40	
Wire thickness (mm)	1.0-1.5	2.0-3.0	2.0-3.0	1.4	4.0	1.4	
Average (mm h ⁻¹)	63.7	57.1	61.5	61.8	64.5	61.2	46.6
Minimum (mm h ⁻¹)	62.2	54.9	59.7	59.8	61.6	58.8	42.6
Maximum (mm h ⁻¹)	64.9	58.1	62.4	63.6	68.1	63.4	48.7
Coef. variation	0.02	0.02	0.02	0.02	0.04	0.03	0.05
Coef. uniformity (%)	98.7	98.1	98.7	98.4	96.5	97.6	96.5

8.3.2. Diameter and fall speed of drops

The diameter and fall speed of the raindrops was analysed for the 4 nozzles tested. The rainfall simulated without using meshes was compared to the rain produced when a plastic

mesh (with a square aperture of 20 mm) was positioned at three distances from the nozzle (200, 400 and 600 mm).

Results suggest that, overall, the presence of meshes increased the mass-weighted mean drop diameter (D_m) of the simulated rainfall; in Figure 53a, the majority of points are located above the 1:1 line. The mass-weighted mean diameter of the drops simulated with all the nozzles without using meshes varied between 0.65 mm and 1.76 mm and between 0.73 mm and 2.69 mm when meshes were used.

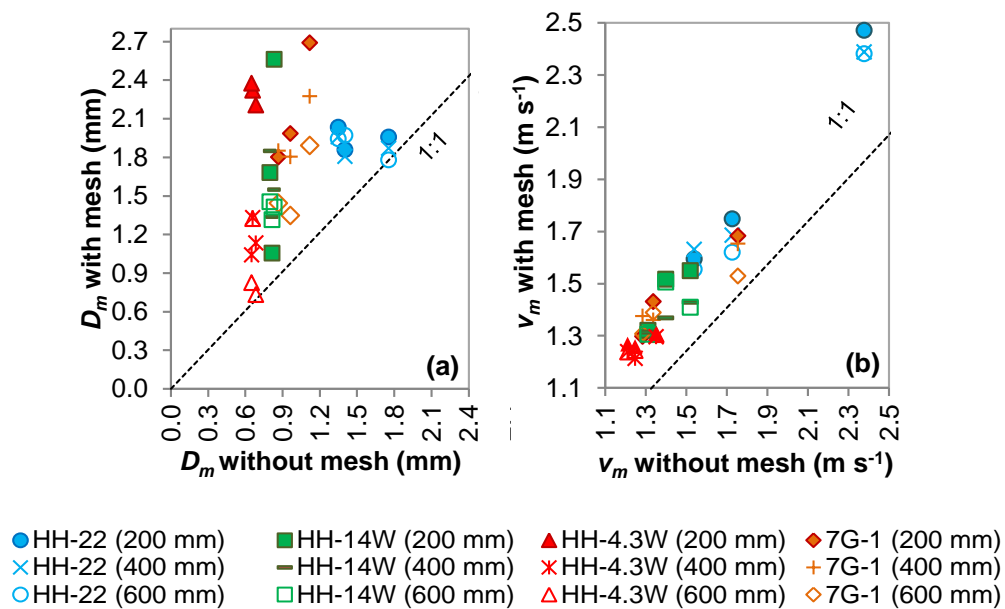


Figure 53. Comparison of simulated raindrops' properties observed combining the spray nozzle with a plastic mesh (square aperture of 20 mm) and without mesh: (a) mass-weighted mean diameter; (b) mean fall speed. The spray nozzles tested are identified in the legend. The results are for meshes positioned at three vertical distances from the nozzles: 200, 400 and 600 mm. The data were collected during 15 s (3 replicates) with a laser disdrometer positioned in three positions that correspond to the 3 data points for each combination nozzle type-distance (see Figure 50d).

The formation of larger drops that are caused by the meshes, in relation to the mesh-free simulations, increased the mass-weighted mean diameter of the simulated raindrops and lead

to a broader range of drop sizes. This is illustrated in Figure 54 that shows the effect of the plastic mesh (square aperture of 20 mm) on the rain simulations recorded just below the 4 nozzles. It is expected that water drops that hit the meshes will detach from it after growing up to a size at which its weight overcomes the surface tension force, thus the number of larger drops increases. We note that the increase in drop size caused by the meshes is less strong for the HH-22 nozzle; this is because the nozzle was nevertheless producing drops larger than the other nozzles, even without the meshes. In particular, just below the nozzle the maximum drop diameter recorded for this case was 6.25 mm. Other properties of the spray formed by this nozzle are discussed below.

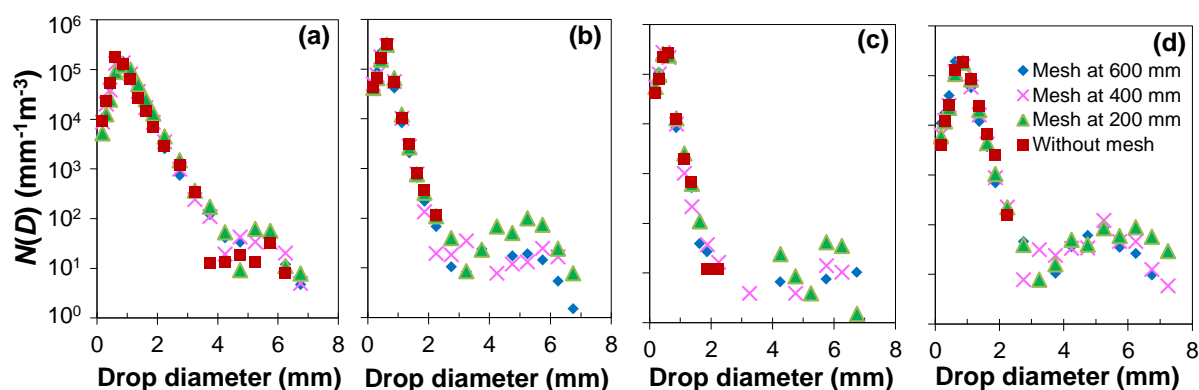


Figure 54. Rain drop size distribution produced by spray nozzles combined with a plastic mesh (square aperture of 20 mm) and without mesh: (a) HH-22; (b) HH-14W; (c) HH-4.3W; (d) 7G-1. The data were collected with the disdrometer positioned in the centered position, on the measuring plane, and the meshes were positioned at three distances from the nozzle.

The fine 7G-1 spray nozzle forms very small droplets, yielding a rather dense spray resembling fog. The expectation is that the smaller number of drops in the lowest drop size class reported by the laser disdrometer (Figure 54d) in comparison to other nozzles (Figure 54a, Figure 54b and Figure 54c) is explained, at least partly, by the lower size-limit detection for the drops (i.e. 0.125 mm diameter) which could lead to undersampling of small drops below this limit. However, this effect, if present, does not affect the qualitative evaluation of the impact of meshes on changing the properties of the drops formed by this nozzle.

The drop fall speed seems not to be much affected by the presence of meshes. Figure 53b shows that drop fall speed ranges from 1.2 m s^{-1} to 2.4 m s^{-1} for the mesh-free simulations and are between 1.2 m s^{-1} and 2.5 m s^{-1} for the simulations conducted with meshes. This figure shows that in 36% of the tests the fall speed was higher in the simulations using meshes, and smaller in 28% of them. Nevertheless, it might be expected that without meshes the fall speed is higher, because drops are forced out of the spray nozzles at high velocities, whereas drops that fall from meshes have an initial velocity of zero. However, despite the short fall distance from the mesh to the ground, the bigger drops that are formed due to the presence of meshes fall faster because of their greater mass; in addition, it is expected that the majority of drops fall to the target surface without hitting the mesh. Similar results were obtained for the plastic mesh of 12 mm aperture (Figure 52b and Table 21).

8.4. Concluding remarks

A laboratory set-up was prepared to evaluate the impact of combining meshes with spray nozzles on rain simulations, with the meshes being positioned underneath the nozzles and intercepting the spray (i.e. the drops trajectories). The meshes were made of plastic and steel, with square apertures from 12 to 40 mm, installed at various vertical distances away from the nozzles. For the control plot, we report the following findings:

(i) Rainfall intensities

- In general, the meshes increased the mean rainfall intensity on the control plot, beneath the nozzle, as most raindrops that hit the meshes fall vertically underneath; nevertheless, this effect on the rain simulations is affected by the distance between the mesh and the nozzle.
- The mean rainfall intensity under the meshes increases as the distance between the meshes and the nozzles decreases; this is also explained by the drop concentration effect caused by the interception of the drop trajectories by the mesh.

– The meshes' material (plastic and steel), wire thickness and square apertures seem not to have much influence on the simulated rain properties; but the limited number of conditions studied restricts the analysis of results and hence the tests were not conclusive.

(ii) Raindrop properties

While intercepting the nozzle sprays, the meshes altered the simulated raindrops' properties. In particular, for the raindrops diameter and fall speed, the main findings were:

- The mass-weighted mean diameter of the simulated raindrops was higher when meshes were used, in relation to the simulations carried out without combining meshes and nozzles. Because spray nozzles generate typically small drop sizes and narrow drop size distributions, when meshes are combined with nozzles they promote the formation of bigger drops and the randomization of their landing positions;
- The mean fall speed of the simulated raindrops was similar for simulations carried out with and without meshes. Results suggest that overall the meshes might not have much influence on the mean fall speed because regardless of the presence of the meshes a large amount of drops still fall directly from the nozzle without hitting the meshes.

Thus, meshes can be used to alter the mean rainfall intensity produced by spray nozzles, and also the drop sizes. Note that by varying the operating nozzle pressure, which was kept constant in this exploratory work, the diameter and fall speed of drops can be changed. Indeed, lower nozzle pressures yield larger drops with lower fall speed, whereas higher pressures produce smaller drops with higher fall speed.

In this study no attempt was made to reproduce natural rainfall. Further research should be done to investigate how nozzle type, operating pressure and meshes can be used to adjust the characteristics of spray nozzle simulated rainfall to those of a specific natural rainfall.

9. INCREASING THE RAINFALL KINETIC ENERGY OF SPRAY NOZZLES BY USING MESHES⁵

Abstract

Rainfall simulators are an important tool in studying soil erosion, which is a key process contributing to land degradation. The kinetic energy of simulated rain is central to these studies and it is used as an indicator of the raindrops' ability to detach particles from the soil surface. The main purpose of this experimental work was to explore the usefulness of incorporating meshes underneath pressurized nozzles' rain simulators, that intercept the drops sprayed out by the nozzles and change the simulated rain characteristics, namely by increasing the rainfall kinetic energy. The laboratory experiments included testing four types of spray nozzles (discharge from 2.3 to 11.9 L min⁻¹), combined with a high-density polyethylene mesh (square aperture of 20 mm). The effect of the mesh was studied for three vertical distances between the nozzle and the mesh (200, 400 and 600 mm). A laser disdrometer was used to measure the diameter and fall speed of the simulated raindrops. For the mesh-free simulations, the nozzles produced drops having on average a mean equivalent diameter of around 0.6 mm and a mean fall speed of about 1.5 m s⁻¹. The mesh increased the formation of bigger drops (>2.5 mm) and, consequently, increased the rainfall kinetic energy of the simulated rain; the magnitude of this increase varied with the spray produced by the nozzles. Results show that meshes can be useful for increasing the kinetic energy of the rainfall simulated by nozzles within soil erosion studies.

⁵ Carvalho, S.C.P., de Lima, J.L.M.P., de Lima, M.I.P. 2014. Increasing the rainfall kinetic energy of spray nozzles by using meshes. *Land Degradation & Development*. (In revision: revised manuscript submitted)

9.1. Introduction

Land degradation is a worldwide process triggered by humankind, highly associated with soil erosion and transport of pollutants. Soil erosion is a key process to understand the role of water, nutrients, sediments and organic matter losses, which reduce soil fertility and contribute to land degradation. Over time, many authors have published on these problems, either by reporting on case studies from different parts of the world (recent works are e.g. Abu Hammad and Tumeizi, 2012; Meshesha et al., 2012; Thomaz and Luiz, 2012; Zhao et al., 2013), which includes discussing solutions by means of sustainable land management practices, or examining relevant processes and mechanisms in detail (e.g. Cerdà, 1998; Ziadat and Taimeh, 2013). Experimental field and laboratory work, relying on simulations of rain, have contributed much to the increased understanding of various hydrological and geomorphological processes. The versatility of rainfall simulators enables them to be used in the laboratory and in the field, providing controlled conditions of rainfall intensity and duration (e.g. Wilcox et al., 1986; Kamphorst, 1987; Kainz et al., 1992; Cerdà et al., 1997; Regmi and Thompson, 2000; Grismer and Hogan, 2004; de Lima et al., 2005; Seeger, 2007; de Lima et al., 2009; 2013c).

However, the capacity of reproducing natural rainfall events through simulations is limited; this has been discussed by e.g. Agassi and Bradford (1999), Dunkerley (2008a), Fernández-Raga et al. (2010), Abudi et al. (2012), and Ries et al. (2014). Namely, some authors (e.g. Hall, 1970; Cerdà, 1997; Fernández-Gálvez et al., 2008) pointed out that in soil water erosion studies simulated raindrops should desirably have the size and fall speed observed in nature, since these are key variables affecting the kinetic energy of individual drops that particularly enhance soil detachment (e.g. Bisal, 1960). Some studies have also revealed important relationships between the kinetic energy of raindrops and soil surface sealing (e.g. Thompson and James, 1985; Ziegler et al., 1997; Assouline, 2004): high kinetic energy of drops can induce soil surface sealing and consequently reduce the infiltration rate. The simulated rainfall kinetic energy is therefore crucial when choosing the most appropriate type of simulator for a particular purpose.

Although a large diversity of rainfall simulators are currently used, the most common types are non-pressurised rainfall simulators (drop-formers) (e.g. Walker et al., 1977; Kamphorst, 1987) and pressurised rainfall simulators (e.g. Dunne et al., 1980; Cerdà et al., 1997; de Lima et al., 2003; Montenegro et al., 2013). Cerdà (1999) gives an extended review on both types of simulators, and discusses their advantages and inconveniences for rainfall simulations.

The advantages of non-pressurised simulators are related to the spatial rainfall uniformity they yield, since these simulators produce uniformly-sized drops; however, this can turn out to be also a disadvantage (e.g. Tossell et al., 1987). In addition, the drops' fall velocities attained (fall under gravity) might hamper the reproduction of the kinetic energy of natural rain. In order to break up the raindrops and create a drop size distribution closer to that of natural rainfall, as well as to random the drops' landing positions, some experimental set-ups include meshes under the non-pressurised drop formers (e.g. Clarke and Walsh, 2007; Fernández-Gálvez et al., 2008).

The pressurised rainfall simulators have spray nozzles that can be characterized by the nozzle discharge, spray angle and pattern, and drop size (e.g. Omer and Ashgriz, 2011). In contrast to drop-formers, in these rainfall simulators drops do not rely on gravity to reach terminal velocity since they are sprayed out under pressure (e.g. Tossell et al., 1987). Moreover, pressurised rainfall simulators provide a wider range of drop sizes than non-pressurised simulators, which randomly land on the surface. However, the drop's properties and hence the entire simulated event will depend on the system operating pressure, the flow rate and the nozzle design (e.g. Kincaid, 1996; Erpul et al., 1998). All these factors could explain why meshes have seldom been used in this type of experimental set-ups. Recently, Schindler Wildhaber et al. (2012) conducted a series of experiments using a rainfall simulator that comprised a wire mesh screen suspended (0.5 m) below a spray nozzle. In their work, the authors stated that despite not being possible to achieve natural rain conditions with the proposed simulator, its performance improved with respect to the mean drop size and kinetic energy of the simulated rain.

As pointed out by e.g. Aksoy et al. (2012), the calculation of simulated rainfall kinetic energy is not common in literature. In addition, some studies (e.g. Iserloh et al., 2013) claim that the kinetic energy of simulated rain is often likely overestimated since the values are typically calculated based on assumptions that diameters and/or velocities from natural rainfall apply for simulated rainfall.

This study is dedicated to explore the effect of meshes on the kinetic energy of rainfall produced by spray nozzle simulators. This modification of the experimental installation, which consists of combining nozzles and meshes, is expected to increase the versatility of nozzles in experimental simulations of rain. Thus, a laboratory set-up was prepared aiming at exploring different combinations of types of nozzles and distances between the mesh and the nozzle. The usefulness of these experiments is to increase our understanding of rain simulations using nozzles, namely on laboratory and field studies of soil erosion and surface hydrology processes.

9.2. Materials and Methods

9.2.1. Laboratory installation

The laboratory installation was prepared by coupling a mesh to a nozzle rainfall simulator (Figure 55). The experimental set-up includes: a constant head reservoir, a submersible pump, flexible hoses, a downward-oriented spray nozzle and a mesh suspended horizontally underneath by a system of cables and pulleys.

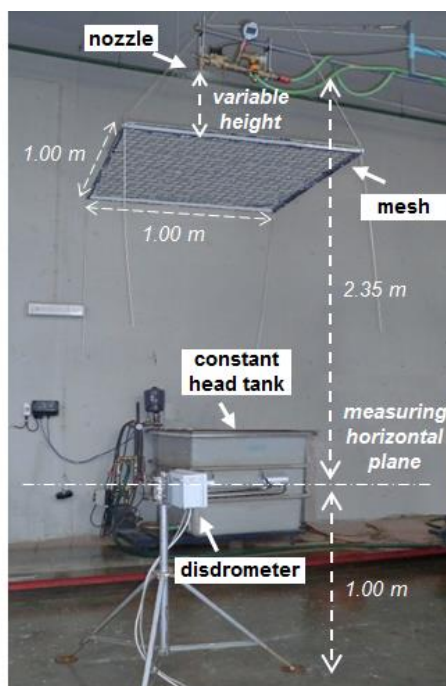






Figure 55. View of the laboratory installation, showing the nozzle, the suspended mesh underneath and the disdrometer.

In order to explore the effect of a mesh on the intensity and drop characteristics of simulated rainfall, four types of spray nozzles manufactured by Spraying Systems Co. were used: three single full-cone nozzles (named HH-22, HH-14W and HH-4.3W); and one multiple full-cone nozzle (7G-1). Table 22 shows the spray angle and discharge for these nozzles, which were operated at a pressure of 1.5 bar. Note that by varying the operating nozzle pressure, the drop characteristics can be changed. Spraying Systems Co. (2013) reported that the angle of the water cone is higher at this pressure (for the studied nozzles); increasing the operating pressure would reduce drop sizes and increase drop velocities, whereas, on the opposite, a pressure reduction would increase drop sizes and decrease drop velocities. In relation to kinetic energy, as it depends on the number, size and fall speed of drops, the effect of changing the nozzle pressure will be determined by the impact caused on these drop's properties; nevertheless, this effect was not studied here.

Table 22. Description of the spray nozzles used in the experiments. All nozzles are manufactured by Spraying Systems Co. The operating pressure was 1.5 bar for all the experiments.

Spray nozzle code	HH-22	HH-14W	HH-4.3W	7G-1
Nozzle photograph				
Discharge (L min ⁻¹)	11.9	7.6	2.3	4.3
Spray angle (°)	90	120	120	170

The mesh, which was attached to a metal square frame of 1 m², is made of high-density polyethylene and has 20 mm square aperture; the thickness of the wire is around 2.5 mm.

The simulated rainfall was measured using a Laser Precipitation Monitor (LPM) from Thies Clima (Thies, 2007). This disdrometer consists of a laser-optical source that produces a parallel light-beam (the area of detection is 4777 mm²). The instrument determines the size and fall speed of drops by measuring the signal reduction caused by the drop falling through the light-beam; the amplitude and duration of the reduced signal is used to estimate the drop size and fall speed, respectively. The instrument provides information on the total number of drops over 21 size classes (from 0.125 mm to 8.000 mm) and 20 fall speed classes (up to 20.0 m s⁻¹); for both drop size and fall speed, the amplitude of the classes is variable.

9.2.2. Methodology

The mesh (1 m²) was positioned centred and at three vertical distances below the nozzles: 200, 400 and 600 mm. Rainfall measurements were performed under the nozzle with and without the presence of the mesh.

The characteristics of the simulated rainfall, namely rain intensity, and size and fall speed of drops, were measured using a disdrometer installed at 2.35 m below the nozzle (Figure 55). The disdrometer was positioned in three locations: just beneath the nozzle and at a horizontal distance of 0.30 m (opposite positions); it was kept recording in each position during 3 minutes. Due to limitations of the disdrometer software in handling a large number of raindrops, the sampling interval adopted in this study was 15 seconds instead of the standard 1-minute interval, defined by the device manufacturer by default. This was achieved by repeatedly covering the disdrometer during 45 seconds of each minute recorded, leaving it exposed to the simulated rain during 15 seconds in each minute (thus, the data were assumed to represent 3 measurements' repetitions, one for each 15 seconds sampled). For each sampled interval, the instrument provided a two dimensional matrix with the count of drops in each of the size and fall speed classes. Thus, for each position of the disdrometer, the three matrices (i.e. for the 3 repetitions) were averaged to obtain one single matrix for each case, which were used for determining the mean drop diameter (Eq. 9.1), the mean drop fall speed (Eq. 9.2), the rainfall intensity (Eqs. 9.3 and 9.4), and the rainfall kinetic energy (Eqs. 9.5 to 9.8).

The mean drop diameter, D_{mean} [mm], was obtained by:

$$D_{\text{mean}} = \frac{\sum_{i=1}^{21} n_i D_i}{N} \quad (9.1)$$

where n_i is the number of detected raindrops in the size class i , D_i [mm] is the drop diameter at the middle of the size class i , and N is the total number of detected raindrops. D is the spherical equivalent diameter of the raindrops.

The mean fall speed, V_{mean} [m s^{-1}], was calculated as:

$$V_{\text{mean}} = \frac{\sum_{j=1}^{20} n_j v_j}{N} \quad (9.2)$$

where, n_j is the number of detected raindrops in the fall speed class j , v_j [m s^{-1}] is the fall speed at the middle of the fall speed class j , and N is the total number of detected raindrops.

The rainfall intensity, R [mm h^{-1}], was obtained by (e.g. Krajewski et al., 2006):

$$R = \sum_{i=1}^{21} R(D_i) \quad (9.3)$$

with $R(D_i)$ being the intensity for a given drop size class i :

$$R(D_i) = \frac{\pi}{6A\Delta t} n_i D_i^3 \quad (9.4)$$

where n_i is the number of drops detected in the size class i during the interval $\Delta t = 15/3600$ h, D_i [mm] is the drop diameter at the middle of the size class i , and A is the disdrometer detection area [m^2].

The time-specific kinetic energy KE_{time} [$\text{J m}^{-2} \text{h}^{-1}$] of the simulated rain was calculated by (e.g. Usón and Ramos, 2001):

$$\text{KE}_{\text{time}} = \sum_{i=1}^{21} \text{KE}_{\text{time}}(D_i) \quad (9.5)$$

with

$$\text{KE}_{\text{time}}(D_i) = \frac{\rho \pi}{12A\Delta t} \sum_{j=1}^{20} n_{ij} v_j^2 D_i^3 \quad (9.6)$$

where ρ is the water density (10^{-6} kg mm^{-3}), n_{ij} is the number of detected raindrops in the size class i and fall speed class j , which is measured during the interval Δt (15/3600 h), v_j [m s^{-1}] is the fall speed of the raindrops at the middle of the fall speed class j , A [m^2] is the detection area, and D_i [mm] is the drop diameter at the middle of the size class i .

The kinetic energy of the simulated rain was also estimated in terms of volume-specific rain kinetic energy, KE_{mm} [$\text{J m}^{-2} \text{mm}^{-1}$], which is given by (e.g. Salles et al., 2002):

$$\text{KE}_{\text{mm}} = \frac{\text{KE}_{\text{time}}}{R} = \frac{\sum_{i=1}^{21} \text{KE}_{\text{time}}(D_i)}{\sum_{i=1}^{21} R(D_i)} \quad (9.7)$$

And $\text{KE}_{\text{mm}}(D_i)$ is the volume-specific rain kinetic energy for a given drop size class i :

$$KE_{mm}(D_i)=10^6 \frac{\rho \sum_{j=1}^{20} n_{ij} v_j^2 D_i^3}{2 n_i D_i^3} \quad (9.8)$$

All variables in Eqs. (9.7) and (9.8) are defined above.

9.3. Results and discussion

This section reports changes observed in rain simulated with four pressurised nozzles (Table 22), caused by suspending a mesh underneath the nozzles; the focus is on rain intensity, and drop size and fall speed. Table 23 shows some properties of the simulated rainfall produced by each nozzle without mesh and with the mesh suspended at three vertical distances from the nozzles: 200, 400 and 600 mm. Data in Table 23 are averages of the measurements recorded for the three positions of the disdrometer, as described above; in each position, 3 replicate measurements were taken, the sampling time being 15 s. For mesh-free simulations, the HH-22 nozzle produced the highest mean rain intensity (174 mm h^{-1}), whereas the HH-4.3 produced the lowest mean rain intensity (22 mm h^{-1}). When the mesh was combined with the nozzles, most of the drops that hit the mesh fell vertically beneath the nozzles and, consequently, the rain intensity increased. The highest (182%) and the lowest (6%) increase were both observed for HH-4.3W nozzle, when the mesh was suspended at 200 mm and 600 mm from the nozzle, respectively. In fact, it was possible to observe that, for all nozzles, the lower the distance between the mesh and the nozzle, the higher the increase in rainfall intensity. On average, for a distance between the mesh and the nozzles of 200, 400 and 600 mm, this increase was, respectively, 120%, 48% and 25%.

Table 23. Description of rainfall characteristics produced by four spray nozzles, for mesh-free simulations and combining a mesh at three vertical positions from the nozzle. Data are averages for the measurements recorded at three positions of the disdrometer (with 3 replicates for each position).

Nozzles	Position of mesh (mm)	R (mm h ⁻¹)	D _{mean} (mm)	Std. deviation of D (mm)	V _{mean} (m s ⁻¹)	Std. deviation of V (m s ⁻¹)	KE _{time} (J m ⁻² h ⁻¹)	KE _{mm} (J m ⁻² mm ⁻¹)
HH-22	-	174.1	0.74	0.36	1.92	1.63	288.5	1.66
	200	285.3	0.88	0.44	1.99	1.78	524.1	1.84
	400	245.9	0.82	0.42	1.96	1.69	436.5	1.77
	600	229.6	0.77	0.41	1.92	1.67	470.4	2.05
HH-14W	-	41.2	0.52	0.21	1.41	1.03	35.7	0.87
	200	95.8	0.58	0.30	1.47	1.13	182.8	1.91
	400	69.2	0.52	0.26	1.37	0.98	146.3	2.11
	600	56.2	0.50	0.24	1.41	0.99	126.1	2.25
HH-4.3W	-	21.6	0.47	0.17	1.27	0.95	12.3	0.57
	200	61.0	0.47	0.27	1.28	0.95	243.6	3.99
	400	28.3	0.44	0.20	1.25	0.89	74.9	2.64
	600	22.9	0.44	0.17	1.26	0.90	32.5	1.41
7G-1	-	68.4	0.67	0.25	1.47	1.37	49.9	0.73
	200	137.0	0.69	0.36	1.47	1.41	292.8	2.14
	400	104.6	0.66	0.33	1.46	1.39	190.3	1.82
	600	87.3	0.65	0.29	1.42	1.33	111.7	1.28

where: R (rainfall intensity), D_{mean} (mean drop diameter), V_{mean} (mean drop fall speed), KE_{time} (time-specific rain kinetic energy) and KE_{mm} (volume-specific rain kinetic energy).

Figure 56 shows the distribution of the total number of drops as a function of the drop diameter and fall speed for mesh-free simulations and for a mesh positioned at 400 mm from the nozzle; the drop diameter and fall speed data were measured with the disdrometer positioned just below the nozzle. For mesh-free simulations (Figure 56, left), the majority of drops had a diameter smaller than 1 mm: 85.4%, for HH.22; 97.9%, for HH.14W; 99.7%, for HH.4.3W; and 86.4%, for 7G.1. Without mesh, the maximum raindrop diameter observed was ~2.5 mm, except for HH-22 nozzle.

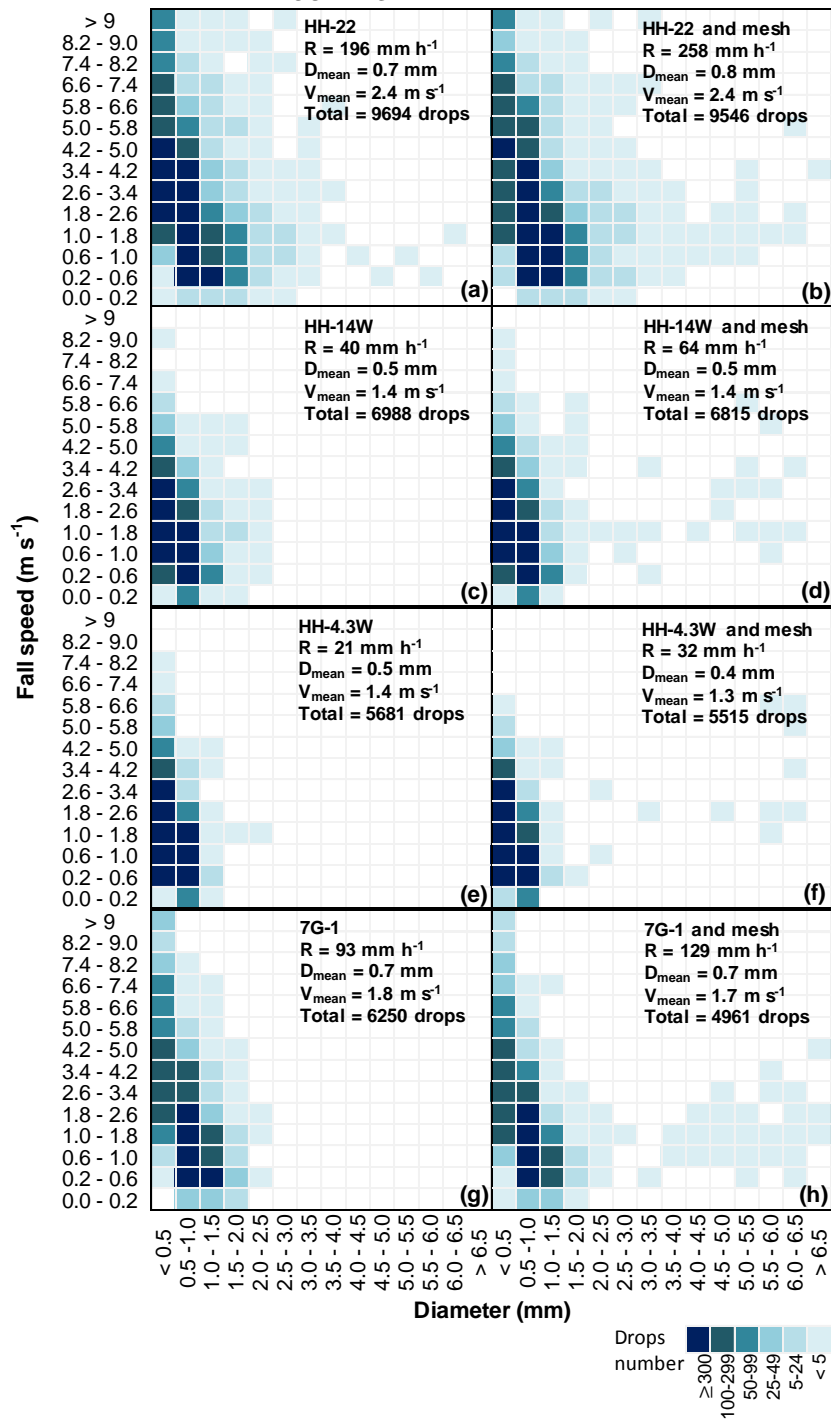


Figure 56. For 4 nozzle types, total number of drops counted in each size and fall speed interval for: mesh-free nozzle simulations (left); and for simulations combining the nozzle with a mesh positioned at 400 mm from the nozzle (right). The data were collected during 15 s (average of 3 replicates) with the disdrometer positioned just below the nozzles. See also Table 23.

For the simulations incorporating the mesh (Figure 56, right), it was found that the mesh affected the simulated raindrops mainly by leading to the formation of bigger drops (i.e. larger than 2.5 mm). Figure 56 also shows that when using the mesh the fall speeds of big drops are typically below 6.6 m s^{-1} , and higher fall speeds are usually reached by drops with small diameters ($< 0.5 \text{ mm}$). This is because larger drops fall from the mesh at an initial zero velocity, while the nozzles produce small drops that are sprayed out at high velocities. Nevertheless, the mean drop fall speed was similar when using, or not, the mesh (Figure 56 and Table 23).

Comparison of the mean drop fall speed recorded for the four spray nozzles show that this speed was much higher for the HH-22 nozzle than for the other nozzles: 2.4 m s^{-1} just below the nozzle compared to e.g. 1.4 m s^{-1} for HH-14W (see Figure 56); moreover, for the HH-22 nozzle, the fall speed of around 16% of drops was higher than 4.2 m s^{-1} (Figure 56a and Figure 56b), while for the other nozzles this percentage was only between 1% (Figure 56f) and 8% (Figure 56g).

The kinetic energy of the simulated rain was also determined for the four nozzles, including the mesh-free simulations and the simulations incorporating the mesh positioned at three vertical distances from the nozzles (Figure 57 and Table 23). Iserloh et al. (2013) report values of the kinetic energy found for a large variety of simulators (e.g. nozzles/drop formers, working pressure, fall height). We highlight that in our study the results obtained for the mesh-free simulations are within the range of reported values and that the rainfall kinetic energy clearly increased when the mesh was used in comparison to the mesh-free simulations. Figure 57a (KE_{time}) and Figure 57b (KE_{mm}) show this tendency: the data points are located well above the 1:1 line, for both types of kinetic energy; but the percentage increase is different for each case (see also Table 23) and it is therefore not viable to distinguish an average percentage increase. In particular, the highest increase of kinetic energy was found for HH-4.3W nozzle with the mesh at 200 mm; whereas the lowest increase of kinetic energy was for the HH-22 with mesh at 400 mm. The experiments show that the kinetic energy is sensitive to the presence of large drops. However, it does not affect the general conclusion about the effect of the mesh on the rainfall simulations.

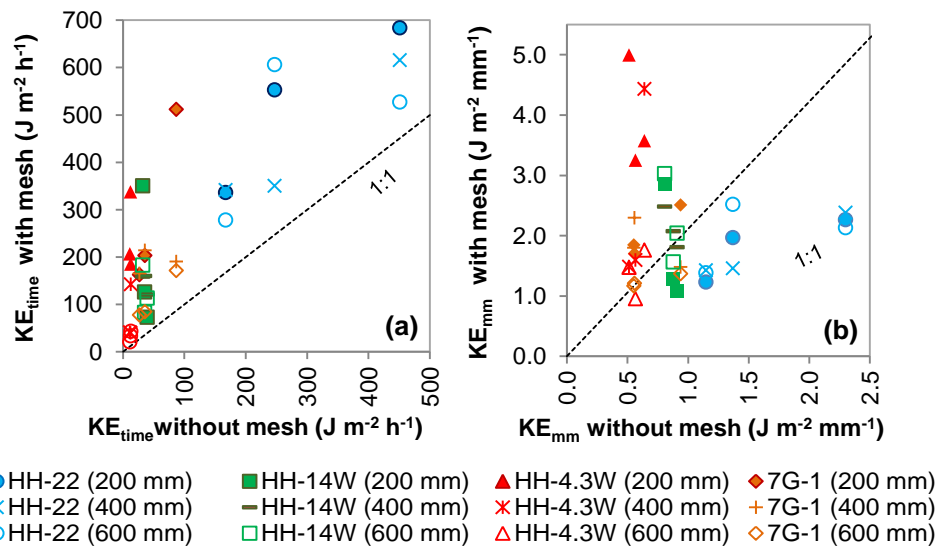


Figure 57. Comparison of the kinetic energy of the rainfall simulated using meshes with the mesh-free simulations: (a) time-specific rainfall kinetic energy; (b) volume-specific rainfall kinetic energy. The results are for the mesh positioned at three vertical distances from the nozzle. The three data points for each combination nozzle type-distance from the nozzle are for the three positions of the disdrometer; data points are averages of 3 measurement replicates.

In general, decreasing the distance of the mesh to the nozzle is expected to lead to increased rainfall kinetic energy, as more drops are intercepted by the mesh and fall vertically underneath. For the HH-4.3W and 7G-1 nozzles, the increase in the rainfall kinetic energy was the highest when the mesh was positioned at 200 mm, and the lowest for mesh positioned at 600 mm from the nozzle. This result was not confirmed for all simulations that involved the HH-22 and HH-14W nozzles.

In order to better understand the effect of the mesh on the rainfall kinetic energy, the distribution of KE_{time} is shown in Figure 58 as a function of the drop size and fall speed (rain data in Figure 56 and Figure 58 are the same). Figure 58 highlight that the KE_{time} distributions are different for each nozzle, but a common pattern is identified: the contribution of bigger drops (>2.5 mm) to the total kinetic energy is particularly relevant, despite the smaller number of drops with larger diameters (see Figure 56).

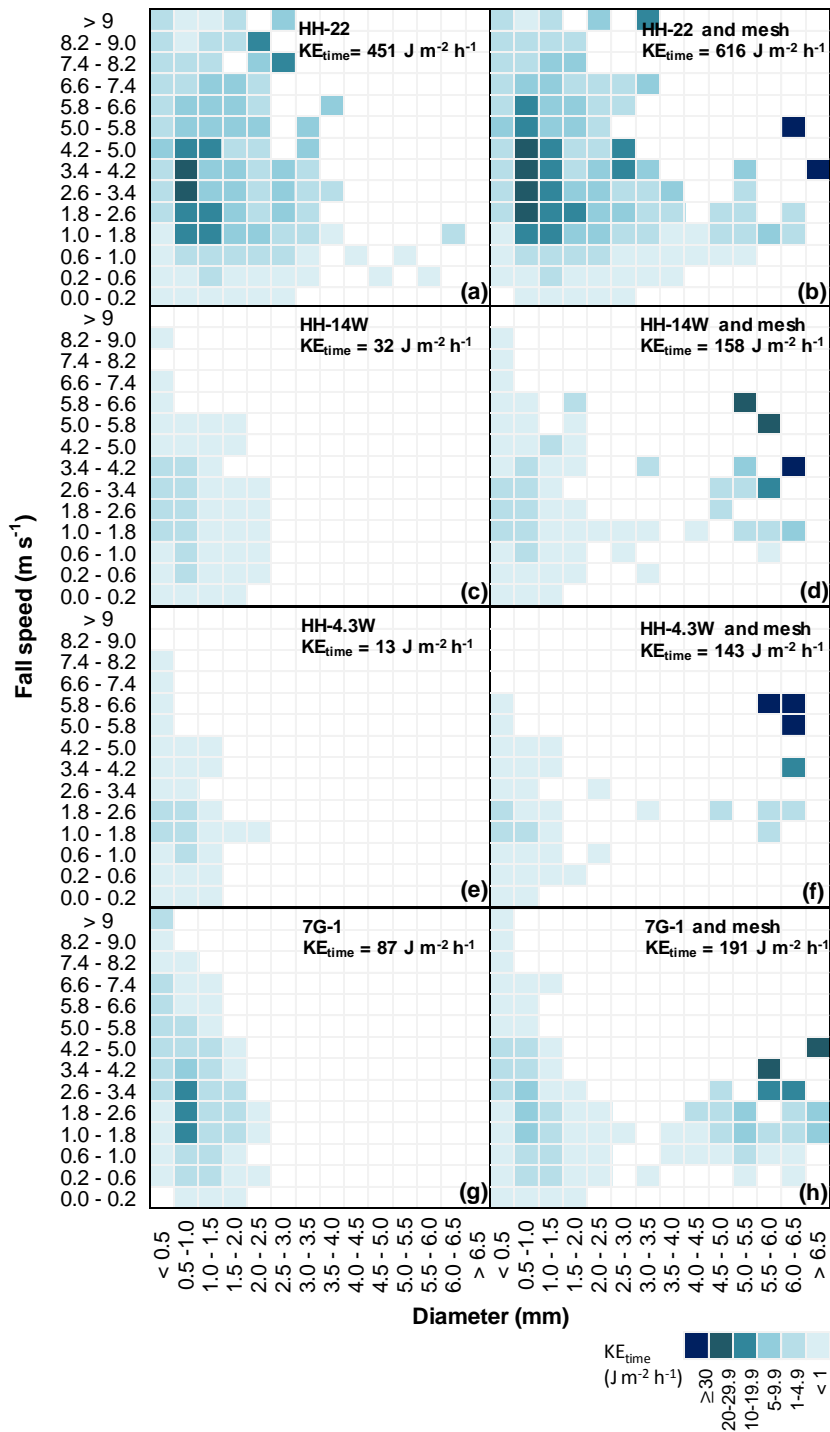


Figure 58. Time-specific kinetic energy, KE_{time} , for each size and fall speed class for mesh-free simulations (left), and combining a mesh positioned at 400 mm from the nozzle (right). The data were collected during 15 s (3 replicates) with the disdrometer positioned just below the nozzle. The KE_{time} data are average values for the 3 measurement replicates.

Figure 59a to Figure 59d show the KE_{time} for each raindrop size class and for all the nozzles. Except for nozzle HH-22, results support that small drops are only responsible for a small proportion of the rainfall kinetic energy, due to their small mass.

The impact of drop fall speeds on the rainfall kinetic energy was also inspected. Figure 59e to Figure 59h show plots of KE_{time} as a function of drop fall speed classes: we note high values (“peaks”) of kinetic energy for some fall speed classes that appear to be specific for each nozzle type; the effect of the position of the mesh is not clear. In spite of the mean drop fall speed being similar for experiments with and without the mesh, the relative contribution of faster drops ($> 3.8 \text{ m s}^{-1}$) to the total kinetic energy was higher for the experiments using the mesh, except for HH-22 (Figure 59e). For example, for the mesh-free simulations using the HH-4.3W nozzle, around 50% of the total kinetic energy was provided by drops that fall slower than 1.8 m s^{-1} (Figure 58e); whereas for simulations with a mesh, the same 50% of the total kinetic energy was provided by drops falling faster than 5 m s^{-1} (Figure 58f). Overall, results show that despite the small number of drops with large diameters and high fall speeds produced when the mesh was used, they contribute highly to the increase of the kinetic energy of the simulated rainfall.

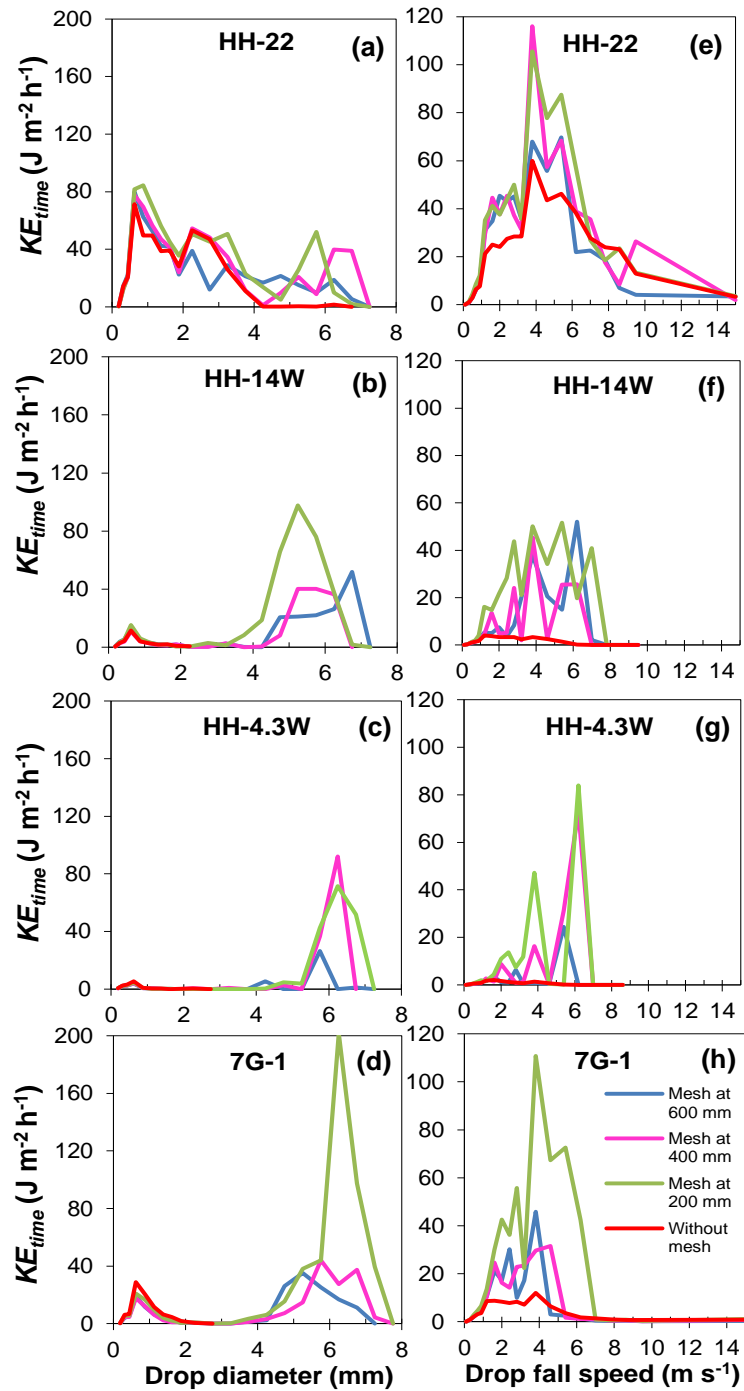


Figure 59. Time-specific kinetic energy, KE_{time} , as a function of raindrop size classes (left), and drop fall speed classes (right). The data are for the disdrometer positioned just below the nozzle (average for 3 replicates).

9.4. Concluding remarks

The main finding of this rainfall simulation laboratory study is that it is possible to increase the rainfall kinetic energy by combining nozzles and meshes; this results mainly from the formation of bigger drops on the mesh's wire since mean raindrop fall speed was similar for simulations conducted with and without meshes. Although the magnitude of that increase differs for each spray nozzle and mesh position, using a mesh systematically increased the rainfall intensity and kinetic energy below the mesh, in comparison to the mesh-free simulations. However, the experimental results highlight that it is difficult to identify a general quantitative model for the expected effect of meshes on rain simulations. Nevertheless, for the majority of cases explored in this work, which involved different combinations of nozzles and installation distances between the nozzles and the mesh underneath, the combination that produced the highest increase in the rainfall intensity and kinetic energy was when the mesh was positioned nearer to the spray nozzles.

We believe that modifying the experimental installation, by incorporating meshes, can increase the versatility of nozzles in experimental simulations of rain, both in the laboratory and in the field; the effect on the simulated rain of combinations involving, for example, different operation pressures and different drop fall heights should be also investigated. The usefulness of changing the characteristics of the rain simulated by nozzle sprays, and the result achieved, depends greatly on the specific experimental conditions and study aims, in particular for studying soil erosion and surface hydrology processes. Therefore, these exploratory experiments were important to understand how the characteristics of the rain simulated using nozzles might be manipulated by combining nozzles and meshes.

10. CONCLUSIONS AND FUTURE RESEARCH

Rainfall is one of the most important meteorological variables and characterizing its distribution, frequency, and variability is crucial for water-related system design and management. Moreover, despite its critical influence on everyday life (e.g. in water supply, agriculture, energy production), it is still complex to measure, estimate and forecast rainfall. The research presented in this thesis focused on some aspects related to rainfall. Special attention was dedicated to measuring and charactering the rainfall variability, both within natural and laboratory conditions.

10.1. Conclusions

The following paragraphs summarize the main conclusions of this thesis according to the objectives listed in Chapter 1.

- Comparison of different instruments for rainfall measurement, in particular, development of an instrument for assessing the variability in rainwater composition

In recent years, considerable efforts have been dedicated to produce quality observational rainfall records. A combination of rain-gauge types is normally used in pluviometric monitoring networks. Chapter 3 provided a comparison of the performance of different types of rain gauges, namely, Hellmann gauges, a tipping bucket gauge, a weighing gauge, optical and impact sensors, installed at the top of the building of the Department of Civil Engineering. The discrepancy of measurements was high, but approximately half of the observations were within the WMO limits of rainfall measurement accuracy (5%). Although the rainfall time series provided by the different gauges were not strictly equivalent, that fact could be expected, as the instruments tested have different designs and measuring principles. For example, the overestimation for the disdrometer can occur from coincident drops, which

are detected by the laser as one single but large drop; or the underestimation from weighing precipitation gauge might result of evaporation processes.

In addition to the instruments used to measure the rain rates and cumulative rain amounts described in Chapter 3, collecting sequential samples of rainwater is crucial to understand the variability of rain composition during short time periods. For example, the rainwater quality is expected to vary from event to event and within individual events. In Chapter 4 a low-cost volume-based sequential rain sampler was developed in a way to accomplish: i) simple manufacturing, set-up and maintenance, and no power requirements; and ii) adequate sampling resolution to monitor single events. The tests carried out under field conditions suggested that the sampling resolution adopted (2 bottles of 0.5 mm, followed by 9 bottles of 1 mm, until a maximum of 10 mm of cumulative rainfall depth) are adequate to detect the inter-event variability of some parameters of rainwater quality; for example, higher turbidity was observed in the beginning of the rain event followed by a rapid decline of the initial values. Nevertheless, due to the simplicity of the design of the rain sampler, it can be easily adapted to include different sample volumes.

- Analysis of the variability of raindrop characteristics measured at an outdoor experimental site

The advances in rainfall measurements by using disdrometers for example, allowed an increased understanding of the rainfall structure at small time scales (e.g. 1 minute). These instruments can monitor rainfall efficiently providing data on raindrop properties (size and fall speed). Chapter 5 showed analysis of the variability of raindrop characteristics based on 35 rainfall events selected from the dataset obtained at an outdoor experimental site (described in Chapter 2); relationships between the rain rate, kinetic energy and raindrop characteristics were estimated. For example, power laws fitted well relationships between the mass-weighted mean diameter and rain rates. Unlike the diameters of raindrops, the mean drop fall speed did not seem to increase progressively with the rain rate. Taking into account different rain rate classes, the gamma distribution was shown to be a proper fit for the drop size distributions presented in this study. The combined measurement of the size and fall

speed of drops was also used for calculating the rainfall kinetic energy. The relationship between rain rate and kinetic energy is of particular interest for e.g. water erosion studies; results showed it was well described by power laws.

- Investigation of the long-term variability of annual and monthly rainfall in Portugal

In addition to the importance of studying the rainfall within individual events and its drop properties (see Chapter 5), the study of longer time periods, e.g. projections of negative trends for annual rainfall, leads to increased concern about water resources management. In order to detect long term patterns of variation in Portugal's climate, in Chapter 6 the monotonic linear trends were investigated in long rainfall time series. Although there was not statistical evidence for rejecting the null hypothesis of no trend in annual rainfall over the full record period, the inspection of 50-year rainfall moving averages series suggested a raise in rainfall in the last decades (since around 1925-30), which was preceded by a period of rainfall decline. The analyses of partial trends also revealed a sequence of alternating periods (with minimum length of 20 years between breakpoints, and 5 years for the first and last segments) of decreasing and increasing trends in annual and monthly rainfall, although not always statistically significant. This study supplements previous investigations of rainfall trends in Portugal emphasizing that the results obtained based on a monotonic linear model should be handled carefully, in particular for small data sets.

- Laboratory experiments on the effects of the temporal variation of rain intensities on runoff and soil loss

Techniques for reproducing natural rain events in laboratory have still room for improvement. For example, despite the common knowledge that the heavy rain rates promote soil loss, constant rain rates are more commonly used in laboratory. Chapter 7 has reiterated the importance of having rainfall simulators that provide variable rain intensities within an event as a way to achieve an in-depth understanding of the processes of overland flow and soil erosion. Laboratory experiments were carried out comprising a single nozzle rainfall simulator that produced time-variable high intensity bursts, guaranteeing the same duration

and mean intensity of the rain event. The results showed that the later the rainfall bursts occurred, the greater was the runoff depth and the total amount of sediment transported; these bursts also led to higher runoff peaks and sediment fluxes than the ones observed for other rain event patterns. These findings are likely to be explained by the changes in the structure of the soil surface and the soil moisture content, as well as from the variability of the infiltration capacity over time. The misestimation of the runoff discharge and soil loss may then occur from disregarding the instant at which rainfall bursts occur during long duration rain events. For engineering purposes, for example to prevent flood hazards, the potential underestimation of runoff discharge from delayed rainfall bursts should be considered as a major concern.

- Study of the performance of rainfall simulators in reproducing rainfall characteristics

Rainfall simulators can be a powerful tool to increase our understanding of hydrological and geomorphological processes, providing attention is paid to the simulated rainfall characteristics (e.g. rain rate, kinetic energy, drop sizes). The research presented in Chapters 8 and 9 characterized the rainfall produced by spray nozzle simulators, and sought for producing simulated rain with different characteristics, which can be important for different application purposes; the effect of combining meshes with spray nozzles was then explored, which has not been a common procedure in rainfall simulator studies. The measurement of rain intensities, number of drops, drop size and fall speed were carried out using a laser disdrometer for a number of different experimental settings (e.g. varying the distance between the nozzle and the mesh, or the material and square aperture of meshes). The presence of meshes gives way to the formation of bigger drops and consequently a broader range of drop sizes, compared to mesh-free simulations. Moreover, as a large amount of drops still fall directly from the nozzles without hitting the meshes, the mean fall speed were similar for simulations with and without meshes. The combined effect of some more (“new”) larger drops and their fall speed was then shown to have particularly importance for increasing the rainfall kinetic energy. The closer the mesh was positioned to the spray nozzle, the higher the mean rain intensities and the increase of rainfall kinetic energy observed. These exploratory experiments were hence relevant to increase the versatility of spray nozzles simulators on providing different rain properties by incorporating a mesh underneath.

10.2. Future Research

Whilst carrying out this research study, some issues that can be further investigated were identified, and are presented in the following paragraphs:

- Using the rainwater sequential sampler proposed in this thesis for assessing the variability of rainwater quality for all the standard parameters required for human consumption, as it could benefit rainwater harvesting systems, namely by helping to understand what volume of water should be diverted in the beginning of a storm;
- Studying the recorded rainfall events, according to the rain types (convective and stratiform), may possibly give important insights on the estimation of the relationships between the rain rate, kinetic energy and raindrop characteristics;
- Simulating complex rainfall hyetograms (e.g. with several high intensity bursts with different magnitudes) in the laboratory in order to quantify their effects on discharge hydrographs and associated transport processes;
- Exploring the way to achieve simulated rain properties similar to observed natural rain. Many variables can be manipulated which affect the outcome properties of the rainfall simulations, e.g. nozzle type, operating pressure, presence of meshes.

11. REFERENCES

- Abu Hammad, A., Tumeizi, A., 2012. Land degradation: socioeconomic and environmental causes and consequences in the eastern Mediterranean. *Land Degradation & Development* 23, 216–226.
- Abudi, I., Carmi, G., Berliner, P., 2012. Rainfall simulator for field runoff studies. *Journal of Hydrology* 454-455, 76–81.
- Agassi, M., Bradford, J.M., 1999. Methodologies for interrill soil erosion studies. *Soil & Tillage Research* 49, 277–287.
- Ahrens, C.D., 2006. *Meteorology today: an introduction to weather climate and the environment*, 8th ed. CengageLearning, 624 p.
- Aksoy, H., Unal, N.E., Cokgor, S., Gedikli, A., Yoon, J., Koca, K., Inci, S.B., Eris, E., 2012. A rainfall simulator for laboratory-scale assessment of rainfall-runoff-sediment transport processes over a two-dimensional flume. *Catena* 98, 63–72.
- Alexandersson, H., Moberg, A., 1997. Homogenization of Swedish temperature data. Part I: Homogeneity test for linear trends. *International Journal of Climatology* 17, 25–34.
- Alfieri, L., Laio, F., Claps, P., 2008. A simulation experiment for optimal design hyetograph selection. *Hydrological Processes* 22, 813–820.
- Arnaez, J., Lasanta, T., Ruiz-Flaño, P., Ortigosa, L., 2007. Factors affecting runoff and erosion under simulated rainfall in Mediterranean vineyards. *Soil and Tillage Research* 93, 324–334.
- Assouline, S., 2004. Rainfall-induced soil surface sealing: a critical review of observations, conceptual models, and solutions. *Vadose Zone Journal* 3, 570–591.

-
- Assouline, S., 2009. Drop size distributions and kinetic energy rates in variable intensity rainfall. *Water Resources Research* 45, 7.
- Assouline, S., Selker, J.S., Parlange, J.-Y., 2007. A simple accurate method to predict time of ponding under variable intensity rainfall. *Water Resources Research* 43, W03426.
- Atlas, D., Srivastava, R.C., Sekhon, R.S., 1973. Doppler radar characteristics of precipitation at vertical incidence. *Reviews of Geophysics and Space Physics* 11, 1–35.
- Barret, E.C., Martin, W.M., 1981. *The use of satellite data in rainfall monitoring*. Academic Press, London, 340 p.
- Battany, M.C., Grismer, M.E., 2000. Development of a portable field rainfall simulator for use in hillside vineyard runoff and erosion studies. *Hydrological Processes* 14, 1119–1129.
- Beard, K.V., 1976. Terminal velocity and shape of cloud and precipitation drops aloft. *Journal of the Atmospheric Sciences* 33, 851–864.
- Beard, K.V., Pruppacher, H.R., 1969. A determination of the terminal velocity and drag of small water drops by means of a wind tunnel. *Journal of the Atmospheric Sciences* 26, 1066–1072.
- Best, A.C., 1950. The size distribution of raindrops. *Quarterly Journal of the Royal Meteorological Society* 76, 16–36.
- Bisal, F., 1960. The effect of raindrop size and impact velocity on sand-splash. *Canadian Journal of Soil Science* 40, 242–245.
- Bjerknes, J., 1919. On the structure of moving cyclones. *Geophys. Publ.* 1, 1–8.
- Black, P.E., 1972. Hydrograph responses to geomorphic model watershed characteristics and precipitation variables. *Journal of Hydrology* 17, 309–329.

-
- Blanchard, D.C., 1953. Raindrop size-distribution in Hawaiian rains. *Journal of Meteorology* 10, 457–473.
- Bonta, J.V., Rao, A.R., 1988. Comparison of four design-storm hyetographs. *Transactions of the ASABE* 31, 102–106.
- Bourgouin, P., 2000. A method to determine precipitation types. *Weather & Forecasting* 15, 583–592.
- Bowyer-Bower, T.A.S., Burt, T.P., 1989. Rainfall simulators for investigating soil response to rainfall. *Soil Technology* 2, 1–16.
- Brandão, C., Rodrigues, R., Costa, J., 2001. Análise de fenómenos extremos, precipitações intensas em Portugal Continental. Lisboa, DSRH, 64 p.
- Brandes, E.A., Zhang, G., Vivekanandan, J., 2002. Experiments in rainfall estimation with a polarimetric radar in a subtropical environment. *Journal of Applied Meteorology* 41, 674–685.
- Brawn, D., Upton, G., 2008. On the measurement of atmospheric gamma drop-size distributions. *Atmospheric Science Letters* 9, 245–247.
- Brodie, I., Rosewell, C., 2007. Theoretical relationships between rainfall intensity and kinetic energy variants associated with stormwater particle washoff. *Journal of Hydrology* 340, 40–47.
- Buishand, T.A., 1982. Some methods for testing the homogeneity of rainfall records. *Journal of Hydrology* 58, 11–27.
- Cao, Q., Zhang, G., 2009. Errors in estimating raindrop size distribution parameters employing disdrometer and simulated raindrop spectra. *Journal of Applied Meteorology and Climatology* 48, 406–425.

-
- Cao, Q., Zhang, G., Brandes, E., Schuur, T., Ryzhkov, A., Ikeda, K., 2008. Analysis of video disdrometer and polarimetric radar data to characterize rain microphysics in Oklahoma. *Journal of Applied Meteorology and Climatology* 47, 2238–2255.
- Caracciolo, C., Prodi, F., Battaglia, A., Porcu', F., 2006. Analysis of the moments and parameters of a gamma DSD to infer precipitation properties: A convective stratiform discrimination algorithm. *Atmospheric Research* 80, 165–186.
- Carter, C.E., Greer, J.D., Braud, H.J., Floyd, J.M., 1974. Raindrop characteristics in South Central United States. *Transactions of the ASABE* 17, 1033–1037.
- Castillo, R., Lala, G., Justo, J.E., 1985. The chemistry and microphysics of intrastorm sequential precipitation samples. *Tellus* 37B, 160–165.
- Cerdà, A., 1997. Rainfall drop size distribution in the western Mediterranean Basin, Valencia, Spain. *Catena* 30, 169–182.
- Cerdà, A., 1998. The influence of aspect and vegetation on seasonal changes in erosion under rainfall simulation on a clay soil in Spain. *Canadian Journal of Soil Science* 78, 321–330.
- Cerdà, A., 1999. Simuladores de lluvia y su aplicación a la Geomorfología. Estado de la cuestión. *Cuadernos I. Geográfica* 25, 45–84.
- Cerdà, A., Doerr, S.H., 2007. Soil wettability, runoff and erodibility of major dry-Mediterranean land use types on calcareous soils. *Hydrological Processes* 21, 2325–2336.
- Cerdà, A., Ibáñez, S., Calvo, A., 1997. Design and operation of a small and portable rainfall simulator for rugged terrain. *Soil Technology* 11, 163–170.
- Chang, C.L., 2007. Influence of moving rainstorms on watershed responses. *Environmental Engineering Science* 24, 1353–1360.
- Chow, V.T., 1964. *Handbook of applied hydrology: a compendium of water-resources technology*. McGraw-Hill, New York, USA, 1495 p.

-
- Chow, V.T., Maidment, D., Mays, L., 1994. Applied hydrology. McGraw-Hill, Colombia, 689 p.
- Christiansen, J.E., 1942. Irrigation by sprinkling, Bulletin 6. ed. University of California, College of Agriculture, Agricultural Experiment Station, Berkeley, California, 124 p.
- Chukwum, G.O., Schwab, G.O., 1983. Procedure for developing design hyetographs for small watersheds. Transactions of the ASAE 26, 1386–1389.
- Ciach, G.J., 2003. Local random errors in tipping-bucket rain gauge measurements. Journal of Atmospheric and Oceanic Technology 20, 752–759.
- Ciach, G.J., Krajewski, W.F., 1999. Radar-rain gauge comparisons under observational uncertainties. Journal of Applied Meteorology 38, 1519–1525.
- Clarke, M.A., Walsh, R.P.D., 2007. A portable rainfall simulator for field assessment of splash and slopewash in remote locations. Earth Surface Processes and Landforms 32, 2052–2069.
- Collier, C.G., 1989. Applications of weather radar systems: a guide to uses of radar data in meteorology and hydrology. Ellis Horwood, Chichester, UK, 294 p.
- Cooper, H.B.H., Demo, J.M., Lopez, J.A., 1976. Chemical composition of acid precipitation in Central Texas. Water, Air, and Soil Pollution 6, 351–359.
- Corte-Real, J., Qian, B., Xu, H., 1998. Regional climate change in Portugal: precipitation variability associated with large-scale atmospheric circulation. International Journal of Climatology 18, 619–635.
- Costa, A.C., Durão, R., Soares, A., Pereira, M.J., 2008. A geostatistical exploratory analysis of precipitation extremes in southern Portugal. REVSTAT – Statistical Journal 6, 21–32.
- Costa, A.C., Soares, A., 2009. Trends in extreme precipitation indices derived from a daily rainfall database for the South of Portugal. International Journal of Climatology 29, 1956–1975.

-
- Costa, M.J., Salgado, R., Santos, D., Levizzani, V., Bortoli, D., Silva, A.M., Pinto, P., 2010. Modelling of orographic precipitation over Iberia: a springtime case study. *Advances in Geosciences* 25, 103–110.
- Coutinho, M.A., Tomás, P.P., 1995. Characterization of raindrop size distributions at the Vale Formoso Experimental Erosion Center. *Catena* 25, 187–197.
- Cubasch, U., von Storch, H., Waszkewitz, J., Zorita, E., 1996. Estimates of climate change in Southern Europe derived from dynamical climate model output. *Climate Research* 7, 129–149.
- Dallal, G.E., Wilkinson, L., 1986. An analytic approximation to the distribution of Lilliefors's test statistic for normality. *The American Statistician* 40, 294–296.
- Dawson, G.A., 1978. Ionic composition of rain during sixteen convective showers. *Atmospheric Environment* 12, 1991–1999.
- de Lima, J.L.M.P., Carvalho, S.C.P., de Lima, M.I.P., 2013c. Rainfall simulator experiments on the importance of when rainfall burst occurs during storm events on runoff and soil loss. *Zeitschrift für Geomorphologie, Supplementary Issues* 57, 91–109.
- de Lima, J.L.M.P., de Lima, M.I.P., Singh, V.P., 2005. The importance of the direction, speed, intensity and length of moving storms on water erosion, in: *Advances in GeoEcology 36 – Sustainable Use and Management of Soils – Arid and Semiarid Regions*. CATENA VERLAG, Reiskirchen, 163–176.
- de Lima, J.L.M.P., Dinis, P.A., Souza, C.S., de Lima, M.I.P., Cunha, P.P., Azevedo, J.M., Singh, V.P., Abreu, J.M., 2011. Patterns of grain-size temporal variation of sediment transported by overland flow associated with moving storms: interpreting soil flume experiments. *Natural Hazards and Earth System Science* 11, 2605–2615.
- de Lima, J.L.M.P., Singh, V.P., 2002. The influence of the pattern of moving rainstorms on overland flow. *Advances in Water Resources* 25, 817–828.

-
- de Lima, J.L.M.P., Singh, V.P., 2003. Laboratory experiments on the influence of storm movement on overland flow. *Physics and Chemistry of the Earth* 28, 277–282.
- de Lima, J.L.M.P., Singh, V.P., de Lima, M.I.P., 2003. The influence of storm movement on water erosion: storm direction and velocity effects. *Catena* 52, 39–56.
- de Lima, J.L.M.P., Souza, C.S., Singh, V.P., 2008. Granulometric characterization of sediments transported by surface runoff generated by moving storms. *Nonlinear Processes in Geophysics* 15, 999–1011.
- de Lima, J.L.M.P., Tavares, P., Singh, V.P., de Lima, M.I.P., 2009. Investigating the nonlinear response of soil loss to storm direction using a circular soil flume. *Geoderma* 152, 9–15.
- de Lima, J.L.M.P., Torfs, P.J.J.F., 1993. Effects of wind on rainfall simulation. Spatial distribution of water application, kinetic energy, and overland flow under single full-cone nozzle sprays, Report n° 40. The Netherlands, 93 p.
- de Lima, M.I.P., Carvalho, S.C.P., de Lima, J.L.M.P., 2010a. Investigating annual and monthly trends in precipitation structure: an overview across Portugal. *Natural Hazards and Earth System Science* 10, 2429–2440.
- de Lima, M.I.P., Carvalho, S.C.P., de Lima, J.L.M.P., Coelho, M.F.E.S., 2010b. Trends in precipitation: analysis of long annual and monthly time series from mainland Portugal. *Advances in Geosciences* 25, 155–160.
- de Lima, M.I.P., de Lima, J.L.M.P., 2009. Investigating the multifractality of point precipitation in the Madeira archipelago. *Nonlinear Processes in Geophysics* 16, 299–311.
- de Lima, M.I.P., Marques, A.C.P., de Lima, J.L.M.P., Coelho, M.F.E.S., 2007. Precipitation trends in mainland Portugal in the period 1941-2000. *IAHS Publ. 310, International Association of Hydrological Sciences* 94–102.

-
- de Lima, M.I.P., Santo, F.E., de Lima, J.L.M.P., Ramos, A.M., 2013a. Recent precipitation variability over 67 years in mainland Portugal. *Die Bodenkultur* 64, 21–26.
- de Lima, M.I.P., Santo, F.E., Ramos, A.M., de Lima, J.L.M.P., 2013b. Recent changes in daily precipitation and surface air temperature extremes in mainland Portugal, in the period 1941–2007. *Atmospheric Research* 127, 195–209.
- de Oliveira, J.R., Pinto, M.F., Souza, W. de J., Guerra, J.G.M., Carvalho, D.F., 2010. Erosão hídrica em um Argissolo Vermelho-Amarelo, sob diferentes padrões de chuva simulada. *Revista Brasileira de Engenharia Agrícola e Ambiental* 14, 140–147.
- De Ploey, J., 1981. Some laboratory techniques of investigating land erosion, in: *Erosion and Sediment Transport Measurement (Proceedings of the Florence Symposium)*. IAHS Publ. no. 133., 423–432.
- Deheuvels, P., 1981. A Kolmogorov-Smirnov type test for independence and multivariate samples. *Rev. Roum. Math. Pure A.* 26, 212–226.
- Do Khac, K., Zanghi, F., Tabary, P., 2004. Radar-disdrometer comparison. *ERAD Publication Series* 2, 272–277.
- Dunkerley, D., 2008a. Rain event properties in nature and in rainfall simulation experiments: a comparative review with recommendations for increasingly systematic study and reporting. *Hydrological Processes* 22, 4415–4435.
- Dunkerley, D., 2008b. Identifying individual rain events from pluviograph records: a review with analysis of data from an Australian dryland site. *Hydrological Processes* 22, 5024–5036.
- Dunkerley, D., 2012. Effects of rainfall intensity fluctuations on infiltration and runoff: rainfall simulation on dryland soils, Fowlers Gap, Australia. *Hydrological Processes* 26, 2211–2224.

-
- Dunne, T., Dietrich, W.E., Brunengo, M.J., 1980. Simple, portable equipment for erosion experiments under artificial rainfall. *Journal of Agricultural Engineering Research* 25, 161–168.
- Durão, R., Pereira, M.J., Costa, A.C., Côrte-Real, J.M., Soares, A., 2009. Indices of precipitation extremes in Southern Portugal - a geostatistical approach. *Natural Hazards and Earth System Science* 9, 241–250.
- Ebert, P., Kibler, M., Mainka, A., Tenberken, B., Baechmann, K., Frank, G., Tschiersch, J., 1998. A field study of particle scavenging by raindrops of different sizes using monodisperse trace aerosol. *Journal of Aerosol Science* 29, 173–186.
- Elbasit, M.A.M.A., Yasuda, H., Salmi, A., Anyoji, H., 2010. Characterization of rainfall generated by dripper-type rainfall simulator using piezoelectric transducers and its impact on splash soil erosion. *Earth Surface Processes and Landforms* 35, 466–475.
- Eliassen, A., 1962. On the vertical circulation in frontal zones. *Geophys. Publ.* 24, 147–160.
- El-Jabi, N., Sarraf, S., 1991. Effect of maximum rainfall position on rainfall-runoff relationship. *Journal of Hydraulic Engineering* 117, 681–685.
- Ellouze, M., Abida, H., Safi, R., 2009. A triangular model for the generation of synthetic hyetographs. *Hydrological Sciences Journal* 54, 287–299.
- Engelmann, R.J., 1968. The calculation of precipitation scavenging, in: *Meteorology and atomic energy, 1968*. US Atomic Energy Commission, Springfield, Virginia, 208–221.
- Erpul, G., Gabriels, D., Janssens, D., 1998. Assessing the drop size distribution of simulated rainfall in a wind tunnel. *Soil and Tillage Research* 45, 455–463.
- Erpul, G., Gabriels, D., Norton, L.D., 2004. Wind effects on sediment transport by raindrop-impacted shallow flow: a wind-tunnel study. *Earth Surface Processes and Landforms* 29, 955–967.

-
- Erpul, G., Norton, L.D., Gabriels, D., 2003. Sediment transport from interrill areas under wind-driven rain. *Journal of Hydrology* 276, 184–197.
- Esteves, M., Planchon, O., Lapetite, J.M., Silvera, N., Cadet, P., 2000. The “emire” large rainfall simulator: design and field testing. *Earth Surface Processes and Landforms* 25, 681–690.
- Fernández-Gálvez, J., Barahona, E., Mingorance, M.D., 2008. Measurement of infiltration in small field plots by a portable rainfall simulator: application to trace-element mobility. *Water, Air, and Soil Pollution* 191, 257–264.
- Fernández-Raga, M., Fraile, R., Keizer, J.J., Varela Teijeiro, M.E., Castro, A., Palencia, C., Calvo, A.I., Koenders, J., Marques, R.L.C., 2010. The kinetic energy of rain measured with an optical disdrometer: An application to splash erosion. *Atmospheric Research* 96, 225–240.
- Fister, W., Iserloh, T., Ries, J.B., Schmidt, R.-G., 2011. Comparison of rainfall characteristics of a small portable rainfall simulator and a portable wind and rainfall simulator. *Zeitschrift für Geomorphologie, Supplementary Issues* 55, 109–126.
- Fister, W., Iserloh, T., Ries, J.B., Schmidt, R.-G., 2012. A portable wind and rainfall simulator for in situ soil erosion measurements. *Catena* 91, 72–84.
- Flanagan, D.C., Foster, G.R., Moldenhauer, W.C., 1988. Storm pattern effect on infiltration, runoff, and erosion. *Transactions of the ASABE* 31, 414–420.
- Fornis, R.L., Vermeulen, H.R., Nieuwenhuis, J.D., 2005. Kinetic energy – rainfall intensity relationship for Central Cebu, Philippines for soil erosion studies. *Journal of Hydrology* 300, 20–32.
- Foroud, N., Broughton, R.S., Austin, G.L., 1984. The effects of a moving rainstorm on direct runoff properties. *Journal of the American Water Resources Association* 20, 87–91.

-
- Frasson, R.P.M., da Cunha, L.K., Krajewski, W.F., 2011. Assessment of the Thies optical disdrometer performance. *Atmospheric Research* 101, 237–255.
- Frauenfeld, B., Truman, C., 2004. Variable rainfall intensity effects on runoff and interrill erosion from two coastal plain ultisols in Georgia. *Soil Science* 169, 143–154.
- Gatz, D.F., Dingle, A.N., 1971. Trace substances in rain water: concentration variations during convective rains, and their interpretation. *Tellus* 23, 14–27.
- Georgakakos, K.P., Kavvas, M.L., 1987. Precipitation analysis, modeling, and prediction in hydrology. *Reviews of Geophysics* 25, 163–178.
- Gerakis, A., Baer, B., 1999. A computer program for soil textural classification. *Soil Science Society of America Journal* 63, 807–808.
- Gertzman, H.S., Atlas, D., 1977. Sampling errors in the measurement of rain and hail parameters. *Journal of Geophysical Research* 82, 4955–4966.
- Ghadiri, H., Payne, D., 1977. Raindrop impact stress and the breakdown of soil crumbs. *Journal of Soil Science* 28, 247–258.
- Gilbert, R.O., 1987. *Statistical methods for environmental pollution monitoring*. John Wiley & Sons, New York, USA, 336 p.
- González-Hidalgo, J.C., Brunetti, M., de Luis, M., 2011. A new tool for monthly precipitation analysis in Spain: MOPREDAS database (monthly precipitation trends December 1945–November 2005). *International Journal of Climatology* 31, 715–731.
- Goodess, C.M., Jones, P.D., 2002. Links between circulation and changes in the characteristics of Iberian rainfall. *International Journal of Climatology* 22, 1593–1615.
- Gray, J., Hage, K.D., Mary, H.W., 1974. An automatic sequential rainfall sampler. *Review of Scientific Instruments* 45, 1517–1519.

-
- Grimaldi, S., Serinaldi, F., 2006. Design hyetograph analysis with 3-copula function. *Hydrological Sciences Journal* 51, 223–238.
- Grismer, M.E., Hogan, M.P., 2004. Simulated rainfall evaluation of revegetation/mulch erosion control in the Lake Tahoe Basin — 1: method assessment. *Land Degradation & Development* 15, 573–588.
- Gunn, R., Kinzer, G.D., 1949. The terminal velocity of fall for water droplets in stagnant air. *Journal of Meteorology* 6, 243–248.
- Habib, E., Lee, G., Kim, D., Ciach, G.J., 2010. Ground-based direct measurement. *Geophysical Monograph Series* 191, 61–77.
- Haddad, Z.S., Durden, S.L., Im, E., 1996. Parameterizing the Raindrop Size Distribution. *Journal of Applied Meteorology* 35, 3–13.
- Hall, M.J., 1970. A Critique of Methods of Simulating Rainfall. *Water Resources Research* 6, 1104–1114.
- Harikumar, R., Sampath, S., Sasi Kumar, V., 2009. An empirical model for the variation of rain drop size distribution with rain rate at a few locations in southern India. *Advances in Space Research* 43, 837–844.
- Hawkins, D.M., 1977. Testing a sequence of observations for a shift in location. *Journal of the American Statistical Association* 72, 180–186.
- Helmreich, B., Horn, H., 2009. Opportunities in rainwater harvesting. *Desalination* 248, 118–124.
- Helsel, D.R., Hirsch, R.M., 2002. *Statistical Methods in Water Resources*, Techniques of Water Resources Investigations, Book 4, chapter A3. U.S. Geological Survey, 522 p.
- Hewlett, J.D., Fortson, J.C., Cunningham, G.B., 1977. The effect of rainfall intensity on storm flow and peak discharge from forest land. *Water Resources Research* 13, 259–266.

-
- Holden, J., Burt, T.P., 2002. Infiltration, runoff and sediment production in blanket peat catchments: implications of field rainfall simulation experiments. *Hydrological Processes* 16, 2537–2557.
- Hosking, J.R.M., Wallis, J.R., 1997. *Regional frequency analysis: an approach based on L-moments*. Cambridge University Press, Cambridge, UK, 244 p.
- Houze Jr., R.A., 1994. *Cloud Dynamics*. Academic Press, California, USA, 573 p.
- Hudson, N., 1995. *Soil conservation*. Iowa State University Press, 391 p.
- Huff, F.A., Stout, G.E., 1964. Distribution of Radioactive Rainout in Convective Rainfall. *Journal of Applied Meteorology* 3, 707–717.
- Huff, F.A., 1967. Time distribution of rainfall in heavy storms. *Water Resources Research* 3, 1007–1019.
- Huffman, G.J., Adler, R.F., Rudolf, B., Schneider, U., Keehn, P.R., 1995. Global precipitation estimates based on a technique for combining satellite-based estimates, rain gauge analysis, and NWP model precipitation information. *Journal of Climate* 8, 1284–1295.
- Humphry, J., Daniel, T., Edwards, D., Sharpley, A., 2002. A Portable Rainfall Simulator for Plot-Scale Runoff Studies. *Transactions of the ASAE* 18, 199–204.
- IPCC, 2007. *Climate Change 2007: Impacts, Adaptation and Vulnerability*. Contribution of Working Group II to the Fourth Assessment Report of the Intergovernmental Panel on Climate Change, in: Parry, M.L., Canziani, O.F., Palutikof, J.P., van der Linden, P.J., Hanson, C.E. (Eds.), Cambridge University Press, Cambridge, UK, 976 p.
- Iserloh, T., Ries, J.B., Arnáez, J., Boix-Fayos, C., Butzen, V., Cerdà, A., Echeverría, M.T., Fernández-Gálvez, J., Fister, W., Geißler, C., Gómez, J.A., Gómez-Macpherson, H., Kuhn, N.J., Lázaro, R., León, F.J., Martínez-Mena, M., Martínez-Murillo, J.F., Marzen, M., Mingorance, M.D., Ortigosa, L., Peters, P., Regüés, D., Ruiz-Sinoga, J.D., Scholten,

-
- T., Seeger, M., Solé-Benet, A., Wengel, R., Wirtz, S., 2013. European small portable rainfall simulators: A comparison of rainfall characteristics. *Catena* 110, 100–112.
- Islam, T., Rico-Ramirez, M. A., Thurai, M., Han, D., 2012. Characteristics of raindrop spectra as normalized gamma distribution from a Joss–Waldvogel disdrometer. *Atmospheric Research* 108, 57–73.
- Jaffrain, J., 2012. Experimental quantification of the variability of the raindrop size distribution at small scales. Doctoral thesis, École Polytechnique Fédérale de Lausanne, Lausanne, Suisse, 157 p.
- Jaffrain, J., Berne, A., 2012. Quantification of the small-scale spatial structure of the raindrop size distribution from a network of disdrometers. *Journal of Applied Meteorology and Climatology* 51, 941–953.
- Jambers, W., Dekov, V., Van Grieken R., 2000. Single particle and inorganic characterization of rainwater collected above the North Sea. *The Science of the Total Environment* 256, 133–150.
- Jones, D., 1959. The shape of raindrops. *Journal of Meteorology* 16, 504–510.
- Kainz, M., Auerswald, K., Vöhringer, R., 1992. Comparison of German and Swiss rainfall simulators - Utility, labour demands and costs. *Zeitschrift für Pflanzenernährung und Bodenkunde* 155, 7–11.
- Kamphorst, A., 1987. A small rainfall simulator for the determination of soil erodibility. *Netherlands Journal of Agricultural Science* 35, 407–415.
- Karl, T.R., Knight, R.W., Baker, B., 2000. The record breaking global temperatures of 1997 and 1998: Evidence for an increase in the rate of global warming? *Geophysical Research Letters* 27, 719–722.
- Kawakubo, S., Hashi, S., Iwatsuki, M., 2001. Physicochemical speciation of molybdenum in rain water. *Water Research* 35, 2489–2495.

-
- Keifer, T.O., Unkrich, C.L., Smith, J.R., Goodrich, D.C., Moran, M.S., Simanton, J.R., 2008. An event-based comparison of two types of automated-recording, weighing bucket rain gauges. *Water Resources Research* 44, W05S12.
- Keifer, C.J., Chu, H.H., 1957. Synthetic storm pattern for drainage design. *Journal of the Hydraulics Division* 83, 1–25.
- Keller, J., Bliesner, R.D., 1990. *Sprinkle and trickle irrigation*. Van Nostrand Reinhold, New York, 652 p.
- Kendall, M.G., 1970. *Rank correlation methods*, 4th ed. Charles Griffin, London, 202 p.
- Kincaid, D.C., 1996. Spraydrop kinetic energy from irrigation sprinklers. *Transactions of the ASAE* 39, 847–853.
- King, B.A., Winward, T.W., Bjorneberg, D.L., 2010. Laser Precipitation Monitor for measurement of drop size and velocity of moving spray-plate sprinklers. *Applied Engineering in Agriculture* 26, 263–272.
- Kinnell, P.I.A., 1976. Some observations on the Joss-Waldvogel rainfall disdrometer. *Journal of Applied Meteorology* 15, 499–502.
- Kinnell, P.I.A., 1981. Rainfall intensity-kinetic energy relationships for soil loss prediction. *Soil Science Society of America Journal* 45, 153–155.
- Kostopoulou, E., Jones, P.D., 2005. Assessment of climate extremes in the Eastern Mediterranean. *Meteorology and Atmospheric Physics* 89, 69–85.
- Kozu, T., Reddy, K.K., Mori, S., Thurai, M., Ong, J.T., Rao, D.N., 2006. Seasonal and diurnal variations of raindrop size distribution in Asian monsoon region. *Journal of the Meteorological Society of Japan* 84, 195–209.
- Krajewski, W.F., Kruger, A., Caracciolo, C., Golé, P., Barthes, L., Creutin, J.-D., Delahaye, J.-Y., Nikolopoulos, E.I., Ogden, F., Vinson, J.-P., 2006. DEVEX-disdrometer

evaluation experiment: Basic results and implications for hydrologic studies. *Advances in Water Resources* 29, 311–325.

Krajewski, W.F., Smith, J.A., 2002. Radar hydrology: rainfall estimation. *Advances in Water Resources* 25, 1387–1394.

Kruger, A., Krajewski, W.F., 2002. Two-dimensional video disdrometer: A description. *Journal of Atmospheric and Oceanic Technology* 19, 602–617.

Krupa, S.V., 2002. Sampling and physico-chemical analysis of precipitation: a review. *Environmental Pollution* 120, 565–594.

Lambourne, J.J., Stephenson, D., 1987. Model study of the effect of temporal storm distributions on peak discharges and volumes. *Hydrological Sciences Journal* 32, 215–226.

Lanza, L.G., Vuerich, E., 2012. Non-parametric analysis of one-minute rain intensity measurements from the WMO Field Intercomparison. *Atmospheric Research* 103, 52–59.

Lanza, L.G., Vuerich, E., Gnecco, I., 2010. Analysis of highly accurate rain intensity measurements from a field test site. *Advances in Geosciences* 25, 37–44.

Laquer, F.C., 1990a. An intercomparison of continuous flow, and automatically segmenting rainwater collection methods for determining precipitation conductivity and pH. *Atmospheric Environment* 24A, 2299–2306.

Laquer, F.C., 1990b. Sequential precipitation samplers: a literature review. *Atmospheric Environment. Part A. General Topics* 24, 2289–2297.

Lascelles, B., Favis-Mortlock, D., Parsons, A.J., Guerra, A.J.T., 2000. Spatial and temporal variation in two rainfall simulators: implications for spatially explicit rainfall simulation experiments. *Earth Surf. Process. Landforms* 25, 709–721.

-
- Laws, J.O., Parsons, D.A., 1943. The relation of raindrop-size to intensity. *Transactions of the American Geophysical Union* 24, 452–60.
- Leijnse, H., Uijlenhoet, R., 2010. The effect of reported high-velocity small raindrops on inferred drop size distributions and derived power laws. *Atmospheric Chemistry and Physics* 10, 6807–6818.
- Lettenmaier, D.P., Wood, E.F., Wallis, J.R., 1994. Hydro-climatological trends in the continental United States, 1948-88. *Journal of Climate* 7, 586–607.
- Levin, L.M., 1954. Size distribution function for cloud-droplets and raindrops. *Dok. Akad. Nauk.* 94, 1045–1048.
- Levine, S.Z., Schwartz, S.E., 1982. In-cloud and below-cloud scavenging of nitric acid vapor. *Atmospheric Environment* 16, 1725–1734.
- Li, X., Gao, S., 2012. *Precipitation modeling and quantitative analysis*. Springer Atmospheric Sciences, XVI, 240 p.
- Lim, B., Jickells, T.D., Davies, T.D., 1991. Sequential sampling of particles, major ions and total trace metals in wet deposition. *Atmospheric Environment* 25A, 745–762.
- Lionello, P., Malanotte-Rizzoli, P., Boscolo, R. (Eds.), 2006. *Developments in Earth & Environmental Science, in: Mediterranean climate variability*. Elsevier, 421 p.
- Löffler-Mang, M., Joss, J., 2000. An optical disdrometer for measuring size and velocity of hydrometeors. *Journal of Atmospheric and Oceanic Technology* 17, 130–139.
- López-Moreno, J.I., Vicente-Serrano, S.M., Gimeno, L., Nieto, R., 2009. Stability of the seasonal distribution of precipitation in the Mediterranean region: Observations since 1950 and projections for the 21st century. *Geophysical Research Letters* 36, L10703.
- Losada, A., Juana, L., Roldan, J., 1990. Operation diagrams for irrigation management. *Agricultural Water Management* 18, 289–300.

-
- Louie, M.J., Selker, J.S., 2000. Sprinkler head maintenance effects on water application uniformity. *Journal of Irrigation and Drainage Engineering* 126, 142–148.
- Lu, J.-Y., Su, C.-C., Lu, T.-F., Maa, M.-M., 2008. Number and volume raindrop size distributions in Taiwan. *Hydrological Processes* 22, 2148–2158.
- Mangoni, M., Udisti, R., Piccardi, G., 1998. Sequential sampling of rain: Construction and operation of an automatic wet-only apparatus. *International Journal of Environmental Analytical Chemistry* 69, 53–66.
- Mann, H.B., 1945. Non-parametric test against trend. *Econometrica* 13, 245–259.
- Mantovan, P., Pastorea, A., Szpyrkowicz, L., Zilio-Grandi, F., 1995. Characterization of rainwater quality from the Venice region network using multiway data analysis. *Science of The Total Environment* 164, 27–43.
- Marques, M.J., Bienes, R., Jiménez, L., Pérez-Rodríguez, R., 2007. Effect of vegetal cover on runoff and soil erosion under light intensity events. Rainfall simulation over USLE plots. *Science of The Total Environment* 378, 161–165.
- Marshall, J.S., Palmer, W.McK., 1948. The distribution of raindrops with size. *Journal of Meteorology* 5, 165–166.
- Marzuki, M., Randeu, W.L., Schönhuber, M., Bringi, V.N., Kozu, T., Shimomai, T., 2010. Raindrop size distribution parameters of distrometer data with different bin sizes. *IEEE Transactions on Geoscience and Remote Sensing* 48, 3075–3080.
- Mason, B.J., Andrews, J.B., 1960. Drop-size distributions from various types of rain. *Quarterly Journal of the Royal Meteorological Society* 86, 346–353.
- McFarquhar, G.M., 2010. Raindrop size distribution and evolution, in: Testik, F.Y., Gebremichael, M. (Eds.), *Rainfall: State of the Science*. American Geophysical Union, 49–60.

-
- Mermut, A.R., Luk, S.H., Römken, M.J.M., Poesen, J.W.A., 1997. Soil loss by splash and wash during rainfall from two loess soils. *Geoderma* 75, 203–214.
- Meshesha, D.T., Tsunekawa, A., Tsubo, M., 2012. Continuing land degradation: cause–effect in Ethiopia’s Central Rift Valley. *Land Degradation & Development* 23, 130–143.
- Meyer, L.D., McCune, D.L., 1958. Rainfall simulator for runoff plots. *Agricultural Engineering* 39, 644–8.
- Michaelides, S., 2008. *Precipitation: advances in measurement, estimation and prediction*. Springer Berlin Heidelberg, Berlin, Heidelberg, 540 p.
- Michaelides, S., Levizzani, V., Anagnostou, E., Bauer, P., Kasparis, T., Lane, J.E., 2009. Precipitation: measurement, remote sensing, climatology and modeling. *Atmospheric Research* 94, 512–533.
- Miranda, P., Coelho, F.E.S., Tomé, A.R., Valente, M.A., Carvalho, A., Pires, C., Pires, H.O., Pires, V.C., Ramalho, C., 2002. 20th Century Portuguese climate and climate change scenarios, in: Santos, F.D., Forbes, K., Moita, R. (Eds.), *Climate change in Portugal: scenarios, impacts and adaptation measures*. Gradiva, Lisbon, Portugal, 27–83.
- Miranda, P.M.A., Valente, M.A., Tomé, A.R., Trigo, R., Coelho, F., Aguiar, A., Azevedo, E.B., 2006. O clima de Portugal nos séculos XX e XXI, in: Santos, F., Miranda, P. (Eds.), *Alterações climáticas em Portugal: cenários, impactos e medidas de adaptação - Projecto SIAM II*. Gradiva, Lisbon, Portugal, 1–89.
- Molini, A., Lanza, L.G., La Barbera, P., 2005. The impact of tipping-bucket raingauge measurement errors on design rainfall for urban-scale applications. *Hydrological Processes* 19, 1073–1088.
- Montenegro, A.A.A., Abrantes, J.R.C.B., de Lima, J.L.M.P., Singh, V.P., Santos, T.E.M., 2013. Impact of mulching on soil and water dynamics under intermittent simulated rainfall. *Catena* 109, 139–149.

-
- Montero-Martínez, G., Kostinski, A.B., Shaw, R.A., García-García, F., 2009. Do all raindrops fall at terminal speed? *Geophysical Research Letters* 36, L11818.
- Morin, E., Krajewski, W.F., Goodrich, D.C., Gao, X., Sorooshian, S., 2003. Estimating rainfall intensities from weather radar data: the scale-dependency problem. *Journal of Hydrometeorology* 4, 782–797.
- Mourato, S., Moreira, M., Corte-Real, J., 2010. Interannual variability of precipitation distribution patterns in Southern Portugal. *International Journal of Climatology* 30, 1784–1794.
- Munn, J.R., Huntington, G.L., 1976. A portable rainfall simulator for erodibility and infiltration measurements on rugged terrain. *Soil Science Society of America Journal* 40, 622–624.
- Mutchler, C.K., Hermsmeier, L.F., 1965. A review of rainfall simulators. *Transactions of the ASABE* 8, 67–68.
- Nešpor, V., Krajewski, W.F., Kruger, A., 2000. Wind-induced error of raindrop size distribution measurement using a two-dimensional video disdrometer. *Journal of Atmospheric and Oceanic Technology* 17, 1483–1492.
- Ng, C.W.W., Wang, B., Tung, Y.K., 2001. Three-dimensional numerical investigations of groundwater responses in an unsaturated slope subjected to various rainfall patterns. *Canadian Geotechnical Journal* 38, 1049–1062.
- Niu, S., Jia, X., Sang, J., Liu, X., Lu, C., Liu, Y., 2010. Distributions of raindrop sizes and fall velocities in a semiarid plateau climate: convective versus stratiform rains. *Journal of Applied Meteorology and Climatology* 49, 632–645.
- Nyika, D., Zhande, E., Zhakata, W., 1996. Rainwater quality during 1991–1993 and constituents of milky rain (November 1992) in Bulawayo, Zimbabwe. *The Science of the Total Environment* 186, 273–281.

-
- Nzeukou, A., Sauvageot, H., Ochou, A.D., Kebe, C.M.F., 2004. Raindrop size distribution and radar parameters at Cape Verde. *Journal of Applied Meteorology* 43, 90–105.
- Okuda, T., Iwase, T., Ueda, H., Suda, Y., Tanaka, S., Dokiya, Y., Fushimi, K., Hosoe, M., 2005. Long-term trend of chemical constituents in precipitation in Tokyo metropolitan area, Japan, from 1990 to 2002. *Science of The Total Environment* 339, 127–41.
- Omer, K., Ashgriz, N., 2011. Chapter 24 - Spray nozzles, in: Ashgriz, N. (Ed.), *Handbook of atomization and sprays*. Springer, 497–579.
- Parsons, A.J., Stone, P.M., 2006. Effects of intra-storm variations in rainfall intensity on interrill runoff and erosion. *Catena* 67, 68–78.
- Partal, T., Kahya, E., 2006. Trend analysis in Turkish precipitation data. *Hydrological Processes* 20, 2011–2026.
- Petan, S., Rusjan, S., Vidmar, A., Mikoš, M., 2010. The rainfall kinetic energy–intensity relationship for rainfall erosivity estimation in the mediterranean part of Slovenia. *Journal of Hydrology* 391, 314–321.
- Pettitt, A.N., 1979. A non-parametric approach to the change-point problem. *Applied Statistics* 28, 126–135.
- Pielke, R.A., Adegoke, J., Beltrán-Przekurat, A., Hiemstra, C.A., Lin, J., Nair, U.S., Niyogi, D., Nobis, T.E., 2007. An overview of regional land-use and land-cover impacts on rainfall. *Tellus B* 59, 587–601.
- Potter, T.L., Truman, C.C., Strickland, T.C., Bosch, D.D., Webster, T.M., Franklin, D.H., Bednarz, C.W., 2006. Combined effects of constant versus variable intensity simulated rainfall and reduced tillage management on cotton preemergence herbicide runoff. *Journal of Environmental Quality* 35, 1894–1902.
- Pruppacher, H.R., Klett, J.D., 2010. *Microphysics of clouds and precipitation*, 2nd ed. Springer, The Netherlands, 976 p.

-
- Rao, T.N., Radhakrishna, B., Nakamura, K., Rao, N.P., 2009. Differences in raindrop size distribution from southwest monsoon to northeast monsoon at Gadanki. *Quarterly Journal of the Royal Meteorological Society* 135, 1630–1637.
- Raynor, G.S., Hayes, J.V., 1981. Acidity and conductivity of precipitation on central Long Island, New York in relation to meteorological variables. *Water, Air, and Soil Pollution* 15, 229–245.
- Regmi, T.P., Thompson, A.L., 2000. Rainfall simulator for laboratory studies. *Applied Engineering in Agriculture* 16, 641–647.
- Ries, J.B., Marzen, M., Iserloh, T., Fister, W., 2014. Soil erosion in Mediterranean landscapes—Experimental investigation on crusted surfaces by means of the Portable Wind and Rainfall Simulator. *Journal of Arid Environments* 100-101, 42–51.
- Ries, J.B., Seeger, M., Iserloh, T., Wistorf, S., Fister, W., 2009. Calibration of simulated rainfall characteristics for the study of soil erosion on agricultural land. *Soil & Tillage Research* 106, 109–116.
- Rodrigo, F.S., Trigo, R.M., 2007. Trends in daily rainfall in the Iberian Peninsula from 1951 to 2002. *International Journal of Climatology* 27, 513–529.
- Rogers, R.R., Yau, M.K., 1989. *A short course in cloud physics*, 3rd ed. Pergamon Press, Oxford, 293 p.
- Ronneau, C., Cara, J., Navarre, J.L., Priest, P., 1978. An automatic sequential rain sampler. *Water, Air, & Soil Pollution* 9, 171–176.
- Rosenfeld, D., Ulbrich, C.W., 2003. Cloud microphysical properties, processes, and rainfall estimation opportunities. *Meteorological Monographs* 52, 237–258.
- Rosewell, C.J., 1986. Rainfall kinetic energy in eastern Australia. *Journal of Climate and Applied Meteorology* 25, 1965–1701.

-
- Royston, J.P., 1982. An extension of Shapiro and Wilk's W test for normality to large samples. *Applied Statistics* 31, 115–124.
- Rudolf, B., Hauschild, H., R uth, W., Schneider, U., 1996. Comparison of raingauge analyses, satellite-based precipitation estimates and forecast model results. *Advances in Space Research* 18, 53–62.
- Salles, C., Poesen, J., Sempere-Torres, D., 2002. Kinetic energy of rain and its functional relationship with intensity. *Journal of Hydrology* 257, 256–270.
- Santos, F.D., Valente, M.A., Miranda, P.M.A., Aguiar, A., Azevedo, E.B., Tom e, A.R., Coelho, F., 2004. Climate change scenarios in the Azores and Madeira islands. *World Resource Review* 16, 473–491.
- Sauvageot, H., Lacaux, J.P., 1995. The shape of averaged drop size distributions. *Journal of the Atmospheric Sciences* 52, 1070–1083.
- Savina, M., Sch appi, B., Molnar, P., Burlando, P., Sevruk, B., 2012. Comparison of a tipping-bucket and electronic weighing precipitation gage for snowfall. *Atmospheric Research* 103, 45–51.
- Schindler Wildhaber, Y., B anninger, D., Burri, K., Alewell, Ch., 2012. Evaluation and application of a portable rainfall simulator on subalpine grassland. *Catena* 91, 56–62.
- Seeger, M., 2007. Uncertainty of factors determining runoff and erosion processes as quantified by rainfall simulations. *Catena* 71, 56–67.
- Segond, M.-L., Wheeler, H.S., Onof, C., 2007. The significance of spatial rainfall representation for flood runoff estimation: a numerical evaluation based on the Lee catchment, UK. *Journal of Hydrology* 347, 116–131.
- Sen, P.K., 1968. Estimates of the regression coefficient based on Kendall's Tau. *Journal of the American Statistical Association* 63, 1379–1389.

-
- Sevruk, B., Hamon, W.R., 1984. International comparison of national precipitation gauges with a reference pit gauge, Instruments and Observing Methods Report. Geneva, Switzerland, 139 p.
- Sevruk, B., Ondrás, M., Chvíla, B., 2009. The WMO precipitation measurement intercomparisons. *Atmospheric Research* 92, 376–380.
- Seymour, M.D., Stout, T., 1983. Observation on the chemical composition of rain using short sampling times during a single event. *Atmospheric Environment* 17, 1483–1487.
- Singh, V.P., 1997. Effect of spatial and temporal variability in rainfall and watershed characteristics on stream flow hydrograph. *Hydrological Processes* 11, 1649–1669.
- Singh, V.P., 2005. Effects of storm direction and duration on infiltrating planar flow with partial coverage. *Hydrological Processes* 19, 969–992.
- Smith, J.A., De Veaux, R.D., 1992. The temporal and spatial variability of rainfall power. *Environmetrics* 3, 29–53.
- Smith, P.L., Kliche, D.V., 2005. The bias in moment estimators for parameters of drop size distribution functions: sampling from exponential distributions. *Journal of Applied Meteorology* 44, 1195–1205.
- Smith, R.B., 1979. The influence of mountains on the atmosphere. *Advances in Geophysics* 21, 87–230.
- Sneyers, R., 1990. On the statistical analysis of series of observations, Technical Note no.143. World Meteorological Organization, Geneva, Switzerland, 192 p.
- Spraying Systems Co., 2013. Industrial Hydraulic Spray Products, Catalog 75 HYD, USA.
- Stedinger, J.R., Vogel, R.M., Efi, F.-G., 1993. Frequency analysis of extreme events, in: Maidment, D. (Ed.), *Handbook of Hydrology*. McGraw-Hill, Inc, New York.

-
- Steiner, M., Smith, J.A., 2000. Reflectivity, rain rate, and kinetic energy flux relationships based on raindrop spectra. *Journal of Applied Meteorology* 39, 1923–1940.
- Strangeways, I., 2007. *Precipitation: theory, measurement and distribution*. Cambridge University Press, Cambridge, UK, 290 p.
- Tarjuelo, J.M., Montero, J., Honrubia, F.T., Ortiz, J.J., Ortega, J.F., 1999. Analysis of uniformity of sprinkle irrigation in a semi-arid area. *Agricultural Water Management* 40, 315–331.
- Testud, J., Oury, S., Black, R.A., Amayenc, P., Dou, X., 2001. The concept of “normalized” distribution to describe raindrop spectra: a tool for cloud physics and cloud remote sensing. *Journal of Applied Meteorology* 40, 1118–1140.
- Thies A., 2007. Instruction for Use 021341/08/07. Laser Precipitation Monitor 5.4110.xx.x00 V2.4x STD. Göttingen, Germany.
- Thomaz, E.L., Luiz, J.C., 2012. Soil loss, soil degradation and rehabilitation in a degraded land area in Guarapuava (Brazil). *Land Degradation & Development* 23, 72–81.
- Thompson, A.L., James, L.G., 1985. Water droplet impact and its effect on infiltration. *Transactions of the ASABE* 28, 1506–1510.
- Tokay, A., Short, D.A., 1996. Evidence from tropical raindrop spectra of the origin of rain from stratiform versus convective clouds. *Journal of Applied Meteorology* 35, 355–371.
- Tokay, A., Wolff, D.B., Wolf, K.R., Bashor, P., 2003. Rain gauge and disdrometer measurements during the Keys Area Microphysics Project (KAMP). *Journal of Atmospheric and Oceanic Technology* 20, 1460–1477.
- Tomé, A.R., Miranda, P.M.A., 2004. Piecewise linear fitting and trend changing points of climate parameters. *Geophysical Research Letters* 31, L02207.
- Tomé, A.R., Miranda, P.M.A., 2005. Continuous partial trends and low-frequency oscillations of time series. *Nonlinear Processes in Geophysics* 12, 451–460.

-
- Tomich, S.D., Dana, M.T., 1990. Computer-Controlled Automated Rain Sampler (CCARS) for rainfall measurement and sequential sampling. *Journal of Atmospheric and Oceanic Technology* 7, 541–549.
- Tossell, R.W., Dickinson, W.T., Rudra, R.P., Wall, G.J., 1987. A portable rainfall simulator. *Canadian Agricultural Engineering* 29, 155–162.
- Trenberth, K.E., 2011. Changes in precipitation with climate change. *Climate Research* 47, 123–138.
- Tsai, T.-L., 2008. The influence of rainstorm pattern on shallow landslide. *Environmental Geology* 53, 1563–1569.
- Türkeş, M., 1996. Spatial and temporal analysis of annual rainfall variations in Turkey. *International Journal of Climatology* 16, 1057–1076.
- Uijlenhoet, R., 1999. Parameterization of rainfall microstructure for radar meteorology and hydrology. Doctoral thesis, Wageningen University, The Netherlands, 279 p.
- Uijlenhoet, R., Stricker, J.N.M., 1999. A consistent rainfall parameterization based on the exponential raindrop size distribution. *Journal of Hydrology* 218, 101–127.
- Ulbrich, C.W., 1983. Natural variations in the analytical form of the raindrop size distribution. *Journal of Climate and Applied Meteorology* 22, 1764–1775.
- University Corporation for Atmospheric Research, 2009. Available from http://www.meted.ucar.edu/hydro/precip_est/part1_measurement/print.htm [Accessed 04-06-2014].
- Usón, A., Ramos, M.C., 2001. An improved rainfall erosivity index obtained from experimental interrill soil losses in soils with a Mediterranean climate. *Catena* 43, 293–305.
- Veneziano, D., Villani, P., 1999. Best linear unbiased design hyetograph. *Water Resources Research* 35, 2725–2738.

-
- Vermang, J., Gabriëls, D., Cornelis, W., Boever, M. De, 2011. Land degradation processes and assessment: wind erosion, interrill erosion, gully erosion, land cover features. Ghent University. UNESCO Chair of Eremology; Research Foundation Flanders (FWO), Ghent, Belgium, 173 p.
- Vicente-Serrano, S.M., Cuadrat-Prats, J.M., 2007. Trends in drought intensity and variability in the middle Ebro valley (NE of the Iberian peninsula) during the second half of the twentieth century. *Theoretical and Applied Climatology* 88, 247–258.
- von Neumann, J., 1941. Distribution of the ratio of the mean square successive difference to the variance. *The Annals of Mathematical Statistics* 12, 367–395.
- Vories, E.D., von Bernuth, R.D., 1986. Single nozzle sprinkler performance in wind. *Transactions of the ASABE* 29, 1325–1330.
- Vuerich, E., Monesi, C., Lanza, L.G., Stagi, L., Lanzinger, E., 2009. WMO Field Intercomparison of rainfall intensity gauges, IOM Report N°99, WMO/TD N° 1504, Data Manager report.
- Walker, P.H., Hutka, J., Moss, A.J., Kinnell, P.I.A., 1977. Use of a versatile experimental system for soil erosion studies. *Soil Science Society of America Journal* 41, 610–612.
- Wijngaard, J.B., Klein Tank, A.M.G., Können, G.P., 2003. Homogeneity of 20th century European daily temperature and precipitation series. *International Journal of Climatology* 23, 679–692.
- Wilcox, B.P., Wood, M.K., Tromble, J.T., Ward, T.J., 1986. A hand-portable single nozzle rainfall simulator designed for use on steep slopes. *Journal of Range Management* 39, 375–377.
- Wischmeier, W.H., Smith, D.D., 1958. Rainfall energy and its relationship to soil loss. *Transactions American Geophysical Union* 39, 285–291.

-
- WMO, 1994. Guide to hydrological practices: data acquisition and processing, analysis, forecasting and other applications, 5th ed. Geneva, Switzerland, 735 p.
- WMO, 2008. Guide to meteorological instruments and methods of observation. 7th ed. Geneva, Switzerland, 681 p.
- Wong, R.K.W., Chidambaram, N., 1985. Gamma size distribution and stochastic sampling errors. *Journal of Climate and Applied Meteorology* 24, 568–579.
- Yen, B.C., Chow, V.T., 1980. Design hyetographs for small drainage structures. *Journal of the Hydraulics Division* 106, 1055–1076.
- Yilmaz, K.K., Hogue, T.S., Hsu, K.-L., Gupta, H.V., Wagener, T., 2005. Intercomparison of rain gauge, radar, and satellite-based precipitation estimates with emphasis on hydrologic forecasting. *Journal of Hydrometeorology* 6, 497–517.
- Young, R.A., Burwell, R.E., 1972. Prediction of runoff and erosion from natural rainfall using a rainfall simulator. *Soil Science Society of America Journal* 36, 827–830.
- Yuter, S.E., Kingsmill, D.E., Nance, L.B., Löffler-Mang, M., 2006. Observations of precipitation size and fall speed characteristics within coexisting rain and wet snow. *Journal of Applied Meteorology and Climatology* 45, 1450–1464.
- Zereini, F., Hötzl, H., 2008. Climatic changes and water resources in the Middle East and North Africa. Springer, 552 p.
- Zhang, G., Xue, M., Cao, Q., Dawson, D., 2008. Diagnosing the intercept parameter for exponential raindrop size distribution based on video disdrometer observations: model development. *Journal of Applied Meteorology and Climatology* 47, 2983–2992.
- Zhang, X.C., Norton, L.D., Hickman, M., 1997. Rain pattern and soil moisture content effects on atrazine and metolachlor losses in runoff. *Journal of Environmental Quality* 26, 1539–1547.

-
- Zhang, X., Vincent, L.A., Hogg, W.D., Niitsoo, A., 2000. Temperature and precipitation trends in Canada during the 20th century. *Atmosphere-Ocean* 38, 395–429.
- Zhang, X., Wang, X.L., Corte-Real, J., 1997. On the relationships between daily circulation patterns and precipitation in Portugal. *Journal of Geophysical Research* 102, 13495–13507.
- Zhao, G., Mu, X., Wen, Z., Wang, F., Gao, P., 2013. Soil erosion, conservation, and eco-environment changes in the loess plateau of China. *Land Degradation & Development* 24, 499–510.
- Ziadat, F.M., Taimeh, A.Y., 2013. Effect of rainfall intensity, slope, land use and antecedent soil moisture on soil erosion in an arid environment. *Land Degradation & Development* 24, 582–590.
- Ziegler, A.D., Sutherland, R.A., Tran, L.T., 1997. Influence of rolled erosion control systems on temporal rainsplash response – a laboratory rainfall simulation experiment. *Land Degradation & Development* 8, 139–157.

**APPENDIX A:
CHARACTERISTICS OF THE USED GAUGES**

APPENDIX A.1. Non-Conventional Rain Gauge (SRG.1)

The RUC (*Rain-gauge University of Coimbra*) is a rain gauge used to gather and measure precipitation accumulated over a given period of time. This rain gauge was developed in the Department of Civil Engineering of the Faculty of Science and Technology, University of Coimbra, and it enables the quantification of precipitation that is comparable to other rain gauges marketed by various manufacturers. Moreover, its manufacturing and maintenance costs are low. The RUC can be useful in scientific research, engineering studies or even in short term densification of national pluviometric networks.

RUC is made of simple components (Figure A.1 and A.2):

1. Outside housing
2. Funnel
3. Inner can
4. Support

Technical Specifications:

Outside housing

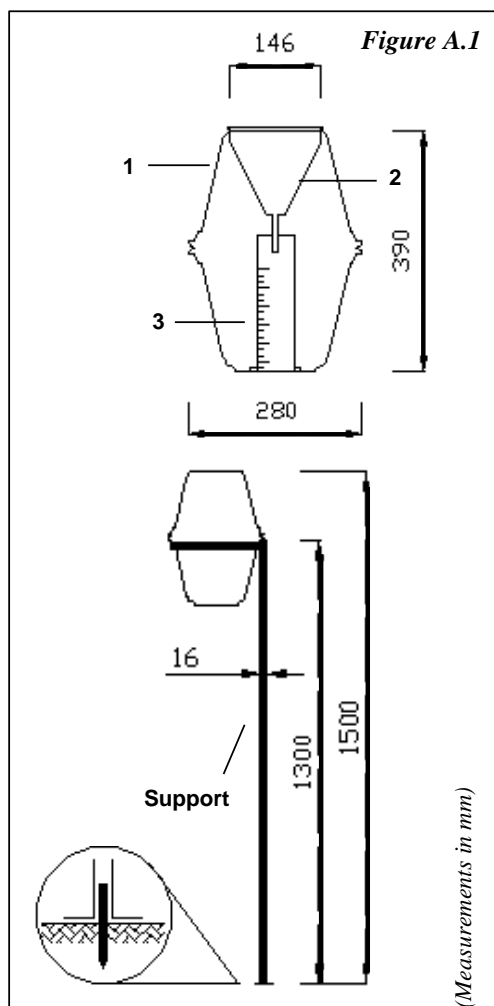
- Colour: white
- Shape: double cone
- Material: polypropylene

Funnel

- Colour: translucent
- Type of rim: curved
- Width of rim: 3.5 mm
- Material: polypropylene

Support

- Galvanized tube with a square cross section of 16 mm
- Iron pile with square section of 12 mm and a height of 800 mm

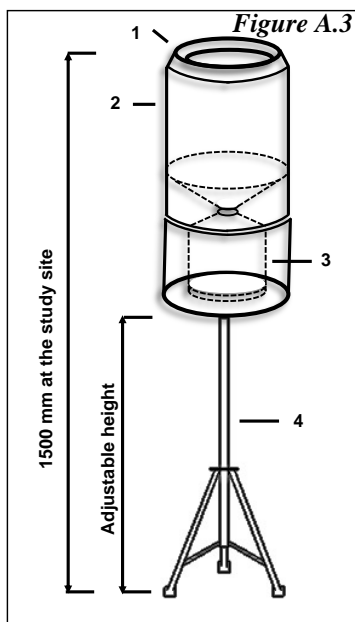


APPENDIX A.2. Standard Rain Gauges (SRG.2 and SRG.3)

The standard rain gauges manufactured by *Wilh.Lambrecht GmbH* and *VWR (model Hellmann rain gauge)* are non-recording rain gauges. Since these instruments only collect the rainfall and do not record it, an operator is required to measure the total rainfall amount at regular intervals. In order to estimate the rainfall depth, the total volume of water stored (in a graduated cylinder) is divided by the collecting area of the instrument.

The main components of the apparatus are (Figure A.3):

1. Knife-edge collector ring
2. Outside housing (upper and lower parts) incorporating a funnel
3. Inner can/graduated cylinder
4. Support



Technical specifications of *VWR* rain gauge (SRG.2, Figure A.4):

Collecting area (mm²)	10000
Dimensions (mm)	Height: 300 Diameter: 115
Range (mm)	0 - 25
Graduated cylinder (L)	0.25
Scale of the graduated cylinder (mm)	1



Technical specifications of *Wilh.Lambrecht GmbH* rain gauge (SRG.3, Figure A.5):

Collecting area (mm²)	20000
Dimensions (mm)	Height: 450 Diameter: 190
Range (mm)	0 - 60
Inner can (L)	1.20



For further information:
<http://www.lambrecht.net>
<https://uk.vwr.com/>

APPENDIX A.3. Tipping Bucket Rain Gauge (TBG.4)

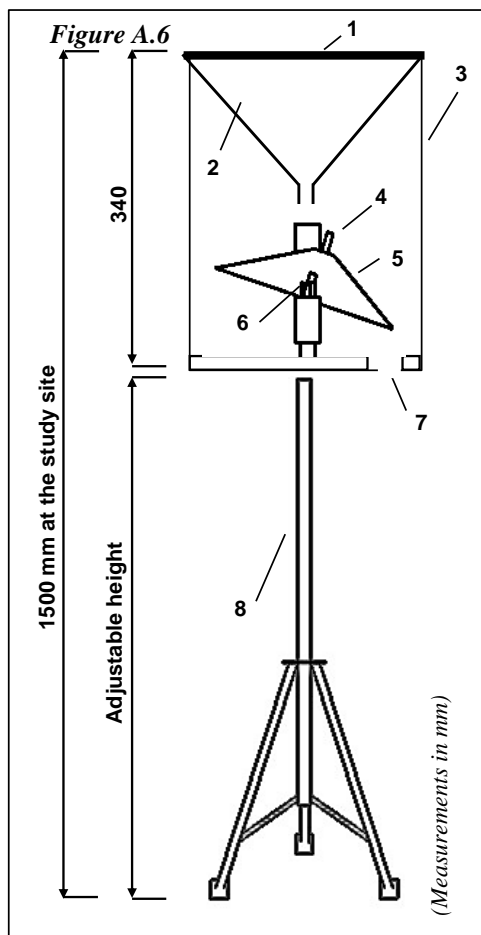
The *Casella CEL Tipping Bucket Rain Gauge* is a meteorological device used for measuring precipitation. The principle consists in harvesting the rainfall which flows down a funnel and drips into one of two calibrated buckets balanced on a pivot; when the calibrated amount of precipitation has been collected, the bucket becomes overbalanced and tips down, activating a magnetic reed switch. The water is discharged by a drainage hole while the other bucket is repositioned under the funnel ready for filling.

The main components of the apparatus are (Figures A.6, A.7, and A.8):

1. Knife-edge collector ring
2. Funnel
3. Cover
4. Magnet
5. Small bucket
6. Reed switch
7. Drain hole
8. Support

Technical specifications:

Collecting area (mm ²)	40000
Bucket size (mm)	0.2
Transducer	Magnet/ Reed switch
Capacity	Unlimited
Accuracy (%)	±1 at 1 L h ⁻¹



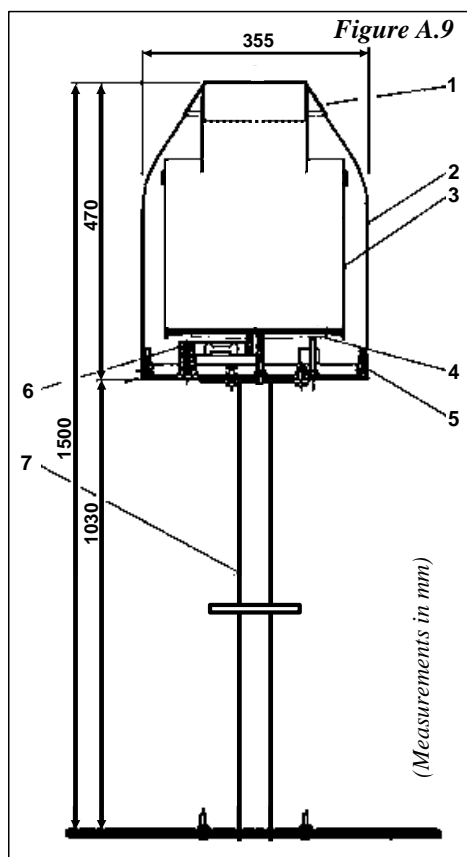
For further information:
<http://www.casellausa.com/>

APPENDIX A.4. Weighing Precipitation Gauge (WPG.5)

The weighing precipitation gauge manufactured by *MPS* (model *TRwS 204*) is an instrument for measuring different forms of precipitation, including rain, hail and snow. It consists of a storage container, that is weighed to record the precipitation amount and rate of accumulation over a set period of time. The increasing weight of the container is calculated by analysing the resonating frequency of wires which support the container. A data logger stores the data.

The main components of the apparatus are (Figures A.9 and A.10):

1. Collecting ring with heating
2. Cover
3. Container
4. Support plate
5. Base plate with box for electronics
6. Support of sensor
7. Pedestal



Technical specifications:

Collecting area (mm²)	20000
Range of weight (g)	0 - 12000
Maximum rain intensity (mm min⁻¹)	60
Resolution (mm)	0.001
Temporal resolution (s)	60
Accuracy of 1 min rain intensity (%)	0.02



For further information:
<http://www.mps-system.sk/>

APPENDIX A.5. Multi-parameter weather sensor (MWS.6)

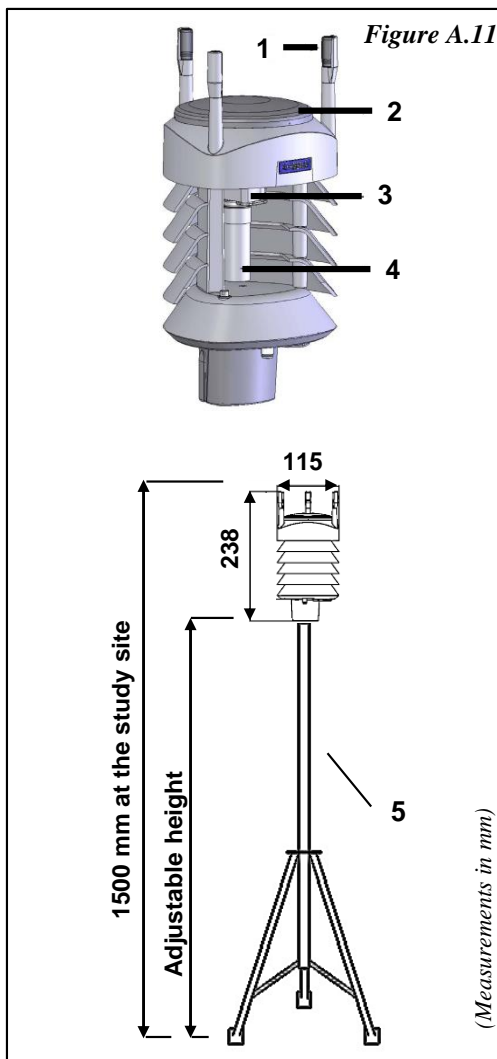
The *Vaisala Weather Transmitter WXT510* is a multi-sensor equipment that enables the measurement of the following parameters: wind speed and direction, precipitation, atmospheric pressure, temperature and relative humidity. In relation to the precipitation, the sensor detects the impact of individual precipitation particles; the mechanical movement of the steel cover is converted in electrical signals, which are proportional to the volume of the precipitation particles; and the output signal is finally converted in accumulated precipitation.

The main components of the equipment are (Figures A.11 and A.12):

1. Wind transducer
2. Precipitation sensor
3. Pressure sensor
4. Humidity and temperature sensors
5. Support

Technical specifications:

Precipitation	Collecting area (mm ²)	6000
	Range (mm h ⁻¹)	0 – 200
	Resolution (mm)	0.01
	Accuracy (%)	< 5
	Temporal resolution (s)	60
Wind	Speed: Range (m s ⁻¹)	0 – 60
	Accuracy (%) at 0–35 m s ⁻¹	3
	at 36–60 m s ⁻¹	5
	Resolution (m s ⁻¹)	0.1
	Direction: Range	0 – 360°
Accuracy	± 3.0°	
Resolution	1°	
Barom. Pressure	Range (hPa)	600 – 1100
	Accuracy (hPa) at 0–30°C	± 0.5
	Resolution (hPa) at -52°C–60°C	±1
Air Temperat.	Range (°C)	-52 to +60
	Accuracy (°C) at 20°C	±0.3
	Resolution (°C)	0.1
Relative humidity	Range (%)	0 – 100
	Accuracy (%) at 0–90 %	±3
	at 90–100 %	±5
Resolution (%)	0.1	

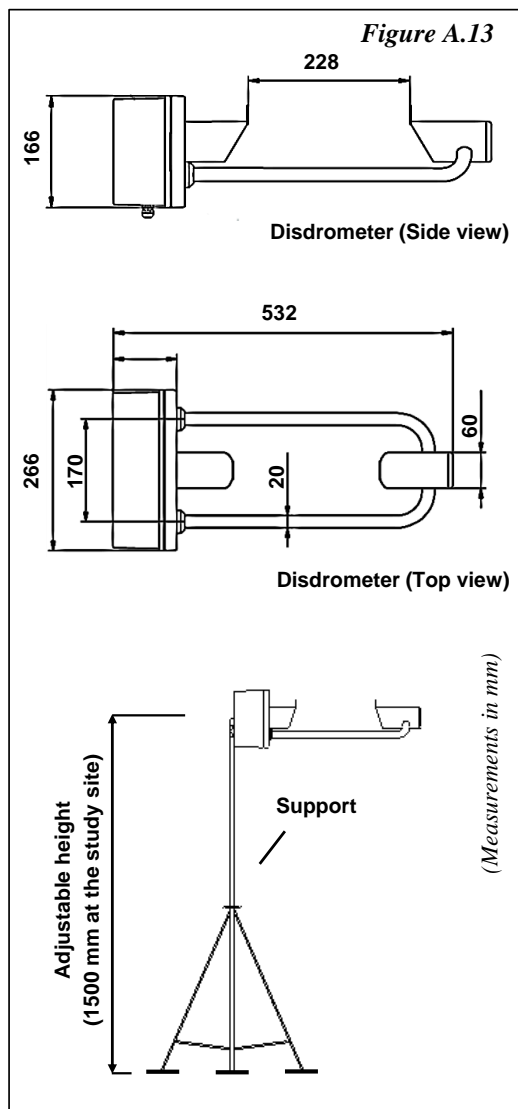


For further information:
<http://www.vaisala.com/>

APPENDIX A.6. Disdrometer (DIS.7)

The *Laser Precipitation Monitor* is a disdrometer manufactured by *Thies Clima* and measures the drop size distribution and velocity of falling precipitation particles. A laser-optical source produces a light-beam which is transformed into an electrical signal in the receiver. When a precipitation particle falls through the light-beam the receiving signal is reduced. The diameter of the particle is calculated from the amplitude of the reduction and the fall speed of the particle is determined from the duration of the reduced signal. The disdrometer also estimates the intensity, quantity and type of precipitation.

The disdrometer and its support are shown in Figures A.13 and A.14:



Technical specifications:

Laser	785 nm; class 1M; max 0.5 mW optical power
Measuring area (mm²)	4776.7
Temporal resolution (s)	60
Particle size (mm)	0.125 – 8.000
Particle speed (m s⁻¹)	0.0 – 20.0
Disdrometer classes	420 (21 diameter × 20 speed)
Intensity of precipitation (mm h⁻¹)	0.001 – 250
Error intensity- quantity	<15% (rain 0.5 – 20 mm h ⁻¹) <30% (snow)



For further information:
<http://www.thiesclima.com/>

**APPENDIX B:
CHRONOGRAM AND LIST OF
MEASURED DATA SERIES**

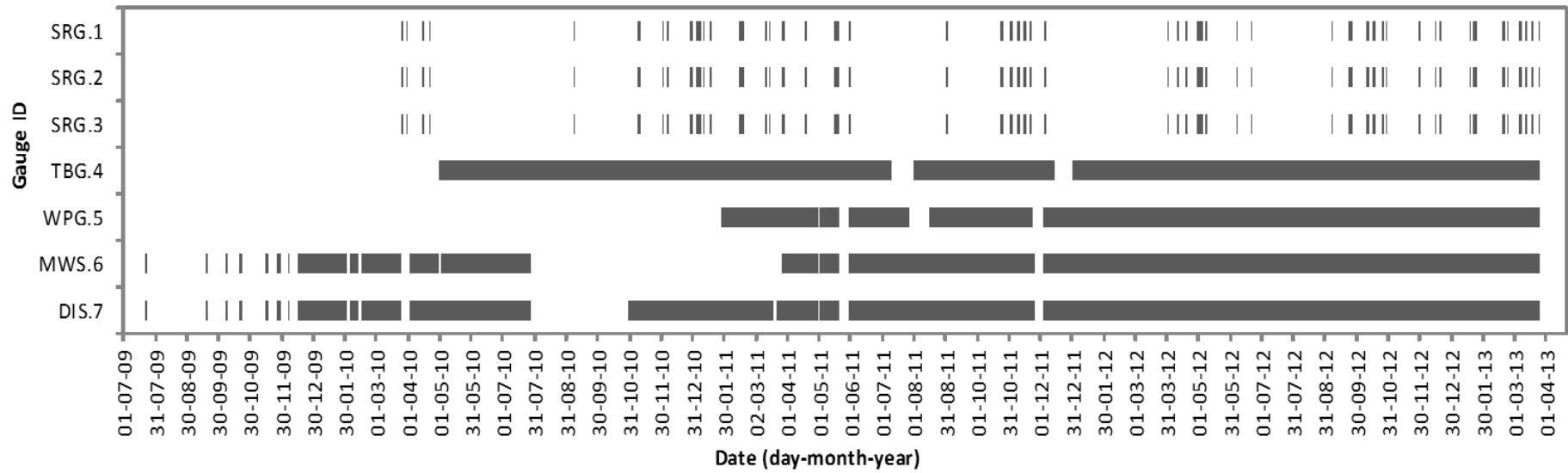


Figure B.1 Chronological distribution of the data collected with the seven instruments: SRG.1, SRG.2, SRG.3, TBG.4, WPG.5, MWS.6, DIS.7.

Table B.1 List of the 60 rainy periods measured with the seven instruments: SRG.1, SRG.2, SRG.3, TBG.4, WPG.5, MWS.6, DIS.7.

Rainy periods	Date (day-month-year) / Time (h:min)		Rainfall depths (mm)						
	start	end	SRG.1	SRG.2	SRG.3	TBG.4	WPG.5	MWS.6	DIS.7
1	26-03-2011 10:00:00	27-03-2011 9:00:00	12.8	12.7	12.9	14.1	13.0	10.5	13.7
2	27-03-2011 9:00:00	28-03-2011 9:30:00	1.9	1.7	1.6	0.8	0.4	0.2	0.8
3	28-03-2011 9:30:00	29-03-2011 9:30:00	21.2	20.9	20.8	21.2	19.4	12.7	20.0
4	18-04-2011 12:00:00	19-04-2011 9:30:00	24.9	24.9	25.0	25.0	23.9	27.2	24.4
5	17-05-2011 9:20:00	18-05-2011 9:30:00	5.6	5.5	5.6	6.0	4.9	6.6	5.5
6	18-05-2011 9:30:00	19-05-2011 9:30:00	1.3	1.6	1.4	1.2	1.2	1.3	1.3
7	19-05-2011 9:30:00	20-05-2011 8:50:00	10.3	9.9	10.0	10.2	9.4	11.9	9.4
8	01-09-2011 13:45:00	02-09-2011 9:45:00	16.2	16.3	16.2	17.8	15.3	12.8	15.7
9	23-10-2011 14:00:00	24-10-2011 9:40:00	19.8	14.1	14.4	16.6	16.7	5.8	20.2
10	24-10-2011 9:40:00	25-10-2011 10:30:00	11.7	11.6	11.4	10.4	11.2	4.9	12.8
11	01-11-2011 17:00:00	02-11-2011 15:30:00	23.5	22.2	22.5	24.0	22.5	23.9	25.0
12	02-11-2011 15:30:00	03-11-2011 9:40:00	4.5	4.1	4.1	4.4	4.2	3.8	4.6
13	03-11-2011 9:40:00	04-11-2011 9:30:00	14.8	13.0	13.2	14.4	13.0	15.2	15.0
14	08-11-2011 10:00:00	09-11-2011 9:00:00	9.6	8.8	8.8	9.5	8.2	5.8	10.3
15	09-11-2011 9:00:00	10-11-2011 9:30:00	0.5	0.4	0.5	0.5	0.4	0.3	0.5
16	10-11-2011 9:30:00	11-11-2011 15:30:00	19.3	16.6	22.1	18.2	16.7	13.8	20.1
17	14-11-2011 13:30:00	15-11-2011 10:00:00	18.7	23.1	23.4	24.5	22.9	23.3	24.8
18	15-11-2011 10:00:00	16-11-2011 12:20:00	0.9	0.9	0.9	1.1	0.8	1.1	1.3
19	21-11-2011 10:00:00	22-11-2011 10:00:00	20.2	20.0	19.8	20.6	19.3	17.9	19.7
20	05-12-2011 14:30:00	06-12-2011 14:00:00	2.3	2.0	2.2	2.2	1.8	0.3	2.1
21	01-04-2012 10:00:00	02-04-2012 10:00:00	2.4	2.2	2.1	2.4	1.9	2.7	2.4
22	11-04-2012 10:00:00	12-04-2012 12:00:00	1.9	1.6	1.6	1.6	1.5	0.3	2.2
23	19-04-2012 14:00:00	20-04-2012 10:00:00	3.5	3.6	3.2	3.2	3.2	0.1	4.1
24	30-04-2012 15:00:00	01-05-2012 19:00:00	3.3	2.5	2.5	3.0	2.3	2.5	2.9
25	01-05-2012 19:00:00	02-05-2012 14:00:00	4.3	3.6	3.4	4.0	3.4	4.3	4.6
26	02-05-2012 14:00:00	03-05-2012 10:30:00	20.2	18.6	19.1	18.8	18.6	21.7	21.2
27	03-05-2012 10:30:00	04-05-2012 10:30:00	10.5	9.8	10.4	10.2	9.7	10.9	11.4
28	04-05-2012 10:30:00	05-05-2012 18:00:00	5.6	5.5	5.3	5.2	5.3	5.3	6.0
29	07-05-2012 10:00:00	08-05-2012 10:00:00	23.8	22.1	21.9	22.2	22.2	14.3	24.0
30	20-06-2012 9:30:00	21-06-2012 9:30:00	2.4	2.1	2.0	2.2	2.0	1.2	2.9
31	06-09-2012 14:00:00	07-09-2012 14:00:00	1.0	1.2	1.1	1.0	1.2	1.9	1.4
32	22-09-2012 9:00:00	23-09-2012 9:00:00	7.5	6.7	6.6	6.6	6.9	6.5	5.6
33	23-09-2012 9:00:00	24-09-2012 10:00:00	2.0	1.9	1.8	2.0	1.9	2.6	0.9
34	24-09-2012 10:00:00	25-09-2012 17:30:00	13.7	13.0	12.8	13.9	13.2	14.4	7.5
35	25-09-2012 17:30:00	26-09-2012 9:00:00	12.8	12.6	12.7	12.7	12.3	9.6	12.0
36	09-10-2012 9:00:00	10-10-2012 18:00:00	1.9	2.4	2.2	1.9	1.5	0.3	2.1
37	10-10-2012 18:00:00	11-10-2012 10:00:00	4.4	4.4	4.3	4.5	4.2	2.4	4.4
38	11-10-2012 10:00:00	11-10-2012 17:30:00	7.8	7.7	7.9	7.7	7.6	6.5	7.3
39	16-10-2012 17:30:00	17-10-2012 11:30:00	11.2	9.1	9.3	9.8	10.1	5.1	11.2
40	17-10-2012 11:30:00	18-10-2012 11:30:00	25.1	25.0	25.1	25.0	24.2	25.9	26.5
41	24-10-2012 17:30:00	25-10-2012 17:30:00	10.7	9.8	10.0	10.6	9.7	10.8	10.9
42	25-10-2012 17:30:00	26-10-2012 18:30:00	19.4	17.3	17.5	18.8	17.9	14.6	20.6
43	29-10-2012 9:30:00	30-10-2012 18:00:00	10.5	10.3	10.1	11.0	9.9	10.7	11.2
44	29-11-2012 14:00:00	30-11-2012 14:00:00	8.4	7.6	8.7	8.6	8.3	9.0	8.3
45	14-12-2012 14:00:00	15-12-2012 18:00:00	23.1	19.7	19.6	18.4	20.5	7.6	20.8
46	19-12-2012 10:00:00	20-12-2012 9:30:00	0.6	0.6	0.6	0.9	0.7	0.4	1.3
47	17-01-2013 10:00:00	18-01-2013 10:00:00	11.5	10.6	10.2	10.3	10.9	2.8	11.7
48	20-01-2013 14:00:00	21-01-2013 9:30:00	11.2	9.0	9.2	7.6	8.5	3.3	9.2
49	21-01-2013 9:30:00	22-01-2013 18:00:00	17.7	16.8	17.0	17.8	16.7	18.9	15.9
50	22-01-2013 18:00:00	23-01-2013 9:30:00	6.9	6.5	6.7	6.8	5.9	6.3	6.2
51	23-01-2013 9:30:00	24-01-2013 10:00:00	9.2	8.2	7.9	8.0	8.4	2.8	9.1
52	19-02-2013 10:30:00	20-02-2013 10:00:00	2.7	2.6	2.5	2.6	2.2	1.4	2.7
53	22-02-2013 10:20:00	22-02-2013 18:00:00	1.7	0.4	1.4	1.5	1.3	1.7	1.9
54	05-03-2013 10:00:00	06-03-2013 14:00:00	6.6	5.7	5.7	6.2	5.5	4.3	7.2
55	06-03-2013 14:00:00	07-03-2013 10:30:00	7.8	6.1	6.0	6.8	6.5	4.0	8.3
56	07-03-2013 10:30:00	08-03-2013 10:00:00	22.5	21.4	21.6	21.8	20.9	18.7	23.3
57	11-03-2013 10:30:00	12-03-2013 9:30:00	6.4	6.0	6.0	6.5	5.6	5.9	6.4
58	12-03-2013 9:30:00	13-03-2013 10:00:00	5.0	5.0	5.1	5.4	4.5	4.1	4.9
59	18-03-2013 10:00:00	19-03-2013 20:00:00	5.5	4.9	4.8	5.2	5.0	4.1	5.2
60	24-03-2013 18:30:00	25-03-2013 19:00:00	28.8	23.1	23.1	24.3	25.9	12.0	28.2